Siôn Marc Lewis

Department of Biochemical Engineering

UCL

Localisation of mTOR complex proteins in embryonic stem cells: relationship with cell division and survival

A thesis submitted for the degree of Doctor of Philosophy

PhD Biochemical Engineering

2011

Abstract

The mammalian target of rapamycin (mTOR) regulates cell growth and proliferation in response to nutrients and growth factors. The role of mTOR in the biology of embryonic stem cells has not been extensively characterised.

The principle aim of this research was to assess the feasibility of manipulating the mTOR pathway to provide bioprocessing improvements for the expansion and differentiation of embryonic stem cells.

In order to achieve this aim, the cellular distribution and localisation of mTOR pathway phosphoproteins was assessed and the effect of pathway inhibition on ES cell proliferation and viability was characterised.

The key findings of this study revealed that in mouse ES cells, mTOR pathway proteins were phosphorylated during mitosis. Secondly, inhibition of mTOR in growth factor-stimulated pluripotent stem cells impaired proliferation but not viability. Upon withdrawal of growth factors, cells lost their compact shape and exhibited a spread morphology. Under these conditions mTOR inhibition reduced the viability and proliferation of ‘compact’ cells but not ‘spread’ cells.

Thus, during the expansion of ES cells the mTOR pathway may be stimulated. During early differentiation, inhibition of the pathway may improve the purity of the final cell preparation and reduce the prevalence of parent stem cells.

In conclusion, the experimental findings discussed here show that temporal manipulation of the mTOR pathway in embryonic stem cells may provide bioprocessing advantages resulting in an increased yield of parent cell populations

during expansion and increased purity of differentiated cells. The sensitivity of the mTOR pathway to the bioavailability of nutrients may offer a cost-effective route to optimising cell production in an industrial scale process.

Further work to elucidate the role of the mTOR complex 2 in ES cell proliferation may provide an additional level of control to independently modulate cell proliferation and growth during expansion and differentiation.

Declaration

I, Sion Marc Lewis confirm that the work presented in this thesis is my own.

Where information has been derived from other sources, I confirm that this has been indicated in the thesis.

Acknowledgements

I wish to thank Dr. Farlan Veraitch for his continued support and advice throughout this project.

I would like to express my sincere gratitude to Dr. Alun Brown for his longstanding support and scientific mentoring.

I wish to express my thanks to Dr. Samir Nuseibeh for his help and advice with gel electrophoresis and western blotting.

I would like to thank Dr. Chris Thrasivoulou and Danial Ciantar for their help and advice with confocal microscopy and colocalisation analysis.

I wish to acknowledge the BBSRC for the financial support of this study.

I am sincerely grateful to Trystan, Bethan and my young niece and nephew for putting it all into perspective and to Melanie who kept me smiling throughout.

This thesis is dedicated to Mum and Dad for their limitless
support and encouragement.

"I may not have gone where I intended to go,
but I think I ended up where I needed to be"

Douglas Adams

Table of Contents

Title…p1

Abstract…p2

Declaration...p4

Acknowledgements…p5

Table of Contents…p6

List of Figures…p13

List of Abbreviations…p20

CHAPTER 1

1.1 Aims of research…p22

1.2 Thesis structure…p22

1.3 Introduction…p24

1.4 Background…p25 .

1.4.1 A historical perspective on embryonic stem cell derivation…p25

1.4.2 Leukaemia inhibitory factor signalling in mouse ES cells…p28

1.4.3 The regulation of pluripotency in mouse ES cells by LIF…p28

1.4.4 The core network regulating pluripotency in mouse ES cells…p33

1.4.5 The ground state of embryonic stem cell self-renewal…p34

1.4.6 Cell cycle regulation in mouse ES cells…p35

1.5. The mammalian target of rapamycin pathway…p36

1.5.1 The discovery of metazoan and mammalian TOR…p36

1.5.2 The rapamycin sensitive mTOR complex (TORC1)…p37

1.5.3 The mTOR complex-1 in the regulation of cell size…p38

1.5.4 The rapamycin insensitive mTOR complex (mTORC2)…p39

1.5.5 Upstream regulation of mTOR signaling…p40

1.5.6 Interactions between the mTOR and PI3K pathway…p41

1.5.7 The mTOR/PI3K pathways regulate cellular metabolism in response to nutrient availability…p42

1.5.8 Substrates of AKT promote cell survival…p44

1.5.9 The mammalian TOR pathway in development…p45

1.5.10 Manipulation of the mTOR pathway as a bioprocessing for the enhanced expansion and differentiation of ES cells…p48

1.6 Research question…p49
1.7 Objectives…p49

CHAPTER 2

Experimental methods…p50

2.1 Expansion and culture of mouse embryonic fibroblasts…p50
2.2 Culture of human embryonic stem cells…p51
2.3 Culture of mouse embryonic fibroblasts...p51
2.4 Culture of mouse embryonic stem cells…p52
2.5 Protein isolation and purification…p52
2.6 SDS-polyacrylamide gel electrophoresis and western blotting…p53
2.7 Immunostaining…p54
2.8 Antibodies…p55
2.9 Image capture and processing…p55
2.10 Live-cell imaging…p56
2.11 Flow cytometry…p56
2.12 Assessment of cell viability and proliferation…p57
2.13 Assessment of apoptosis in mES cells…p57
2.14 Hypothesis testing and statistical significance…p58
2.15 Determination of statistical significance in multivariate data sets…p59
2.16 Assessment of significance in multivariate data with multiple treatment groups…p60
2.17 Biological replicates and n-values…p60

CHAPTER 3

Characterisation of the cell culture system for analysis of the mTOR pathway in the pluripotent cells…p61

3.1. Characterisation of human embryonic stem cells in vitro…p61

3.2 Assessment of the effect of rapamycin on human embryonal carcinoma cell proliferation…p79

3.3 The mTOR pathway in E14 mouse embryonic stem cells…p82

3.4 The effect of rapamycin on TORC1 substrate phosphorylation…p91

3.5. The effect of rapamycin on TORC2 substrate phosphorylation…p94

3.6 Activation of the mTOR pathway during in vitro culture…p98

3.7 The effect of rapamycin treatment on the PI3K and MAPK pathways…p99

3.8 Summary of findings…p103

CHAPTER 4

Microscopic analysis of mTOR pathway phosphoprotein expression in mouse embryonic stem cells in vitro…p109

4.1 The cellular distribution of phosphorylated mTOR in mES cells…p109

4.2 The cellular distribution and localisation of phosphorylated p70S6K in mES cells…p122

4.3 The cellular distribution and localisation of the mTORC2 complex substrate AKT ser473 in mES cells…p129

4.4. Colocalisation of phospho-AKT serine-473 with α-tubulin in mitotic mES cells…p139

4.5 Colocalisation of phospho-AKT serine-473 with α-tubulin in mouse embryonic fibroblasts...p151

4.6 Effect of mTOR inhibition on mitosis on mouse embryonic stem cells…p152

4.7 Summary of findings…p159

CHAPTER 5

The mammalian target of rapamycin pathway in the proliferation and viability of embryonic stem cells…p161

5.1 Assessment of the effect of the PI3K inhibitor LY294002 on mES cell proliferation and viability…p162

5.2 Combined inhibition of the mTOR complex 1 and the PI3K pathway on mES cell proliferation and viability…p165

5.3 The effect of the dual mTOR kinase inhibitor Ku-0063 on mES cell proliferation…p168

5.4 The effect of mTOR and PI3K inhibitors on mES cell viability…p170

5.5 The effect of serum deprivation on mES colony formation…p174

5.6 The effect of mTOR inhibition on mES colony expansion during differentiation…p178

5.7 The effect of mTOR inhibition on mES cell apoptosis…p182

5.8 Summary of findings...p193

CHAPTER 6

Discussion…p197

6.1 Preliminary observations…p198

6.2 Subcellular localisation of mTOR phosphoproteins…p198

6.3 The viability of differentiating stem cells in response to mTOR inhibition…p207

6.4 Wider implications of mTOR signaling in mES cells…p209

6.5 Conclusion…p215

6.6 Future work…p217

CHAPTER 7

References…p219

CHAPTER 8

Appendix 1 Development and characterisation of an image analysis tool to enable the assessment of stem cell expansion from phase contrast images…p233

8.1 Intensity thresholding for determination of cell confluence from phase-contrast images (Method 1A)…p234

8.2 Characterisation of Method A for determination of mES expansion from time-course images…p246

8.3 Optimisation of dual threshold technique - Method B…p255

8.4 Characterisation of a robust, local contrast variation technique - Method C…p261

8.5 The relationship between mean colony area measurements and total number of colonies by the three methods…p266

8.6 Characterisation of mES cell phase and morphology from phase-contrast micrographs by Method 2…p270

8.7 Summary of findings…p282

8.8 Appendix 2…p287

8.9 Appendix 3…p288

List of Figures

Chapter 1 Figures

Figure 1.4.1 LIF-mediated activation of JAK/STAT pathway in mouse ES cells…p29

Figure 1.4.2 Activation of AKT via PI3K mediated phosphorylation of PIP2…p31

Figure 1.4.3 The regulation of stem cell pluripotency in the mouse…p34

Figure 1.5.1 Functional structure of mammalian TOR protein…p37

Figure 1.5.2 Key outputs of mTOR mediating cell growth…p38

Figure 1.5.3 Kinase substrates of TORC2…p40

Figure 1.5.4 Pathway map of key mTORC1 interactions…p42

Figure 1.5.5 Mechanisms of cell survival mediated by AKT…p44

Table 1.1 Summary of key signalling events in mES cells…p47

Chapter 2 figures

Table 2.1 Bonferroni adjustment for significance testing with multiple comparisons…p59

Chapter 3 figures

Figure 3.1.1 Human ES cell colonies exhibit distinct morphology and express OCT4…p63

Figure 3.1.2 Mouse embryonic fibroblasts do not express OCT4…p64

Figure 3.1.3 Expression of OCT4 in hES and MEF co-cultures…p65

Figure 3.1.4.1 Morphology and OCT4 expression in hES and MEF co-cultures…p67

Figure 3.1.4.2 Mean fluorescence intensity of OCT4 in morphologically distinct cell areas…p68

Figure 3.1.5 Expression of OCT4 may relate to density of hES cells in a colony…p70

Figure 3.1.6.1 Relationship between OCT4 expression and cell density in single hES cells…p71

Figure 3.1.6.2 Relationship between OCT4 expression and cell density in hES colonies…p73

Figure 3.1.6.3 Relationship between OCT4 expression and nuclear size in hES…p74

Figure 3.1.7 Effect of rapamycin on human embryonic stem cell colony formation…p77

Figure 3.1.8 Expression of mTOR and phospho-p70S6K in mouse embryonic fibroblasts…p78

Figures 3.2.1 Rapamycin mediated inhibition of human embryonal carcinoma cell proliferation is time-dependent…p81

Figure 3.3.1 Typical morphology of E14 mouse embryonic stem cells in culture…84

Figure 3.3.2 Treatment of mouse ES cells with rapamycin for 24h inhibits proliferation at high concentrations…p85

Figure 3.3.3 Rapamycin treatment for 48h inhibits mES cell proliferation in a dose-dependent manner…p86

Figure 3.3.4.1 Rapamycin treatment does not alter OCT4/GFP expression in mES cells…p88

Figure 3.3.4.2 Rapamycin increases the mean intensity of OCT4 expression in mES cells…p89

Figure 3.3.5 Rapamycin does not reduce mES cell size under normal growth conditions…p90

Figure 3.4.1 Rapamycin inhibits the phosphorylation of the mTORC1 substrate p70S6K…p92

Figure 3.5.1 The effect of rapamycin treatment on TORC2 kinase activity…p95

Figure 3.5.2 Rapamycin treatment increases the phospho-AKT at serine residue 473 during serum starvation and normal culture…p96

Figure 3.6 Levels of total and phosphorylated mTOR protein during in vitro culture…p100

Figure 3.7 Rapamycin treatment increases ERK1/2 and reduces AKT th308 phosphorylation in serum starved mES cells…p102

Chapter 4 figures

Figure 4.1.1 The cellular distribution of native mTOR mES cells in vitro…p111

Figure 4.1.2 Cellular distribution of phospho-mTOR at serine-2448 in mES cells…p112

Figure 4.1.3 Mitotic phosphorylation of mTOR serine-2448 in mES cells…p113

Figure 4.1.4 Non-uniform distribution of phospho-mTOR serine-2481 in mES cells…p114

Figure 4.1.5 Nuclear localisation and mitotic phosphorylation of mTOR serine 2448 in mES cells…p115

Figure 4.1.6 Localisation of phospho-mTOR serine 2481 in cells during early differentiation…p118

Figure 4.1.7 Relationship between OCT4 staining and mTOR ser2481 in compact and spread mES cells…p119

Figure 4.1.8 Phospho-mTOR ser2481 is present at the midbody of dividing cells…p121.

Figure 4.2.1 Cellular distribution of total p70S6K protein in mES cells…p124

Figure 4.2.2 Cellular distribution of phospho-p70S6K (tth389) in mES cells…p125

Figure 4.2.3 Cellular distribution of phospho-p70S6K (th421) in mES cells…p126

Figure 4.2.4 Phosphorylation of p70S6K th421 during mES mitosis…p127

Figure 4.2.5 Phosphorylation of p70S6K th421 is downregulated during late mitosis…p128

Figure 4.3.1 Non-uniform distribution of phospho-AKT (ser473) in mES cells…p131

Figure 4.3.2 Nuclear localisation and patterned phosphorylation of AKT at serine-473 in mES cells…p132

Figure 4.3.3 Phosphorylation of AKT at serine-473 during mitosis in mES cells…p133

Figure 4.3.4 Concordance between phospho-AKT (ser473) and mitosis in mES cells…p136

Figure 4.3.4 Mitotic localisation of AKT (ser473) in mES cells with compact and compact and spread morphologies…p137

Figure 4.4.1 Distribution of AKT (ser473) and α-tubulin in a metaphase mES cell…p142

Figure 4.4.2.1 Colocalisation of AKT (ser473) with α-tubulin in a metaphase mES cell…p143

Figure 4.4.2.2 Colocalisation of AKT (ser473) with α-tubulin in a metaphase mES cell from confocal z-series image stack…p145

Figure 4.4.2.3 Colocalisation of phospho-AKT (ser473) with α-tubulin in mES cells during mid and late mitosis…p146

Figure 4.4.3.1 Nocodazole treatment disrupts both tubulin and AKT (ser473) organisation in metaphase mES cell…p148

Figure 4.4.3.2 Confocal z-stacks of individual mES cells treated with nocodazole…p149

Figure 4.5.1 Co-localisation of AKT ser473 with α-tubulin in a proliferating mouse embryonic fibroblast…p154

Figure 4.5.2 Short-term paclitaxel treatment does not impair the association of phospho-AKT (ser473) with α-tubulin in MEF cells…p155

Figure 4.6.1 Assessment of mitotic index by phospho-histone H3(ser10) staining…p157

Figure 4.6.2 Treatment of mES cells for 24h with TORC1 andmTORC2 inhibitors reduces the number of cells in mitosis…p158

Chapter 5 figures

Figure 5.1.1 Dose-dependent effect of LY294002 on mES cell proliferation…p163
Figure 5.1.2 Dose dependent effect of LY294002 on mES cell proliferation…p164
Figure 5.2.1 Comparison between the effects of rapamycin, LY-294003 and combined inhibition on mES cell proliferation…p166
Figure 5.2.2 Low doses of rapamycin and LY294002 do not reduce mES cell viability…p167
Figure 5.3.1 Dose-dependent effect of Ku-0063 treatment on mES cell proliferation…p169
Figure 5.4.1 Inhibitors of the mTOR and PI3K pathways inhibit proliferation but not viability of LIF stimulated mES cells…p171
Figure 5.4.2 Inhibitors of the mTOR and PI3K pathways inhibit proliferation but not viability mES cells deprived of LIF…p172
Figure 5.4.2 Inhibitors of the mTOR and PI3K pathways increase the numbers of detached mES cells when deprived of LIF…p173
Figure 5.5.1 Representative phase contrast and results images of mES cells following serum deprivation…p175
Figure 5.5.2 Mouse ES cell colony expansion is impaired by LIF withdrawal during serum starvation…p176
Figure 5.5.3 Rapamycin treatment promotes mES viability independently of LIF during serum starvation…p177
Figure 5.6.1 Mammalian TOR complexes inhibitors reduce the expansion of cells with compact but not spread morphology…p179
Figure 5.6.2 Mammalian TOR complexes inhibitors reduce the expansion of cells with compact but not spread morphology during differentiation…p180
Figure 5.6.3 Representative phase contrast and results images from Method 2 analysis of expansion of compact and spread cells during differentiation…p181
Figure 5.7.1 Short term treatment of pluripotent mES cells with mTOR inhibitors does not induce apoptosis…p184

Figure 5.7.2 Short-term mTOR inhibition (3h) does not induce apoptosis in mES cells in LIF deficient growth medium…p185

Figure 5.7.3 Extended mTOR inhibition affects the viability and apoptosis of E14 mES cells cultured with LIF…p187

Figure 5.7.4 Extended mTOR inhibition affects the viability of E14 mES cells cultured in LIF deficient growth medium…p188

Figure 5.7.5 Inhibition of mTOR treatment increases the viability of detached cells in LIF-deficient growth medium…p189

Figure 5.7.6 Treatment but not pretreatment of differentiating mES cells with mTOR kinase inhibitors reduces viability…p191

Chapter 6 Figures

Chapter 7 Figures

Chapter 8 Figures

Figure 8.1.1 Method A analysis of confluence of OCT4/GFP mES colonies from phase-contrast micrographs…p238

Figure 8.1.2 Relationship between the calculated cell area from Method A and OCT4+ve cell areas…p239

Figure 8.1.3 Image analysis based method for assessment of mES cell confluence following 48h treatment with DMSO…p242

Figure 8.1.4 Method A for assessment of mES cell confluence following 48h treatment with 10nM rapamycin…p243

Figure 8.1.5 Method A assessment of mES cell confluence following 48h treatment with 100nM rapamycin…p244

Figure 8.1.6 Assessment of the effect of rapamycin on cell area coverage by Method A image analysis…p245

Figure 8.2.1 Analysis of mES cell expansion from triplicate fields of view over 48h by Method A…p248

Figure 8.2.2 Method A analysis of triplicate fields of view describing mES colony expansion over 48h…p249

Figure 8.2.3 The mean number of mES cell colonies measured over 48h by Method A was highly variable…p250

Figure 8.2.4 High variance in the mean area of mES cell colonies over 48h calculated by Method A…p251

Figure 8.2.5 Images of mES cells in culture 4h after seeding analysed by Method A…p253

Figure 8.2.6 Representative images of Method A analysis of mES cells in culture 12h after seeding…p254

Figure 8.3.1 Visual inspection of selected binary mask area from Method A and Method B for analysis of mES cell colony area in phase-contrast images 12h post-seeding…p257

Figure 8.3.2 Comparison between positive threshold analysis (Method A) and dual threshold analysis (Method B) for total cell area measurement from phase-contrast micrographs…p258

Figure 8.3.3 Correlation of total cell area measurements calculated by two methods…p259

Figure 8.3.4 Relationship between total cell area measurements by two methods…p260

Figure 8.4.1 Visual representation of total cell area measurements of mES cells at 24h in culture by Methods A, B and C…p263

Figure 8.4.2 Total cell area measurement by Methods A, B and C…p264

Figure 8.4.3 Cell area measurements by Method C closely align with Method B but not Method A…p265

Figure 8.5.1 Relationship between mean colony size and the total number of colonies by Method A…p267

Figure 8.5.2 Relationship between mean colony size and the total number of colonies by Method B…p268

Figure 8.5.3 Concordance between the mean colony size and total number of mES cell colonies by Method C…p269

Figure 8.6.1 Representative sample library of mES cells for phase distinction…p275

Figure 8.6.2 Representative sample library of mES cells for morphology distinction…p276

Figure 8.6.3 Representative phase-contrast and results images of mES cells after 24h and 48h in culture by Method 2…p277

Figure 8.6.4 Comparison of three computation methods to document mES cell confluence from phase-contrast images over 48h…p278

Figure 8.6.5 The difference between cell area calculations by Method 2 and Methods B and C varies as cell confluence increases…p279

Figure 8.6.6 The relationship between Method 2 and Methods B and C for the analysis of mES cell confluence from phase-contrast images…p280

Figure 8.6.8 Characterisation of mES cell morphology and phase by Method 2 image analysis technique…p281

Figure 8.8 Cytoskeletal α-tubulin and nuclei in spread and compact cells from mES cultures. ..p287

Figure 8.9 Total AKT protein staining in mES cells…p288

List of Abbreviations

7-AAD	7-aminoactinomycin D
AMP	adenosine monophosphate
AMPK	adenosine monophosphate kinase
ATP	adenosine triphospate
bcl-2	B-cell lymphoma
BMP	bone morphogenic protein
BSA	bovine serum albumin
CO_2	carbon dioxide
DAPI	4',6-diamidino-2-phenylindole, dihydrochloride
DMSO	dimethylsulphoxide
DMEM	Dulbecco's modified Eagle's medium
dPBS	Dulbecco's phosphate buffered saline
EC	embryocarcinoma cell
ES	embryonic stem cell
ECL	enhanced chemiluminescence
ERas	ES cell-expressed Ras
EtOH	ethanol
EDTA	ethylenediaminetetraacetic acid
4EBP1	translation initiation factor 4E binding protein
EST	Expression sequence tag
ERK	extracellular signal-regulated kinase
FCS	foetal calf serum
GMEM	Glasgow minimum essential medium
GSK-3	glycogen synthase kinase
GßL	G-protein beta-subunit-like
GPCR	G-protein coupled receptors
GTP	Guanosine-5'-triphosphate
hES	human embryonic stem cell
HM	hydrophobic motif
IgG	immunoglibulin G
IVF	*in vitro* fertilisation
Id	inhibitor of differentiation
ICM	inner cell mass
JAK	janus associated kinase
LIF	leukaemia inhibitory factor
MAPK	mitogen activated protein kinase
MW	molecular weight
MEF	mouse embryonic fibroblast
mES	mouse embryonic stem cell

mTOR	mammalian target of rapamycin
myr	myristolated
OCT 4	octamer binding transcription factor 4
OCT4	octamer-binding transcription factor 4
P70S6K	p70 S6 protein kinase
PTEN	phosphatase and tensin homolog
PI3K	Phosphatidylinositol 3-OH Kinase
PH	plekstrin homology
PDK1	protein dependent kinase
AKT	protein kinase B
PKC	protein kinase C
RIPA	radioimmunoprecipitation assay buffer
rictor	rapamycin insensitive companion of mTOR
Rheb	ras enriched in the brain
RTK	receptor trosine kinase
Rb	retinoblastoma
RNA	ribonucleic acid
S6K	Ribosomal S6 protein kinase
SGK-1	serum glucocorticoid-dependent kinase 1
Sox-2	sex determining region Y-box 2
STAT	signal transducer and activator of transcription
SDS	sodium dodecyl sulfate
TORC1	mTOR complex 1
TORC2	mTOR complex 2

Chapter 1

1.1 Aims of research.

The principle aim of this research was to assess the feasibility of manipulating the mTOR intracellular signalling pathway to provide a bioprocess advantage in the expansion and differentiation of embryonic stem cells.

1.2 Thesis structure.

Chapter 1 provides background information pertinent to the study. This includes a historical perspective and the current understanding of the molecular mechanisms regulating embryonic stem cell biology, with a focus on the mouse embryonic stem cell self-renewal. The mammalian TOR signalling pathway is described in the context of molecular regulation, its role in development and pertinent pathway interactions. Finally, the current understanding of the impact of mTOR signalling on embryonic stem cell biology is reviewed.

Chapter 2 provides details of the methodology utilised for experimental studies Proceeding chapters incorporate the analysis of experimental data and conclude with a summary of findings. Chapter 3 includes preliminary experimental findings relating to pluripotent cell culture conditions and biology. Chapter 4 details a microscopic investigation into distribution and localisation of mTOR phosphoproteins in mouse ES cells.

Chapter 5 documents experimental findings relating to the assessment of mES cell viability and expansion under different in vitro growth conditions.

Chapter 6 incorporates a detailed discussion of research findings within a wider context of the current understanding of mTOR biology. This is followed by a conclusion and description of future studies. References are provided in Chapter 7, and the appendices in Chapter 8 include a methodological approach to develop and characterise image analysis techniques to assess stem cell expansion and morphology from phase contrast micrographs.

1.3 Introduction

Embryonic stem cells (ES) are immortal progenitor cells isolated from the inner cell mass of a developing blastocyst[1]. These cells are pluripotent and can be propagated indefinitely in vitro whilst retaining this potential[2]. Pluripotency is defined by the ability to differentiate into cells of the three primary germ layers; endoderm, ectoderm and mesoderm[3]. Morphologically, ES cells are small and compact with a large nuclear to cytoplasmic ratio. *In vitro*, ES cells form compact colonies and express phenotypic markers associated with pluripotency[4].

Pluripotent cells have great potential as novel *in vitro* platforms for drug discovery and toxicology studies and for future cell-based therapies in clinical medicine[5,6]. Currently there is strong demand for cell-based assays to assist preclinical screening of candidate drug targets from small-molecule libraries. The use of these cell-based assays is desirable as it may facilitate the screening of potential cytotoxic effects of novel compounds.

For the clinical application of cell therapies, material derived from embryonic stem cells must be devoid of pluripotent cells as injection of these cells into recipients can result in benign or malignant teratoma formation[7]. The robust and reliable expansion of stem cells and the generation of uniform populations of differentiated cells will be important for both industrial and clinical applications[8].

1.4 Background

1.4.1 A historical perspective on embryonic stem cell derivation.

The inception of the field of stem cell biology followed the clinical observation that teratocarcinomas consisted of solid tumours containing malignant cells of diverse origins. During the 1950’s these malignancies were thought to occur following metastasis of a primary tumour. However, they are now understood to be a consequence of the malignant transformation of primary germ cells. In 1964, cells cloned from teratocarcinomas led to the hypothesis that the malignant cells may arise from progenitor cells with the capacity to differentiate into derivatives of the three primordial germ layers. Certainly this could explain the diverse tumour ontology observed in teratocarcinoma patients[9].

The first instance of the culture and retention of multipotency in teratocarcinoma cells in vitro occurred in 1967[10], but it was not until 1972 that Martin Evans isolated these embryonal carcinoma cells (EC) from primary teratomas and showed that they had the ability to differentiate into non-malignant progeny[11]. It was hypothesised at the time that this transition was the converse of the malignant transformation of cancer cells. Therefore, these EC cells could serve as a model to investigate ontology and development *in vitro* and would also serve as a system for studying malignancy. Interestingly, the injection of embryonal carcinoma cells into experimental animals resulted in adoptive transfer of teratocarcinoma[12]. However, when these cells were injected into the mouse blastocyst they were incorporated, and normal development ensued[13]. That EC cells were integrated into the viable embryo yet exhibited malignant properties when injected into the adult suggested that they were highly sensitive to their nutritional and structural microenvironment; and have the potential to be reprogrammed by the niche.

The first reports of the derivation of immortal, pluripotent stem cells isolated from the mouse were published by two independent groups in 1981[1,2]. Evans and Kaufman isolated cells by immunosurgical dissection of the inner cell mass (ICM) of the developing blastocyst. Culture of these ICM cells generated clonal lines that could be maintained indefinitely in vitro. These cells were karyotypically normal and morphologically and phenotypically similar to the original EC cells. Injection of these ICM cells into control animals resulted in the formation of teratomas. These neoplasms contained derivatives of the three embryonic germ layers, thus it was confirmed that they were pluripotent. Reimplantation of pluripotent ICM cells into the developing blastocyst resulted in viable chimeric animals. Almost simultaneously, a similar protocol for the derivation of embryonic stem (ES) cells was published by Gail Martin. These ES cells were successfully maintained by co-culture with inactivated fibroblasts and provision of conditioned medium from EC cell cultures. This protocol enabled the ES cells to be maintained in an undifferentiated, pluripotent state over extended passage. Parallels were then drawn between the metabolic requirements of cancer cells and these ES cells. It was this metabolic similarity that enabled the *in vitro* culture of mouse, and later human embryonic stem cells.

The early work to optimise mouse ES cell (mES) expansion has since enabled these lines to be grown as without co-culture with feeder cells. It was found that direct supplementation of mES cells with the growth factor leukaemia inhibitory factor (LIF) maintained the pluripotent phenotype[16,15,16]. Mouse ES cells have since been adapted to passaging by enzymatic treatment.

A major development arising from mouse ES cell research was the ability to generate transgenic animals. This was achieved by the insertion or deletion of genetic elements in ES cells and re-implantation of the donor blastocyst into a pseudopregnant female. Successful incorporation of the modified ES cells into the blastocyst results in chimeric progeny. These chimeric animals are then bred with other heterozygous animals with the same deletion; offspring will then bear the homozygous mutation in accordance with Mendelian patterns of inheritance[17]. This technique has enabled the generation of animal models bearing disease specific modifications and has been invaluable to the study of molecular and cellular biology of disease.

Human ES cells were first derived by JA Thompson in 1998 [18]. The first published hES lines are still in use today and have broadened the scope of cell-based therapies for regenerative medicine. Inactivated feeder cells were necessary to support derivation and the maintenance of pluripotency of hES over extended passage. Human ES cells have since been adapted to feeder-free culture using combinations of extracellular matrix proteins such as found in Matrigel®; which is produced by Kaposi’s sarcoma cells; and conditioned medium from mouse embryonic fibroblasts [19,20]. However, the specific factors that can support and maintain the pluripotent phenotype in hES cells have not been fully characterised. Thus, the successful hES culture is still dependent upon using by-products from complex biological systems.

1.4.2. Leukaemia inhibitory factor signalling in mouse ES cells.

The leukaemia inhibitory factor (LIF) is a pleiotropic cytokine of the interleukin-6 (IL-6) family that binds to the gp-130 cell surface receptor[21]. Ligand binding induces gp-130 dimerisation with the IL-6 receptor (IL-6R) and stimulates signal transduction cascades[22]. The binding of LIF to gp-130 receptor complexes drives the phosphorylation of the membrane localised janus-associated kinase proteins (JAKs). These tyrosine kinases then directly phosphorylate members of the signal transducer and activator of transcription pathway (STAT). Phosphorylation of Stat1 or Stat3 results in the formation of hetero- and homodimers that shuttle to the nucleus[26]. The binding of STAT dimers to DNA subsequently initiates gene transcription events[27]. Thus STAT pathway components transduce signals derived from extracellular factors to initiate cellular responses at the transcriptional level. The actions of LIF however are not limited to JAK/STAT pathway activation. It is widely accepted that LIF signalling also activates the phosphotidylinositide 3-kinase (PI3K) and mitogen activated kinase pathways (MAPK).

1.4.3. The regulation of pluripotency in mouse ES cells by leukaemia inhibitory factor.

In mouse ES cells, LIF signalling promotes pluripotent self-renewal. Consequently, the downstream actions of LIF have been studied to identify factors that may regulate the pluripotent state. The ligation of gp-130/IL-6R induces the phosphorylation and dimerisation of Stat3, and nuclear localisation of phospho-Stat3 dimers promotes mouse ES cell self renewal[25]. Consequently Stat3 was understood to be a core component of the pluripotency network in mES cells. Indeed, a fusion protein containing the coding region of Stat3 was demonstrated to maintain pluripotency independently of LIF[26]. However, mouse ES cell self-renewal is not exclusively dependent upon Stat3 activation as it has since been proven to be dispensable for the maintenance of pluripotency[27]. Although Stat3 was considered a major factor driving mouse ES cell self-renewal it is not the principle mediator of the pluripotent phenotype maintained by LIF.

Figure 1.4.1

LIF-mediated activation of JAK/STAT pathway in mouse ES cells [28]

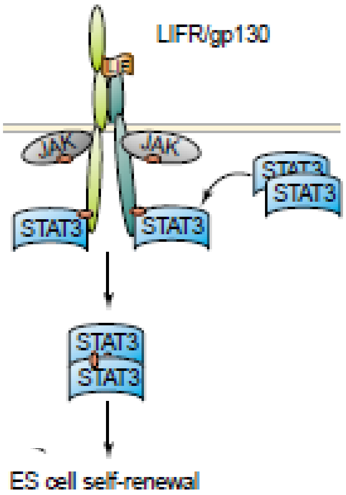

The c-myc proto-oncogene is induced downstream of Stat3. Removal of LIF from mES growth medium results in downregulation of c-myc protein and transcript levels. Expression of constitutively active c-myc supports pluripotent self-renewal independently of LIF/Stat3. Additionally, dominant negative c-myc mutant mES cells spontaneously differentiate in the presence of LIF[27]. Therefore c-myc supports self-renewal and inhibits the differentiation of mES cells and is the principle mediator of LIF-mediated pluripotency.

As LIF stimulates the PI3K pathway, the importance of this signal transduction cascade in mouse ES cell biology has been extensively studied. The PI3K pathway mediates an array of cellular responses including survival, cell cycle progression, motility and proliferation[29,30,31]. Ligation of cell surface receptors including receptor tyrosine kinases (RTK), G-protein coupled receptors (GPCR) by growth factors or insulin stimulates the phosphorylation of membrane phospholipids by PI3K. Membrane localised phosphoinositides are phosphorylated at the 3'OH ring by PI3K.

Activation of PI3K signalling pathway initiates a signal transduction cascade involving the protein dependent kinase-1 (PDK1) mediated phosphorylation of protein kinase-B (AKT). The downstream biological effects of PI3K signalling is orchestrated by AKT. The plekstrin homology domain (PH) of AKT elicits recruitment to the plasma membrane where it is binds PIP_3 and interacts with PDK1. This kinase then phosphorylates AKT at threonine residue 308 (th308). The actions of PDK1 are inhibited by the tumour suppressor PTEN. Genetic mutations at the PTEN locus are implicated in the pathogenesis of numerous site-specific cancers and myeloproliferative diseases[31,32]. Conditional knockout of the PTEN gene results in embryonic lethality and mouse ES cells derived from PTEN $^{-/+}$ blastocysts exhibit increased tumourogenic potential. This arises from the loss of anchorage-dependent growth inhibition, thus PTEN null ($^{-/-}$) ES cells exhibit aberrant differentiation potential[33]. It was therefore concluded that PTEN is essential for normal development, and the impaired regulation of PI3K signalling upon loss of PTEN promotes the proliferative phenotype that is a hallmark of cancer.

Figure 1.4.2

Activation of AKT and PI3K-mediated phosphorylation of PIP_2. [35]

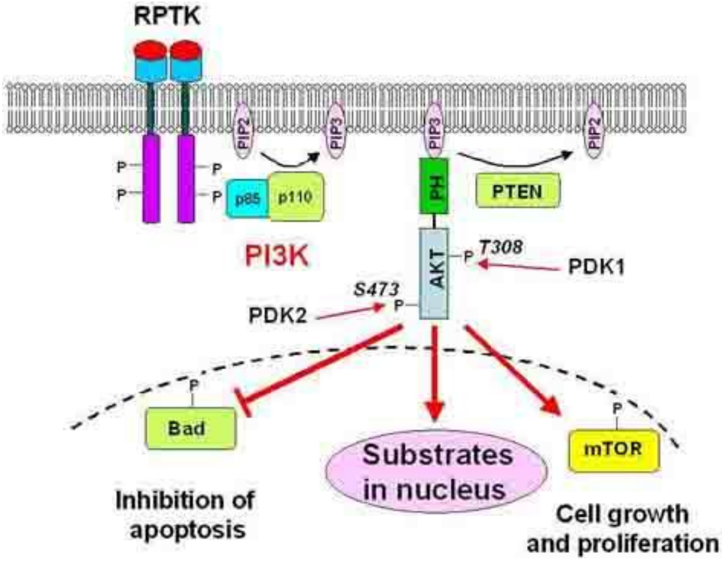
RPTK
PIP2
PIP3
PIP3
PIP2
P
P
P
P
p85
p110
PI3K
PH
PTEN
AKT
P
T308
PDK1
S473
P
PDK2
P
Bad
Substrates in nucleus
P
mTOR
Inhibition of apoptosis
Cell growth and proliferation

Figure 1.4.2 documents the key interactions resulting in AKT phosphorylation at th308 by PDK1. The phosphorylation of AKT at the serine-473 residue (ser473) by the protein dependent kinase-2 (PDK2) will be discussed in later sections. Activation of AKT via the PI3K pathway promotes mES proliferation, survival and self-renewal. In mouse ES cells the inhibition of AKT results in cellular differentiation. The pluripotent phenotype is rescued by expression of constitutively active myristolated AKT (myr-AKT). Thus myr-AKT-mES cells maintain pluripotent self renewal in the absence of LIF. This highlights the importance of the PI3K-AKT pathway in the LIF-dependent maintenance of pluripotency in mES cells[36], however this pathway operates upstream of c-myc.

In 2005, Takahashi, Murakami and Yamanaka documented the role of the PI3K pathway in the tumourogenic potential of mouse ES cells. Prior analysis of the mouse expression sequence tag database (EST) led to the identification of the ES cell-expressed Ras (ERas) in ES cells but not in differentiated cells. Near constitutive activation of ERas was observed in pluripotent cells. The expression of ERas in NIH3T3 fibroblasts induced malignant transformation and led to tumour formation when injected into adult mice. Additionally, ERas expression induced the proliferation of mouse embryonic fibroblasts. As ERas was a potent PI3K pathway agonist it was speculated that the tumourogenic properties of mES cells may be driven by the ERas-PI3K axis. However, injection of ERas-null ES cells into mouse blastocysts resulted in the generation of developmentally normal chimeric mice. While ERas did not therefore regulate pluripotency in mouse ES cells, it did appear to promote proliferation and tumorigenicity. While ERas-null ES cells retained their teratogenic potential, teratomas were smaller in size. Additional pathway interactions were speculated to regulate the ERas/PI3K mediated teratogenic potential of mouse ES cells[37]. It is now understood that this effect is mediated by downstream signalling via the mTOR pathway.

Leukaemia inhibitory factor signalling also stimulates the mitogen activated kinase pathway (MAPK) pathway leading to phosphorylation of ERK1 and ERK2. Phospho-ERK promotes cell proliferation and has been strongly associated with the differentiation of mouse embryonic stem cells[38]. Inhibition of ERK phosphorylation or the upstream kinase promotes mouse ES cell self-renewal by potentiating the actions of Stat3[41]. It was postulated that the LIF/Stat3 pathway dominates cell fate in mouse ES cells, upon removal of LIF, the ERK pathway gains prominence and differentiation is induced[28]. The inclusion of serum in mES culture medium supports the LIF-mediated maintenance of pluripotency by inhibiting the downstream consequences of ERK phosphorylation. This has been shown to involve the actions of a class of compounds entitled the inhibitor of differentiation (Id) proteins arising from the bone-morphogenic protein (BMP) signalling pathway[40].

1.4.4 The core network regulating pluripotency in mouse ES cells.

The transcription factors octamer-binding transcription factor-4 (OCT4) and the homeobox protein Nanog have been implicated as major regulators of the pluripotent phenotype[41,42,43]. Constitutive expression of Nanog was considered to be a hallmark of stem cell pluripotency[46], and genetic mutation of the Nanog gene results in lethality early in development[43]. Investigations into the levels of the Nanog in mouse ES cells revealed fluctuations in expression levels that may act as discrete windows whereby stem cells are prone to differentiate in response to environmental signals[47]. It has been postulated that Nanog acts as a negative regulator of differentiation especially toward the endodermal and mesodermal lineages by promoting pluripotent self renewal.

The transcription factor OCT4 is first detected at the 4 cell stage of mouse development and has been shown to be closely associated with pluripotency both *in vivo* and *in vitro* [42, 43]. The expression of OCT4 diminishes as cells differentiate, and somatic cells can be reprogrammed to display the pluripotent phenotype by transfection with OCT4 mRNA and at least one other transcription factor[46]. These findings provide the strongest case for the OCT4-mediated regulation of the pluripotency network. The observation that OCT4 is detected in some adult cancers may be support the ‘cancer stem cell’ hypothesis, whereby undifferentiated stem-like cells act as cellular drivers of neoplasia.

The transcription factor Sox2 is key factor in the core network regulating pluripotency. Inhibition of Sox2 by RNA interference induces the differentiation of mouse ES cells[47]. Both OCT4 and Sox2 have been shown to bind to the Nanog promoter to enhance transcription[48], and cooperate to maintain the pluripotent state.

1.4.5 The ground state of embryonic stem cell self-renewal.

Austin Smith and colleagues have extensively documented the molecular regulation of mouse ES pluripotency in response to LIF stimulation. It was found that ERK inhibition is essential to maintain pluripotency in mouse ES cells. Additionally inhibition of the PI3K/AKT pathway results in accumulation of glycogen synthase kinase-3 (GSK3) in the nucleus. The kinase activity of AKT antagonises the function of GSK3 by phosphorylating specific threonine and serine residues. Phosphorylation of GSK3 by AKT is important for the maintenance of mouse ES cell pluripotency. Extrapolating these findings, Smith *et al* proved that mouse ES cell self-renewal could be maintained by the combined inhibition of GSK3 and ERK phosphorylation with small molecule inhibitors. Thus, pluripotent self renewal can be maintained by inhibiting intrinsic differentiation signals rather than providing extrinsic growth factors to promote pluripotency. That Stat3-null cells proliferate under these conditions implies that mouse ES cells have an innate capacity for self-renewal. It was postulated that it is this innate capacity that underpins tumorigenic potential. This concept was termed the ‘ground state of embryonic self renewal’[49, 50].

Figure 1.4.3

The regulation of stem cell pluripotency in the mouse [51].

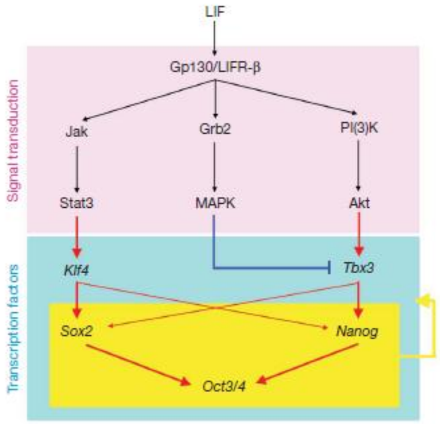

1.4.6 Cell cycle regulation in mouse ES cells.

The mammalian cell cycle is regulated by proteins and protein kinases of the cyclin and cyclin-dependent kinase (cdk) family. In somatic cells and differentiated stem cells a series of interactions regulates progression from the G_0/G_1 phase to the DNA synthesis (S) phase, and G_2 to mitosis (M) phase. A major checkpoint of the cell cycle occurs during G_1-S transition. For progression through this checkpoint cyclin-D is necessary to induce retinoblastoma protein (Rb) phosphorylation. This results in the release of the E2F transcription factor and subsequent cyclin-E activation. Cyclin-E then is free to induce the transcription of S-phase genes necessary for DNA synthesis.

In pluripotent embryonic stem cells this G_1 checkpoint is compromised as Rb protein is hyperphosphorylated and cells transit rapidly through the G_1 phase. The length of the G_1 phase is reported to be approximately 1 to 1.5 hrs in these ES cells[28]. Interestingly, it has been documented that mES cells are refractory to cell cycle inhibition upon deletion of regulatory proteins involved in G_1-S transition. When cellular differentiation proceeds following LIF withdrawal, Rb checkpoint control is then acquired. The proto-oncogene c-myc appears to be directly involved in the production of S-phase genes via activation of cyclin-E, and Stat3 may also act directly upon cell cycle regulators to promote S-phase transition. Thus LIF-mediated induction of Stat3/c-myc may supersede the Rb checkpoint at G_1 of the cell cycle. Activation of the PI3K pathway downstream of LIF also induces cyclin-D expression and activation, thereby promoting the transition through the G_1 phase of the cell cycle in mES cells.

1.5 The mammalian target of rapamycin pathway.

1.5.1 The discovery of metazoan and mammalian TOR.

The mammalian target of rapamycin (mTOR) is a highly conserved serine/threonine protein kinase that links the availability of extracellular nutrients to key checkpoints of cell growth and proliferation, cytoskeletal commitment and autophagy. The discovery of rapamycin followed observations of the inhibitory effects of the soil bacterium Streptomyces hygroscopicus on the growth of *Candida albicans* and other fungi. Canadian researchers isolated the organism responsible and purified the active compound. It was termed rapamycin after Rapa Nui, the indigenous name for Easter Island where the samples were first obtained [52].

Rapamycin binds to the highly conserved 12kb molecule FKBP12 and inhibits the action of an associated protein. The identification of two TOR genes was reported in 1993 following drug resistance screening of the yeast *Saccharomyces cerevisaie*[53]. Disruption of the TOR2 gene was lethal, whereas rapamycin treatment induced cell cycle arrest at the G_1 phase[54]. The mammalian orthologue of the yeast TOR gene was cloned a year later by three independent groups[55,56,57]. Mammalian TOR is transcribed from a single locus and is structurally similar to metazoan TOR. The mammalian TOR protein was observed to have close homology with PI3K.

Upstream regulators of mTOR include amino acids, growth factors, insulin, energy availability, hypoxia and reactive oxygen species. Of note is the sensitivity of mTOR signalling to the bioavailability of the branched-chain amino acid leucine[58].

1.5.2 The rapamycin sensitive mTOR complex (TORC1).

Mammalian TOR is a high molecular weight protein (290 kDa) and has a number of highly conserved domains with catalytic activity. The N-terminus contains tandem repeat domains that are implicated in protein interactions while the C-terminus retains the kinase activity. The structure of mTOR is represented below.

Figure 1.5.1

Functional structure of mammalian TOR protein [59]

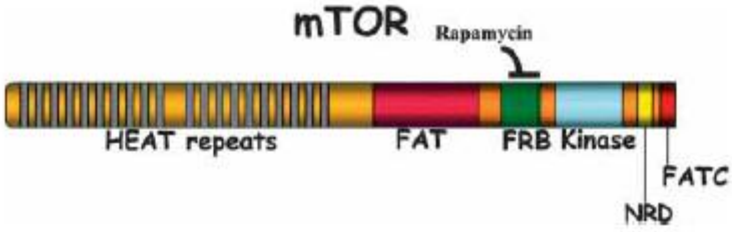

Mammalian TOR forms two distinct heteromeric complexes, TORC1 and TORC2. The TORC1 complex consists of mTOR bound to the protein raptor[60]. Additional subunits of the complex include GβL (LST8) [61], and PRAS40 [62]. The activity of the TORC1-raptor complex is sensitive to nutrients and growth factors, kinase activity is dependent upon the formation of this stable complex[63 64].

The TORC1 kinase phosphorylates p70S6-kinase (p70S6K) and the eukaryotic translation initiation factor 4E binding protein 1 (4EBP1). These substrates regulate protein translation. The mechanisms of the regulation of protein translation downstream of mTOR have been relatively well characterised. Phosphorylation of the mRNA translation repressor 4EBP1 leads to its inactivation and liberates the eIF4E translation initiation factor from an inhibitory complex with 4EBP1. This promotes translation initiation and the production of new proteins. The detection of phosphorylation of distinct sites on these two proteins acts as a reporter of the mTOR/raptor complex activity[65,66]. Of particular significance is the phosphorylation of the threonine 389 residue of p70S6K by TORC1[67].

1.5.3 The mTOR complex-1 in the regulation cell size.

Rapamycin treatment results in a reduction in cell size in proliferating cells. Dividing cells must double their mass at each round of division, proliferation and cell growth are closely regulated to match metabolic processes to nutrient availability. Cell growth occurs predominantly in the G_1 phase of the cell cycle, occurring after cell division, although protein translation is necessary in the G_2 phase prior to mitosis. The TORC1 mediated effectors of cell growth are p70S6K and 4EBP1, together they induce protein translation and ribosome biogenesis. Inhibition of TORC1 reduces cell size, and a rapamycin-resistant mutant of mTOR ablated this cell size defect, the S6K mutant only partially rescued this size-defective phenotype[68]. However, the rapamycin mediated effects on cell size and proliferation in yeast are separable. Changing nutrient provision from a nitrogen-rich to nitrogen-poor source results in continued cell division at the expense of cell growth. Inhibition of cell proliferation does not affect cell size, whereas cells deprived of nutrients continue to progress through the cell cycle, progeny are of a smaller size[69].

Figure 1.5.2

Key outputs of mTOR mediating cell growth[70]

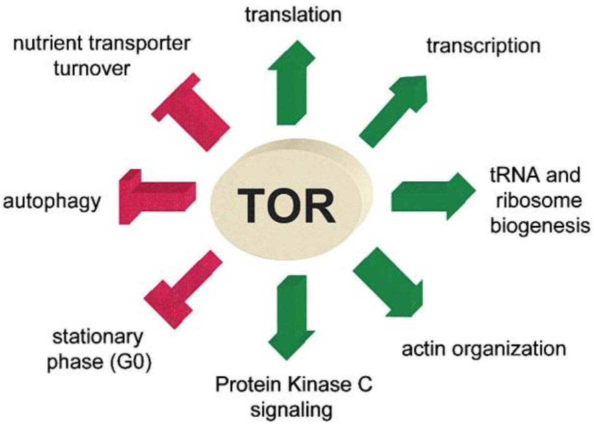
translation
nutrient transporter turnover
transcription
autophagy
TOR
tRNA and ribosome biogenesis
stationary phase (G0)
actin organization
Protein Kinase C signaling

1.5.4 The rapamycin insensitive mTOR complex (mTORC2).

The formation of the mTOR-raptor complex is inhibited by rapamycin; however mTOR also forms an additional heteromeric complex that competes for free mTOR protein. In budding yeast cells, two TOR genes form independent complexes transcribed from different genes Tor1 and Tor2 [64]. In the mammalian system, only one TOR homologue was identified. However, as mTOR was shown to exhibit rapamycin insensitive functions, it was postulated that two independent TOR complexes might exist in the mammalian system. Jacinto and colleagues demonstrated that mammalian TOR did indeed form two functional protein complexes[71]. A second binding partner was identified and termed 'rapamycin insensitive companion of mTOR' (rictor)[72]. It is now known that the mTOR complex-2 contains mTOR, rictor, sin1 [73], protor[74], PRR5[75] and LST8[76].

The mTOR complex-2 exhibits discrete kinase activity from mTORC1. The first substrate for mTORC2 was identified as the serine-473 residue in the hydrophobic loop of AKT[77]. Other substrates have been identified, namely the serum- and glucocorticoid-dependent kinase-1 (SGK1) and Protein Kinase C-α (PKC-α)[78,79]. Reports indicate that TORC2 may signal to the cytoskeleton, inducing actin polymerization and cell spreading[71,72]. Knockdown of rictor in mouse blastocysts results in growth arrest at E9.5 and death by E11.5. This is in contrast to the homozygous mTOR kinase-dead mutant whereby embryonic lethality occurs at E6.5 [80]. It appears that intact TORC2 signalling is necessary for midgestation whereas TORC1 is required for early development. Interestingly mTORC2 is necessary for the adoptive transfer of prostate cancer in PTEN null mice. This implies an unrecognised role for TORC2 in cellular proliferation[81].

Figure 1.5.3

Kinase substrates of TORC2[82].

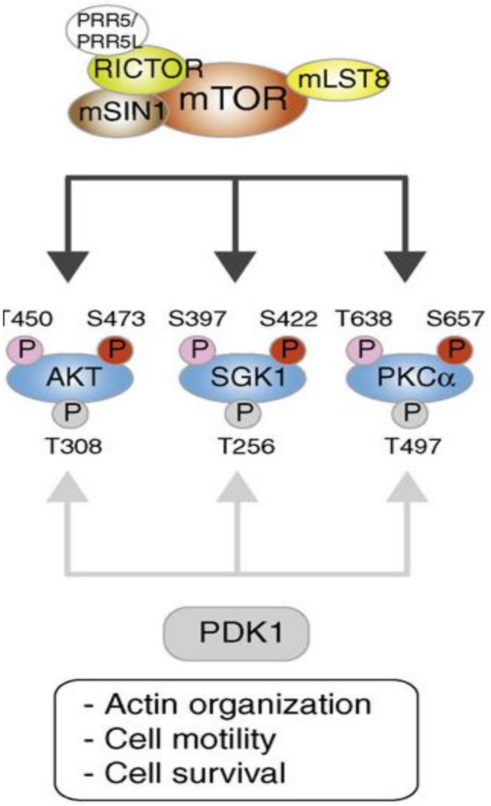
PRR5/
PRR5L
RICTOR
mSIN1
mTOR
mLST8
450
S473
S397
S422
T638
S657
P
AKT
SGK1
PKCα
T308
T256
T497
PDK1
- Actin organization
- Cell motility
- Cell survival

The protein kinase A/G/C family proteins (AGC) share common mechanisms of activation involving phosphorylation at the T-loop motif by PDK1 and the hydrophobic motif (HM). Full activation of AGC kinases depends upon these two modifications. Phosphorylation of the turn motif (TM) by TORC2 may stabilise newly synthesised protein and prevent proteosomal degradation.

1.5.5 Upstream regulation of mTOR signalling.

The tuberous sclerosis complex (TSC) is a key regulator of mTOR activation. Benign tumours called harmatomas arise from mutations in the TSC genes[83]. These neoplasms result from the impaired negative regulation of mTOR signalling. Two TSC proteins form a complex that ultimately inhibits mTOR via the GTPase Rheb (ras enriched in the brain). Phosphorylation of TSC2 by PI3K or MAPK related kinases release Rheb, and activate mTOR[84,85,86]. The TSC complex is known to regulate TORC2 activation as mutations in the TSC genes impairs the TORC2 mediated phosphorylation of AKT in some cell types[87].

1.5.6 Interactions between the mTOR and PI3K pathway.

Mammalian TOR signalling is closely integrated with the phosphoinositide kinase (PI3K) pathway. The interaction between AKT and mTOR is complex and multifaceted involving both upstream and downstream regulation. A substrate of the AKT kinase includes the tuberous sclerosis complex molecule TSC2. The AKT mediated phosphorylation of TSC2 results in disruption of TSC1/TSC2 complex and releases the inhibition of TORC1 via the GDP exchange factor Rheb[62]. Thus PI3K/AKT potentiates mTOR signalling. Downstream interactions involve the mTOR complex-2. Phosphorylation of the serine-473 residue of AKT by TORC2 results in full activation of AKT. It has been documented that the serine-473 phosphorylation induces a conformational change exposing the PH-membrane localisation sequence. This brings AKT into contact with PDK1 at the plasma membrane and elicits phosphorylation of the threonine-308 residue[88]. Mammalian TOR also regulates its own activity through a feedback mechanism involving PI3K. High levels of phospho-p70S6K, resulting from TORC1 activation, inhibits PDK1-mediated phosphorylation of AKT. This mechanism process occurs at the cell membrane via the insulin-response unit, IRS-1. This feedback inhibition may serve to prevent unregulated cell growth and proliferation in response to mTOR over-activation[89].

Figure 1.5.4

Pathway map of key TORC1 interactions[90].

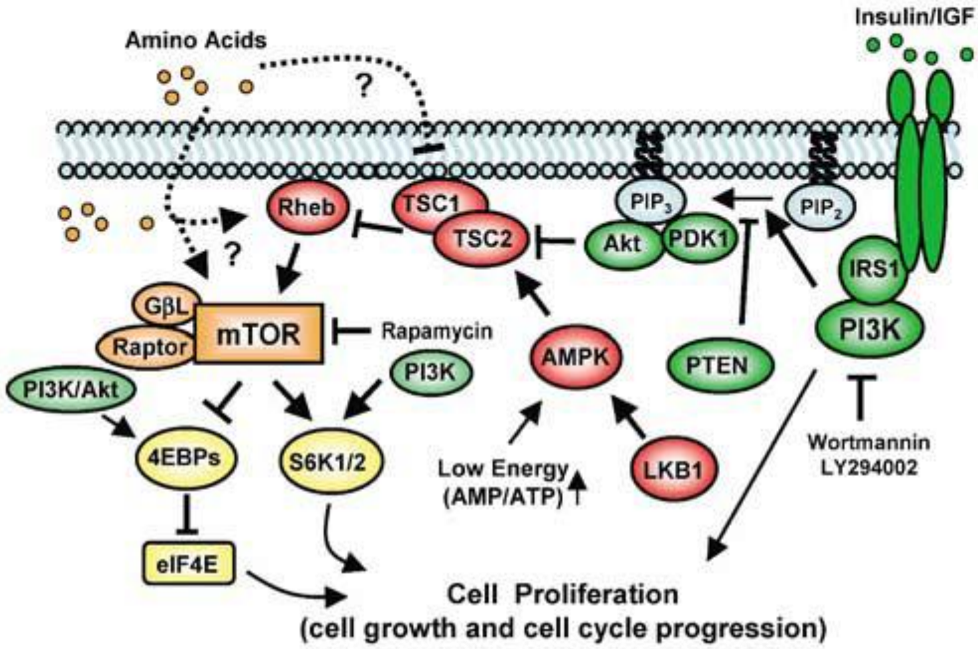
Amino Acids
?
Insulin/IGF
?
Rheb
TSC1
TSC2
PIP3
Akt
PDK1
PIP2
IRS1
PI3K
GβL
Raptor
mTOR
Rapamycin
PI3K
PI3K/Akt
AMPK
PTEN
4EBPs
S6K1/2
Low Energy
(AMP/ATP)
LKB1
Wortmannin
LY294002
eIF4E
Cell Proliferation
(cell growth and cell cycle progression)

1.5.7 The mTOR/PI3K pathways regulate cellular metabolism in response to nutrient availability.

The mammalian TOR pathway is known to regulate cellular survival under conditions of nutritional stress. Depletion of key nutrients such as branched-chain amino acids[91,92], glucose and oxygen results in the inactivation of mTOR. The regulation of these processes may however depend upon cell type and microenvironmental conditions.

Branched-chain amino acids such as leucine are known agonists of mTOR activation and protein translation. It has been widely reported that amino acid availability stimulates protein production in skeletal muscle[93], adipose tissue[58] and myoblasts[94]. The effect of amino-acid availability on protein translation is not restricted only to these cells types. Indeed the converse may be true and mTOR signalling appears to provide a fundamental checkpoint in cell growth control in response to nutrient availability. This is exemplified by pathological nutrient restriction during development. During intrauterine growth restriction, the transport of amino-acids via the expression of A- and L-type amino acid receptors is impaired resulting in reduced placental nutrient transport. The mTOR pathway is implicated in the regulation of placental nutrient sensing as impaired mTOR signalling reduces foetal growth[95]. Insulin is increases growth via the upregulation of nutrient transporter expression, an effect that is impaired by AKT deletion[96]. The B0+ amino acid transporter system regulates the uptake of branched-chain amino acids and affects both blastocyst implantation and differentiation by an mTOR mediated mechanism[97, 98].

Energy stress is also a modulator of the mTOR pathway. The adenosine monophosphate kinase (AMPK) regulates cellular metabolism in response to glucose availability. This kinase becomes activated when cellular ATP is depleted and the ratio of AMP to ATP rises. The level of ATP correlates directly with glucose bio-availability. Consequently, AMPK slows cell metabolism and inhibits proliferation by activating repressor proteins upstream of the mTOR pathway. Adenosine monophosphate protein kinase activity inhibits mTOR activation via the TSC complex[99]. And phosphorylation of raptor by AMPK impairs TORC1 complex formation and activity[100]. High levels of glucose have been documented to have a positive effect on embryonic stem cell proliferation via an increase in AKT signalling[101]. Therefore, high glucose stimulates proliferation through the PI3K and mTOR pathways whereas low glucose inhibits proliferation by inactivating the mTOR/raptor pathway.

Inhibition of mTOR also results in the stimulation autophagy, an intracellular catabolic process involving lysosomal degradation and recycling of cellular material. Recent research has shed light on the molecular mechanism of the mTOR-mediated induction of autophagy[102]. The restriction of nutrients inhibits mTOR activation which in turn induces autophagy. This mechanism enables cells to regulate their metabolism in dynamic equilibrium with the availability of nutrients.

1.5.8 Substrates of AKT promote cell survival.

Many substrates of the AKT serine/threonine kinase have been identified. These substrates are broadly categorised as type1 or type2. Type 1A substrates become activated following phosphorylation by AKT whereas type 1B phosphorylations are predominantly inhibitory. The type2 substrate interactions involve serine/threonine phosphorylations that promote binding to 14-3-3 proteins[103]. Binding of intracellular proteins to 14-3-3 commonly results in degradation or dephosphorylation of the substrate and therefore represents a major regulatory system to limit signal transduction pathway activation. One such interaction involves the Bcl-2 mediated inhibition of apoptosis. The phosphorylation of the BAD protein by AKT promotes its binding to 14-3-3 and consequently inhibits this association with Bcl-2. Unbound Bcl-2 is anti-apoptotic and promotes cell survival following AKT activation[104] .

Figure 1.5.5

Mechanisms of cell survival mediated by AKT[105].

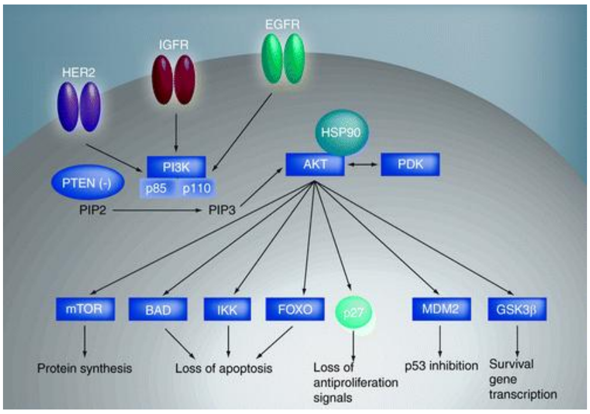
EGFR
IGFR
HER2
HSP90
PI3K
AKT
PDK
PTEN (-)
p85
p110
PIP2
PIP3
mTOR
BAD
IKK
FOXO
p27
MDM2
GSK3β
Protein synthesis
Loss of apoptosis
Loss of antiproliferation signals
p53 inhibition
Survival gene transcription

1.5.9 The mammalian TOR pathway during development.

The mammalian target of rapamycin (mTOR) signalling pathway has been implicated as a regulator of cell growth and proliferation in response to nutrient availability. In 2004, two publications independently assessed the effect of mTOR inactivation or depletion on embryonic development in the mouse[106] [107]. The first study published by Murikami and colleagues documented the levels of mTOR protein in developing and adult mouse tissues. Relatively high levels of protein were identified in mouse ES cells compared with many adult tissues. Genetic disruption of the kinase domain of mTOR by homozygous recombination impaired proliferation of both embryonic and extra-embryonic tissues and resulted in embryonic lethality. Embryonic stem cells derived from the inner cell mass of homozygous mutant blastocysts failed to proliferate in vitro. Utilising a conditional deletion approach to target mTOR, homozygous mutant ES clones (mTOR $^{flox/flox}$) were tested for their ability to proliferate in vitro. Interestingly, the severe reduction in the proliferative capacity of these ES mutant cells was not seen with rapamycin treatment alone. Although rapamycin did reduce cell proliferation it was clear that the role of mTOR in ES cell proliferation extended beyond the rapamycin sensitive effects. Additionally, the ERas-null phenotype described by Takahashi and colleagues resembles that of mTOR deficient ES cells. It was therefore speculated that the teratogenic potential of mouse ES cells may be driven by the mTOR pathway.

The second study by Gangloff *et al* demonstrated that heterozygous mutation of the mTOR gene resulted in reduced mTOR protein levels and phosphorylation of the mTORC1 substrate p70S6K in embryonic fibroblasts. However no phenotypic traits were observed and cell size and cell cycle transit were not affected. Homozygous mutation resulted in severe phenotypic abnormalities and embryonic lethality at E5.5. Embryonic stem cells could not be derived from these homozygous mTOR mutant blastocysts[107]. It has been postulated that developmental arrest at this time is due to impaired blastocyst implantation. This is consistent with the observations that rapamycin treatment impairs trophoblast outgrowth, which occurs at E4.5 in the mouse[98], and that amino acid deprivation impairs blastocyst implantation and outgrowth in vivo[108]. Interestingly, Gangloff *et al* observed that cell cycle transit was not impaired in preimplantation blastocysts. This may relate to the low requirement for amino acid uptake at this stage of development, and the increase in amino acid dependency at implantation when embryo size begins to increase rapidly[109]. Loss-of function mutations in the mTOR gene inhibit proliferation and embryonic development in the mouse, however, cell size was not affected in these flat-top mutants[110].

In human ES cells, mTOR was found to be important for the maintenance of pluripotent self-renewal. Inhibition of mTOR resulted in loss of pluripotency and a tendency towards the formation of endoderm and mesoderm lineage specification. Interestingly, in mouse ES cells, this effect was not observed and mTOR inhibition had no effect on pluripotent marker expression or self-renewal. Colony size was reduced indicating that mTOR is important for mES cell proliferation but not pluirpotency. The compact morphology of pluripotent mES cells was also maintained[111].

The mTOR/PI3K axis is strongly associated with cell proliferation and survival in mouse and human ES cells. Genetic mutations in components of the mTOR and PI3K pathways result in embryonic lethality. Excessive PI3K activation drives rapid cell cycling, and the loss of regulation of PI3K/AKT promotes cell survival. Of particular interest to this investigation is the finding that the depletion of serum results in PI3K/mTOR pathway activation, an effect that is postulated to provide a survival advantage under conditions of nutritional depletion[112]. The role of the mTOR complex-2 is not well understood in ES cells or somatic cells. There is evidence implicating TORC2 in cytoskeletal commitment and polarity, and there is a body of evidence to suggest that mTORC2 may play a role in the regulation of cellular proliferation.

Table 1.1. Summary of key signalling events in mES cells.

Agonist	Target	Downstream	Effector	Outcome in mES cells
LIF	gp130/LIFR	PI3K STAT3 MAPK	p-AKT (th308) p-STAT3 dimer p-ERK 1/2	Survival, proliferation Self-renewal Differentiation
Leucine	Unknown	mTORC1	p-S6K (th389) p-4EBP1	Protein translation/cell growth Translation initiation/cell growth
Unknown	mTORC2	AKT	p-AKT (ser473)	Unknown

In summary, mTOR is at a nexus of intracellular signalling pathways that regulate cell growth, cell cycle progression, survival and proliferation in response to the availability of nutrients and growth factors. The impact of the mTOR pathway on the behaviour of mES cells has not been fully characterised and the role of the mTORC2 complex in mammalian cells is poorly understood.

1.5.10 Manipulation of the mTOR pathway as a bioprocessing tool for the enhanced expansion and differentiation of ES cells.

Embryonic stem cells are currently attracting great interest as a potential source of cellular material for novel regenerative medicines. Currently the first ES cell based therapies are undergoing clinical trials for macular degeneration. Furthermore, industrial application of stem cell technologies is centred upon developing cell-based assay systems for toxicology testing in pre-clinical drug discovery and validation programmes.

Critical to the success of ES cell therapies is the development of robust protocols to generated pure population of target cells. As the injection of pluripotent cells into recipients may result in teratoma formation it is critical to ensure that final cell preparations are devoid of contaminating parent cells. The use of ES cells in pre-clinical screening programmes also necessitates high levels of purity and reproducibility. Consequently, there is demand for bioprocess improvements that are cost-effective at an industrial scale. Manipulation of the mTOR pathway has not been previously considered as a route to bioprocess optimisation however this pathway is an ideal candidate as it is central to the regulation of cellular growth and proliferation. Whereas cell proliferation rate is relevant to cell expansion, cell growth is an important biological process during cellular differentiation. Furthermore, the mTOR pathway is sensitive to the bioavailability of glucose and branched-chain amino acids such as leucine. As amino acids are relatively cheap to produce compared with recombinant proteins, the mTOR pathway offers a unique opportunity for the cost-effective manipulation of ES cell fate at an industrial scale.

1.6 Research question

Does the mTOR pathway offer a route to bioprocess optimisation during the expansion and differentiation of embryonic stem cells?

1.7 Objectives

The principle objective of this research is to characterise mTOR pathway signalling in a model pluripotent stem cell system.

Secondly to advance the understanding of the role of the two mTOR complexes in the proliferation of embryonic stem cells.

Finally to assess the impact of manipulating the mTOR pathway on the expansion and early differentiation of embryonic stem cells.

Chapter 2

Experimental Methods

2.1 Expansion and culture of mouse embryonic fibroblasts.

Primary mouse embryonic fibroblasts (MEF) at passage 1 were thawed in a water bath and seeded into T-75 tissue-culture flasks (Nunc; Stafford, UK) with Dulbecco’s modified Eagle’s medium (DMEM), (4500mg/ml glucose; Lonza-Bio-Whittaker*;* Wokingham, UK) supplemented with L-glutamine and 10% foetal calf serum (FCS), (both Gibco Invitrogen; Paisley, UK*)*. Cells were cultured until confluence and split (1:10 ratio) by enzymatic detachment (0.25% trypsin/EDTA; Gibco-Invitrogen) and grown until passage 5. Every 2 weeks confluent MEFs were mitotically inactivated by treatment for 2hr with mitomycin-C (1mg/ml, Sigma-Aldrich, Poole, UK). Flasks were washed with dPBS and cells detached with 0.1% (w/v) trypsin (both Sigma-Aldrich) at 37 ºC. After 5min incubation, enzyme was neutralised with growth medium (DMEM) containing 10% FCS, detached cells were centrifuged for 3min at 280g and seeded at a density of 4000 cells/T-25 flask or 1000 cells/IVF dish. Fresh inactivated feeders were then sustained for 2 weeks to support human embryonic stem cell growth. Inactivated feeders were also cryopreserved in 90% FCS containing 10% dimethylsulphoxide (DMSO; Sigma-Aldrich) and stored at -80 ºC. When needed cryopreserved cells were thawed and seeded at a density of 7000 cells/T25 flask.

2.2 Culture of human embryonic stem cells

Human Shef3 embryonic stem cells (UK Stem Cell Bank) were maintained on primary inactivated mouse embryonic fibroblasts (MEFs) and cultured upon 0.1% gelatin (Sigma-Aldrich) coated T-25 flasks or IVF culture dishes (Nunc) in a humidified atmosphere at 37 ºC, 5% CO_2. Human Shef3 cultures were cut by surgical microdissection under a microscope with a heated glass element in the presence of collagenase (0.025mg/ml. Invitrogen) for 3 minutes at 37℃. Cell suspensions were collected in 2ml DMEM containing 100mM ß- mercaptoethanol, 1mM L-glutamine, 1% (v/v) non-essential amino acids (all Sigma) and seeded into tissue culture flasks containing adherent inactivated MEFs. Colonies were passaged every 3-4 days during expansion.

2.3 Culture of human embryonic carcinoma cells

Cryopreserved embryonic carcinoma cells N-Tera2 were rapidly thawed at 37ºC and diluted with 9mls of warmed DMEM containing 10% foetal calf serum (FCS) and centrifuged for 3min at 280xg. The cell pellet was resuspended in 5mls of growth medium, placed into 25cm^2 tissue culture treated flasks (T-25, Nunc) and cultured in a humidified environment containing 5% CO_2 at 37°C. Confluence was determined by visual inspection under light microscopy. Cultures were manually passaged by mechanical dissociation using sterile 5mm glass beads. The monolayer of cells was first washed with fresh growth medium and then broken into clumps by the addition of approximately 15-20 glass beads in 4mls of medium followed by a gentle shaking of the flask for 20-30 seconds. Detachment was assessed by microscopy and the cell suspension removed and reseeded into tissue culture flasks at a ratio of 1:2 for confluence within 2 days or 1:3 for confluence within 3 days.

2.4 Culture of mouse embryonic stem cells.

Mouse embryonic stem cells clone E14-Tga2 were cultured at 37 ºC and 5% CO_2 in a humidified atmosphere for 2 days with Glasgow modified eagle's medium (GMEM) supplemented with sodium pyruvate, 1mM L-glutamine, 100mM β-mercaptoethanol (all Sigma), 10^3 u/ml LIF (ESGRO; Millipore, Watford, UK) and 10% foetal bovine serum (Gibco-Invitrogen). Monolayers were passaged by enzymatic dissociation with 0.01% trypsin containing 0.2M EDTA and 5% chick serum (all Sigma) at 37ºC for 3 min. Cells were liberated by gently tapping flasks under phase-contrast microscope. Enzyme was then inactivated with growth medium containing 10% FCS and cell suspensions centrifuged at 300xG for 3min. Cell pellets were resuspended and seeded at a 1:6 ratio onto gelatin-coated (0.1%) tissue culture plastic (Iwaki™; Thermo-Fisher, Waltham, UK). Mouse E14 Tga2 cells were observed to exhibit monolayer growth when cultured on Iwaki™ tissue culture treated plastic with 10% serum and 10^3u/ml LIF and passaged every 48h by the method described.

2.5 Protein isolation and purification.

Protein isolates were prepared from cellular material for gel electrophoresis and western blotting. Cells were washed with ice-cold dPBS, harvested by scraping in 1ml dPBS and centrifuged at 300xG for 5min. Cell pellets were lysed for 30min on ice with 100µL commercially available RIPA lysis buffer (Gibco; Invitrogen) containing phosphatase and protease inhibitors (Roche; Welwyn Garden City, UK). Lysates were collected and centrifuged at 13000 x g for 30min at 4°C, the supernatant was collected and transferred pre-cooled 1.2ml micro-centrifuge tubes (Eppendorf; Cambridge, UK). Protein lysates were then stored at -80°C. Protein concentrations were assessed by the Bradford method (Bio-Rad, Hemel Hempstead, UK) and quantified against a standard curve generated by serial dilution of bovine serum albumin (BSA; Sigma-Aldrich). Optical density was measured at 597nm and sample protein concentrations determined by linear regression from the standard curve.

2.6 SDS-polyacrylamide gel electrophoresis (SDS-PAGE) and western blotting.

Each lane of a pre-cast 10% Tris-glycine/SDS gel (Invitrogen) was loaded with 30µg of protein in Laemlli sample buffer. Protein samples were run alongside Western Blotting ECL™ molecular weight markers and Full-Range Rainbow™ markers (both GE Medical) and loading controls (see Antibodies) at 145 V, 50 mA for 1hr in a X-Cell II Sure-Lock system™ (Invitrogen). Proteins were transferred onto Hy-Bond-ECL™ nitrocellulose membranes (GE-Heatlhcare-Amersham; Lt Chalfont, UK) pre-activated with methanol (Sigma-Aldrich). Protein transfer using the X-Cell II™ blot module (Invitrogen) and standard transfer buffer was undertaken for 2hrs at 20V/450mA. Membranes were equilibrated with wash buffer for 5mins prior to incubation with 5% milk blocking solution for1hr. Membranes were then washed 3 times with tris-glycine buffer (15mls). Membranes were cut at specific positions according to the molecular weight band identified by the Full-Range Rainbow marker lane relevant for the target protein. Subsequently, membranes were incubated overnight on a rotating shaker with a 1:500 dilution of primary antibodies at 4ºC (see Antibodies). Membranes were washed 3 times and incubated for a further1hr at room temperature with goat-anti rabbit secondary antibodies conjugated with horseradish peroxidase (HRP). Membranes were again washed 5 times with 5ml wash buffer and visualised by enhanced chemiluminescence. A 10ml solution of ECL+ (GE Healthcare-Amersham) was prepared (1:1 ECL A: ECL B) and applied to labelled membranes. Chemiluminescence was detected by exposing Hyperfilm™ x-ray sensitive photographic film for between 30sec and 5 min in a hyperfilm cassette (GE-Healthcare-Amersham).

2.7 Immunostaining

Cells were fixed with 1% paraformaldehyde (Sigma) for 10min and washed with dPBS at room temperature, cultures were cooled to 4°C, washed again with pre-cooled dPBS and fixed with 70% Etoh at -20°C for 10 min at 4°C. Solution was removed and wells were washed with a 50% ratio of EtOH/dPBS, 25% EtOH/dPBS and then left at room temperature in dPBS alone to rehydrate. Cells were incubated for 30min in XT-image enhancer blocking solution (Invitrogen) and then incubated for 1-2h with isotype control or antigen-specific primary antibodies at room temperature on a rotating shaker, or overnight at 4°C for phosphospecific antibodies. Primary antibody solutions were removed and cells washed with dPBS 3x and incubated with AlexaFluor-conjugated secondary antibodies (Invitrogen) for 1h at room temperature. Wells were washed 3x for a minimum of 30min and treated with 0.5μg/ml DAPI (Invitrogen). Solution was removed and cells washed 2x with dPBS and kept at 4°C in the dark.

2.8 Antibodies

Primary antibodies were used at the manufacturer recommended concentrations or as specified. Anti-mTOR, phospho-p70S6K (th389/th412 human/mouse), phospho-p70S6K (th421/ser424); rabbit monoclonal IgG (Upstate/Millipore). Primary monoclonal p70S6K, mTOR, phospho-mTOR (ser2448), phospho-mTOR (ser2481), raptor, rictor, AKT, phospho AKT (ser473), phospho-AKT (th308), p44/p42 ERK, phospho p44/p42 ERK, phospho-histone H3 (ser10), ß-actin (all rabbit monoclonal IgG; Cell Signaling Technology/New England Biolabs, Hichin, UK). Phospho-specific antibodies were used at minimum dilution of 1:100 overnight at 4°C. Monoclonal mouse anti-Oct4,1:400 (Invitrogen). Secondary antibodies; AlexFluor 488nm, 555nm, 597nm, 647nm; goat anti rabbit IgG or goat anti-mouse IgG used at manufacture recommended concentrations.

2.9 Image capture and processing

Wide-field microscopy was performed with a Nikon Eclipse TE-2000U fluorescence microscope with NIS Elements-BR™ capture software. Test samples were background corrected with secondary antibody and isotype specific controls except where specified. Confocal microscopy performed with Leica SP1-UV with LCS capture software. All post-processing and image analysis was undertaken with ImageJ (MacBiophotonics ImageJ package)

2.10 Live-cell imaging.

Mouse ES cells were cultured into triplicate wells of a 6-well tissue culture plate (Iwaki) coated with 0.1% gelatin (Sigma-Aldrich). Cells were seeded at a density of $5x10^4$ cells/cm^2 and placed into the incubated stage of the Cell-IQ™ automated image analysis platform with 5% CO_2 at 37°C.. Phase contrast images were captured at 5 locations per well by an automated protocol with an enhanced depth of field function that ensured in-focus images were obtained. Image capture locations were manually specified by a grid matrix using the integrated image capture software. Images were captured sequentially over a period of 48h

2.11 Flow cytometry

All flow cytometry performed with a Guava-EasyCyte benchtop cytometer with EasyCyte Express™ (Guava.) *or DAKO* CyAN ADP, 3 laser analyser, (Beckman Coulter, High Wycombe, UK). Post-processing performed with Cytomation Summit v.4.3 (DAKO). Single cells were gated by their characteristic forward scatter (linear scale) and peak width profile. At least 10000 gated events were recorded on the FL-2 channel with the voltage settings modified so that the primary peak fell within the specified range. Calibration performed daily using standard bead kits. Flow cytometry was not undertaken to quantify protein phosphorylation. Alternatively cellular distribution and sub-cellular localisation of phosphoproteins was documented by fluorescence and confocal microscopy relative to cell morphology and cytoskeletal protein expression.

2.12 Assessment of cell viability and proliferation

Mouse ES cells were harvested by treatment with trypsin as described. Cells were liberated by gently tapping flasks on the stage of a phase contrast microscope. Trypsin was quenched with 10mls dPBS containing 10% FCS and centrifuged for 5min at 300xG. Cell pellets were resuspended in 1ml dPBS containing 0.1% BSA (fractionV) (Sigma-Aldrich) and held on ice until analysis was complete. Cell counts were obtained manually by trypin blue exclusion with an Enhanced Neubauer™ haemocytometer by phase contrast microscopy. Automated analysis was performed using the Vi-Cell™ Cell Viability Analyzer (Beckman-Coulter). Cell suspensions were diluted 1:1 with 0.5ml dPBS for analysis.

2.13 Assessment of apoptosis in mES cells.

Mouse E14 cells were cultured for 48h in complete growth medium supplemented with LIF (10^3u/ml). At specified time-points cell cultures were washed with dPBS and supplied with fresh growth medium with or without LIF. Wells were then with 1µl DMSO or small molecule inhibitors. The effect of mTORC1 kinase activity on apoptosis induction was determined by treatment with rapamycin (100nM) and mTORC1/mTORC2 kinase activity determined by treatment with the dual kinase inhibitor Ku-0063 (100nM).).To assess the effect of short-term inhibition cultures were washed after 45h and incubated for a further 3h with kinase inhibitors whereas for extended inhibition, cells were washed after 24h and incubated for a further 24h in growth medium containing inhibitors. After a total of 48h of incubation, all cultures were washed and cells harvested and processed for apoptosis assessment by flow cytometry or for viability assessment by trypin blue exclusion. All analysis was performed within 1h of the end of the reaction. The percentages of viable, apoptotic and necrotic cells were assessed by immunostaining for cell membrane bound annexin IV and nuclear incorporation of the fluorescent dye 7-AAD. The percentages of viable cells (annexin negative, 7-AAD negative), early apoptotic cells (annexin positive, 7-AAD negative), late apoptotic cells (annexin positive, 7-AAD positive) and necrotic cells/nuclear debris (annexin negative, 7-AAD positive) were determined according to the standard protocol for apoptosis assessment using the Guava-Nexin™ kit.

2.14 Hypothesis testing and statistical significance

The assessment of differences between the mean values of data sets generated from biological assays was undertaken using standard statistical tests. Statistical significance was determined when the null hypothesis was rejected at an alpha level of $p<0.05$, differences between treatment groups in parametric data sets (normal frequency distribution) was determined by paired or unpaired t-test (Minitab 3.1 statistical software). Differences between treatment groups in non-parametric data were assessed by the Mann-Whitney U test (Minitab 3.1). Multiple comparisons within single data sets were treated with post-hoc correction calculations for parametric or non-parametric data. The Pearson’s product moment correlation coefficient was used to identify statistical concordance between normally distributed data sets.

2.15 Determination of statistical significance in multivariate data sets.

In certain biological assays, multivariate data was generated from a single data set. In order to limit the chance of generating type 1 errors resulting from multiple statistical comparisons within a single data set, post-hoc corrections were applied in accordance with the Bonferroni method for normally distributed data. Briefly, the alpha value (α) of $p<0.05$ was selected for determination of statistical significance. In order to correct for multiple testing, alpha was then divided by the number of independent statistical tests (n) performed within a single data set (α/n).

Table 2.1

Bonferroni adjustment for significance testing with multiple comparisons.

number of tests (n)	alpha level (α)	alpha level (α)
1	0.05	0.01
2	0.0250	0.0050
3	0.0167	0.0033
4	0.0125	0.0025
5	0.0102	0.0020
6	0.0083	0.0017
7	0.0071	0.0014
8	0.0064	0.0013

2.16 Assessment of significance in multivariate data with multiple treatment groups.

Multiple testing errors were negated by defining a primary outcome measure, hypothesis testing was then performed on the primary outcome data. Additionally, within the same data sets, secondary outcome measures were defined and tested for significance. In some cases statistical significance was observed in the secondary outcome variables, these findings were classed as preliminary observations. In such cases, repeat experiments were performed and new primary outcome measures defined. Secondary outcome measures that were not subject to independent validation were defined as preliminary or exploratory.

2.17 Biological replicates and n-values.

Where stated, biological replicates are denoted by n=*(value)*. In certain cases a single cell culture was split and assayed as parallel cultures/technical replicates, in such cases this is clearly stated in the figure legend and denoted by n=$(value^{tech})$.

Chapter 3

Introduction

The experimental data presented in this chapter will primarily serve to detail the model system to be utilised throughout this investigation and secondly to assess the impact of inhibition of the mTOR pathway on the proliferation of pluripotent and multipotent cells in vitro. Additionally, substrates of the mTOR kinase will be assayed to define the experimental conditions for the manipulation of the mTOR pathway in later experiments.

Three pluripotent cell types were assessed in preliminary experiments to define the culture system for further investigation. Human embryonic stem cells, human embryonal carcinoma cells and mouse embryonic stem cells were cultured and assayed for their sensitivity to rapamycin. The practicality of cell culture was also considered.

3.1. Characterisation of human embryonic stem cells *in vitro*.

Preliminary experiments were undertaken to characterise the Shef3 line of human ES cells. These cells were a natural choice for further investigation as they have been used extensively in- house and are stable over extended passaging.

Figure 3.1.1 displays the typical morphology of Shef3 colonies by phase contrast and fluorescence microscopy. These ES cells were manually dissected and seeded into tissue-culture flasks containing a low density monolayer of primary inactivated MEF feeder cells. After 3 days growth, cells were fixed and stained with primary monoclonal antibodies specific for OCT4 and Alexa Fluor-488 conjugated secondary antibodies. Expression of OCT4 and nuclear counterstaining with DAPI was visualised by fluorescence microscopy with the corresponding excitation and emission filters. The typical morphology of these hES colonies can be observed (A) and is indicated by white triangles. Expression of OCT4 was associated with colonies containing densely packed cells (image C).

To confirm that OCT4 was not expressed by the feeder cells, mouse embryonic fibroblasts were cultured alone and stained for OCT4 expression. No immunoreactivity was observed in MEF cells (Figure 3.1.2). Data presented in Figure 3.1.3 confirmed that OCT immunoreactivity was restricted to densely packed cells within hES colonies (white triangles). Again, no staining for OCT4 was observed in individual feeder cells (yellow triangles).

Figure 3.1.1

Human ES cell colonies exhibit distinct morphology and express OCT4.

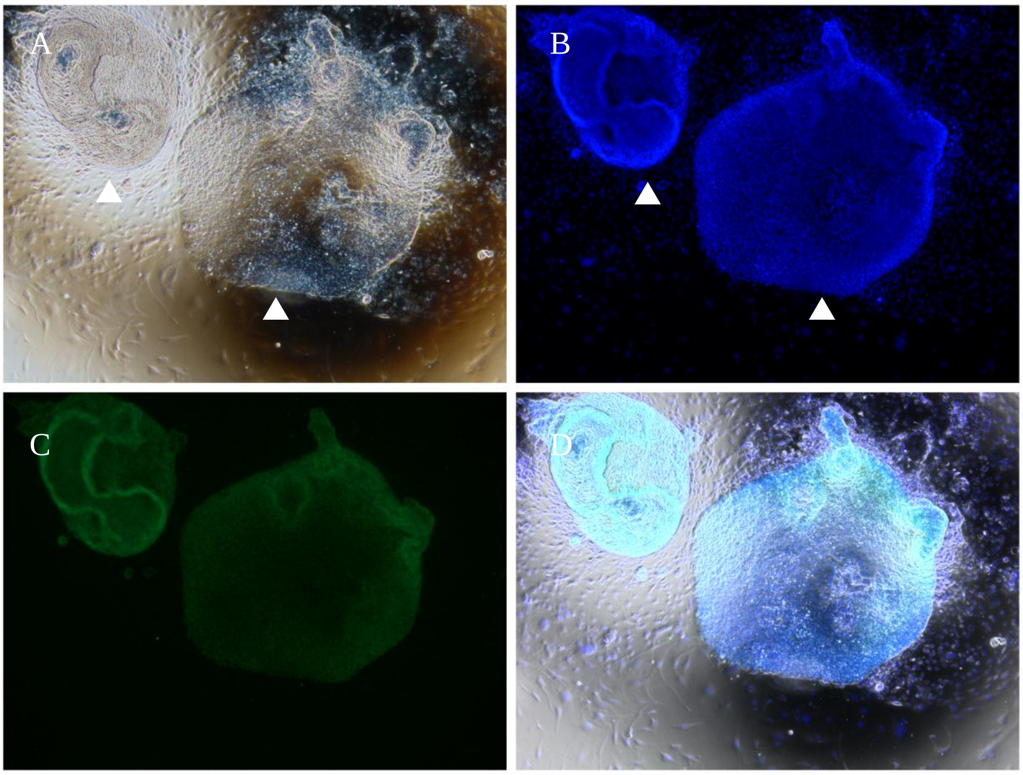

Fig. 3.1.1

Morphology and expression of OCT4 in Shef3 human embryonic stem cell colonies. Human ES cells were cultured *in vitro* on a layer of inactivated mouse embryonic fibroblasts. Cells were fixed with PFA and OCT4 expression determined by staining with monoclonal primary and Alexa-488 conjugated secondary antibodies. Nuclear counterstaining was achieved by DAPI uptake. Cultures were visualised by phase-contrast and fluorescence microscopy with a Nikon-Eclipse TE2000 microscope (4x magnification). Colony morphology and staining was visualised by phase-contrast (image A), DAPI fluorescence (image B), OCT4 fluorescence (image C). Image D represents a merged composite of the three channels. White triangles specify hES colonies. Representative images from 3 independent cultures.

Figure 3.1.2

Mouse embryonic fibroblasts do not express OCT4.

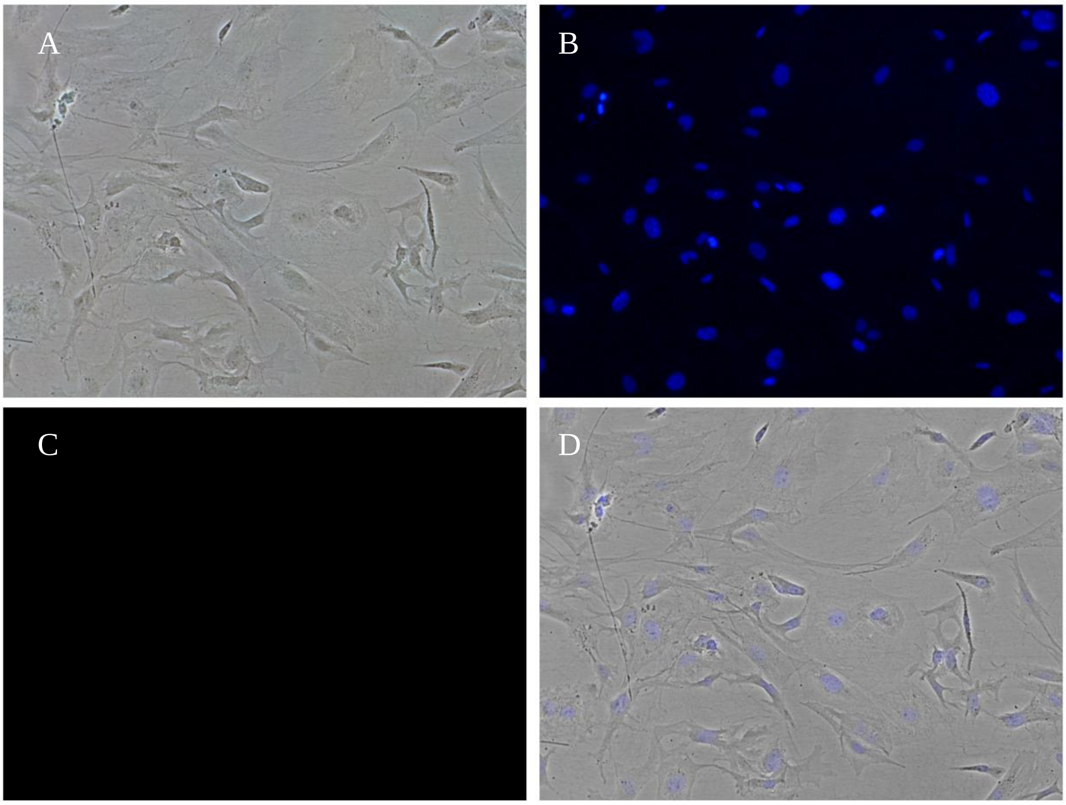

Fig 3.1.2

Morphology and expression of OCT4 in inactivated mouse embryonic fibroblasts. Cells were fixed with PFA and OCT4 expression determined by staining with monoclonal primary and Alexa-488 conjugated secondary antibodies. Nuclear counterstaining was achieved by DAPI uptake. Cultures were visualised by phase-contrast and fluorescence microscopy with a Nikon-Eclipse TE2000 microscope and Nikon Elements BR software. Images were captured at 10x magnification. Colony morphology and staining was visualised by phase-contrast (image A), DAPI fluorescence (image B), OCT4 fluorescence (image C). Image D represents a merged composite of the three channels. Representative images from 3 independent cultures.

Figure 3.1.3

Expression of OCT4 in hES and MEF co-cultures.

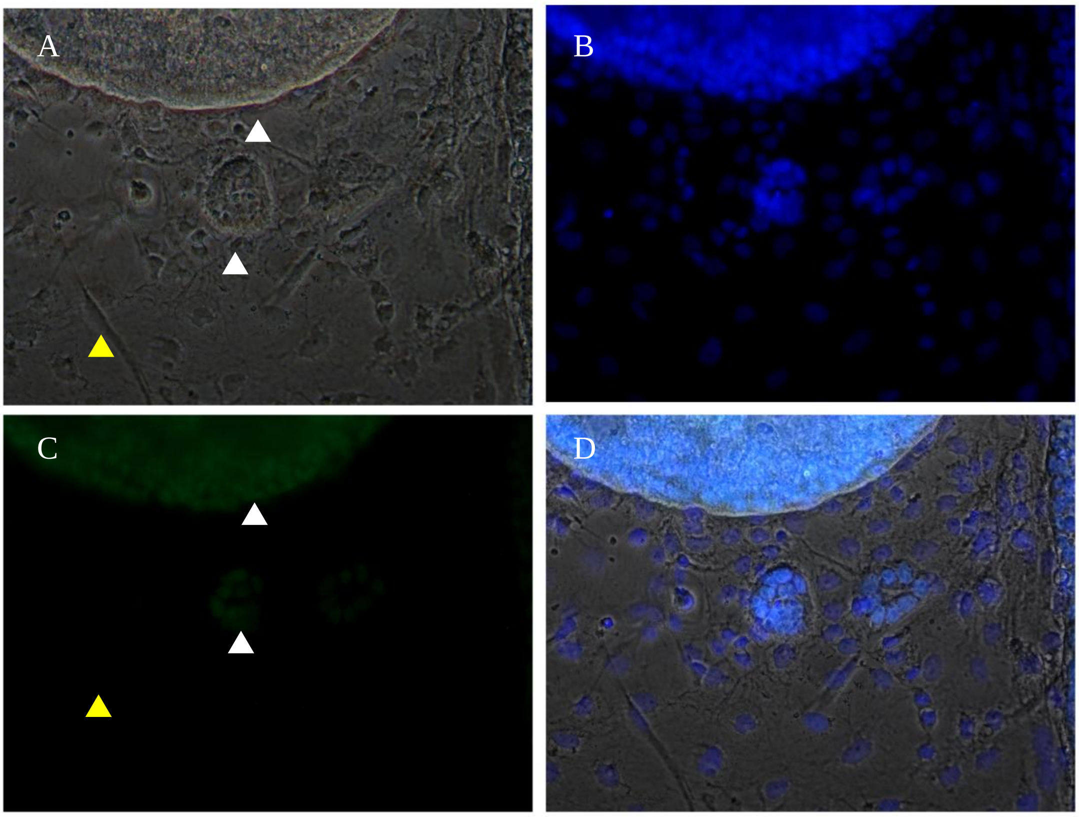

Fig.3.1.3

Morphology and expression of OCT4 in Shef3 hES and MEF co-cultures by fluorescence microscopy. Images were captured at 10x magnification. Colony morphology and staining was visualised by phase-contrast (image A), DAPI fluorescence (image B), OCT4 fluorescence (image C). Image D represents a merged composite of the three channels. White triangles indicate OCT4+ve hES cells, yellow triangles specify OCT4-ve MEF cells. Representative images from 3 independent cultures.

During the culture of hES cells, spontaneous differentiation often proceeds from the edge of the colony. Pluripotent marker expression is maintained within compact, high density areas in the centre. Cells within these compact areas are selected for sub-culture. These observations are made by visual inspection under by phase contrast microscopy. Therefore, the maintenance of pluripotency in these hES cells is supported by a subjective process at the passaging stage.

Figure 3.1.4.1 shows the relationship between the morphology of Shef3 colonies and OCT4 staining by phase-contrast and fluorescence microscopy. Three areas with distinct morphology can be observed in images A and B. White triangles indicate compact cells within the colony. The surrounding layer of less compact cells at the edge of the colony is indicated by red triangles (spread morphology) and the low density monolayer of feeder cells is indicated by yellow triangles (diffuse morphology).

The mean fluorescence intensity of OCT4 in these defined areas is shown in Figure 3.1.4.2. Areas of the images were selected using image analysis software, and the intensity of OCT4 staining was recorded. Areas containing cells with a compact morphology exhibited strong staining for OCT4. Cells with spread morphology exhibited reduced OCT4 staining and diffuse cells were devoid of OCT4 immunoreactivity. Statistical analysis of the difference between OCT4 intensity in these groups was assessed by paired t-test. There was a significantly reduced level of OCT4 staining in the spread areas compared with compact areas ($p=0.01$) and diffuse areas ($p<0.01$). Additionally, OCT4 expression in the spread areas was significantly greater than in diffuse cell areas ($p<0.05$).

Figure 3.1.4.1

Morphology and OCT4 expression in hES and MEF co-cultures.

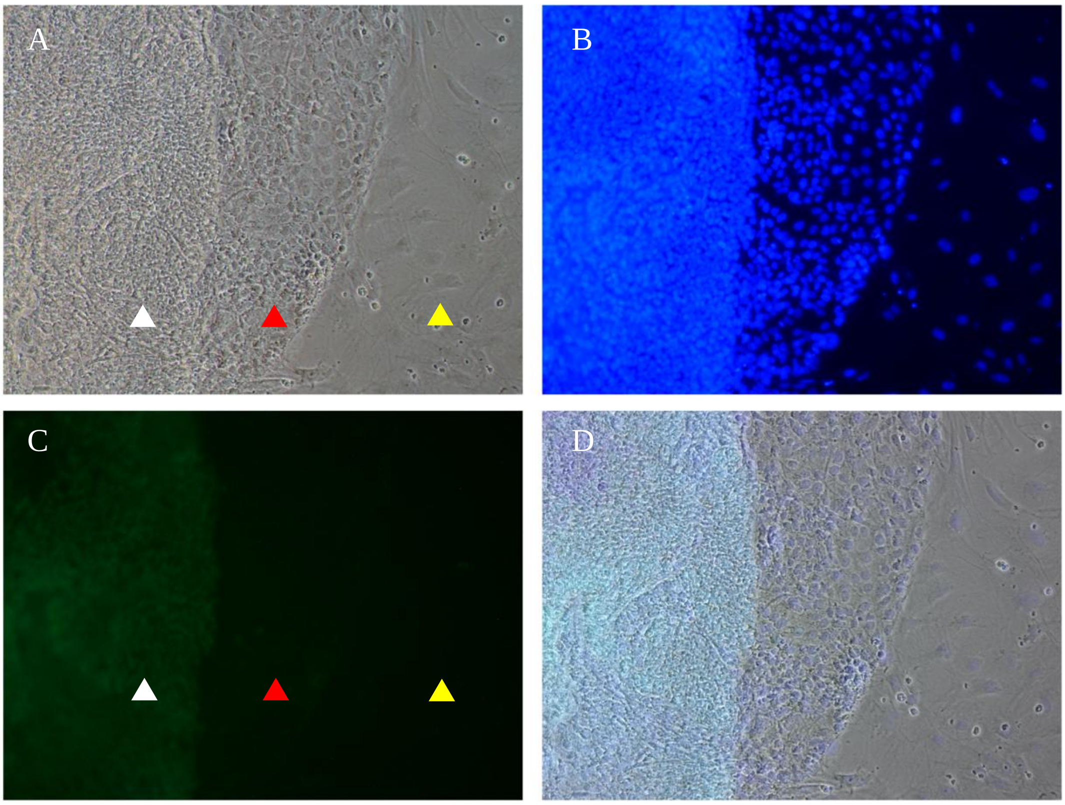

Fig. 3.1.4.1

Morphology and expression of OCT4 in Shef3 hES and MEF co-cultures by fluorescence microscopy at 10x magnification. White triangles indicate dense, tightly packed cells within the colony (compact morphology). The surrounding layer of less compact cells at the edge of the colony is indicated by red triangles (spread morphology) and the low density monolayer of feeder cells indicated by yellow triangles (diffuse morphology). Representative images from 3 independent cultures.

Figure 3.1.4.2

Mean fluorescence intensity of OCT4 in morphologically distinct cell areas.

Colony morphology	Compact	Spread	Diffuse
Mean fluorescence intensity (MFI)	25.15	9.75	6.15
Standard deviation	5.24	2.41	3.44

Fig. 3.1.4.2

Mean fluorescence intensity of OCT4 from fluorescence micrographs. Human ES (Shef3) and MEF co-cultures were stained with OCT4-Alexa488 and DAPI. Morphologically distinct areas containing cells from four fields of view were sampled and the mean intensity of OCT4 fluorescence was measured and presented in tabular form. Sampled areas were identified visually from phase-contrast micrographs and categorised as in Figure 3.1.4.1. Dense, tightly packed cells within the hES colony (i. compact morphology), areas of less compact cells at the edge of the colony (ii. spread morphology) and the low density monolayer of feeder cells (iii. diffuse morphology). Methodology and results of statistical analysis is described in the text.

Human ES cells were stained with OCT4 antibodies and DAPI after 4 days in culture. This was visualised by phase contrast and fluorescence microscopy (Figure 3.1.5.i.). This figure shows that areas of high cell density indicated by bright DAPI staining (white triangles) exhibited high OCT4 expression whereas staining was lower in areas with low cell density (red triangle). The intensity of OCT4 expression was measured along a line drawn through the colony (Figure 3.1.5.ii.A). The intensity of OCT4 expression was high within areas containing a high density of cells (Figure 3.1.5.ii.B).

To assess whether these differences arose from the increased density of cells or the elevated expression of OCT4 within individual cells; data was collected from two hES colonies (Colony 1, 2) (Figure 3.1.6.1.i). Individual nuclei were selected from Colony 1 (n=50) and Colony 2 (n=100) and the mean intensity of OCT4 expression of each selected nucleus was measured (Figure 3.1.6.1.ii).

The number of nuclei within 100µm^2 of the selected nucleus were counted and plotted as a scatter graph of cell density versus nuclear OCT4 expression (Figure 3.1.6.2). The Pearson’s correlation statistic was utilised to assess the relationship between local cell density and nuclear OCT4 expression in Colony 1 (i) and Colony 2 (ii). There was no correlation between cell density and OCT4 expression in either colony.

Scatter graphs of OCT4 expression and nuclear size were generated for both colonies assessed in the previous figure (Figure 3.1.6.3). No statistical concordance was observed in either Colony 1 (i) or Colony 2 (ii). These findings indicate that the high levels of OCT4 expression observed in compact cells did not correlate with the number of cells within the measured area or the size of sampled nuclei.

Figure 3.1.5

Expression of OCT4 may relate to density of hES cells in a colony.

i.

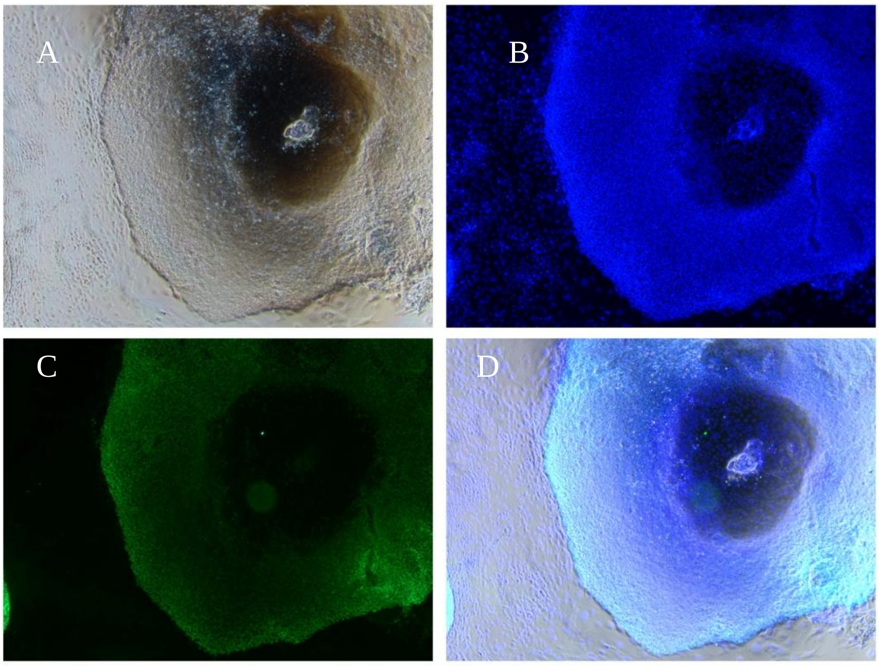

ii.

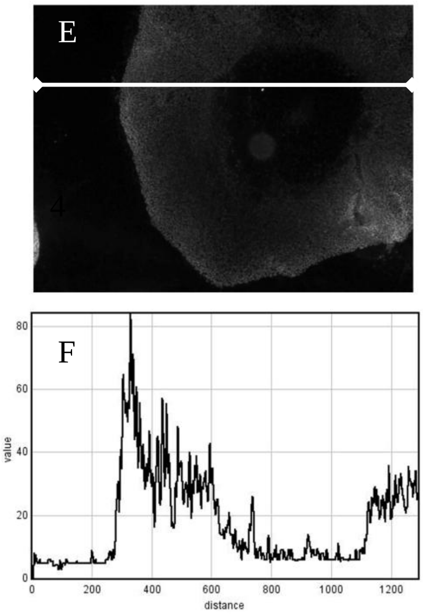

Fig. 3.1.5

Human Shef3 ES cells were cultured for 96h and stained with DAPI and OCT4 antibodies (i). Micrographs of phase contrast (A), DAPI (B) and OCT4 fluorescence (C) were merged to form a composite image (D). The intensity of OCT4 expression was measured across the colony (ii), along a line that crosses high density and low density areas (E). The mean fluorescence intensity of the line measurement is presented graphically (F).

Figure 3.1.6.1

Relationship between OCT4 expression and cell density in single hES cells.

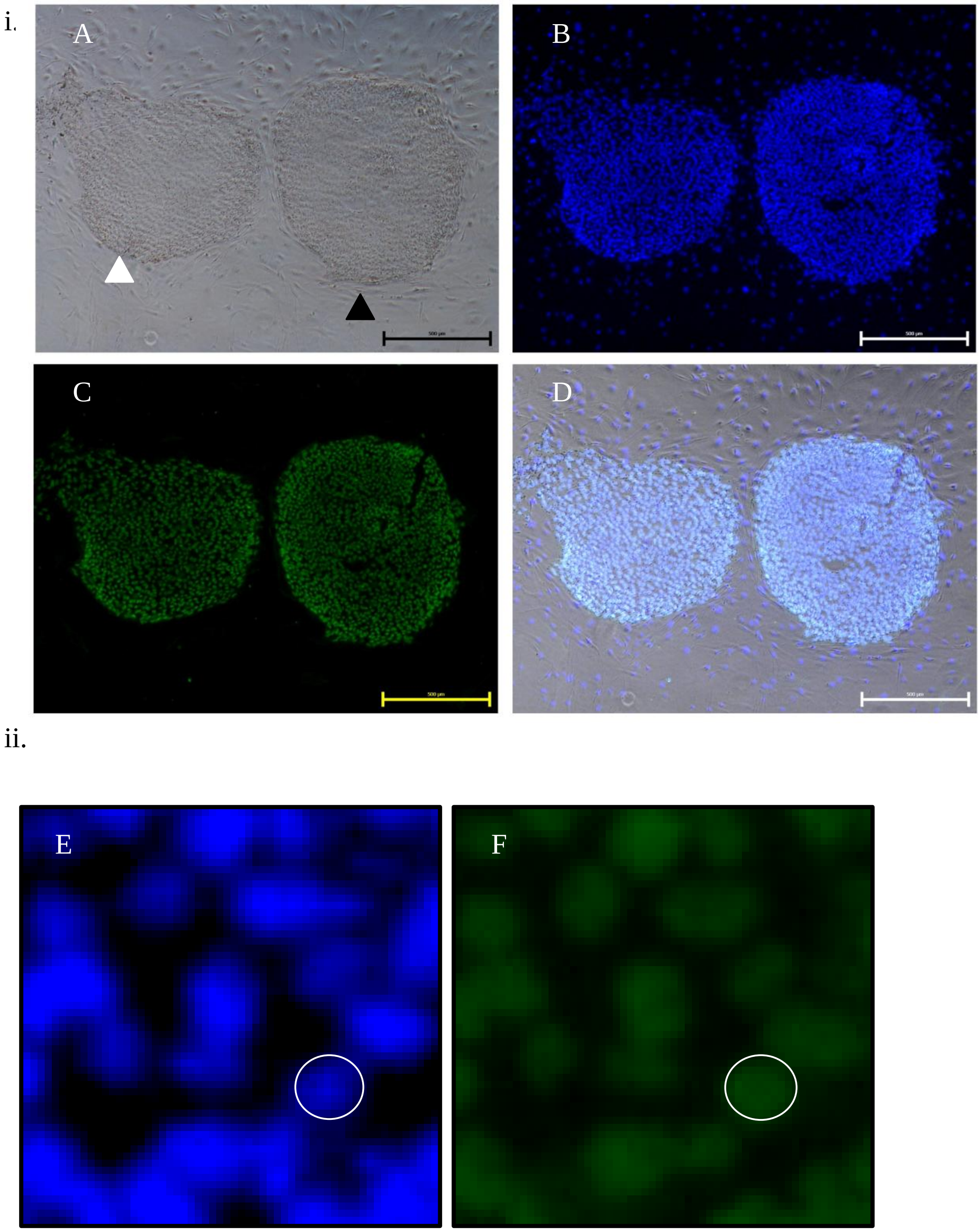

Figure legend

Fig. 3.1.6.1

Human Shef3 ES cells were cultured for 48h and imaged by phase contrast (A) and fluorescence microscopy. Two colonies were selected; Colony1 is indicated by a white triangle and Colony 2 by a black triangle. Individual nuclei were selected (E) and a region of interest (ROI) was drawn around the nucleus (red triangle). At least 50 nuclei were selected from each colony in a raster pattern and the nuclear OCT4 expression with each ROI was measured (F). Image analysis was performed using ImageJ analytical software. An area of 100µm^2 was around each ROI and the number of nuclei within the area was counted and recorded by excluding nuclei at the edges on the right and lower sides. The size of each nuclear ROI was also recorded. The images of OCT4 staining in hES colonies in this figure kindly provided by Dae-Kyeong Bae, Department of Biochemical Engineering, UCL.

Figure 3.1.6.2

Relationship between OCT4 expression and cell density in hES colonies.

i. Colony 1

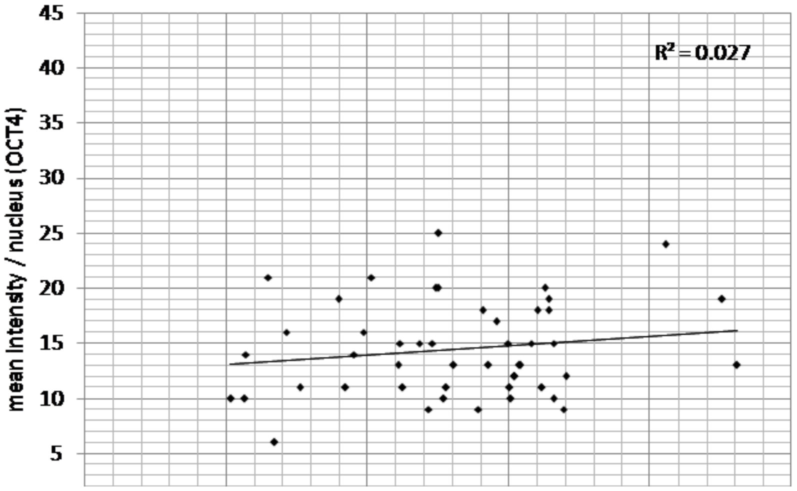

ii. Colony 2

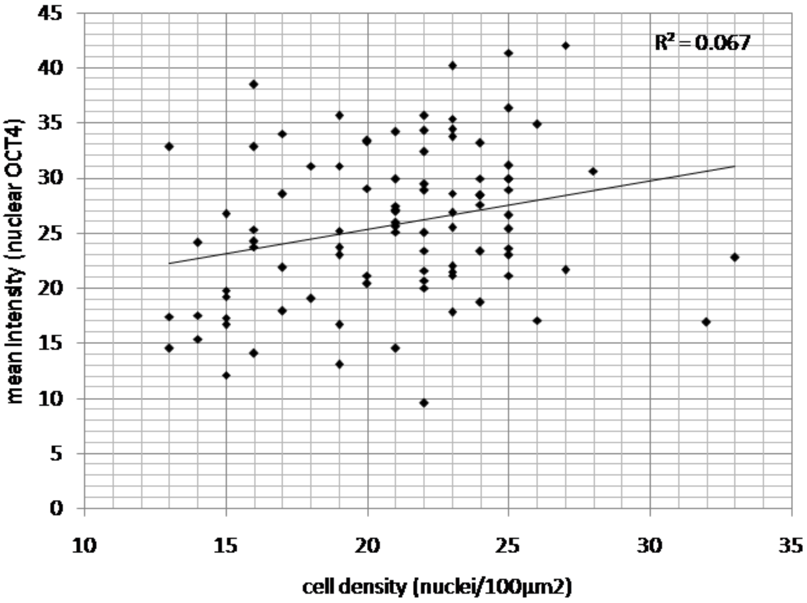

Figure 3.1.6.3

Relationship between OCT4 expression and nuclear size in hES.

i. Colony 1

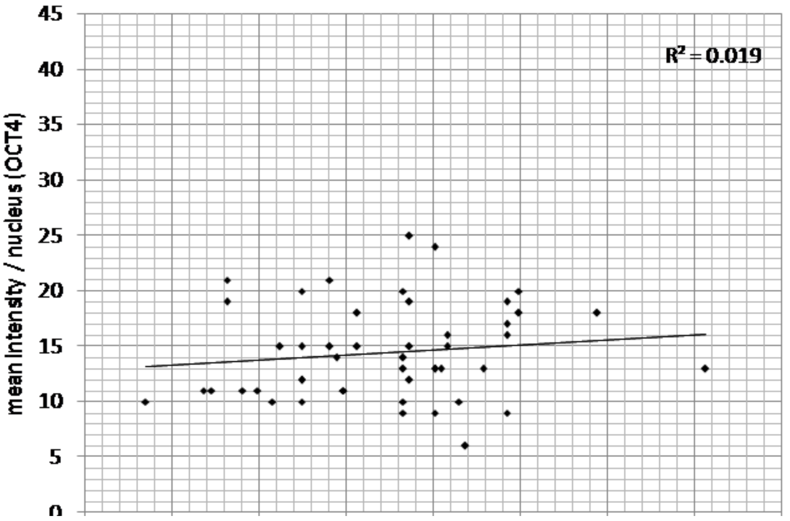

ii. Colony 2

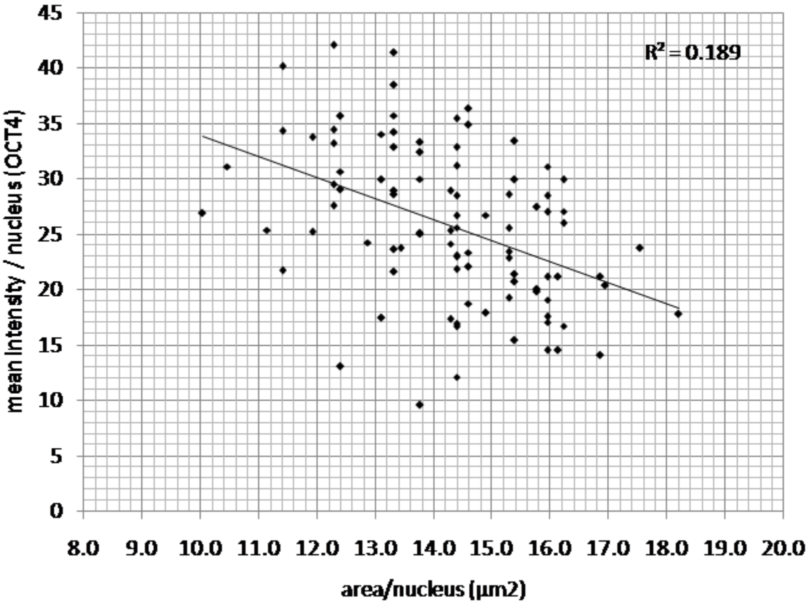

Figure legends.

Fig.3.1.6.2

Data generated from Figure 3.1.6 presented as a scatter graph of mean OCT4 intensity within the selected nuclei versus the number of nuclei within $100\mu m^2$ of the selected cell. Data collected from 50 cells from Colony 1 (i) and 100 cells from Colony 2 (ii). Statistical analysis was performed using the Pearson's product moment correlation statistic to assess the relationship between OCT4 expression and cell density.

Fig.3.1.6.3

Data generated from Figure 3.1.6 was also presented as a scatter graph of mean nuclear OCT4 intensity versus the area of the selected nucleus. Individual nuclei were selected from micrographs by drawing a region of interest (ROI) from the DAPI channel using ImageJ .The mean intensity of OCT4 and area of DAPI staining were recorded for each ROI. Statistical analysis was performed using the Pearson's product moment correlation statistic to assess concordance between nuclear OCT4 intensity and nuclear size.

The effect of the mTOR complex1 (TORC1) kinase inhibitor rapamycin on Shef3 colony formation was assessed in a preliminary experiment. Figure 3.1.7 shows the effect of TORC1 inhibition on the number of hES colonies after 72h growth. The number of colonies was determined manually by counting under phase-contrast microscopy. Rapamycin treatment dramatically reduced the total number of colonies compared with DMSO treated controls. This preliminary experiment suggests that hES colony formation is rapamycin sensitive.

In order to assess the impact of contaminating feeder material on the molecular analysis of protein expression in hES cultures, lysates of MEF and human ES cells co-cultured with MEFs. Lysates were also taken from a breast cancer cell line (MCF7) as a positive control. Proteins were separated by gel electrophoresis and probed with monoclonal antibodies for mTOR and p70S6K by western blotting. Figure 3.1.8 shows the expression of total mTOR protein and phospho-p70S6K in MEF cells, hES/MEF co-cultures and breast cancer cells. All three cell preparations exhibited immunopositive bands for both mTOR and phospho-p70S6K.

Evaluation of mTOR pathway activation in hES would require an efficient purification step to remove contaminating material originating from the supporting feeder cells. The maintenance of pluirpotency in Shef3 cultures was at this time refractory to enzymatic passaging necessitating the mechanical dissociation of colonies under a dissecting microscope. Plating single cell suspensions of Shef3 hES was therefore not possible. This inability to precisely regulate colony size during mechanical dissociation was a major obstacle to quantifying cell seeding density and considered to be a major drawback to the use of Shef3 cells in this investigation.

Figure 3.1.7

Effect of rapamycin on human embryonic stem cell colony formation.

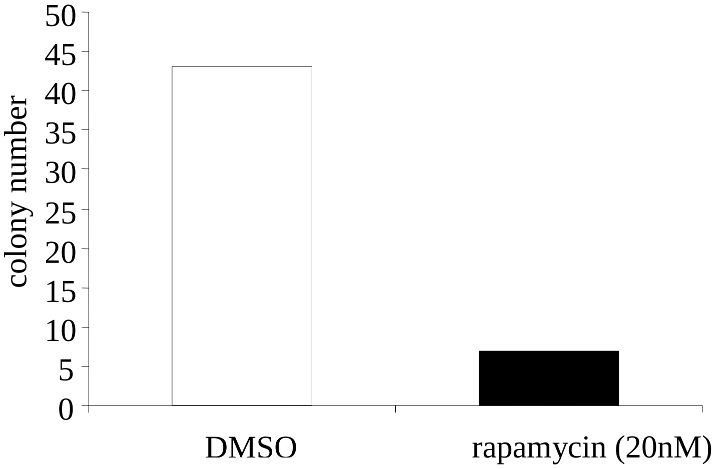

Fig.3.1.7

Human embryonic stem cells were mechanically dissociated under a dissecting microscope and suspended in hES growth medium. Equal volumes of cell suspension were seeded into gelatin-coated T25 flasks containing adherent MEF feeder cells. Cultures were treated with DMSO or rapamycin (20nM) and cultured under standard conditions for 72h. At the designated time-point colonies were counted by phase-contrast microscopy. Preliminary data from a single experiment.

Figure 3.1.8

Expression of mTOR and phospho-p70S6K in mouse embryonic fibroblasts, human embryonic stem cell co-cultures and human breast cancer cells.

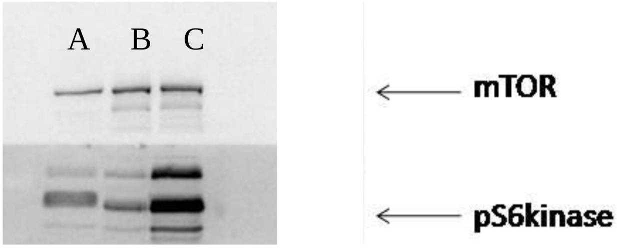

Fig.3.1.8

Mouse embryonic fibroblasts (a), human embryonic stem cell co-cultures containing MEF cells (b) and human breast cancer cells BRCA2 (c) were lysed and equal quantity of protein were separated by gel electrophoresis and transferred onto PVDF membrane by western blotting. Levels of total mTOR protein and phosphorylated p70S6K were probed with primary anti-rabbit monoclonal antibodies and HRP-conjugated anti-mouse secondary antibodies visualised by ECL chemiluminescence detection.

3.2 Assessment of the effect of rapamycin on human embryonal carcinoma cell proliferation

Embryonal carcinoma (EC) cells are pluripotent cells isolated from primary germ line tumours. The biology of mouse EC cells has been extensively studied since they were first identified in 1964 [9] and propagated *in vitro* as permanent cell lines in the 1970's. Embryonal carcinoma cells share many similar properties with embryonic stem cells in that they are immortal and can be induced to differentiate into somatic cells of the three primary germ layers *in vitro* [113, 114]. Human embryonic carcinoma cells (N-Tera2) can be grown *in vitro* without co-culture with feeder cells. Therefore the applicability of EC cells as a model system for this investigation was assessed.

Figure 3.2.1 shows the effect of rapamycin treatment on EC cell proliferation over 72h. Human N-Tera2 cells were seeded in triplicate into 6-well plates and cultured in a humidified atmosphere at 37°C containing 5% $CO_{2.}$ At each time point, cells were harvested by trypsinisation and manually counted in a haemocytometer by light microscopy. The proliferation of EC cells was inhibited by rapamycin treatment. Cell numbers were significantly reduced at all time points compared with DMSO treated control cultures and the inhibitory effect of rapamycin was exacerbated by prolonged treatment (72h).

The utilisation of human EC cells as a model system for the investigation presented limitations. Practical concerns related to the passaging technique for expansion. Self-renewal of N-Tera2 cells is refractory to repeated enzymatic treatment for propagation. Therefore, the long-term passage of EC cultures is achieved by mechanical dissociation of cell monolayers with sterile glass beads. This inability to plate N-Tera2 cells as suspensions of single cells presented complications in both quantitative and qualitative assays. Seeding density could not be accurately controlled and mechanical dissociation resulted in variable colony size, the use of human EC cells for further study was discounted.

Figure 3.2.1

Rapamycin mediated inhibits the proliferation of human embryonal carcinoma cells.

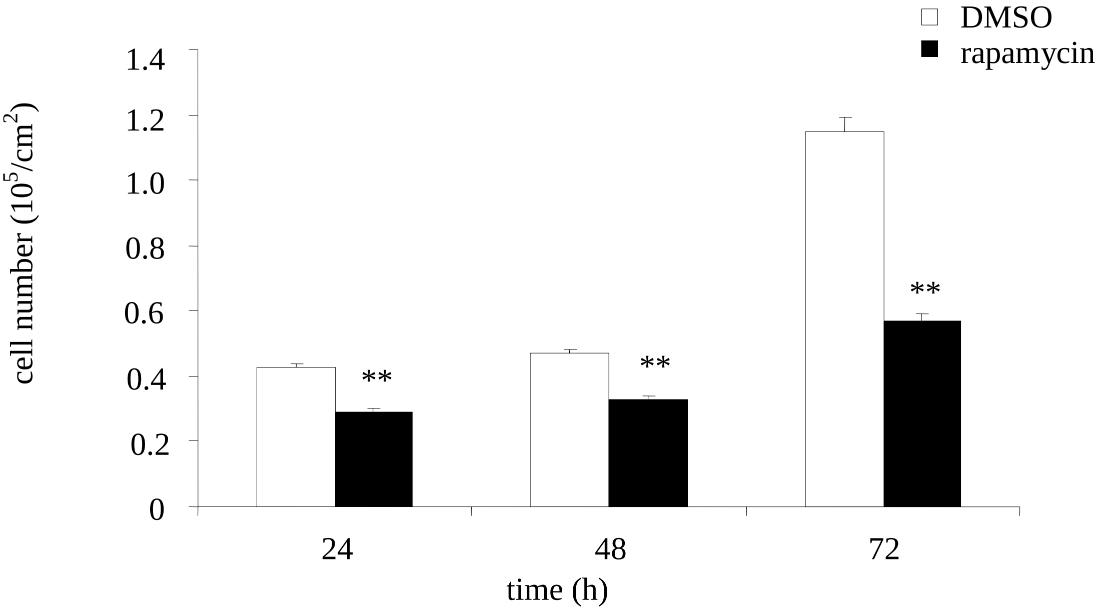

Fig 3.2.1

Human embryonic carcinoma cells (N-tera2) were seeded into 6-well plates and cultured for 24, 48 or 72h under standard growth conditions. Cultures were treated with DMSO or rapamycin (20nM), fresh medium and inhibitor treatments were replaced daily. At the designated time-points cells were harvested by enzymatic detachment and counted by trypin blue exclusion in a haemocytometer counting chamber under light microscopy. Error bars represent standard deviation of the mean from three independent cultures (n=3). Statistical significance at an alpha level of $p<0.01$ (**) was assessed by students t-test.

3.3 The mTOR pathway in E14 mouse embryonic stem cells.

The biology of mouse ES cells has been the subject of intense research since they were first isolated and cultured *in vitro* in 1981[1,2]. The use of mouse ES cells in this study offered practical advantages over both human ES and EC cells. Significant advances in the understanding of the nutritional and growth factor requirements of mES cells have enabled researchers to maintain the pluripotent phenotype *in vitro* indefinitely without the requirement for co-culture with feeder cells. Additionally mES cells will readily grow as monolayer colonies under certain conditions. Mouse ES cells have been adapted to enzymatic passaging and therefore can be seeded as single cells thus affording precise regulation of seeding density.

The in vitro culture of mouse ES cells without co-culture with feeders was enabled by the discovery that supplementation with the cytokine leukaemia inhibitory factor (LIF) supported pluripotent self renewal. That human ES cells do not maintain pluripotency when supplemented with LIF suggests that the regulation of the pluripotency network exhibits key differences with the mouse system. It is now apparent that although both human and mouse ES cells share the same core components of the pluripotency network (OCT4, Nanog). Consequently, the extrapolation of data generated from mouse ES cells to the human system must be interpreted with caution.

The typical morphology of mouse ES cells can be observed in the phase-contrast micrograph presented in Figure 3.3.1. Mouse E14 cells were imaged after 48h growth in complete growth medium containing LIF and serum. Under these conditions E14 cells form a densely packed monolayer colony. Individual cells are small and compact with a large nuclear to cytoplasmic ratio. During routine culture the morphology and confluence of cells is monitored by visual inspection under phase-contrast illumination. Loss of the compact colony morphology observed in this image would be the first indicator of cellular differentiation arising from batch variations in growth medium components.

The effect of rapamycin treatment on the proliferation of mouse embryonic stem cells (E14-TGA2) was assessed and shown in Figure 3.3.2. Incubation with rapamycin at a concentration of 10 or 100 nM resulted in a significant inhibition of total cell numbers after 24h. This observation was confirmed by treatment of mES cells for 48h with a serial dilution of rapamycin. In this assay, cell counts were performed with the Vi-Cell™ automated counting system. At the assay end-point, cells were harvested by trypsinisation, washed and then resuspended in dPBS containing 0.1% BSA. All analysis was performed within 1h. Figure 3.3.3 shows that rapamycin treatment significantly inhibited mES cell proliferation at all concentrations tested. Statistical differences were determined by parametric t-test. The concentration of 100 nM resulted in approximately 50% inhibition in total cell numbers after 48h.

Figure 3.3.1

Typical morphology of E14 mouse embryonic stem cells in culture.

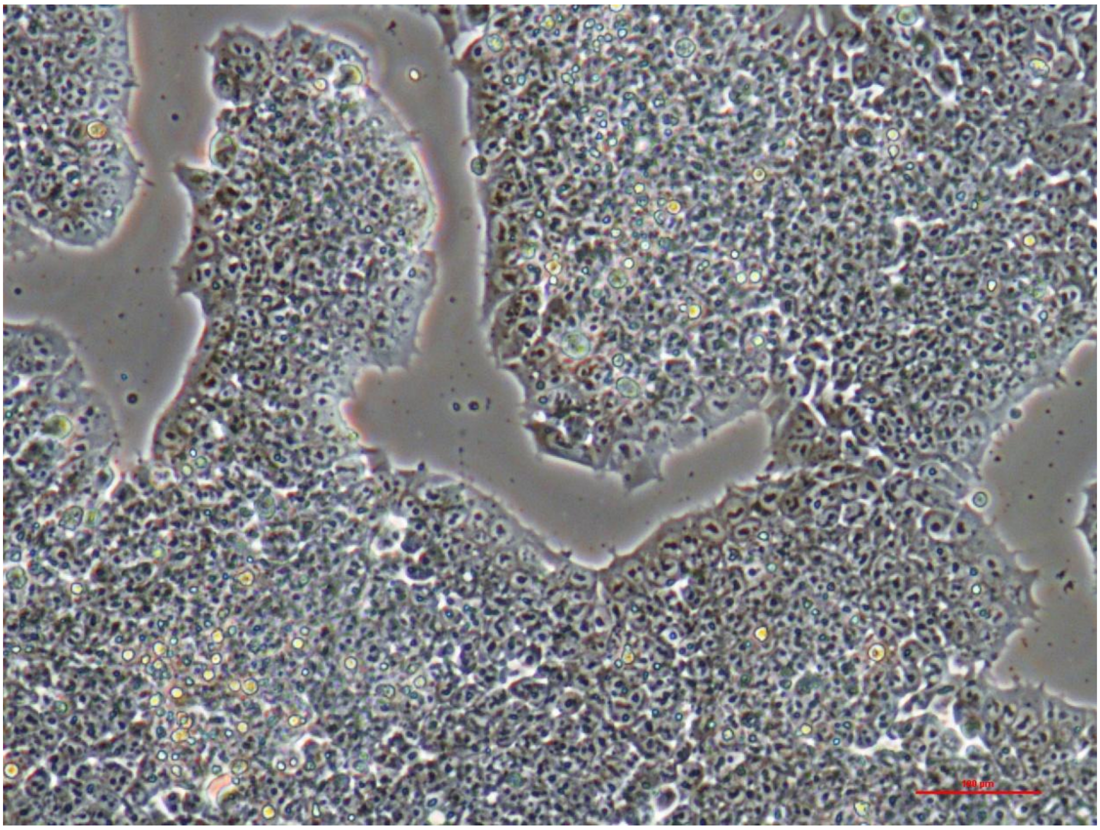

Fig 3.3.1

Typical morphology of mouse ES cells in vitro. Mouse E14-tga2 cells were cultured under standard culture conditions with complete growth medium (GMEM) containing 10% serum and 10^3 U/ml LIF. After 48h, cultures were imaged by phase-contrast microscopy at 10x magnification. Scale is represented by a red line (100µm). Mouse ES cells exhibit compact morphology and are densely packed within monolayer colonies.

Figure 3.3.2

Treatment of mouse ES cells with rapamycin for 24h inhibits proliferation at high concentrations.

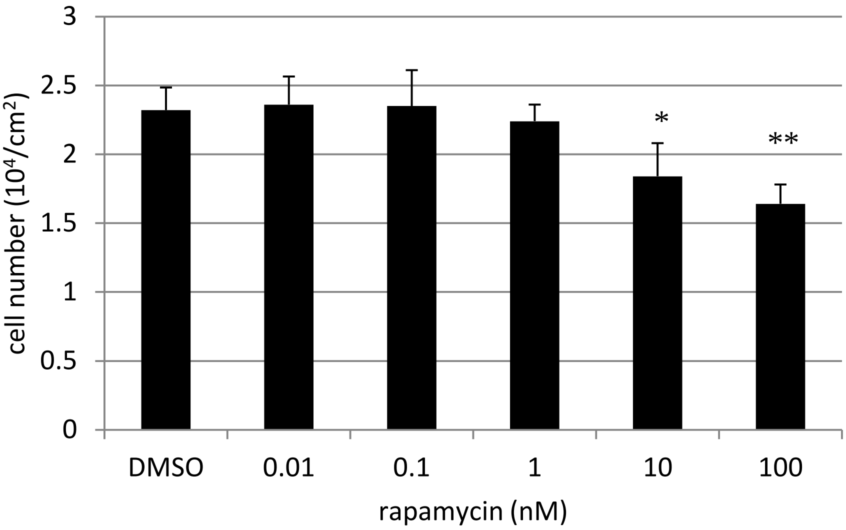

Fig. 3.3.2

Mouse embryonic stem cells (E14TGa2) were cultured in gelatin-coated T25 flasks with complete growth medium supplemented with 10^3 U/ml LIF. After 24h, triplicate cultures were treated with DMSO or rapamycin at the designated concentration and incubated for a further 24h. Cells were harvested and manually counted by trypin blue exclusion assay in haemocytometer counting chamber by phase contrast microscopy. Statistical differences from the DMSO treated control were determined by students T-test at an alpha level of $p<0.05$ (*) or $p<0.01$ (**), n=3.

Figure 3.3.3

Rapamycin treatment for 48h inhibits mES cell proliferation in a dose-dependent manner.

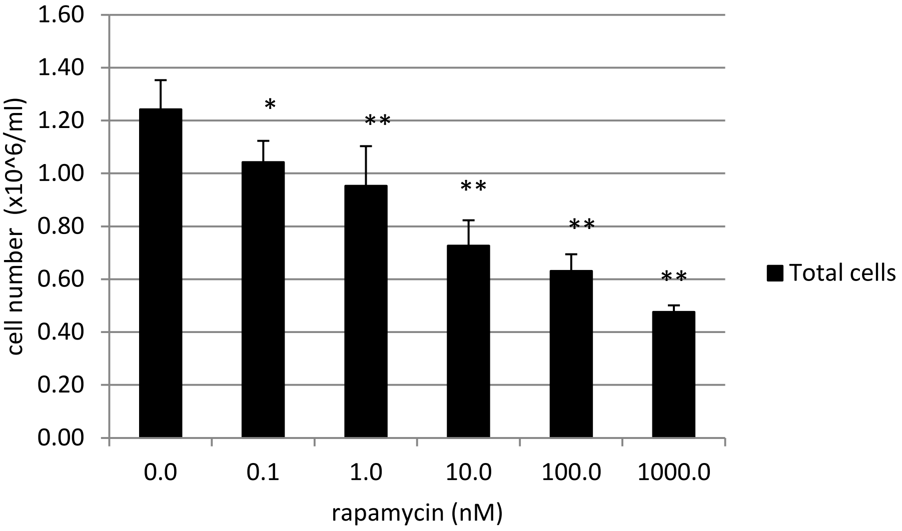

Fig. 3.3.3

Dose-dependent effect of rapamycin on mES cell proliferation. Single-cell suspensions of Mouse E14 tga2 cells were seeded into 6-well plates supplemented with complete growth medium containing 10^3 U/ml LIF. After an initial seeding period, cells were treated with DMSO or rapamycin at the specified concentrations. Cells were harvested and counted by trypin exclusion with the Vi-Cell™ counting system. Data is presented as the mean and standard deviation of three independent experiments (n=3). Statistical significance was determined by t-test (p<0.05 *, p<0.01 **).

The effect of rapamycin treatment on OCT4 expression was assessed by flow cytometry. Figure 3.3.4.1 shows that 72h treatment with rapamycin had no effect the percentage of GFP positive cells at any concentrations tested. Cellular GFP is transcribed from the promoter region of the OCT4 gene in these cells, therefore, levels of GFP protein is related to the transcription of OCT4 mRNA. Consequently, the level cellular of GFP may not precisely correlate with OCT4 protein levels. Mouse E14 cells were incubated with rapamycin and OCT4 expression was also assessed by immunostaining. Figure 3.3.4.2.i also shows that concentration of rapamycin did not alter the percentage of OCT4+ve mES cells. However, the mean intensity of cellular OCT4 expression increased in a dose-dependent manner. This is shown in Figure 3.3.4.2.ii.

The effect of rapamycin of the size of mES cells was assessed by flow cytometry. It was observed that 48h treatment with rapamycin significantly reduced mES cell size in a dose-dependent manner. Analysis was performed by flow cytometry, measurements were taken from the forward scatter channel and data is expressed as the mean and standard deviation of cell size. Differences in mES cell size were assessed by parametric t-test at and significance determined at the alpha level of $p<0.05$ (*) and $p<0.01$ (**).

Mouse E14 ES cells were selected for further investigation as the practicality of the culture system would afford greater precision and flexibility in the design and implementation of specific cellular and biochemical assays. Subsequently, mES cells were assayed for the levels and phosphorylation of mTOR and mTOR substrates under different culture conditions.

Figure 3.3.4.1

Rapamycin treatment does not alter OCT4/GFP expression in mES cells.

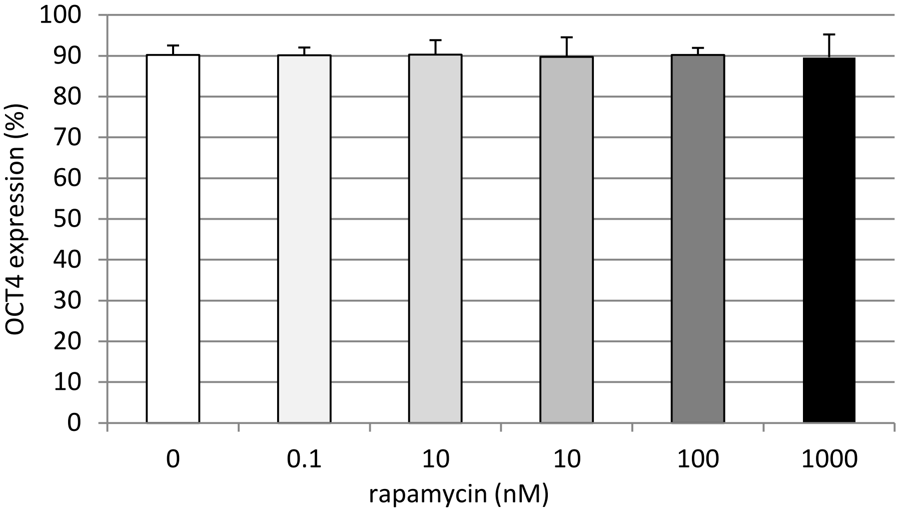

Fig 3.3.4.1

Mouse ES cells (E14-OCT4/GFP) were cultured in complete growth medium supplemented with 103u/ml LIF. Cells were treated for 48h with DMSO or rapamycin at the specified concentrations. Expression of OCT4 GFP was determined by flow cytometry using the Guava EasyCyte™ system. Channel gating was determined with parent E14 control cells. Data is expressed as the percentage of OCT4/GFP cells in suspension from triplicate experiments (n=3). Statistical analysis by parametric t-test revealed no differences between treatment groups.

Figure 3.3.4.2

Rapamycin increases the mean intensity of OCT4 expression in mES cells.

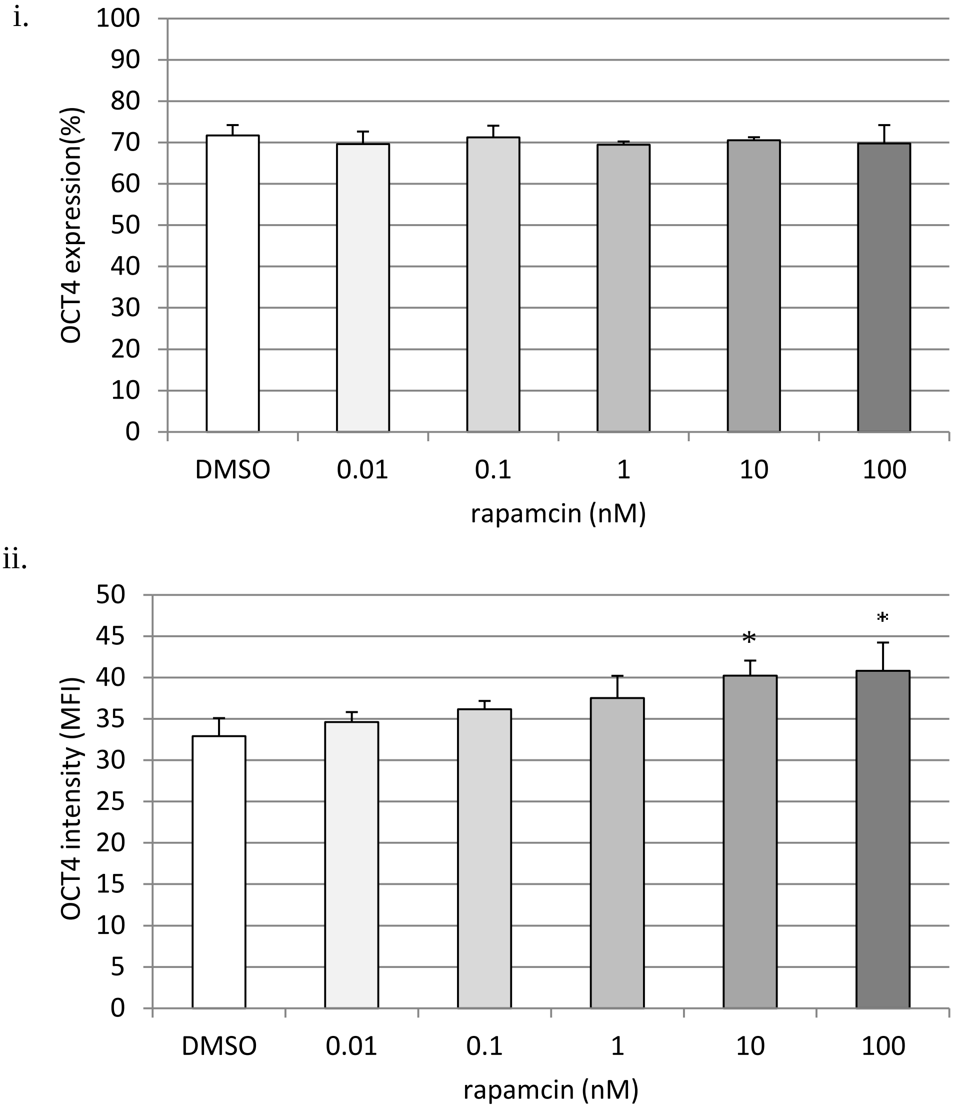

Fig.3.3.4.2

Flow cytometric analysis of OCT4 expression. Mouse E14 tga2 parental cells were cultured for 48h with DMSO or increasing concentrations of rapamycin. Cells were harvested, fixed with PFA and permeabilised before staining with OCT4 monoclonal antibodies and alexa-488 conjugated secondary antibodies. Percentage of OCT-4 +ve cells (i) and the mean intensity of OCT4 expression (ii) from triplicate cultures (n=3). Statistical analysis by paired-test (* $p<0.05$).

Figure 3.3.5

Rapamycin reduces the size of mES cells under normal growth conditions.

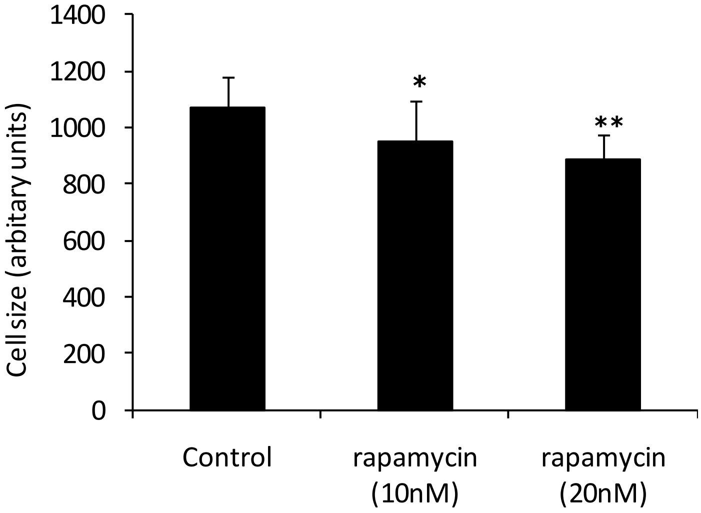

Fig 3.3.5

Mouse ES cells (E14-Tg2a) were treated with DMSO or rapamycin at the specified concentrations for 48h. Cells were harvested by enzymatic detachment and re-suspended in 1ml of dPBS containing 10% FCS. Triplicate cultures were analysed by flow cytometry and cell size determined from the linear forward scatter channel. Parametric t-test revealed statistical differences between DMSO and rapamycin treated cells at a level of $p<0.05$(*) and $p<0.01$(*), (n=3).

3.4 The effect of rapamycin on TORC1substrate phosphorylation.

This experiment was designed to assess the effect of rapamycin treatment on the levels of mTOR and the TORC1 substrate p70S6K in mES cell cultures. Figures 3.4.1.i and 3.4.1.ii show the effect of rapamycin treatment on total mTOR protein levels and TORC1 activity under normal culture conditions (lanes 1,2). Rapamycin treatment exerted no effect on total mTOR protein levels after 48h. The activity of the TORC1 kinase was assessed by levels of phosphorylation of p70S6K at the threonine-389 residue.

Treatment with rapamycin for 48h inhibited the phosphorylation of p70S6K th389. The effect of medium supplementation and rapamycin treatment for 1h was also assessed after 48h of normal growth (lanes 3, 4). Supplementing cultures with fresh growth medium increased the phosphorylation of p70S6K and 1h rapamycin treatment inhibited this effect. Total levels of mTOR protein were unaffected. These findings confirm that in mES cells, rapamycin treatment inhibited the basal and induced phosphorylation of p70S6K. As rapamycin is known to be a specific inhibitor of the TORC1 complex it was inferred that the phosphorylation of p70S6K at th389 is mTOR dependent in mES cells and this phosphorylation is an effective read-out of TORC1 activity.

The mTOR complex 2 has been shown to directly phosphorylate the serine-473 residue of the PI3K pathway protein AKT. Thus, the serine-473 phosphorylation of AKT is considered a reporter of TORC2 kinase activity. Figure 3.4.1.iii shows the effect of rapamycin treatment and medium supplementation on the phosphorylation of the AKT serine-473. Medium supplementation increased this phosphorylation independently of rapamycin treatment.

Figure 3.4.1

Rapamycin inhibits the phosphorylation of the TORC1 substrate p70S6K.

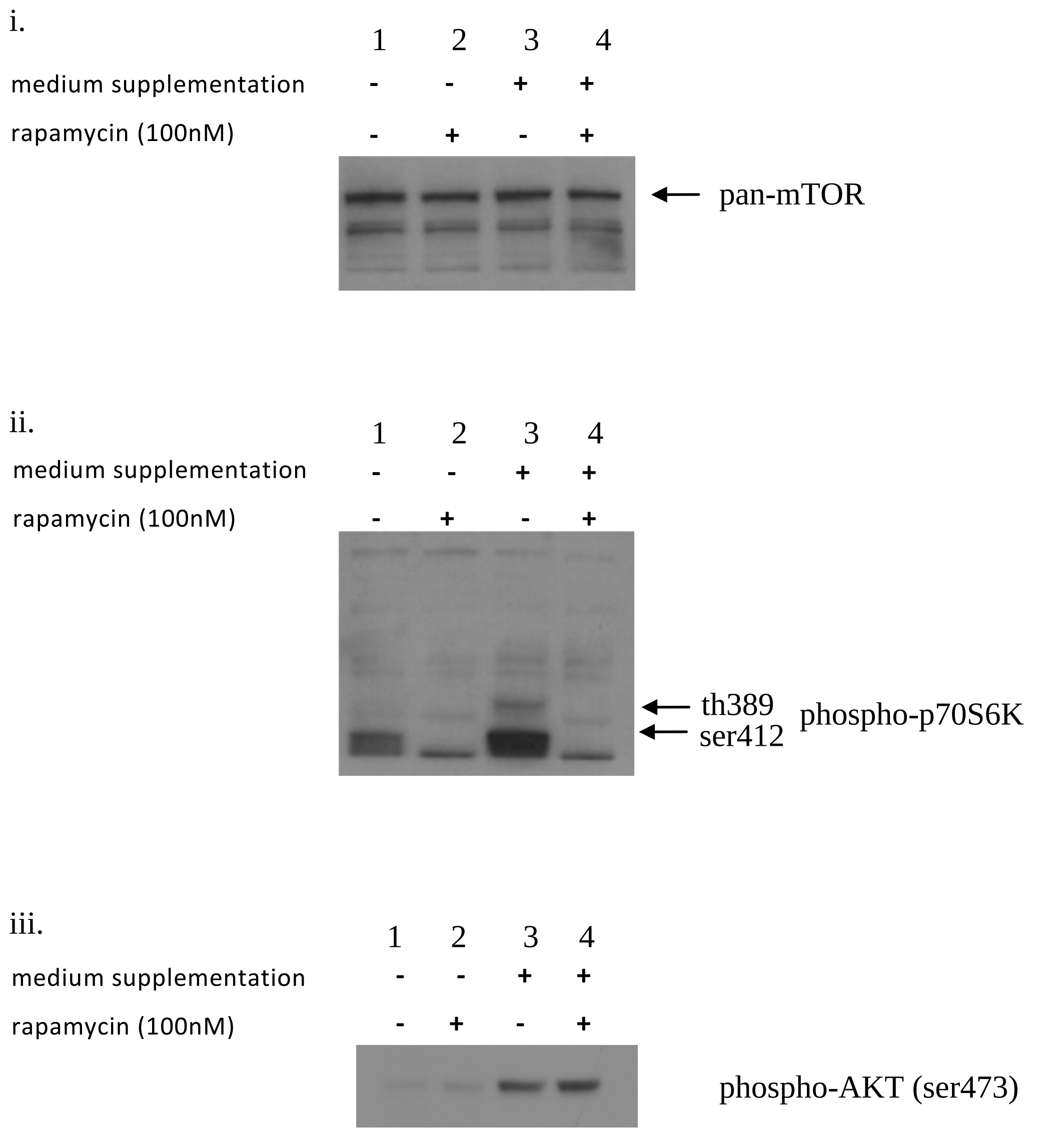
i.
1 2 3 4
medium supplementation - - + +
rapamycin (100nM) - + - +
pan-mTOR
ii.
1 2 3 4
medium supplementation - - + +
rapamycin (100nM) - + - +
th389
ser412
phospho-p70S6K
iii.
1 2 3 4
medium supplementation - - + +
rapamycin (100nM) - + - +
phospho-AKT (ser473)

Figure Legend

Fig.3.4.1

Gel electrophoresis and western blot of mouse ES cell lysates probed for pan-mTOR (i) and phosphorylated p70S6K th389 (ii) with rabbit anti-mouse monoclonal antibodies and HRP-conjugated anti-rabbit secondary antibodies. Immunoreactivity bands were visualised by enhanced chemiluminescence on x-ray sensitive film. Cells were cultured for 48h in complete growth medium containing DMSO or 100nM rapamycin (lanes 1,2) or 47h in complete growth medium followed by supplementation for 1h with fresh medium containing DMSO or 100nMl rapamycin. Representative images from 2 independent experiments are displayed.

3.5. The effect of rapamycin on TORC2 substrate phosphorylation.

The relationship between the activity of the TORC1 and TORC2 kinases remains unclear. Reports indicate that inhibition of mTORC1 with rapamycin results in the compensatory phosphorylation of AKT at serine residue 473[72]. This implies that that the two TORC complexes may compete for free mTOR protein. However, extended rapamycin treatment does inhibit this serine-473 phosphorylation in some cell types[115,116].

To assess the effect of extended rapamycin treatment on AKT serine-473 phosphorylation in mES cells, cultures were treated for 48h with medium containing or devoid of serum. At the designated time-point cells were harvested and protein lysates were separated by gel electrophoresis and subjected to immunoblotting for total mTOR protein and phospho-AKT ser473.

Figure 3.5.1 shows the effect of rapamycin treatment on total mTOR protein levels and phospho-AKT ser473 in representative immunoblots. Quantification of band density was performed from triplicate data with the ImageJ gel analyser tool (Figure 3.5.2). Optical density measurements of phospho-AKT levels were normalised with mean total-mTOR levels for each lane. Whereas rapamycin treatment marginally increased AKT ser473 phosphorylation (1-2 fold increase), this effect was exacerbated in serum-free conditions (3-4 fold increase). Thus, rapamycin treatment for 48h resulted in a dose-dependent increase in the phosphorylation of the TORC2 substrate AKT ser473, an effect that is impaired by serum.

Figure 3.5.1

The effect of rapamycin treatment on TORC2 kinase activity.

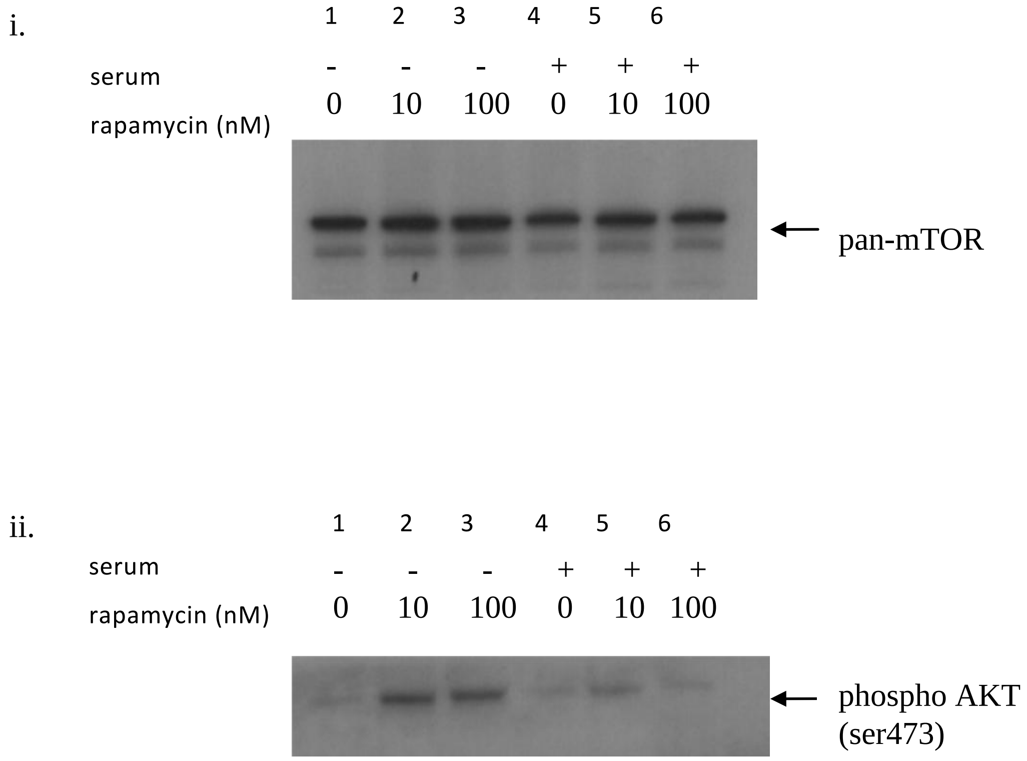
i.
1 2 3 4 5 6
serum
- - - + + +
rapamycin (nM)
0 10 100 0 10 100
pan-mTOR
ii.
1 2 3 4 5 6
serum
- - - + + +
rapamycin (nM)
0 10 100 0 10 100
phospho AKT
(ser473)

Fig.3.5.1

Mouse ES cells were seeded into 6 well plates and cultured with complete growth medium containing LIF. After an initial attachment period, cultures were either starved of FCS (lanes 1-3) or supplemented with 10% FCS (lanes 4-6) for the duration of the incubation. Cells were treated with DMSO or rapamycin at a concentration of 10nM or 100nM. After 48h cells were harvested and lysed for protein extraction. Proteins were separated by gel electrophoresis and specific protein bands identified by western blotting and immunostaining with monoclonal antibodies for pan-mTOR (A) or phospho-AKT ser473 (B). Representative immunoblots from three independent experiments are presented (n=3).

Figure 3.5.2

Rapamycin treatment increases phospho-AKT ser473 during serum starvation and normal culture.

i. Relative expression of total mTOR.

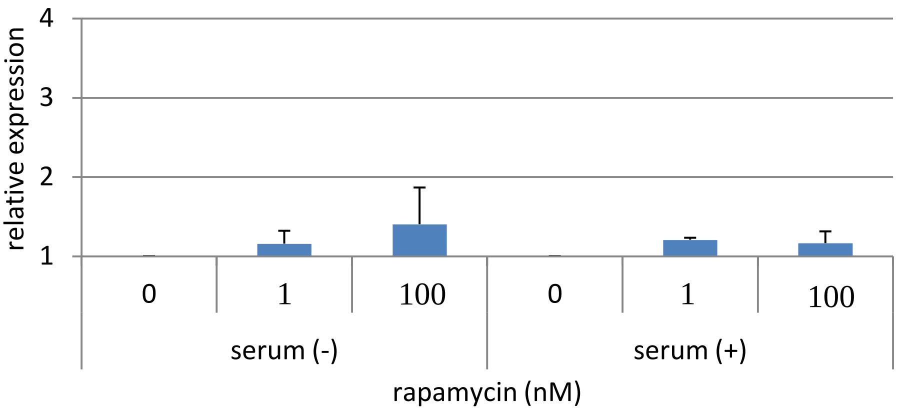

ii. Relative expression of phospho-AKT ser 473.

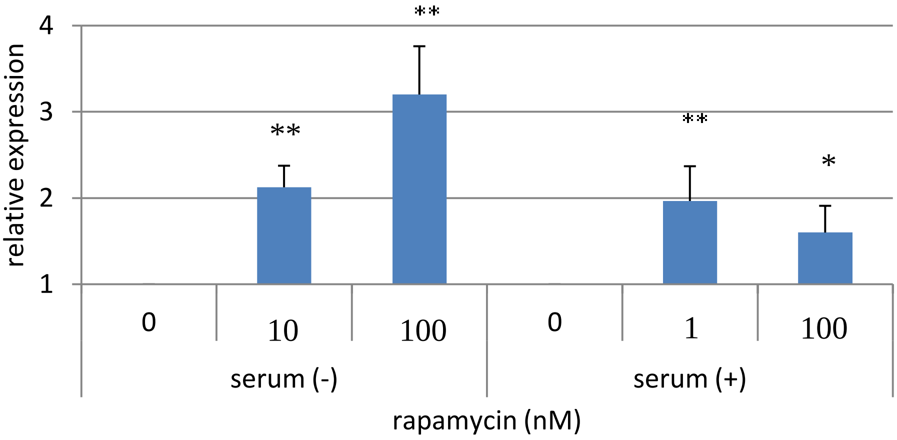

Figure legend.

Fig.3.5.2

Immunopositive bands from triplicate blots were quantified with the ImageJ gel analyser tool and represented graphically as expression relative to DMSO control. Data is expressed as the mean and standard deviation from three independent experiments (n=3). The mean levels of total mTOR protein for each condition were utilised to normalise AKT serine473 levels. Data is presented as fold increase in optical density relative to the DMSO treated control.

3.6 Activation of the mTOR pathway during *in vitro* culture.

The proliferation and pluripotency of mouse embryonic stem cells *in vitro* is maintained by regular passaging every 48h. Parental E14-Tg2a cells were grown on Iwaki brand tissue culture plastic with GMEM growth medium supplemented with 10% FCS and 10^3 u/ml LIF. It was observed that under these conditions regular passaging by enzymatic detachment maintained both cell expansion rate and colony morphology.

It is not known what effect the passage cycle has on activity of the mTOR pathway. To explore this, mES cells were expanded in T-25 flasks under normal culture conditions for 48h and protein lysates were taken at specific time-points over following passage cycle (Fig 3.6). The first sample was taken prior to enzymatic detachment (A), remaining cultures were then detached and seeded into fresh gelatinised flasks and harvested after a further 2h (B), after 24h (C) and 48h. Protein was purified from cell lysates and equal quantities loaded into Tris-HCL gels and separated by electrophoresis. The total level of mTOR protein and phosphorylated mTOR ser2448, ser2481 or p70S6K th389 was determined by western blotting

Figure 3.6 demonstrates that the total level of mTOR protein did not change over the course of the passage cycle (i). Phosphorylation of mTOR at serine 2448 (ii) and serine 2481 (iii) were also not altered by passaging. Levels of p70-S6K phosphorylation at th389 were low after 48h culture and directly before passaging (A). Phosphorylation of S6K then increased steadily at 2h (B), peaked at 24h (C) and then reduced by 48h (D). These findings demonstrate that the activity of mTORC1 varies over the passage cycle.

3.7 The effect of rapamycin treatment on the PI3K and MAPK pathways.

The mTOR pathway is closely integrated with PI3K signaling and AKT phosphorylation Figure 3.7 shows the impact of TORC1 inhibition on the phosphorylation of the th308 residue (T-loop) and the hydrophobic motif ser473 (HM). PI3K mediated signalling at the cell membrane in response to growth factors such as LIF initiates the T-loop phosphorylation by PDK1. The HM phosphorylation is mediated by putative PDK2 enzymes such as TORC2. Data shown suggests that mTOR inhibition affects both AKT phosphorylation events. Activation of the MAPK pathway is initiated by receptor tyrosine kinases at the cell membrane, culminating in the phosphorylation of extracellular signal-related kinase (ERK) proteins. The growth factor LIF is an agonist of ERK phosphorylation via this pathway. Figure 3.7 shows the impact of rapamycin treatment on ERK1/2 phosphorylation from two independent cell culture experiments Rapamycin treatment induced the phosphorylation of both the p42 and p44 subunits of ERK1 and ERK2 respectively (i). This effect was dependent upon the dose of rapamycin and was exacerbated by serum deprivation (ii).

Figure 3.6

Levels of total and phosphorylated mTOR protein during in vitro culture.

i. Total mTOR.

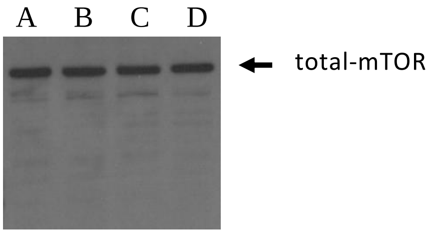
A
B
C
D
total-mTOR

ii. Phospho-mTOR ser 2448.

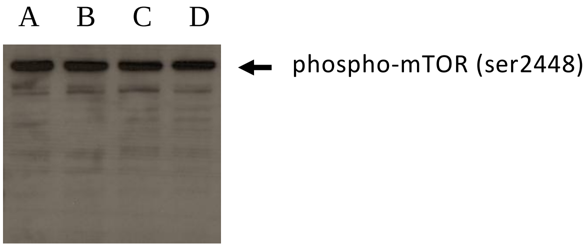
A
B
C
D
phospho-mTOR (ser2448)

iii. Phospho-mTOR ser2481.

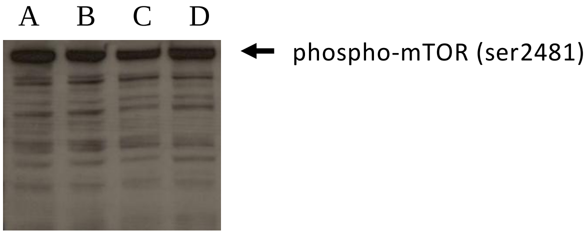
A
B
C
D
phospho-mTOR (ser2481)

iv. Phospho-p70-S6K th389

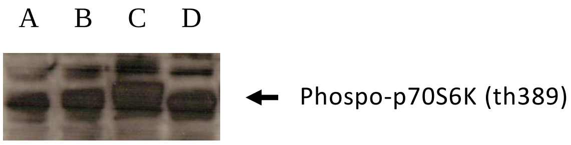
A
B
C
D
Phospo-p70S6K (th389)

Figure legend.

Fig. 3.6

The phosphorylation of mTOR pathway proteins in mouse E14 tga2 ES cells was assessed by western blotting over passage cycle. Cells were cultured in T25 flasks for 48h and harvested for protein extraction (A), and 2h after enzymatic detachment (B), after 24h growth (lane C) and 48h growth (D). Proteins were separated by gel electrophoresis; immunoblotting was performed to assess the levels of mTOR protein (i) and phosphorylation of mTOR at serine 2448 (ii), serine residue 2481 (iii) and p70S6K (iv) during the passaging cycle. Representative plots of 3 independent culture experiments (n=3).

Figure 3.7

Rapamycin treatment increases ERK1/2 and reduces AKT th308 phosphorylation in serum starved mES cells.

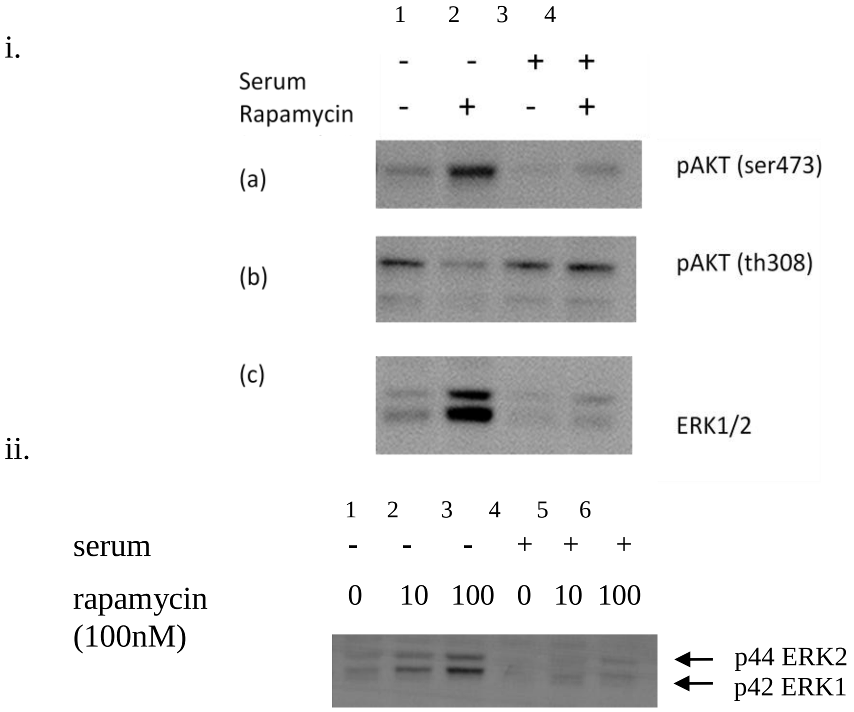
i.
1 2 3 4
Serum - - + +
Rapamycin - + - +
(a)
pAKT (ser473)
(b)
pAKT (th308)
(c)
ERK1/2
ii.
1 2 3 4 5 6
serum - - - + + +
rapamycin (100nM) 0 10 100 0 10 100
p44 ERK2
p42 ERK1

Fig.3.7

Mouse ES cells were seeded into 6 well plates and cultured with complete growth medium containing 103 u/ml LIF. After an initial attachment period, cultures were either starved (i; lanes 1,2; ii; lanes 1-3 or supplemented with 10% FCS (lanes 4-6) for the duration of the incubation. Cells were treated with DMSO or rapamycin at a concentration of 10nM or 100nM. After 48h cells were harvested and lysed for protein extraction. Proteins were separated by gel electrophoresis and specific protein bands identified by western blotting and immunostaining with monoclonal antibodies for AKT ser473 (i.a), AKT-th308 (i.b) or p42 ERK1 or p44 ERK2 (i.c; ii). Representative immunoblots from three independent experiments are presented (n=3).

3.8 Summary of findings

In this chapter, the practical applicability of the *in vitro* culture of three cell lines was assessed. The principle aim was to identify a suitable system to enable the investigation into the cellular distribution and localisation of mTOR pathway proteins. Human embryonic stem cells (hES), embryonal carcinoma cells (EC) and mouse ES cells (mES) were cultured according to established protocols and the limitations of each system was assessed.

Human Shef3 embryonic stem cells were available within the laboratory. This cell line exhibited a stable phenotype over extended culture. Expansion and pluripotency of these cells was dependent upon co-culture with mitotically inactivated mouse embryonic fibroblasts. At the time of this investigation, these cells had not been adapted to culture without feeder cells and were refractory to enzymatic passaging. Consequently, sub-culture and expansion required manual passaging by mechanical microdissection. This method involved visual selection of stem cell colonies, which were then cut by hand under a dissection microscope. Suspensions containing irregular clumps of cells were then seeded into fresh culture flasks. Passaging by microdissection therefore does not control for variables such as colony size and so the seeding density of Shef3 hES cells could not be precisely regulated. Recently, Shef3 hES cells have been adapted to feeder-free culture with a combination of extracellular matrix proteins and a defined medium formulation[117]. However, this system was not available at the time of this study. Inactivated feeders secrete factors that support hES self-renewal[111] but contamination of mEF derived growth factors in cell lysates from hES cultures was a concern as it may have obscured the molecular analysis of signal pathways.

It was noted that the pluripotency marker OCT4 was present in hES colonies, but not in feeder cells (MEF) alone or in co-culture with hES. Its expression related to colony morphology in that compact cells exhibited greater OCT4 expression than morphologically distinct spread cells present at the colony edges. This observation is consistent with expectations as OCT4 is central to the maintenance of the pluripotent phenotype[42, 119], and the classical stem cell morphology is lost upon lineage-specific differentiation.

In this study, the level of OCT4 staining in individual cells from hES colonies expressing OCT4. Expression of OCT4 in single cells did not correlate with local cell density or individual nuclear size. The morphology of hES colonies may serve as a preliminary indicator of pluripotency. This morphological assessment is widely used for the selection of colonies for sub-culture, thus, the maintenance of pluripotency during *in vitro* expansion is influenced by a subjective process during passaging. The relationship between spatial organisation of cells and pluripotent marker expression in mouse ES cells was studied by Zandstra *et al*[120]. It was found that mouse ES cells formed an autoregulatory niche whereby densely packed cells supported the maintenance of pluripotent marker expression independently of growth factor stimulation. Paracrine signalling from adjacent cells may also contribute to the maintenance of the stem cell phenotype.

Although human embryonal carcinoma cells do not require co-culture with feeder cells, mechanical dissociation is necessary for sub-culture and expansion. This is performed by gently shaking sterile glass beads within the culture flask to detach the cells from the surface. This culture system has disadvantages as the sizes of individual clumps produced by this process cannot be regulated and mechanical detachment may damage the cells.

Another problem with EC cells arises from the heterogeneity in the differentiation capacity of clonal lines[9]. Human EC cells were documented to exhibit variability in their differentiation capacity[11], and the N-Tera2 line investigated here, have been reported to exhibit restricted lineage specific differentiation *in vitro*[109]. Although these cells were found to be sensitive to mTOR inhibition, the analysis of embryonal carcinoma cells was not pursued further.

The E14-Tga2 mES cell line proliferates rapidly *in vitro* and can be sub-cultured by enzymatic treatment. These cells were observed to form monolayers when cultured with growth medium supplemented with LIF and 10% serum and plated on Iwaki™ tissue culture plastic. Monolayer growth was a desirable characteristic as the homogeneous distribution of cells may restrict niche development and monolayer cells are useful for microscopic imaging.

The current investigation documented that effect of rapamycin treatment exhibited a dose- and time- dependent inhibition of proliferation. Treatment with rapamycin for 72h did not reduce OCT4-GFP levels. As this may have been due to the persistence of GFP in the cells after OCT4 levels had declined, levels of OCT4 were also assessed by immunostaining. It was found that rapamycin did not affect the number of OCT4 positive cells but did increase the mean fluorescence intensity of OCT4 staining. In a report that showed concordance between OCT4 and GFP levels, it was noted that as the percentage of OCT4-positive cells increased, the standard deviation of the mean also increased[122]. This suggests that GFP is not an accurate indicator of OCT4 levels in pluripotent cells.

Treatment of mouse ES cells with rapamycin for 48h significantly reduced cell size. That rapamycin had this effect was anticipated as this has been demonstrated in other cell types[123], and is consistent with the documented role of TORC1 in cell growth.

Embryonic stem cells are typically characterised by their morphology as they are smaller than most somatic cells. Mouse ES cells also exhibit a large nuclear to cytoplasmic ratio and maintain a compact spherical morphology in dense colonies. These cells may therefore have less requirements for cell growth after each round of division than do many large somatic cells. It has been reported that the amount of total protein in mES cells increases upon differentiation[124] as do mRNA transcript levels[125]. Cellular differentiation requires the expansion of the cytoplasmic compartment and production of new proteins that confers phenotype and function. It has previously been reported that rapamycin reduces the size of mES cells.

When mES cells were stimulated with fresh growth medium containing LIF and serum, the phosphorylation of the TORC1 substrate p70S6K at the threonine 389 residue increased. During normal culture, passaging and medium replacement is scheduled every 48h. By this time mTOR activation declined indicating that key nutrients or growth factors may be depleted. Given that TORC1 inhibition with rapamycin impaired the proliferation of mouse ES cells in this study and other published investigations[111] it is possible that the expansion of mES cells may be enhanced by optimising mTOR activation. The conclusions drawn here are supported by the observation that the levels of phospho-S6K (th389) modulated over the course of the passage cycle.

Medium supplementation also increased the phosphorylation of the mTORC2 substrate AKT (ser473), an effect that was promoted by rapamycin and potentiated by serum deprivation. The phosphorylation of ERK in response to rapamycin treatment was also potentiated by serum withdrawal.

The primary aim of this aspect of the study was to characterise the pluripotent cell systems for further investigation of the mTOR pathway. The use of human ES cells was limited by their dependence upon co-culture with mouse embryonic fibroblasts. Furthermore, mechanical dissociation of cell clumps is required for sub-culture and expansion. The human ES cell line available at this time was refractory to enzymatic passaging and retained an inherent dependence on the stem cell niche to maintain self-renewal.

Human embryonal carcinoma cells do not require co-culture to maintain their phenotype. They were found to be sensitive to the growth inhibitory effects of rapamycin, however, as they are also refractory to enzymatic passaging and require mechanical dissociation with glass beads for sub-culture. This process may damage cells and introduce undesirable variables into the system. Moreover, EC cells are by their nature cancer progenitor cells that exhibit a stem cell phenotype.

The E14 line of mouse ES cells have been extensively characterised by others and exhibit three key features. They are pluripotent in nature, do not require co-culture with feeder cells and can be passaged by enzymatic dissociation and seeded as single cells. Preliminary experiments revealed that these mES cells were sensitive to the anti-proliferative effects of rapamycin. Treatment with rapamycin inhibited the phosphorylation of the TORC1 substrate and increased the phosphorylation of the TORC2 substrate AKT. These findings confirm that the basic regulation of the mTOR pathway in mES cells operates in a similar fashion to other mammalian cells.

The secondary aim of this chapter was to characterise the experimental conditions for the manipulation of the mTOR pathway in pluripotent cells *in vitro*. The use of rapamycin as an mTOR inhibitor in ES cells was confirmed and the effect concentration and incubation time on cell proliferation documented. It is clear from the data presented within this chapter that rapamycin is an effective inhibitor of ES cell proliferation in a concentration- and time-dependent manner.

Additionally the activation of the mTOR pathway in mouse ES cells during the normal passage cycle was characterised. Results generated suggest that over the 48h passage cycle the activation of mTOR pathway is not uniform and exhibits maximal activation after 24h post-seeding and sub-maximal activation after 48h. Thus it is concluded that regular nutrient supplementation may be necessary to ensure that mTOR activity and consequently cellular proliferation is optimised. During the expansion of embryonic stem cells mTOR activation should be maintained to optimise cell expansion rate.

Chapter 4

The principle objective of this chapter is to further characterise the mTOR pathway in mouse embryonic stem cells with an emphasis on the distribution and localisation of components and substrates of the two mTOR complexes, mTORC1 and mTORC2. Better understanding of the spatio-temporal regulation of the two mTOR complexes in ES cells may aid in selective targeting of the proliferative and cell growth-promoting effects of this pathway. This would be advantageous as pluripotent cells exhibit rapid proliferation with little requirement for cell growth whereas cell growth is increasing important for cell specification during differentiation.

4.1 The cellular distribution of phosphorylated mTOR in mES cells.

Mouse ES cells were cultured for 48h and then fixed, permeabilised and stained with monoclonal phosphospecific antibodies and AlexaFluor-conjugated secondary antibodies, nuclear counterstaining was visualised with DAPI. Analysis was performed by phase-contrast, fluorescence and confocal microscopy. Further details of the immunostaining and image capture protocols are documented in Experimental Methods.

Figure 4.1.1 shows that mES cells expressed mTOR protein and distinct staining was observed in the nuclear compartment. Figure 4.1.2 shows that phospho-mTOR ser2448 was not uniformly distributed in these cells. Representative cropped images are of single cells are presented in Figure 4.1.3. The level of phospho-mTOR in cells at interphase (i) appeared lower than during mitotic prophase (ii) and metaphase (iii).

Similar analysis was performed to assess the distribution of the phospho- mTOR ser2481 (Figure 4.1.4). Staining was not uniform and some cells exhibited strong nuclear phosphorylation (red triangles). Cropped enlargements of individual cells highlight these staining patterns (Figure 4.1.5). Distinct phosphorylation patterns were observed in mitotic cells. Cropped enlargements of single cells at metaphase (iii; white triangles), anaphase (iv), and telophase (v). Phospho-mTOR ser2481 was localised to midbody of dividing cells (vi; red triangle). These observations show that the phosphorylation of mTOR protein is not uniformly distributed in mES cells in culture and phospho-mTOR ser2481 exhibits distinct patterning within cells at specific stages of mitosis.

Figure 4.1.1

The cellular distribution of native mTOR in mES cells in vitro.

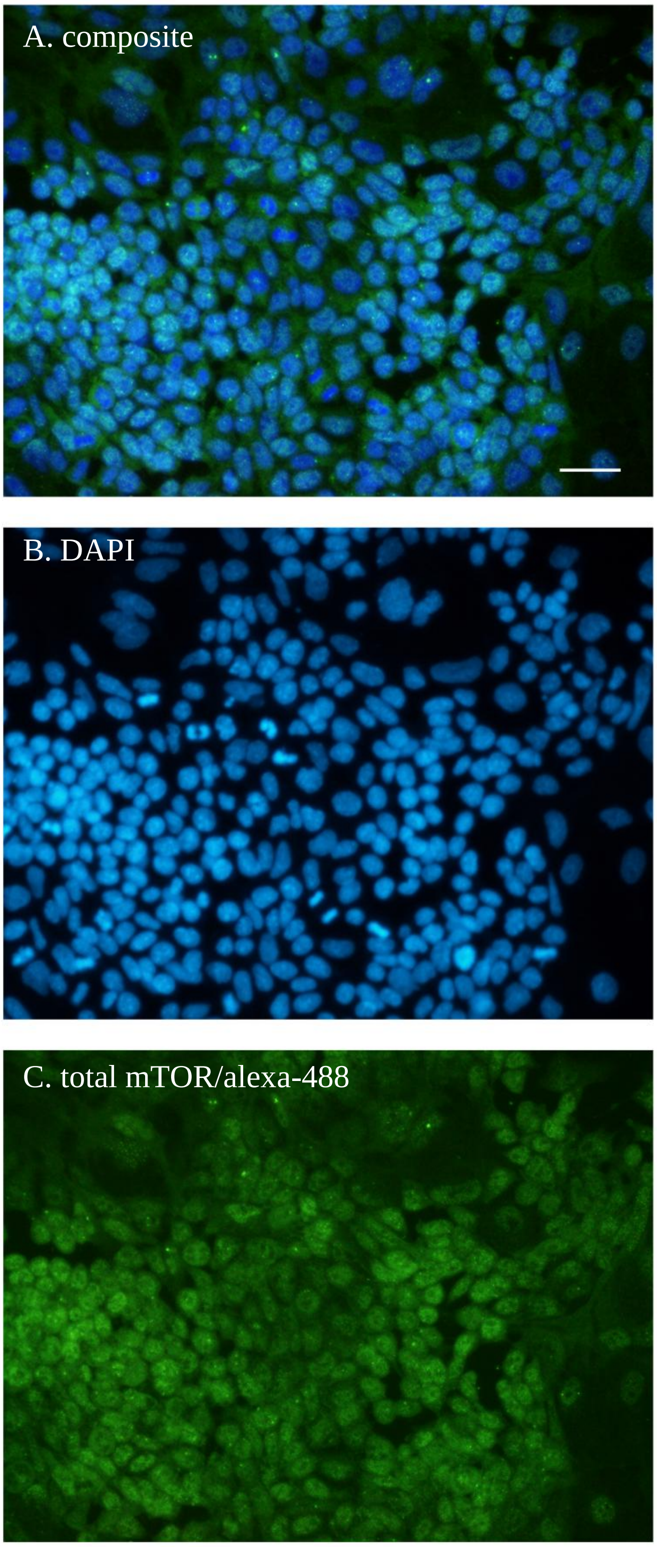

Fig.4.1.1

Representative micrographs of the cellular distribution of total mTOR protein. Merged composite (A) of DAPI (B) and pan-mTOR fluorescence (C) in mES cells under standard culture conditions. Mouse ES cells were cultured for 48h then fixed and permeabilised prior to staining with rabbit anti-mouse IgG monoclonal antibodies. Specific staining was visualised by anti-rabbit Alexa-488 secondary antibodies by fluorescence microscopy. Non-specific staining was assessed with IgG isotype control antibodies (not shown). Representative images from at least 3 independent culture assays. (50µm scale bar)

Figure 4.1.2

Cellular distribution of phospho-mTOR at serine residue 2448 in mES cells.

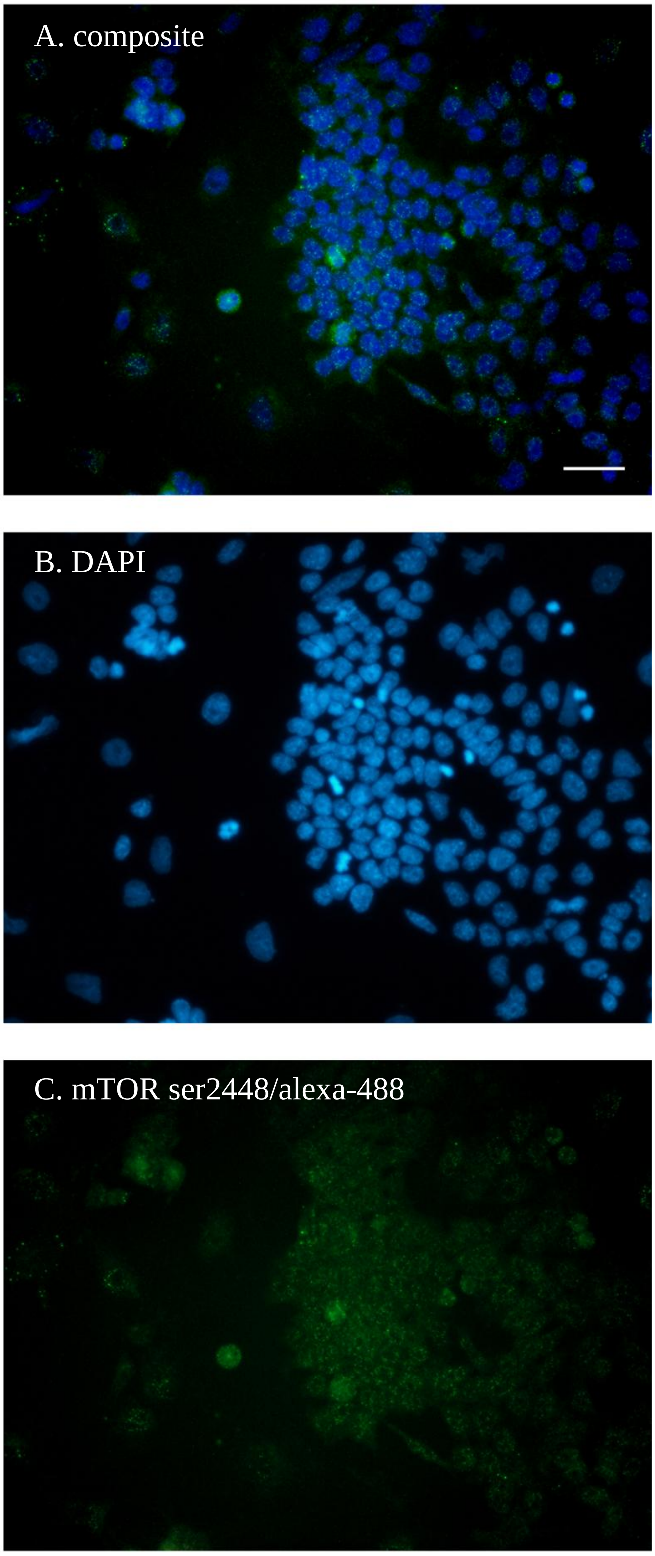

Fig.4.1.2

Representative micrographs of the cellular distribution of total mTOR protein in mES cells. Merged composite (A) of DAPI (B) and phospho-mTOR serine 2448 fluorescence (C) in mES cells under standard culture conditions. Mouse ES cells were cultured for 48h then fixed and permeabilised prior to staining with rabbit anti-mouse IgG monoclonal antibodies. Specific staining was visualised by anti-rabbit Alexa-488 secondary antibodies by fluorescence microscopy. Non-specific staining was assessed with IgG isotype control antibodies (not shown). Representative images from at least 3 independent culture assays. (50µm scale bar)

Figure 4.1.3

Mitotic phosphorylation of mTOR at serine 2448 in mES cells.

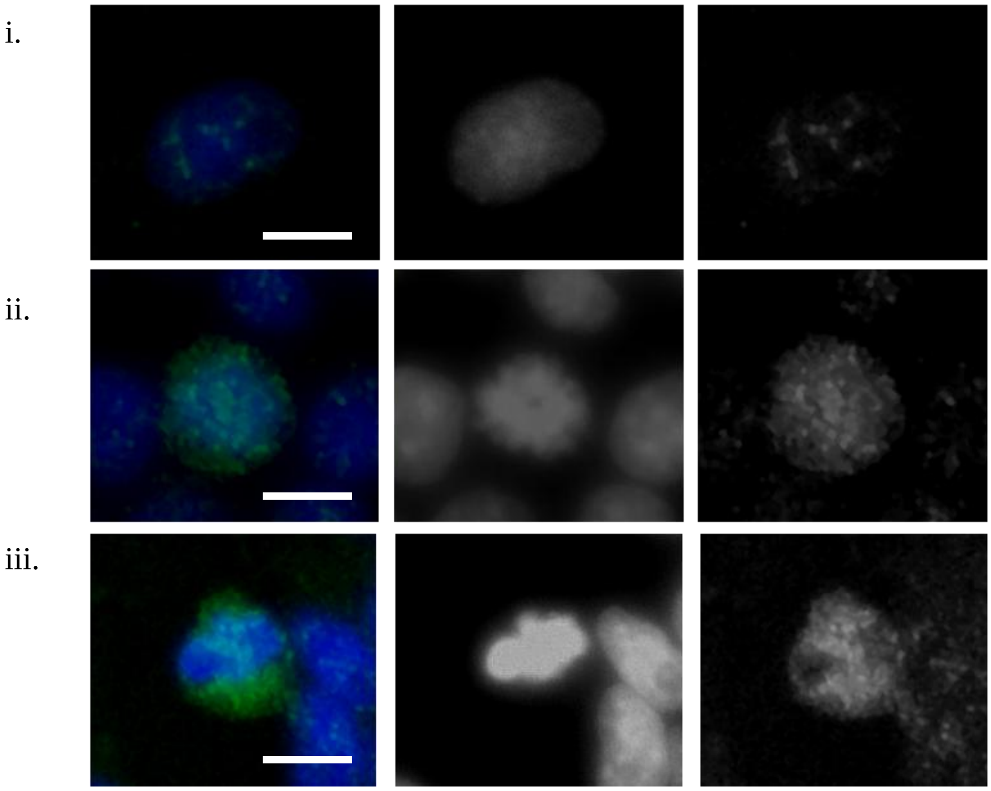

Fig. 3.8.3

Merged composite (A) of cropped images at 100% magnification from micrographs of fixed mES cells stained with DAPI (B) and anti-mTOR serine 2448 monoclonal antibodies(C). Cell cycle phase was determined by visual inspection of nuclear condensation from DAPI micrographs. Panels show cellular expression of phospho-mTOR at interphase (i), prophase (ii) and metaphase (iii). Representative images of single cells from micrographs from at least 3 independent culture assays. 5µm scale bar.

Figure 4.1.4

Non-uniform distribution of phospho-mTOR serine-2481 in mES cells.

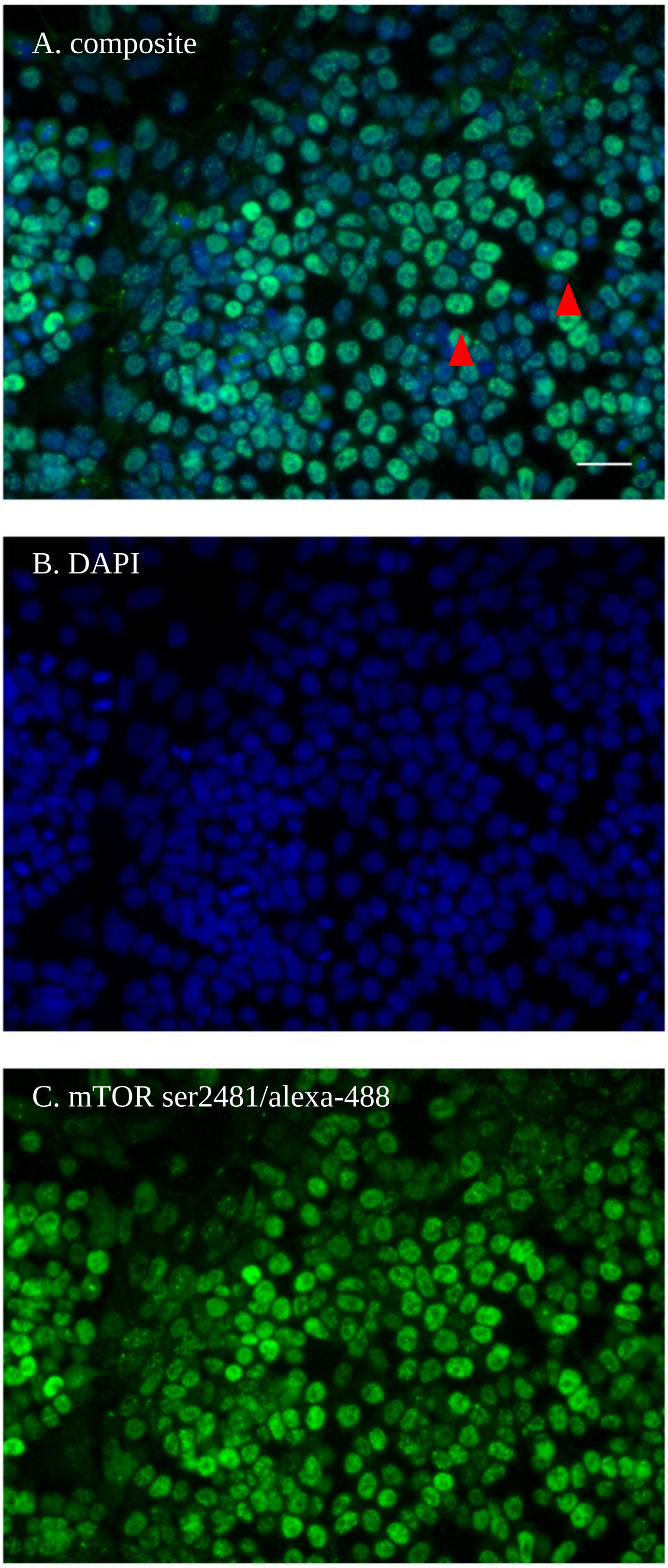

A. composite

B. DAPI

C. mTOR ser2481/alexa-488

Fig.3.8.2

Representative micrographs of the cellular distribution of phospho-mTOR at ser2481. Merged composite (A) of DAPI (B) and mTOR ser2481 fluorescence (C) in mES cells. Mouse ES cells were cultured for 48h and stained with rabbit anti-mouse IgG monoclonal antibodies. Specific staining was visualised by anti-rabbit Alexa-488 secondary antibodies imaging by fluorescence microscopy. Non-specific staining was assessed with IgG isotype control antibodies (not shown). Representative images from at least 3 independent culture assays. (50µm scale bar)

Figure 4.1.5

Nuclear localisation and mitotic phospho-mTOR serine-2481 in mES cells.

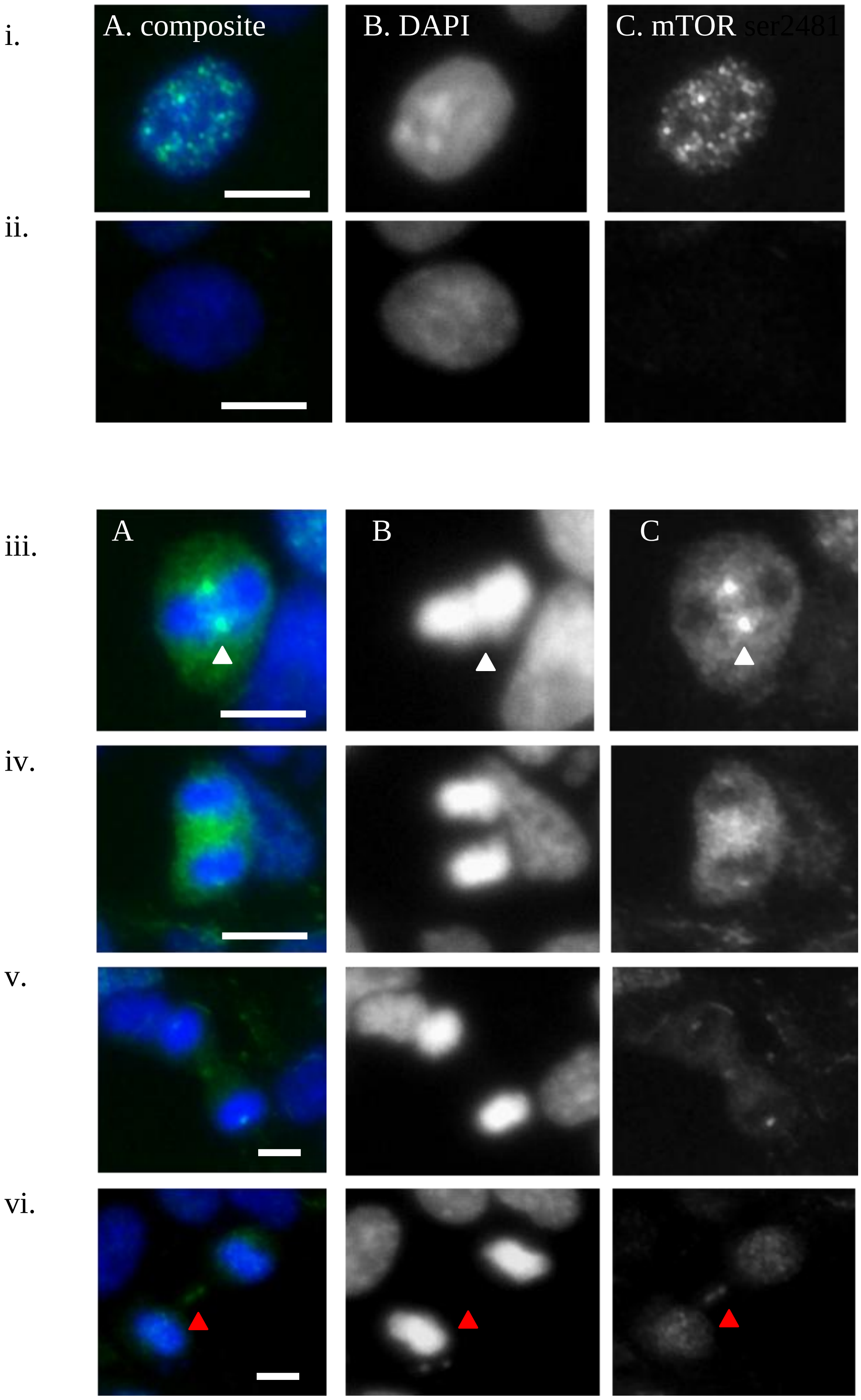
i.
A. composite
B. DAPI
C. mTOR ser2481
ii.
iii.
A
B
C
iv.
v.
vi.

Figure legend.

Fig. 4.1.5

Cropped enlargements of single cells from micrographs of mES cells. Merged composite (A) of DAPI (B) and phospho-mTOR ser2481 (C). Distribution of mTOR ser2481 is not uniform in equivalent cells (i, ii). Intracellular localisation of phospho-mTOR at metaphase (iii, white triangle), anaphase (iv), telophase (v) and cytokinesis (vi, red triangle). Representative images of single cells from at least 3 independent culture assays. white line represents scale (50µm).

To document the cellular distribution and localisation of phospho-mTOR ser2481 in mES-derived cells during early differentiation, mES cells were cultured without LIF for 48h. Cultures were then fixed and stained with DAPI and phosphospecific antibodies. Withdrawal of LIF induces the spontaneous differentiation of mES cells but many cells retain their stem cell phenotype as paracrine signaling may support pluripotency. Therefore, compact colonies were present alongside spread, differentiated cells

Figure 4.1.6 shows a representative micrograph of mES cells stained with phospho-mTOR ser2481 monoclonal antibodies. Examination of this image revealed that compact colony morphology was retained in some areas (white triangle). Large cells with spread morphology were also present (red triangle). These morphologically distinct cells are identified by an increased cell area and reduced nuclear to cytoplasmic ratio. There were differences in the intracellular localisation of phospho-mTOR ser2481 in cells exhibiting this spread morphology with localisation at cell borders. This staining pattern is indicated by yellow triangles. Spread cells undergoing mitosis also exhibited increased staining for phospho-mTOR, consistent with the observations made in compact mES cells.

Figure 4.1.6

Localisation of phospho-mTOR serine 2481 in cells during early differentiation.

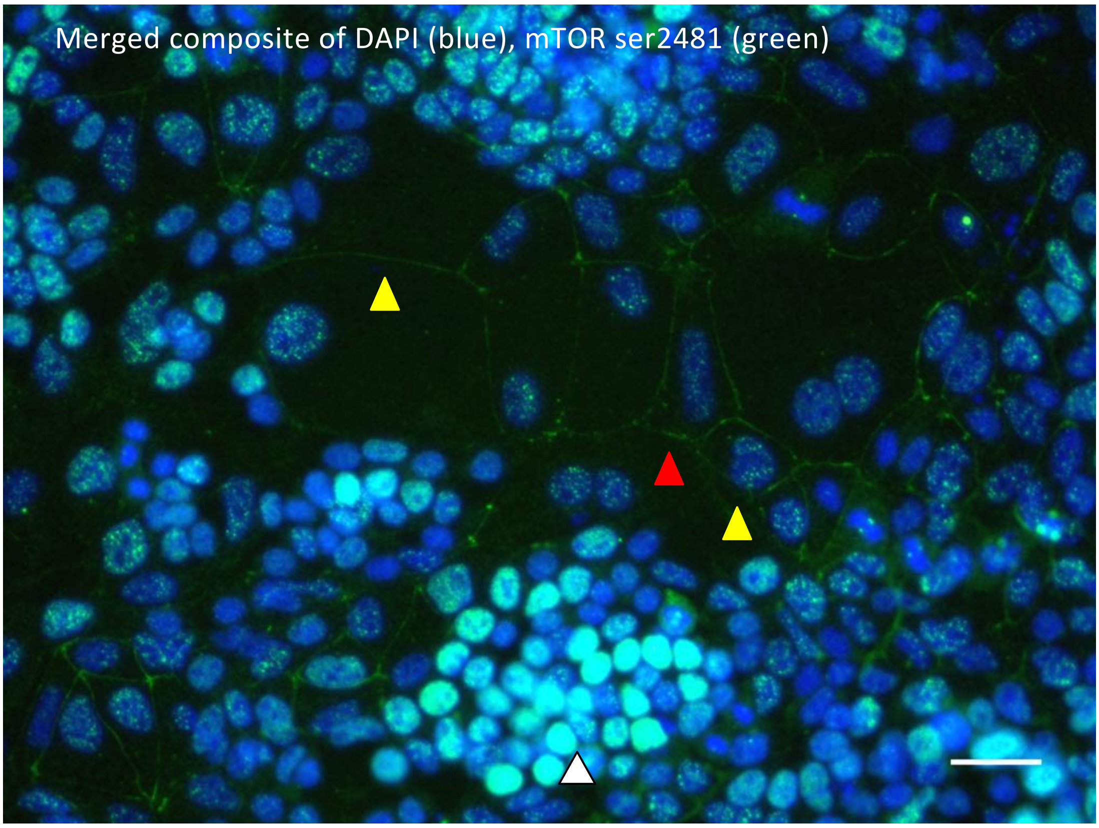

Figure 4.1.6

Representative micrographs of the cellular distribution of phospho-mTOR ser2481. Merged composite (A) of DAPI (B) and phospho-mTOR serine-2481 fluorescence (C) in mES-derived cells following LIF deprivation. Mouse ES cells were cultured for 48h then fixed and permeabilised prior to staining with rabbit anti-mouse IgG monoclonal antibodies. Specific staining was visualised by anti-rabbit Alexa-488 secondary antibodies by fluorescence microscopy. Non-specific staining was assessed with IgG isotype control antibodies (not shown). Representative images from at least 3 independent culture assays. (50µm scale bar)

Figure 4.1.7

Relationship between OCT4 staining and mTOR ser2481 in compact and spread mES cells.

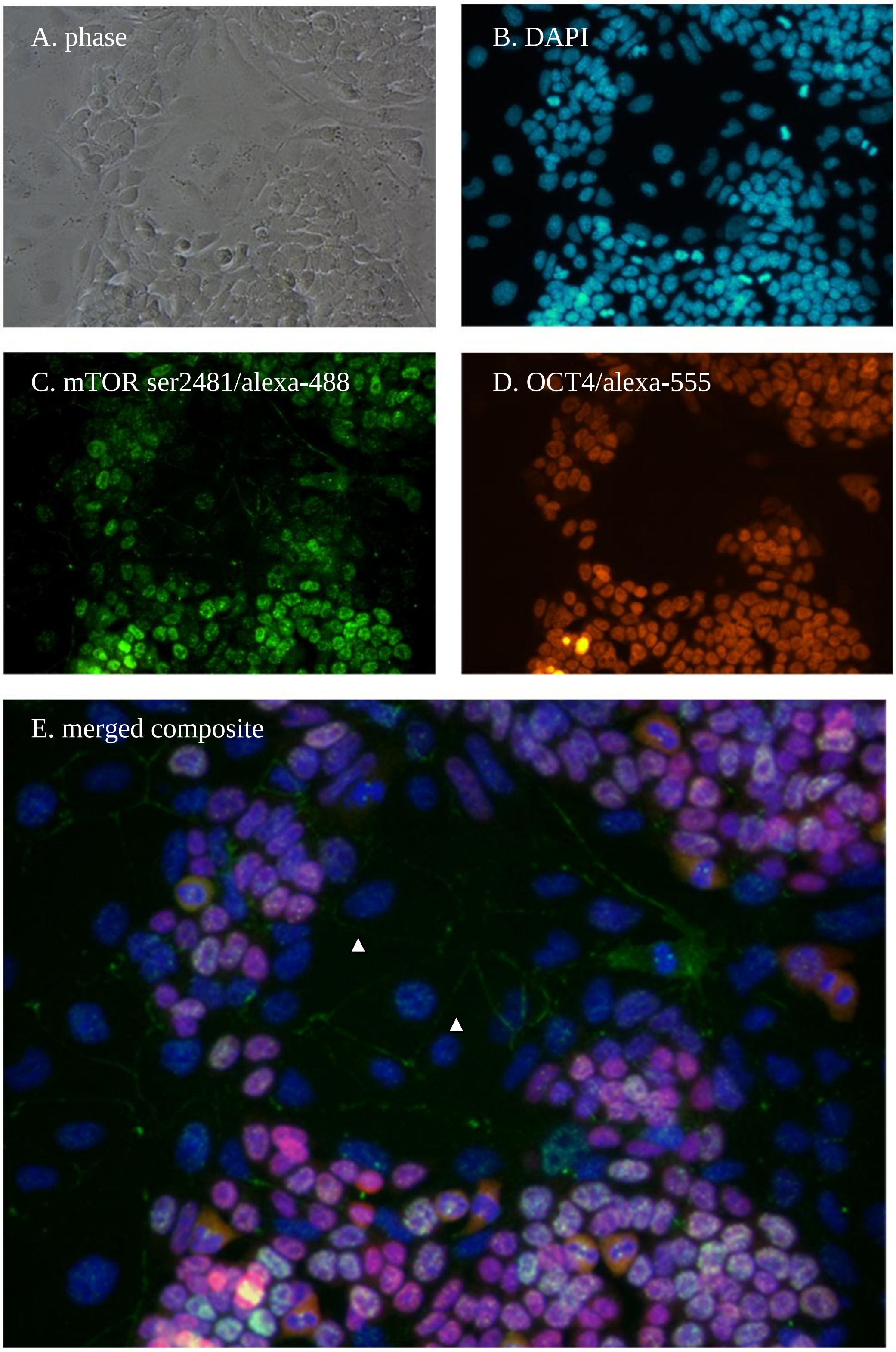
A. phase
B. DAPI
C. mTOR ser2481/alexa-488
D. OCT4/alexa-555
E. merged composite

Figure legend

Fig.4.1.7

Intracellular localisation of phospho-mTOR in OCT4 negative cells. Cell spreading was induced by 48h LIF deprivation and cells were stained with DAPI, phospho-mTOR ser2481 and OCT4 monoclonal antibodies. Cultures were imaged by phase contrast (A) and fluorescence microscopy. Image panel shows DAPI (B), phospho-mTOR ser2481/Alexa-488 (C) and OCT4/alexa-555 (D) fluorescence. Merged composite of three fluorescence channels (E), white triangles indicate localisation of phospho-mTOR ser2481 at cell borders in OCT4-ve spread cells. 50µm scale bar.

Figure 4.1.8

Phospho-mTOR ser2481 is present at the midbody of dividing cells.

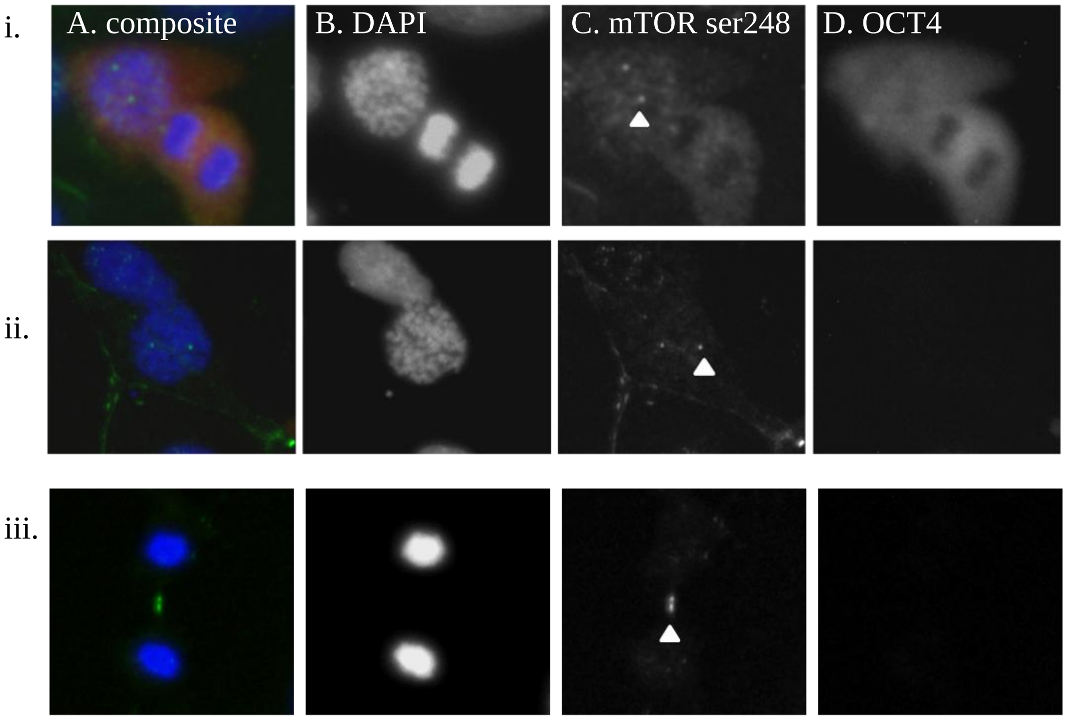
i.
A. composite
B. DAPI
C. mTOR ser248
D. OCT4
ii.
iii.

Fig.4.1.8

Localisation of phospho-mTOR ser2481 at centrosomal and midbody regions of dividing cells. Cropped enlargements of single cells Representative images of merged composite (A) of DAPI (B) phospho-mTOR ser2481 (C) and OCT4 (D)in mES cells during differentiation.

4.2 The cellular distribution and localisation of phosphorylated p70S6K in mES cells.

The ribosomal S6 protein regulates protein translation and is activated by phosphorylation by the S6 kinases. The phosphorylation of p70S6K is mediated by TORC1. The threonine-389, residue is the substrate for this kinase and the activity of p70S6K is closely correlated with this phosphorylation event[70]. Additional serine/threonine specific sites are present on p70S6K, including the threonine-421 residue which is located within the autoinhibitory domain[126]. Other phosphorylation sites present on p70S6K were not investigated in this study.

In the proceeding assays, the cellular distribution and localisation of total p70S6K, phospho-th389 and phospho-th421 were assessed in pluripotent mES cells after 48h in culture. This was achieved by fluorescence microscopy according to the protocols as described previously. The staining of total p70S6K protein is represented in Figure 4.2.1. Expression was ubiquitous and was present in nuclear and cytoplasmic compartments. Phospho-p70S6K th389 staining was also repeatedly observed in all cultures, representative image of this staining is shown in (Figure 4.2.2). Whereas distribution was uniform in mES colonies, high expression was observed in the nuclear compartment of individual cells.

A different pattern was observed when cells were stained with phosphospecific antibodies to the threonine-421 residue of p70S6K (Figure 4.2.3). Expression of phospho-th421 was almost undetectable in most cells, however strong and distinct staining was observed in a small number. Individual cells exhibiting this staining pattern were examined to identify shared morphological features. Detailed inspection revealed that these cells exhibited nuclear condensation that was indicative of mitosis. Individual cells were selected and cropped from composite micrographs to highlight the association with specific stages of mitosis (Figure 4.2.4). High expression was prevalent in all cells from prometaphase to anaphase. During cytokinesis, expression had reduced to basal levels, this can be seen in Figure 4.4.5. Strong staining for phospho-th421 can be seen in two cells during anaphase (red triangles) whereas the three cells at telophase/cytokines did not express phospho-th421 (yellow triangles). Non-mitotic cells did not exhibit strong staining. In summary, p70S6K is phosphorylated at the threonine-412 residue during mitosis. This phosphorylation persists until late mitosis after which staining levels are reduced.

Figure 4.2.1

Cellular distribution of total p70S6K protein in mES cells.

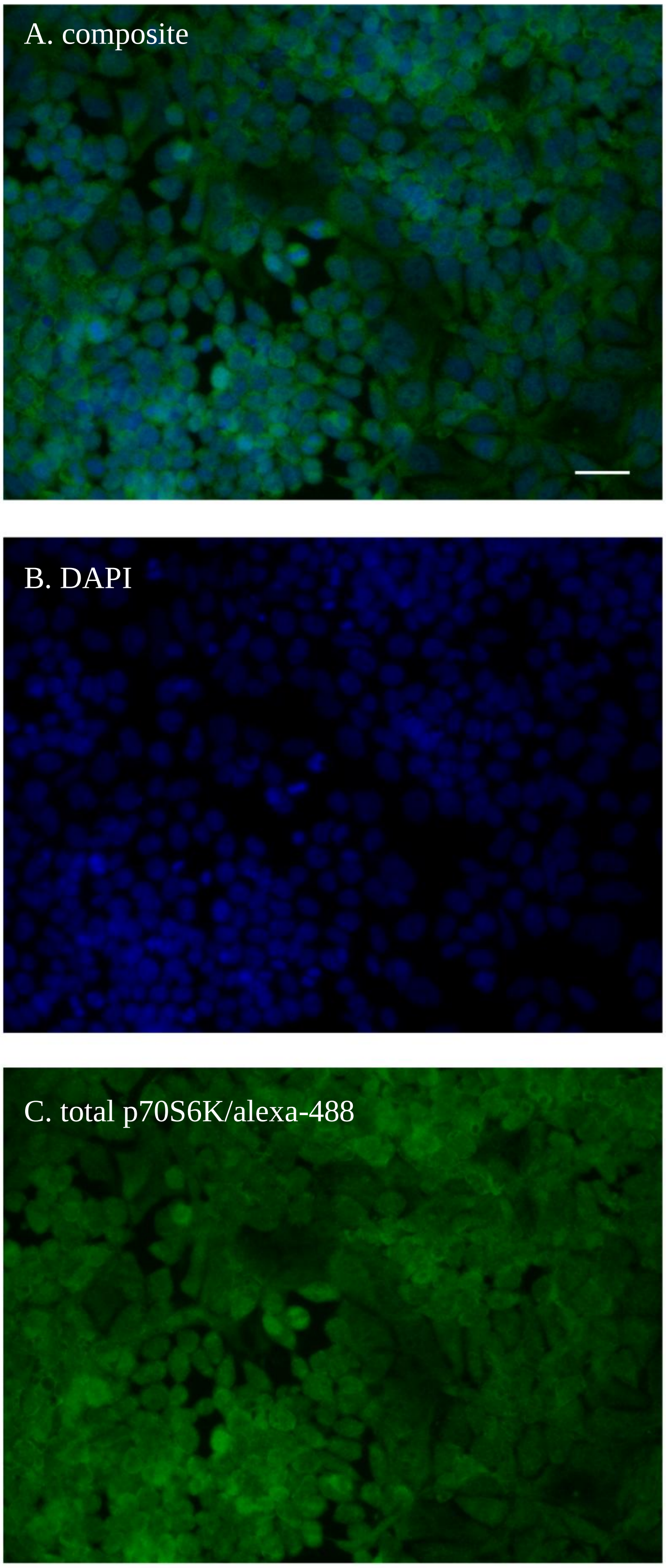

Fig. 4.2.1

Representative micrographs of the cellular distribution total p70S6K. Merged composite (A) of DAPI (B) and total-p70S6K fluorescence (C) in mES cells under standard conditions. Mouse ES cells were cultured for 48h then fixed and permeabilised prior to staining with rabbit anti-mouse IgG monoclonal antibodies. Specific staining was visualised by anti-rabbit Alexa-488 secondary antibodies by fluorescence microscopy. Non-specific staining was assessed with IgG isotype control antibodies (not shown). Representative images from at least 3 independent culture assays n=3. (50µm scale bar)

Figure 4.2.2

Cellular distribution of phospho-p70S6K th389 in mES cells.

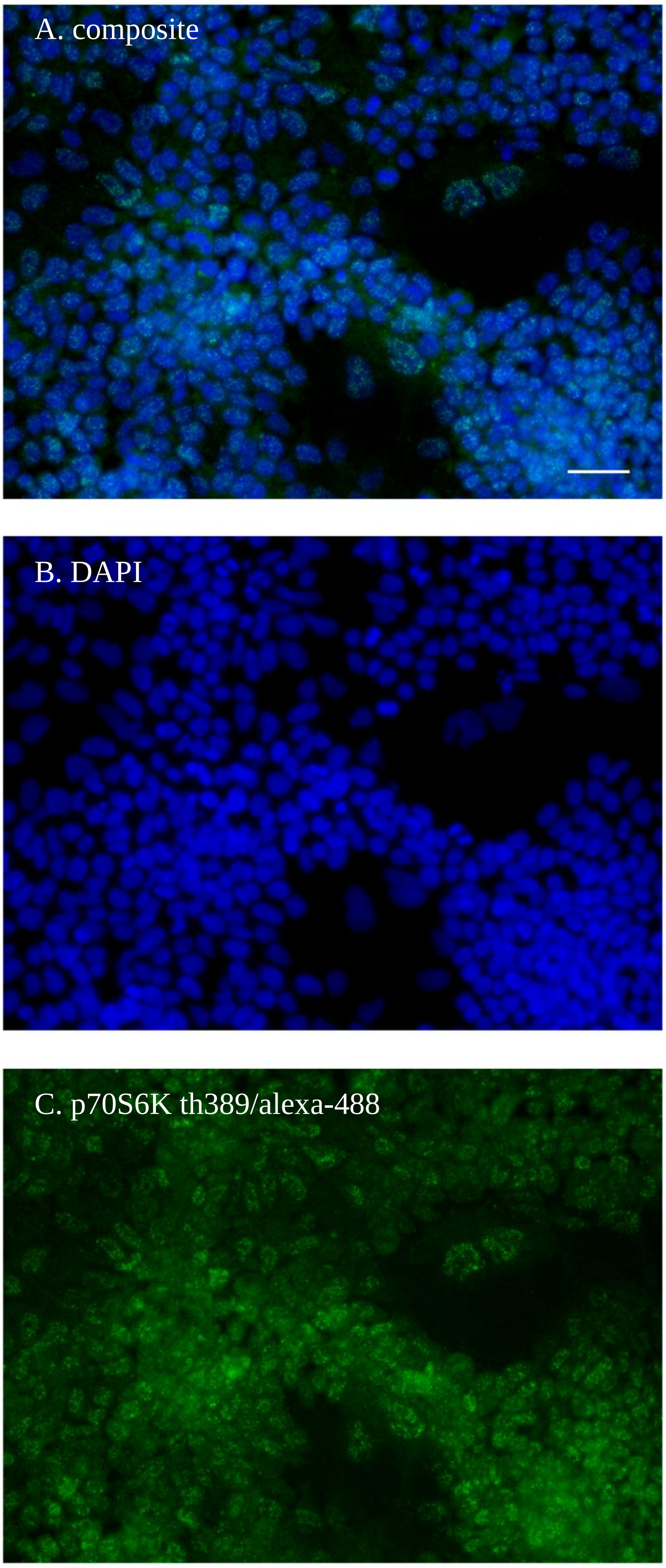

Fig. 4.2.2

Representative micrographs of the cellular distribution phospho-th389 p70S6K. Merged composite (A) of DAPI (B) and phsopho-th389 fluorescence (C) in mES cells under standard conditions. Mouse ES cells were cultured for 48h then fixed and permeabilised prior to staining with rabbit anti-mouse IgG monoclonal antibodies. Specific staining was visualised by anti-rabbit Alexa-488 secondary antibodies by fluorescence microscopy. Non-specific staining was assessed with IgG isotype control antibodies (not shown). Representative images from at least 3 independent culture assays n=3. (50µm scale bar)

Figure 4.2.3

Cellular distribution of phospho-p70S6K th421 in mES cells.

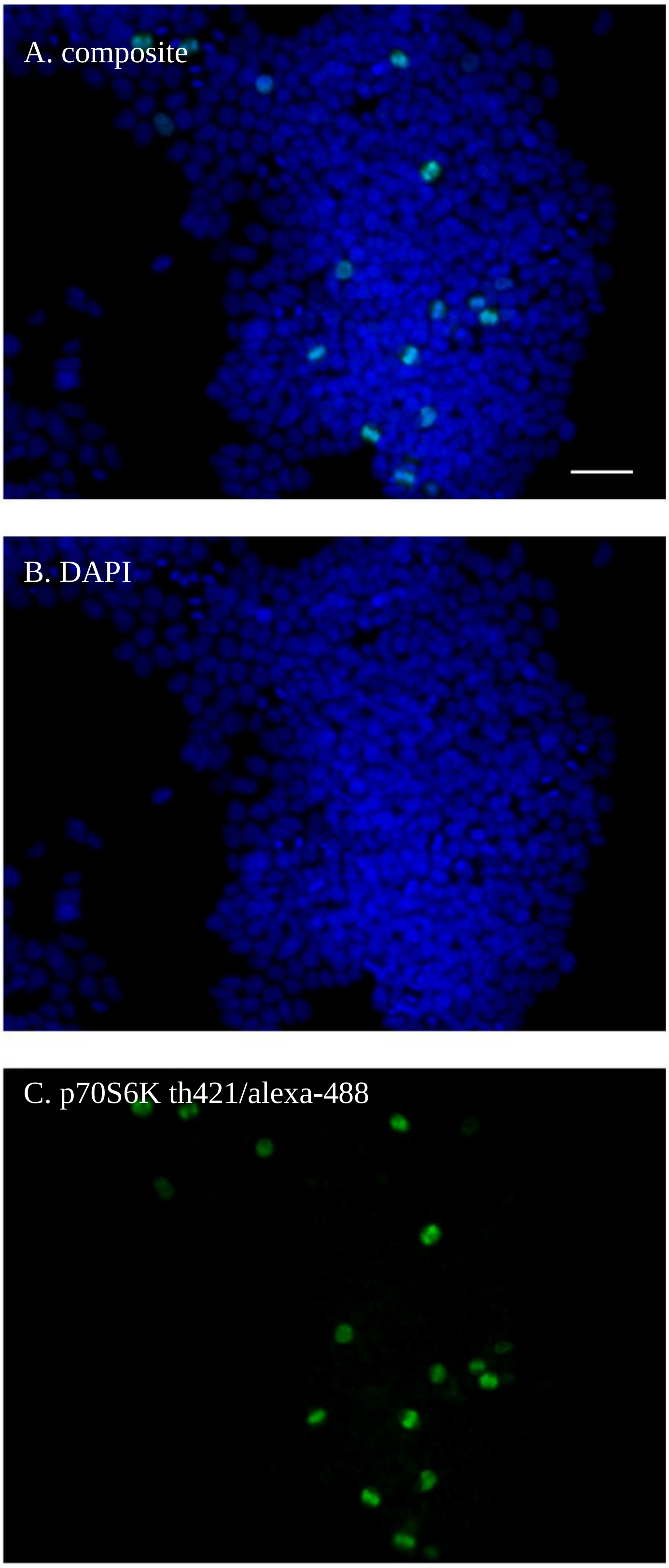

Fig. 4.2.3

Representative micrographs of the cellular distribution phospho-th421 p70S6K. Merged composite (A) of DAPI (B) and phospho-th421 fluorescence (C) in mES cells under standard conditions. Mouse ES cells were cultured for 48h then fixed and permeabilised prior to staining with rabbit anti-mouse IgG monoclonal antibodies. Specific staining was visualised by anti-rabbit Alexa-488 secondary antibodies by fluorescence microscopy. Non-specific staining was assessed with IgG isotype control antibodies (not shown). Representative images from at least 3 independent culture assays. (50µm scale bar)

Figure 4.2.4

Phosphorylation of p70S6K th421 during mES mitosis.

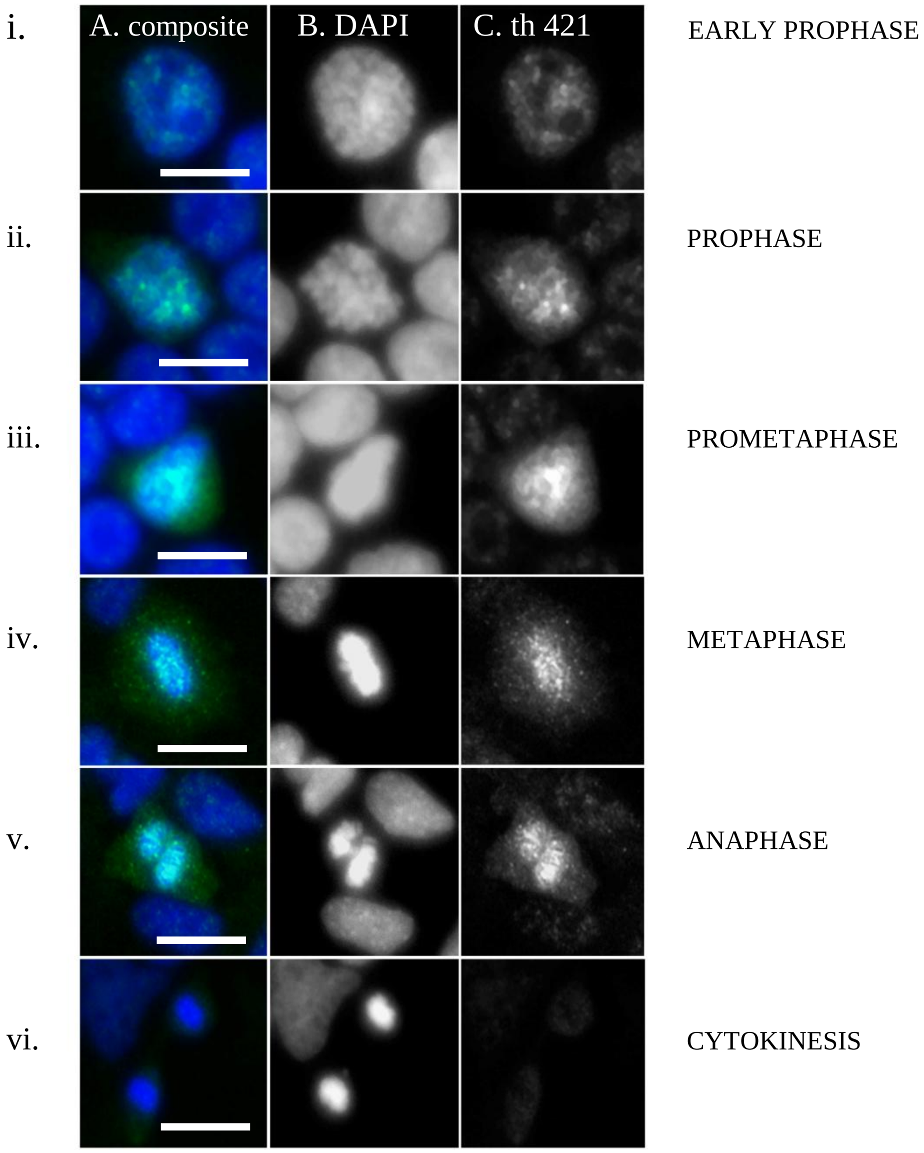
i.
A. composite
B. DAPI
C. th 421
EARLY PROPHASE
ii.
PROPHASE
iii.
PROMETAPHASE
iv.
METAPHASE
v.
ANAPHASE
vi.
CYTOKINESIS

Fig.4.2.4

Cropped images of single mES cells during mitosis. Image panel A is a composite of DAPI (B) and p70S6K th421 fluorescence. A cell at early prophase (i) was identified by nuclear condensation. At early prophase nuclear condensation is apparent and phospho-th421 staining is increased (ii). Staining is distinct at prometaphase (iii) and metaphase (iv). At mitotic anaphase phsopho-p70S6K appears localised with DAPI staining (v). At the stage of cytokinesis strong staining is no longer observed. White line represents 10µm scale.

Figure 4.2.5

Phosphorylation p70S6K th421 is downregulated during late mitosis.

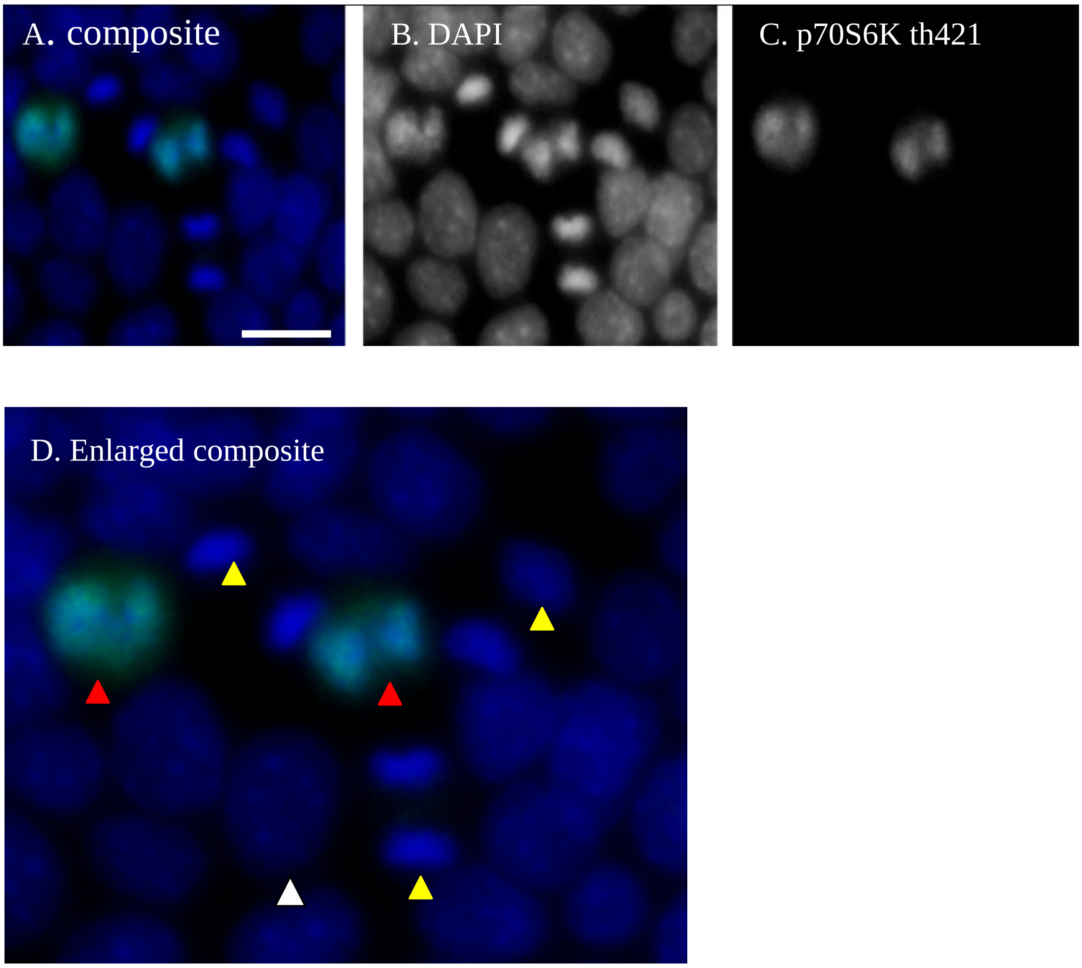

Fig.4.2.5

Panel of images of p70S6K th421 phosphorylation in non-mitotic and mitotic mES cells. Merged composite (A) of DAPI (B) and p70S6K th421 fluorescence (C). Composite image D represents image A repeated and enlarged to highlight nuclear morphology. White triangle indicates a typical non-mitotic mES cells. Two cells at mitotic anaphase exhibiting strong p70S6K phosphorylation are indicated by red triangles and three cells at late telophase/cytokinesis are indicated by yellow triangles. White line represents 20 µm scale.

4.3 The cellular distribution and localisation of the mTORC2 complex substrate AKT ser473 in mES cells.

Protein kinase B (AKT) is a serine/threonine kinase that mediates an array of cellular processes including survival, proliferation, and motility. The activity and stability of AKT is regulated by specific phosphorylation events. It is widely accepted that the phosphorylation of the th308 residue is mediated by PDK1 at the cell membrane in response to insulin and growth factor stimilation[144]. The kinase responsible for the phosphorylation of the ser473 residue was termed the PDK2. A number of putative PDK2 candidates have been identified. Enzymes responsible for this phosphorylation include, the mTOR complex-2 (TORC2), the integrin linked kinase (ILK) and DNA-protein kinase (DNA-PK). In the previous chapter it was demonstrated that inhibition of TORC1 by rapamycin increases the phosphorylation of AKT ser473. This effect has been widely reported and may arise from a dynamic equilibrium between TORC1 and TORC2 activity.

The cellular distribution of phospho-AKT ser473 in mES cells was documented by fluorescence microscopy. Mouse ES cells were cultured for 48h with complete growth medium, serum and LIF according to the previously established protocol. Cells were fixed with paraformaldehyde and ethanol and stained with phosphospecific antibodies. Images were captured and examined for the distribution and localisation of phospho-specific protein.

Data presented in figure 4.3.1 shows the distribution of phospho-AKT (ser473) in mES cells. The distribution of phospho-AKT was not uniform in mES cells in culture. The majority of cells did not express high levels of AKT (ser473), however strong staining was observed in some cells. Close examination of individual cells exhibiting AKT phosphorylation revealed distinctive patterning (Figure 4.3.2). Cropped images of AKT (ser473) positive nuclei were presented as a composite image (A) of DAPI (B) and phospho-AKT fluorescence. Clear patterning of AKT phosphorylation can be observed in these images.

To assess whether AKT (ser473) phosphorylation was associated with mitosis, mouse ES cells were cultured for 48h under standard conditions and stained for AKT (ser473) as described. Additionally, microtubules were visualised by immunostaining for α-tubulin and alexa-555 (red). Micrographs of DAPI, alexa-488 and alexa-555 fluorescence were captured and merged into a composite image. Mitotic nuclei were identified by characteristic nuclear morphology and tubulin patterning. Individual cells were selected and cropped from these composite images (Figure 4.3.3) and displayed according to the stage of mitosis. AKT serine-473 phosphorylation appeared to be strongly expressed from prometaphase (Image iii) until anaphase (Image v.). The staining patterns observed in these representative images were observed repeatedly in independent culture assays.

Figure 4.3.1

Non-uniform distribution of phospho-AKT (ser473) in mES cells.

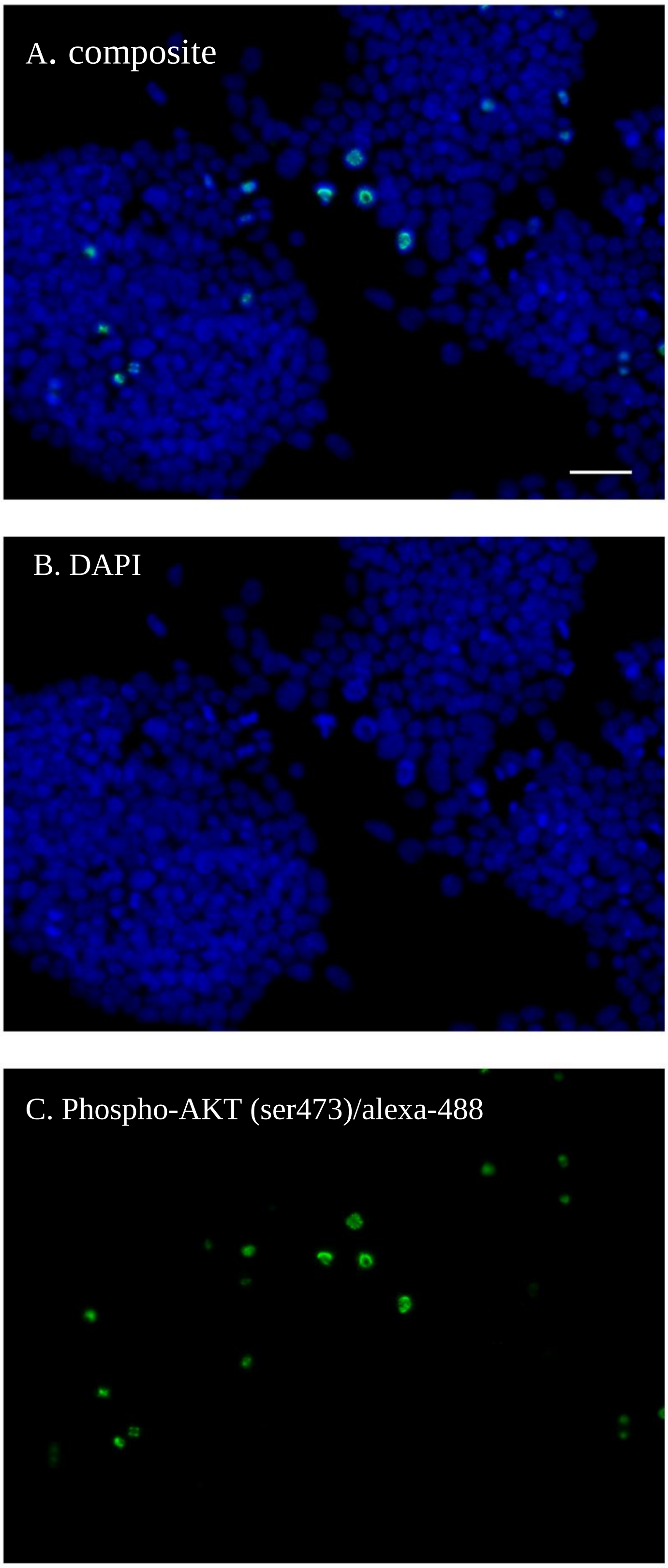

Fig.4.3.1

Mouse E14-Tga2 cultures were stained with DAPI and phospho-AKT (ser473) monoclonal antibodies visualised with alexa-488 secondary antibodies by fluorescence microscopy. Non-uniform distribution of phospho-AKT (ser47) can be observed in mES cells with colonies. Composite image (A) of DAPI fluorescence (B) overlayed with phospho-AKT (ser473) fluorescence (C). Representative images from at least three independent culture experiments. White line represents scale (100µm).

Figure 4.3.2

Nuclear localisation and patterned phosphorylation of AKT at serine -473 in mES cells.

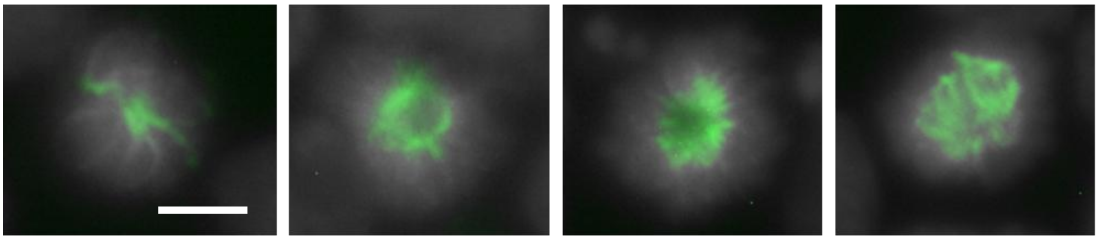

Fig.4.3.2

Distinct patterning of phospho-AKT can be observed in cropped images of single mES nuclei from fluorescence micrographs. Composite images of DAPI fluorescence (greyscale) overlayed with phospho-AKT ser473 fluorescence (green). Representative images from at least three independent culture experiments. White line represents scale (7.5μm).

Figure 4.3.3

Phosphorylation of AKT at serine-473 during mitosis in mES cells.

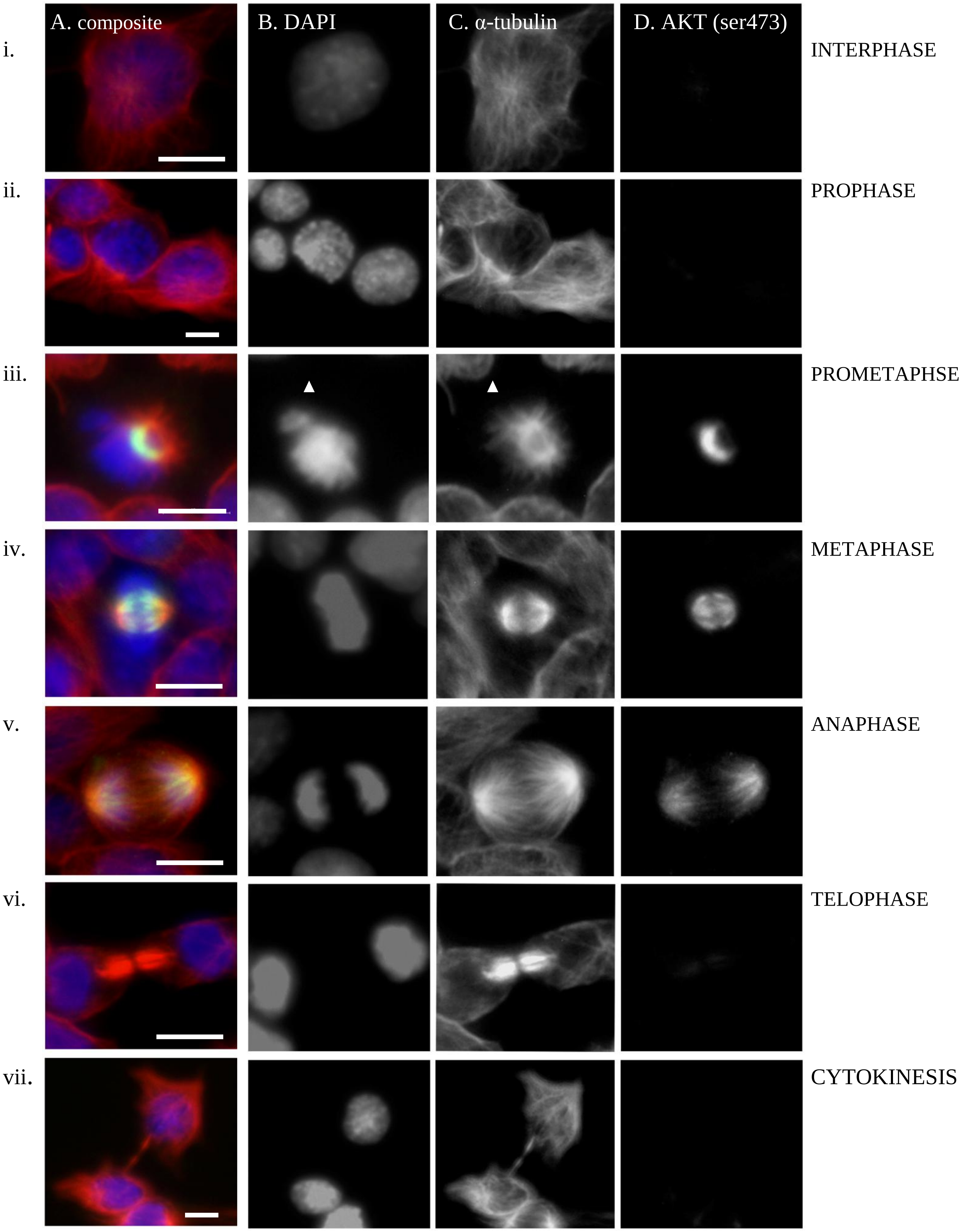
A. composite
B. DAPI
C. α-tubulin
D. AKT (ser473)
i.
INTERPHASE
ii.
PROPHASE
iii.
PROMETAPHSE
iv.
METAPHASE
v.
ANAPHASE
vi.
TELOPHASE
vii.
CYTOKINESIS

Figure legend

Fig.4.3.3

Mouse ES cells exhibit distinct AKT (ser473) phosphorylation during mitosis. mES cells were seeded in into 6 well plates and cultured for 48h in complete growth medium without LIF. Wells were washed and fixed as described in Experimental Methods. Samples were stained with monoclonal antibodies specific for mouse α-tubulin. rabbit anti–phospho-AKT ser473 or isotype control antibodies. Specific staining was visualized with anti-mouse alexa 488 and anti-rabbit alexa 555 secondary antibodies, nuclear counterstaining with DAPI. Triplicate wells were imaged with 20x objective lens using a Nikon TE2000U fluorescence microscope with the corresponding filter blocks for UV, 488 nm and 555 nm excitation. Cropped images of composite and single channel fluorescence of single mES cells at different Stages of mitosis

In order to assess whether there was concordance between the strong nuclear AKT (ser473) staining and mitosis in mES cells, fluorescent micrographs of DAPI and tubulin staining were analysed. Numbers of total nuclei (DAPI) and mitotic nuclei (DAPI + α-tubulin) were counted and compared with AKT ser473 positive staining to generate data for significance testing. The results of this analysis are presented in Figure 4.3.4. It was found that there was a strong concordance between mitotic nuclei and AKT (ser473) positive nuclei that was statistically significant by the Fisher's exact test. This statistic was selected in preference to the typical chi-square analysis as sample numbers within some of the groups were low.

Mouse ES cells were deprived of LIF for 48h to allow cells to begin to differentiate. The justification for this was to assess AKT staining patterns in cells that had lost the typical compact morphology of pluripotent ES cells. Figure 4.3.5 shows that colonies of compact mES cells persist but are surrounded by areas of cells with a developed cytoskeleton, large nucleus and extensive cytoplasmic compartment. These cells are consistent with the 'spread' cells documented throughout this investigation. Mitotic cells were identified from three areas, the compact densely packed area (compact morphology), intermediate area (spread morphology adjacent to compact cells) and spread area. It was observed that AKT serine-473 phosphorylation was maintained in these mitotic cells.

Figure 4.3.4

Concordance between phospho-AKT (ser473) and mitosis in mES cells.

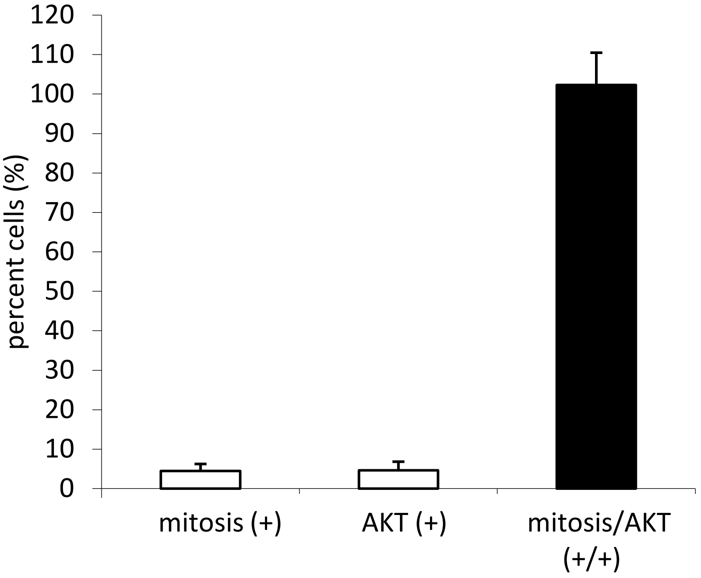

	AKT (-ve)	AKT (+ve)
Non-mitotic cells	2070	4
Mitotic cells	0	94

Fig. 4.3.4

Concordance between the number of mitotic cells and AKT (ser473) positive cells in mES cell cultures. Fluorescence micrographs of mES cells stained with DAPI, α-tubulin and AKT (ser473). Total nuclei were counted from micrographs (10x magnification) of DAPI fluorescence (blue channel) and corresponding numbers of mitotic nuclei and AKT+ve nuclei were counted from the α-tubulin (red) and AKT (green) channels respectively. Data expressed as mean number of total nuclei in 4 fields of view from triplicate culture assays .The positive association between AKT (ser473) and mitosis was statistically relevant ($p<0.001$, Fisher’s exact test).

Figure 4.3.5

Mitotic localisation of AKT (ser473) in mES cells with compact and compact and spread morphologies.

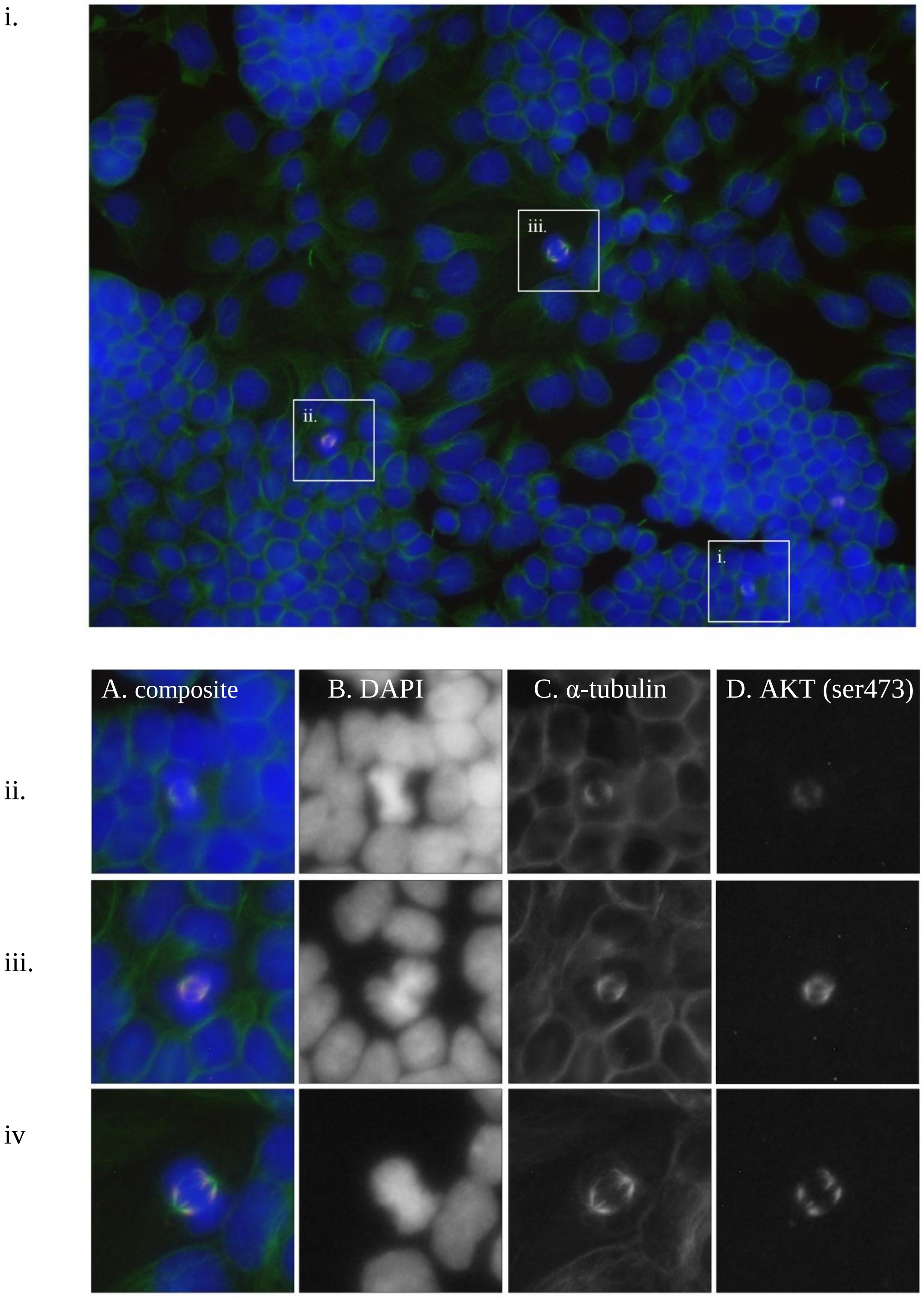
i.
iii.
ii.
i.
A. composite
B. DAPI
C. α-tubulin
D. AKT (ser473)
ii.
iii.
iv

Figure legend.

Fig. 4.3.5

The mitotic localisation of AKT ser473 in can be observed in compact and spread cells upon LIF deprivation. Mouse ES cells were seeded in into 6 well plates and cultured for 48h in complete growth medium without LIF. Wells were washed and fixed as described. Samples were stained with monoclonal antibodies specific for mouse α-tubulin, rabbit anti–phospho-AKT ser473 or isotype control antibodies. Specific staining was visualized with anti-mouse alexa-488 and anti-rabbit alexa-555 secondary antibodies, nuclear counterstaining with DAPI. Triplicate wells were imaged with 20x objective lens using a Nikon TE2000U fluorescence microscope with the corresponding filter blocks for UV, 488nm and 555nm excitation. Ten fields of view were captured for each sample under identical exposure conditions. A representative fluorescence micrograph of the composite RGB image generated by merging the 3 fluorescence channels (image i). Cropped enlargements are presented as a merged composite image (A) and the corresponding greyscale images from the DAPI (B), α-tubulin (C) and phospho-AKT (C) channels. Mitotic cells were identified by the distinctive microtubular structures visualized by α-tubulin staining. A mitotic cell within the compact colony area (Image panel ii), a mitotic cell at within the intermediated area (image pane iii) and a mitotic cell within the spread cell area (image panel iv) exhibit AKT ser473 phosphorylation. Representative image from two independent culture experiments (n=2).

4.4. Colocalisation of AKT serine-473 with α-tubulin in mitotic mES cells.

The assessment of colocalisation between proteins is performed by confocal microscopy. There are numerous methods for this type of analysis that are subject to drawbacks and limitations that have been widely discussed and reviewed in the literature[128]. Interpretation of colocalisation data can be either qualitative or quantitative. A simple qualitative approach involves merging the colour channels of interest (e.g. red and green) and observing the areas of overlap (yellow pixels). Quantitative approaches require more complex statistical analysis of the relationship between pixel intensities at specific positions in the x, y and z-planes. Furthermore, background intensity levels must be normalised and correlation statistics generated from single slices of a z-stack. These methods are also prone to interpretation errors as thresholds are defined subjectively. At the image capture stage it is important to ensure that is no bleed-through of signal occurs between the channels of interest and that the z-planes of each frame are aligned.

Colocalisation provides a description of the correlation of pixel intensities in the x, y and z-planes but it does not provide proof of a direct association between two proteins as the resolution limit of a standard confocal microscope is around 0.2μm. Therefore, in this study, a combined approach was undertaken. Firstly, confocal z-stacks were capture at the maximum resolution possible and intensity level thresholding colocalisation analysis was performed. This is the presented visually as a merged image of the colour channels displaying colocalisation above the threshold at designated levels. Secondly, microtubular polymerising and depolymerising agents were used to disrupt microtubular organisation to assess the effect on the localisation and patterning of the molecule of interest, phospho-AKT (ser473). The techniques used in this study are detailed in Experimental Methods. Briefly, staining for α-tubulin was visualised with anti-mouse, alexa-488 conjugated secondary antibodies and phospho-AKT (ser473) visualised with anti-rabbit, alexa-597 conjugated antibodies. Nuclear counterstaining was performed with DAPI and images were captured ‘between-frames’ to ensure z-plane alignment. Isotype controls and single staining controls were performed; single-slice images were taken but not shown.

Confocal microscopy and the ImageJ analytical software was utilised to assess the colocalisation between phospho-AKT (ser473) and mitotic microtubules in mouse ES cells. The proceeding figures demonstrate that phospho-AKT (ser473) is associated with α-tubulin during mitotic metaphase. Figure 4.4.1 shows that similar patterning of AKT and tubulin was observed when the image stack was combined into a sum-projection of the individual z-slices. This supports the hypothesis that there is a close association between the two proteins during mitosis.

The assay was repeated and an image stack of a whole colony was captured. Figure 4.4.2.1A shows that phospho-AKT (ser473) was restricted to the cells undergoing division as the majority of cells did not exhibit strong staining. Image B is a cropped enlargement of a metaphase cell. This image represents a projection of the individual slices of the z-stack showing DAPI (blue), α-tubulin (green) and phospho-AKT (red). The areas of colocalisation where equivalent staining intensity was greater than the 85% threshold level are indicated by white pixels in image C. This figure is a sum projection of α-tubulin (green pixels) and AKT serine-473 (red pixels) with the colocalised points. The individual z-step slices of this projection are presented in Figure 4.4.2.2A. Enlargements of two individual slices of the metaphase cell showing colocalisation with intensity level thresholding at the 95% level are shown in Figure 4.4.2.2.B and 4.4.2.2.C. Examination of these images reveals that at the highest level of threshold discrimination, colocalised points (white pixels) are in close proximity to kinetochore microtubules. Colocalisation is also seen during mES cell anaphase and telophase (Figure 4.4.2.3. Low levels of phospho-AKT (ser473) are seen during telophase; however, colocalisation can be observed at the polar microtubules between the dividing cells (Figure 4.4.2.3.C)

Treatment of mouse ES cells with nocodazole impaired the association of phospho-AKT (ser473) with α-tubulin in metaphase cells (Figure 4.4.3). Is was hypothesised that if phospho-AKT (ser473) was in direct association with microtubules during mitosis that treatment with the microtubule depolymerising agent nocodazole would impair the AKT patterning that was observed in mitotic cells. This was found to be true, a sum projection of z-stack cropped images of single cells at metaphase (B) and interphase (C) show that the organisation of α-tubulin is lost and cells do not exhibit a structured cytoskeleton. In the metaphase cell, the distinctive AKT patterning is lost. The z-plane slices of these projections are presented in Figure 4.3.4.A (metaphase) and B (interphase).

Figure 4.4.1

Distribution of AKT (ser473) and α-tubulin in a metaphase mES cell.

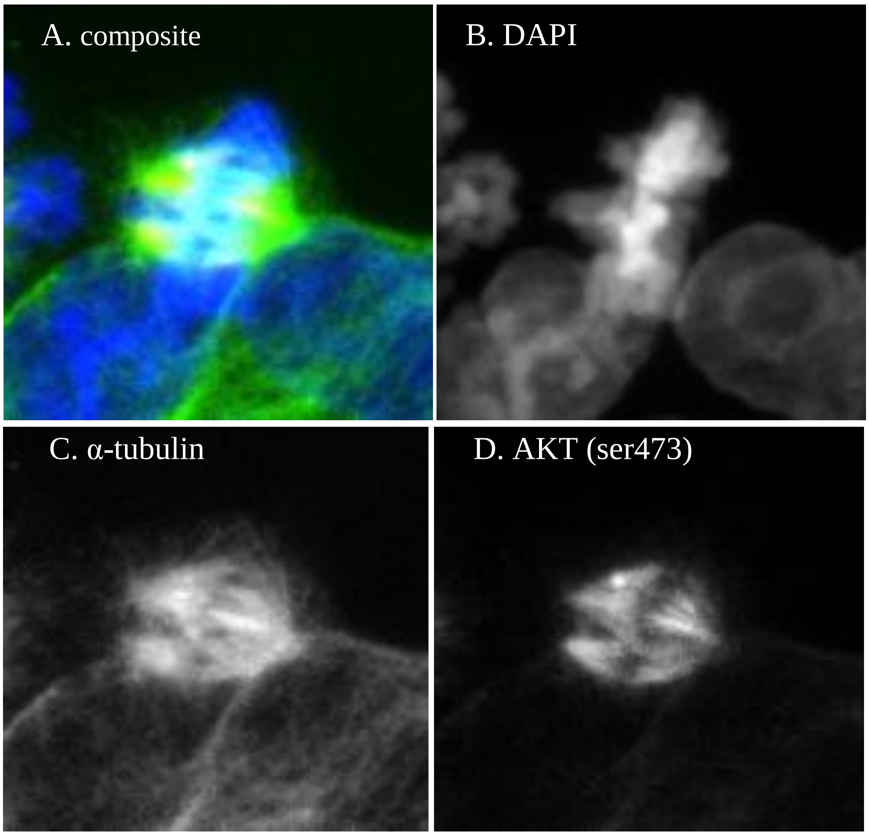

Fig. 4.4.1

Nuclear localisation of phospho-AKT (ser473) in mouse ES cell during metaphase. Mouse E14-Tga2 cells were cultured for 48h in Iwaki™ tissue culture plates under standard growth conditions and fixed with PFA/EtOH as previously described. Cells were stained with DAPI and primary rabbit anti-mouse IgG monoclonal antibodies and fluorochrome-conjugated secondary antibodies. Composite image of DAPI, α-tubulin/alexa-488 and AKT phospho-ser473/alexa-597 (image A). Single channel images of DAPI (B), tubulin (C) and AKT ser473 (D) are shown. Projection of sum slices from confocal microscopy image stack (63x objective, 2.81x zoom).

Figure 4.4.2.1

Colocalisation of AKT (ser473) with α-tubulin in a metaphase mES cell.

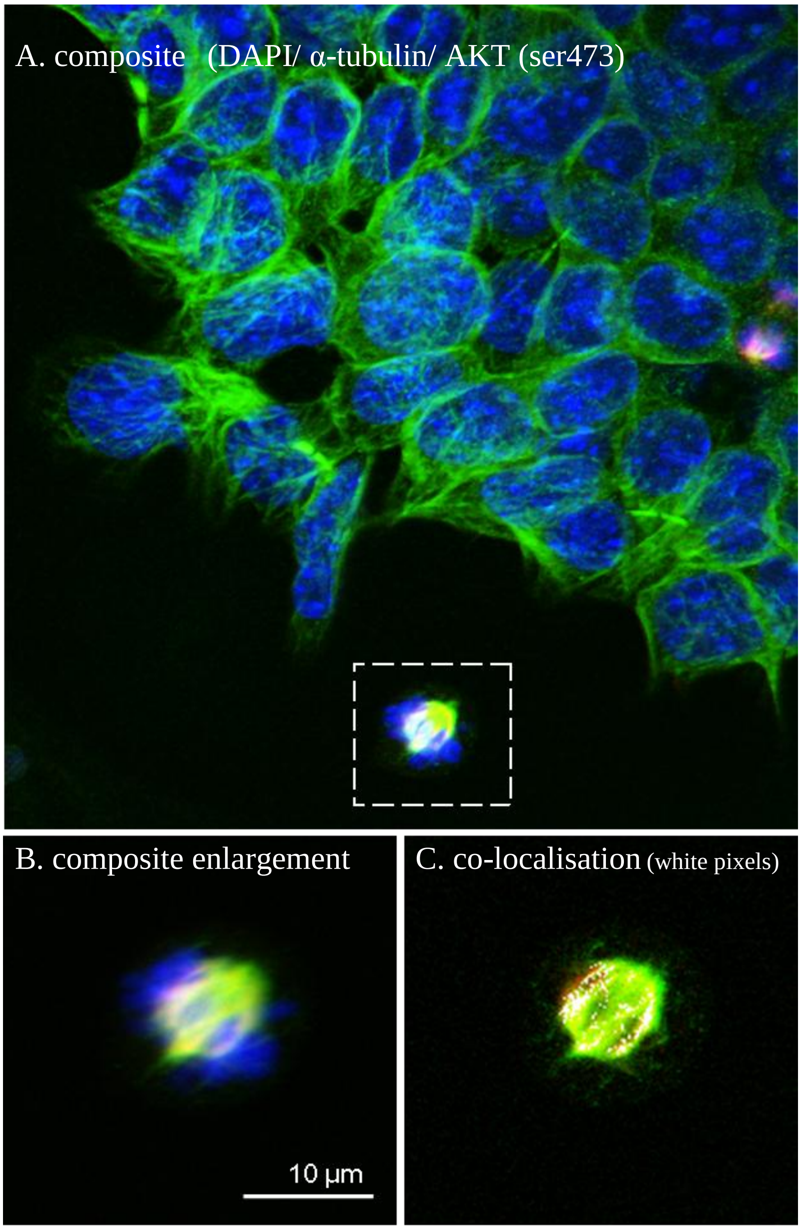
A. composite (DAPI/ α-tubulin/ AKT (ser473)
B. composite enlargement
10 µm
C. co-localisation (white pixels)

Figure legends

Fig.4.4.2.1

Sum projection of colocalisation of phospho-AKT (ser473) with α-tubulin in a metaphase mES cell. Composite image of DAPI, α-tubulin/alexa-488 and AKT phospho-ser473/alexa-597 (image A). Cropped enlargement of metaphase cell (image B) showing DAPI (blue), α-tubulin (green) and AKT ser473 (red). Colocalisation of tubulin (green) with AKT (red) (image C) at threshold level of 85% indicated by white pixels. Projection of sum slices from confocal microscopy image stack, analysis performed with ImageJ colocalisation tool (63x objective, 2.81x zoom, resolution x/y= 216.9nm, z=625nm)

Fig. 4.4.2.2 (overleaf)

Co-localisation of AKT (ser473) with α-tubulin in cropped z-stack of image presented in Figure 4.4.3.C. DAPI channel (blue) and α-tubulin (green) overlayed with white pixels representing co-localisation at 85% threshold (image panel A). White triangle indicates point of colocalisation at kinetochore microtubules. Enlargement of individual z-plane slices showing colocalisation at 95% threshold, images B and C. Image series at 63x objective, 2.81x zoom.

Figure 4.4.2.2

Co-localisation of AKT (ser473) with α-tubulin in a metaphase mES cell from confocal z-series image stack.

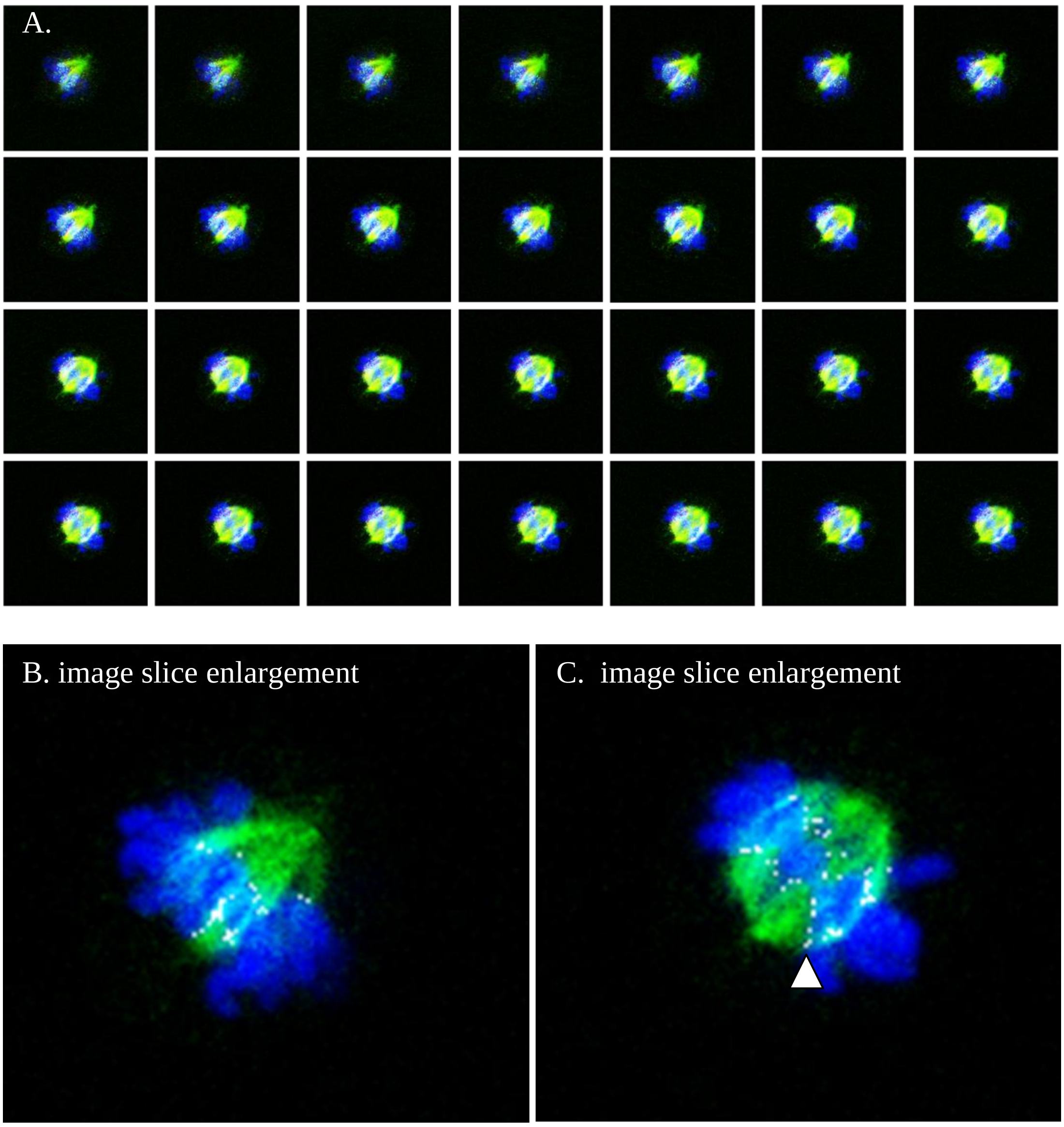
A.
B. image slice enlargement
C. image slice enlargement

Figure 4.4.2.3

Colocalisation of phospho-AKT (ser473) with α-tubulin in mES cells during mid and late mitosis.

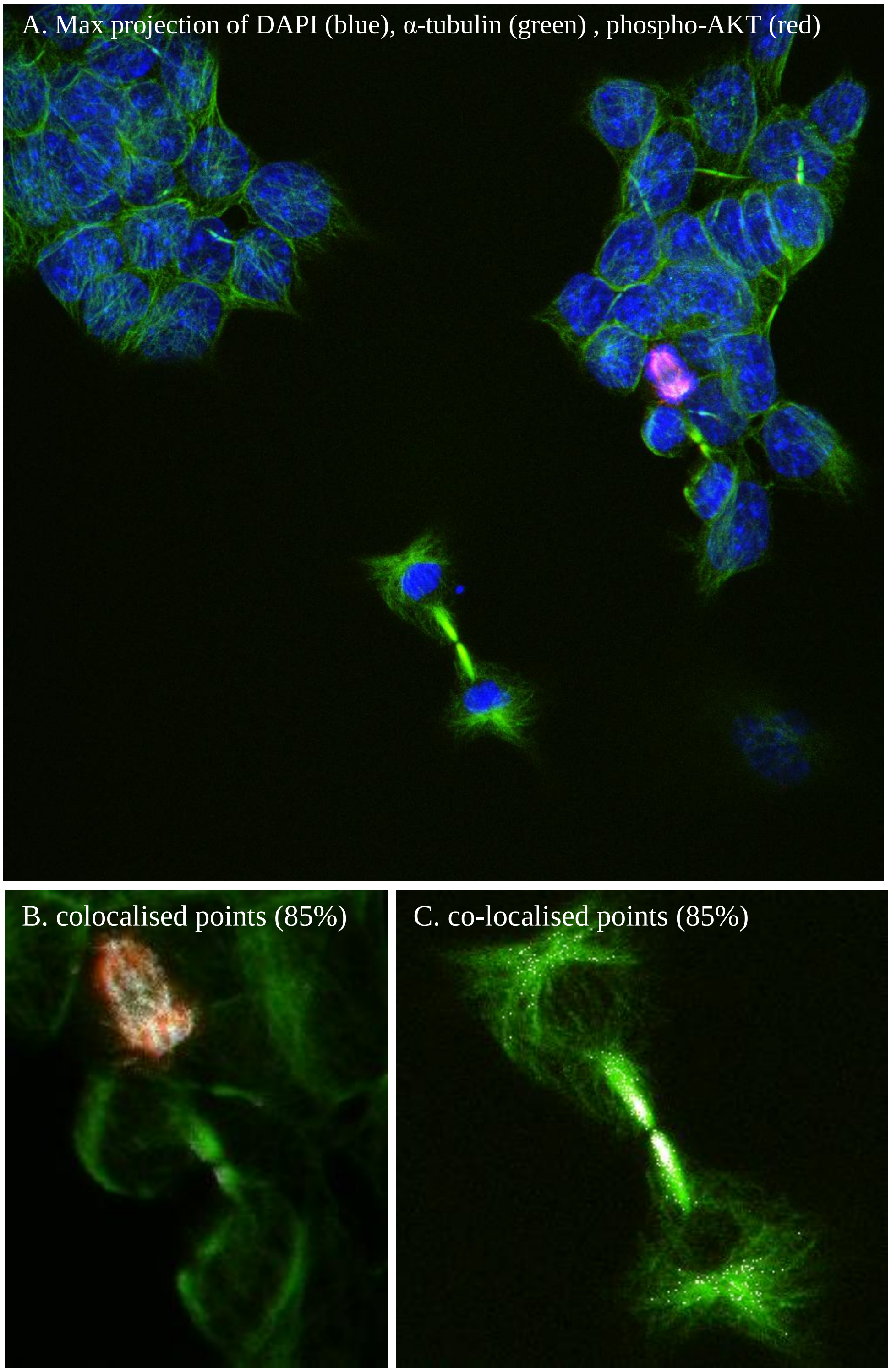
A. Max projection of DAPI (blue), α-tubulin (green) , phospho-AKT (red)
B. colocalised points (85%)
C. co-localised points (85%)

Fig. 4.4.2.3

Maximum projection of mouse E14 ES cells stained with DAPI, α-tubulin/alexa-488, phospho-AKT (ser473)/alexa-543 by confocal microscopy. Colocalisation of proteins by intensity level thresholding at 85% in cropped enlargements of a cell at anaphase (B) and cytokinesis (C). White pixels represent colocalised points at 85% threshold. Colocalisation determined in x/y plane single slices and displayed as maximum projections of the z-stack. Imaging undertaken with Leica SPE2 confocal with HCX APO 63x objective lens (0.9 NA), 2.81x zoom, resolution x/y= 216.9nm, z=625nm. DAPI excitation at 405nm; detector range 415-510nm Green fluorescence excitation at 488nm; detector range 500--560nm. Red fluorescence excitation at 543nm; detector range 583-640nm. images captured with between frames, raster scan.

Figure 4.4.3.1

Nocodazole treatment disrupts both tubulin and AKT (ser473) organisation in metaphase mES cell.

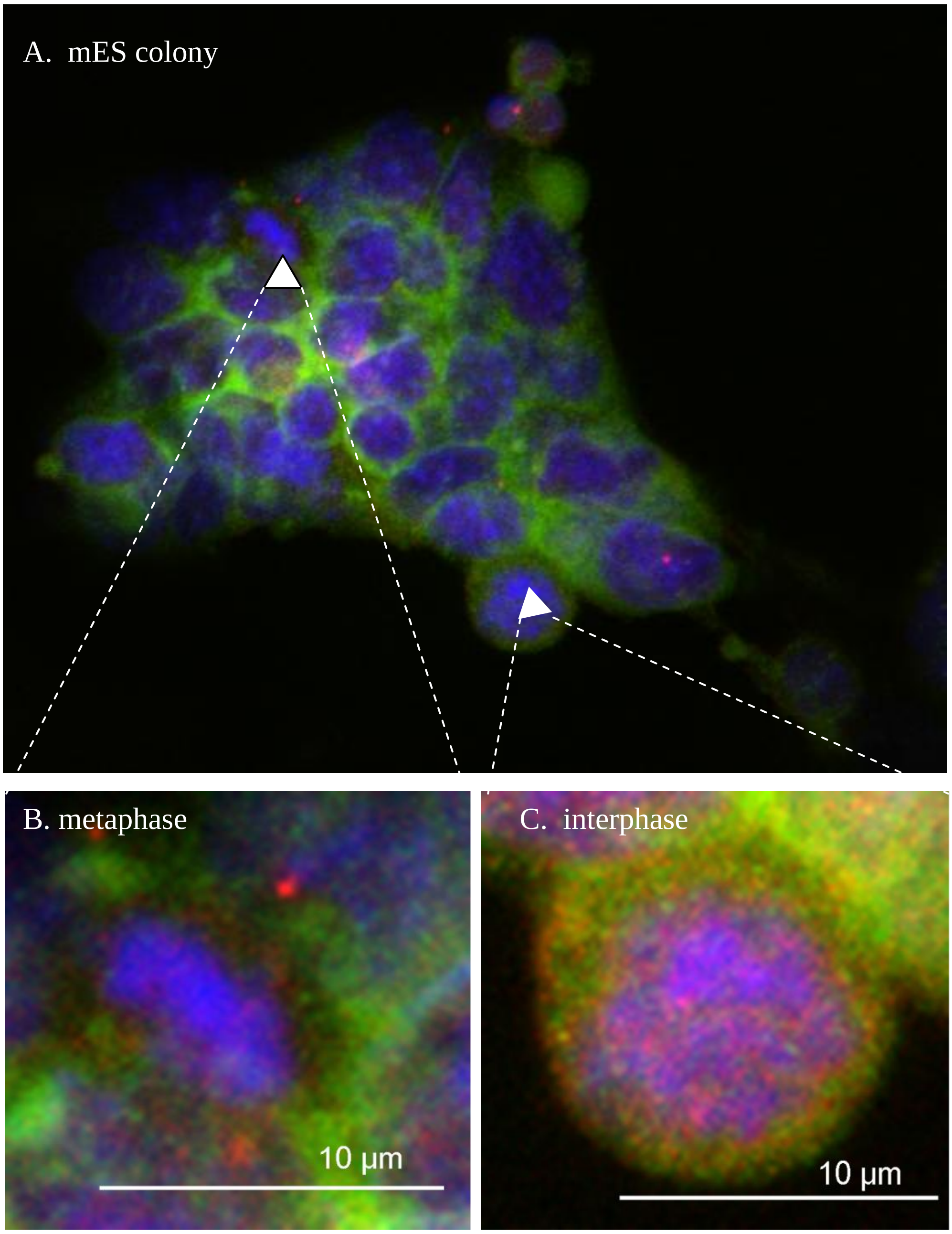
A. mES colony
B. metaphase
10 µm
C. interphase
10 µm

Figure 4.4.3.2

Confocal z-stacks of individual mES cells treated with nocodazole.

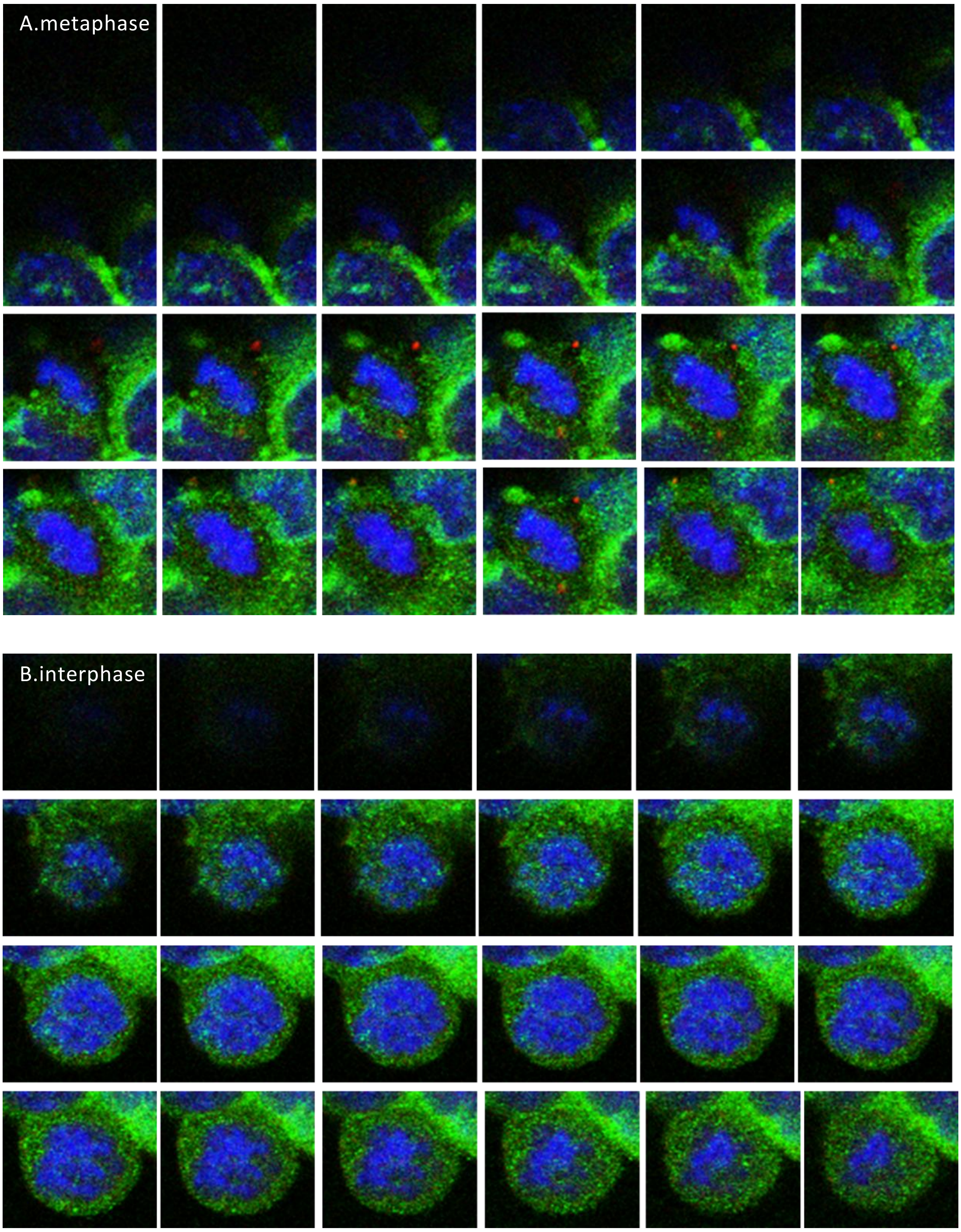
A.metaphase
B.interphase

Figure legends

Fig.4.4.3.1

Nocodazole treatment disrupts microtubular organisation and AKT (ser473) patterning at metaphase. Projection of sum slices from confocal microscopy z-stack of mES cells stained with DAPI (blue), α-tubulin (green), phospho-AKT serine-473 (red). Mouse ES cells were cultured for 48h in complete growth medium containing 103u/ml LIF and 10% FCS and treated with 50nM nocodazole for 1h. Composite image of DAPI, α-tubulin/alexa-488 and phospho-AKT ser473/alexa-597 (image A). Cropped enlargement of a single cell at metaphase (image B). Co-localisation of tubulin (green) with AKT (red) (image C) at the 85% level indicated by white pixels. Image analysis and colocalisation performed with ImageJ co-localisation tool (63x objective, 2.81x zoom; resolution x/y= 216.9nm, z=625nm)

Fig.4.4.3.2

Individual confocal slices of the z-stack presented in Fig.4.4.3.1 displaying a mES cell at interphase (image series A) and metaphase (image series B) following treatment with nocodazole.

4.5 Colocalisation of phospho-AKT (ser473) with α-tubulin in mouse embryonic fibroblasts.

The association between phospho-AKT (ser473) and α-tubulin during mitosis was then investigated in MEF cells by confocal microscopy. Figure 4.5.1 shows a sum projection of a z-stack of a single metaphase MEF cell stained with DAPI and the two proteins of interest (A). It is clear from this image that both proteins are in close association. Colocalisation by the intensity thresholding method is shown in image B; white pixels represent coexpression of the two proteins above the 85% threshold. Quantitative colocalisation was inferred from the Pearson's product moment and Mander's correlation coefficients. Image C shows the PDM values (product of the differences between the means) for each pixel from a single z-slice image. The Pearson's correlation statistic returned a value of 0.937 indicating that there is close concordance between the localisation and intensities of the two proteins. Mander's correlation coefficeint values for AKT phospho-serine 473 show close concordance with green fluorescence (0.97) whereas coefficient for α-tubulin is lower (0.878). The implication of this finding is that phospho-AKT is associated with α-tubulin staining. However, α-tubulin staining is observed independently of phospho-AKT. This is indicated by white triangles in image B and image C. Negative PDM values (blue pixels) are seen at the location of astral microtubules during metaphase.

Figure 4.5.2 shows the effect of short-term paclitaxel treatment on the organisation of phospho-AKT (ser473) in MEF cells. Image panels represent individual cells stained for DAPI, α-tubulin and phospho-AKT (ser473). Paclitaxel stabilises microtubules and disrupts spindle formation during polymerisation. This can be seen in panel D where abnormal spindle formation is observed in a single cell. Phospho-AKT patterning is consistent with this abnormal spindle structure. This supports the notion that phospho-AKT is physically associated with microtubules during mitosis in embryonic stage cells in the mouse. Phosphorylation patterns during anaphase and cytokinesis are consistent with observations made in mouse ES cells.

4.6 Effect of mTOR inhibition on mitosis in mouse embryonic stem cells.

In order to assess the effect of mTOR kinase inhibition on the percentages of mitotic cells in mES cultures, an immunostaining assay was developed to visualise mitotic cells by the expression of phospho-histone H3 (ser10). The relationship between H3 phosphorylation and the stages of mitosis can be observed in Figure 4.6.1. Histone H3 phosphorylation is commonly used to generate mitotic index data as it is not phosphorylated during interphase. Sequential phosphorylation of histone H3 residues culminates in ser10 phosphorylation at early prophase. This phosphorylation is maintained throughout mitosis until late telophase when it is dephosphorylated by mitotic proteinases[146,147]. This can be seen in Figure 5.6.1, phospho H3 staining shown in red with α-tubulin (green) and nuclear DAPI staining (blue).

Mouse ES cell cultures were treated with mTOR kinase inhibitors for 3h or 24h before fixation and staining for phospho-histone H3 and DAPI. Images were captured by fluorescence microscopy and total nuclei and phospho-H3 positive nuclei were counted. A mitotic index statistic was generated by dividing the number of H3 positive nuclei by the total number of DAPI nuclei. The effect of mTORC1 inhibition was determined by rapamycin treatment. Also investigated was the effect of the dual mTOR complex kinase inhibitor Ku-0063. The concentration of inhibitors was determined by the titration assays shown in Figures 3.3.3 and 6.3.1. Concentrations were selected that inhibited mES cell proliferation by 50% after 48h. Short-term treatment (3h) of mES cells with rapamycin or Ku-0063 had no effect on the numbers of cells in mitosis; this can be seen in Figure 4.6.2.i. Treatment of mES cells for 24h with rapamycin significantly reduced the numbers of mitotic cells, and treatment with Ku-0063 resulted in a greater reduction in the mitotic index. These findings were statistically significant and are shown in Figure 4.6.2.ii.

Figure 4.5.1

Co-localisation of AKT ser473 with α-tubulin in a proliferating mouse embryonic fibroblasts.

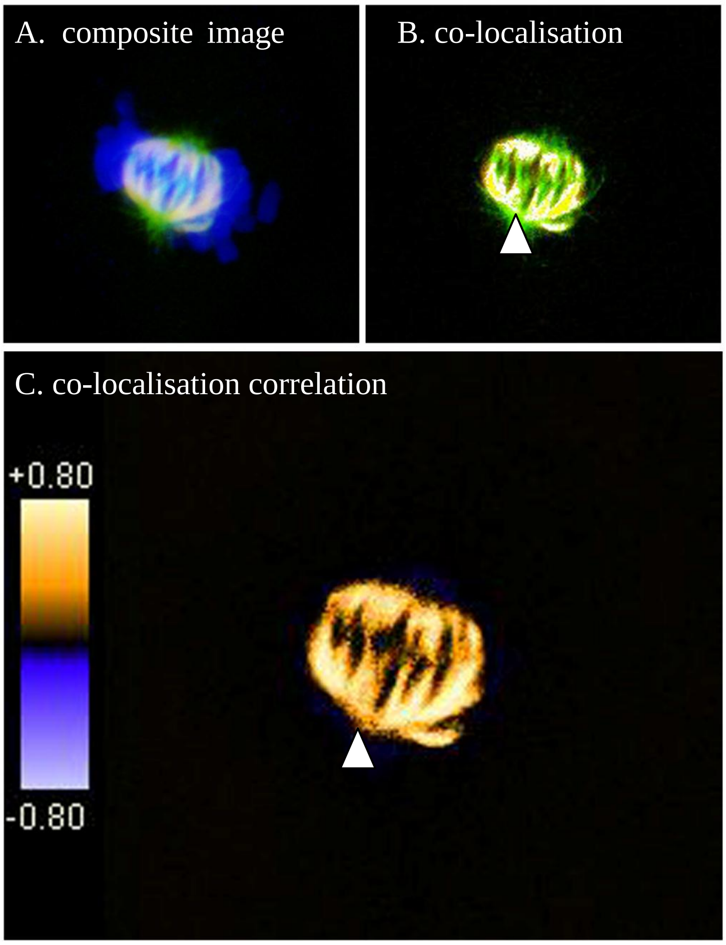

Fig.4.5.1

Mouse embryonic fibroblasts (MEF) were fixed and stained on glass coverslips for analysis by confocal microscopy as previously described. Single slice from z-series image stack. Composite image (A) of nuclear staining with DAPI (blue), α-tubulin/alexa-488 (green) and AKT ser473/alexa-597 (red) of a single metaphase MEF cell. Image B represents merged composite of α-tubulin (green), AKT ser473 (red) colocalised points at 85% threshold. Image C is a graphical representation of PDM values (Product of the Differences from the Mean = (red intensity-mean red intensity) × (green intensity - mean green intensity)). Pearson's correlation value = 0.937. Mander's correlation coefficient M1 = 0.97 (red); M2 = 0.878 (green).

Figure 4.5.2

Short-term paclitaxel treatment does not impair the association of phospho-AKT (ser473) with α-tubulin in MEF cells.

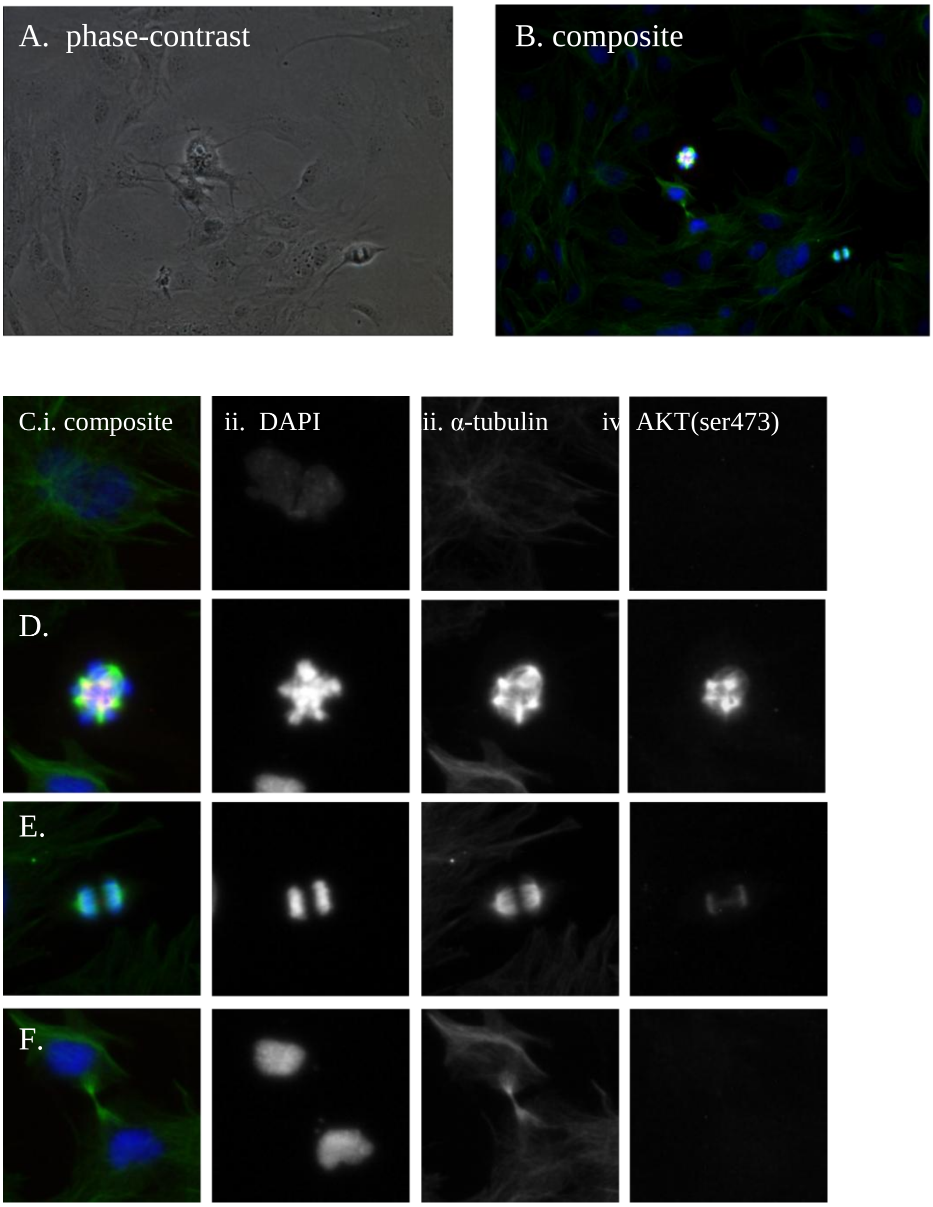
A. phase-contrast
B. composite
C.i. composite
ii. DAPI
ii. α-tubulin
iv AKT(ser473)
D.
E.
F.

Fig.4.5.2

Proliferating mouse embryonic fibroblasts were treated with paclitaxel (5nM) for 4min then fixed and stained to generate composite fluorescence micrographs (image panel i) of DAPI (ii), α-tubulin/alexa-488 (iii) and AKT (ser473)/alexa-555 staining (iv). Selected cells from the phase-contrast image (A) and composite image (B) were identified according to cell cycle phase. Cropped images of cells at interphase (image panel C), prophase/metaphase (image panel D), anaphase (image pane E) and cytokinesis (image panel F) are displayed. The staining of AKT (ser 473) was maintained in paclitaxel treated MEF cells and was associated with mitosis.

Figure 4.6.1

Assessment of mitotic index by phospho-histone H3(ser10) staining.

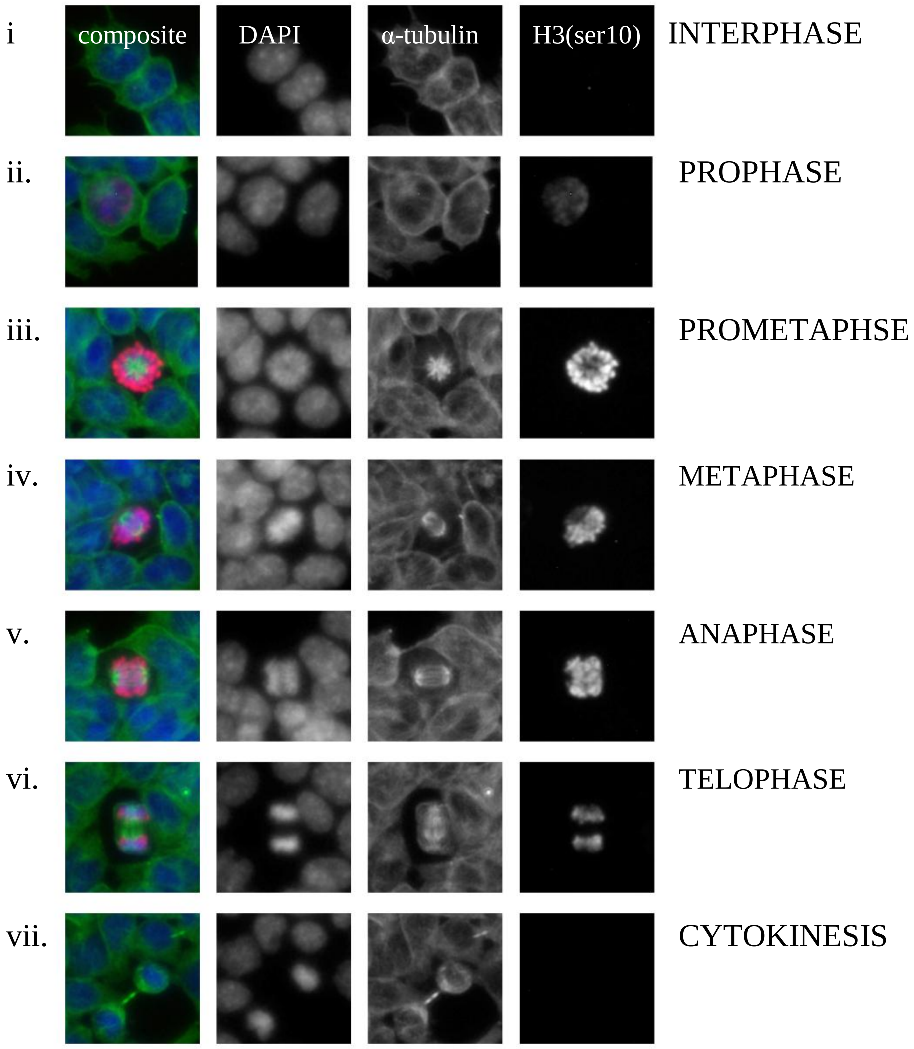
i
composite
DAPI
α-tubulin
H3(ser10)
INTERPHASE
ii.
PROPHASE
iii.
PROMETAPHSE
iv.
METAPHASE
v.
ANAPHASE
vi.
TELOPHASE
vii.
CYTOKINESIS

Fig.4.6.1

Mouse E14 Tga2 cells were cultured under standard growth conditions for 48h and fixed for immunostaining according to a pre-established protocol Cells were stained with DAPI and phospho-histone H3 (ser10) and imaged by fluorescence microscopy at 10x magnification. Individual cells at interphase (i) and successive stages of mitosis were identified by nuclear morphology and α-tubulin patterning. The corresponding expression of phospho-histone-H3 was assessed at each stage of mitosis to enable the use of this antibody to generate mitotic index data from fluorescence micrographs.

Figure 4.6.2

Treatment of mES cells for 24h with TORC1 and TORC2 inhibitors reduces the number of cells in mitosis.

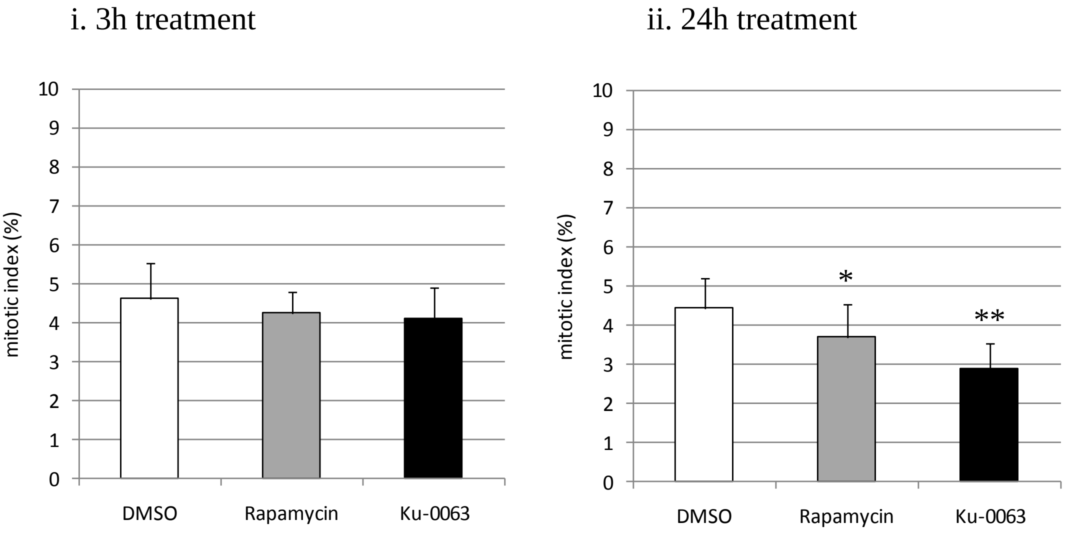
i. 3h treatment

ii. 24h treatment

Fig.4.6.2

Mouse E14 Tga2 cells were cultured under standard growth conditions for 48h and fixed for immunostaining according to a pre-established protocol. Triplicate cultures (n=3) were treated with mTORC1 kinase inhibitor rapamycin (100nM) or the dual mTORC1/mTORC2 kinase inhibitor Ku-0063 (5µM) for the final 24h or 3h of the assay. Cells were stained with DAPI and phospho-histone H3 (ser10) and imaged by fluorescence microscopy. Total numbers of DAPI nuclei and histone-H3+ve nuclei were counted from single channel micrographs from 5 fields of view at 10x magnification. Data presented as the mean percentage of histone-H3+ve nuclei (mitotic index) and standard deviation of the mean. Statistical analysis by parametric t-test, alpha level of $p<0.05$ (*) or $p<0.01$ (**).

4.7 Summary of findings.

The aims of this study were to document the cellular distribution and localisation of mTOR pathway phosphoproteins in mES cells. The methods used here involved the culture E14 cells under standard conditions that had been defined in the previous chapter. Immunostaining protocols were developed to enable the visualisation of phosphoproteins by fluorescence and confocal microscopy.

It was shown that mTOR protein was present in both the nuclear and cytoplasmic compartments. Phosphorylated mTOR was not homogenously distributed or localised within mES cells. Phospho-mTOR serine-2448 was found to be upregulated in some cells. Upon examination it was noted that mitotic cells exhibited increased expression of this phosphospecific form of mTOR. Similar findings were documented with the phospho-serine (2481) specific mTOR as high expression was observed in the nuclei of some cells and mitotic cells exhibited enhanced staining. Examination of these mitotic cells revealed staining patterns that were consistent with localisation to the centrosome and spindle during metaphase. During late mitosis mTOR ser2481 was localised to the midbody between dividing cells. When mES cells were induced to differentiate, they acquired spread morphology and phospho-serine2481 was distributed at cell borders. This was not seen in compact cells that maintained stem cell marker expression. The localisation patterns of phosphospecific mTOR during mitosis were also observed in these spread cells.

The cellular distribution of the TORC1 substrate S6K threonine-389 was homogenous throughout cells in mES cell colonies. However, staining patterns of a different phosphospecific residue of S6K (threonine-412) exhibited dramatic upregulation in some cells. These cells were observed to be in the mitotic phase of the cell cycle as staining was increased in all cells at prophase and was evident until late anaphase. Cells at telophase or cytokinesis exhibited a marked downregulation of phospho-S6K th412.

Findings revealed that the TORC2 substrate phospho-AKT serine-473 exhibited similar patterns of staining. All cells exhibiting high AKT expression were found to be undergoing mitosis. It was noted that the pattern of staining was distinct at each stage of mitosis and appeared to localise with spindle microtubules. This association was confirmed by confocal microscopy as phospho-AKT colocalised with α-tubulin. Disruption of the microtubular network with nocodazole inhibited the AKT patterning in mitotic cells. This mitotic AKT localisation was maintained in early differentiated mES-derived cells that exhibited a spread morphology following LIF deprivation. Mouse embryonic fibroblasts also exhibited this expression pattern, colocalisation was maintained when the spindle organisation but not microtubular polymerisation was disrupted. Extended treatment with inhibitors of mTOR activity reduced the mitotic index of mES cells. This effect was observed following inhibition of TORC1 alone and was potentiated by dual inhibition of TORC1 and TORC2.

In conclusion it was documented that mTOR proteins are phosphorylated during mitosis and exhibit discrete spatio-temporal localisation. During differentiation, mES cells acquired a spread morphology, in these cells mTOR proteins localised at cell borders. This suggests that the mTOR pathway may be regulated differently in compact, pluripotent cells compared with spread, differentiated cells. The implication of this finding is that pluripotent stem cells may exhibit discrete sensitivity to mTOR inhibition and this may enable selective targeting of ES cell proliferation in mixed cell preparations.

Chapter 5

The principle aims of this chapter are to assess the impact of inhibition of the two mTOR complexes and related pathways on the proliferation and viability of mES cells during early differentiation. These experiments follow on from previous findings that show that mTOR pathway proteins may be differentially regulated in compact, pluripotent stem cells and spread, differentiated cells. Furthermore previous experimental finding indicate that components and substrates of the mTOR complex-2 are activated in spatio-temporal manner during cell division. The use of dual-TORC inhibitors in this part of the study will aim to dissect the mTORC1 and mTORC2 mediated effects and strengthen the hypothesis that the timely manipulation of the mTOR pathway in ES cells may provide a bioprocessing tool for industrial scale expansion and differentiation of stem cells. Data presented in this chapter will draw upon image analysis tools that have been developed for this study. Details of the development and validation of these image analysis tools are presented in Appendix 1. Pertinent to this series of experiments is the impact of mTOR inhibition during early differentiation. It is anticipated that development of image analysis tools will enable quantification of the expansion of morphologically distinct pluripotent (compact) and differentiated (spread) cells in mixed cell populations.

The mammalian TOR pathway in the proliferation and viability of mouse embryonic stem cells.

Mammalian TOR sits at a nexus of signal transduction cascades that regulate cellular proliferation and survival. In mouse ES cells, LIF stimulation of the gp-130 receptor activates AKT via the PI3K pathway and promotes TORC1 activation. The TORC2 kinase phosphorylates AKT serine-473, therefore the PI3K pathway interacts both up-stream and down-stream of mTOR. Comparing the inhibition of the PI3K pathway with mTORC1 inhibition alone and dual-TORC inhibition will serve to dissociate the mTOR complex specific effects from global pathway activation.

5.1 Assessment of the effect of the PI3K inhibitor LY294002 on mES cell proliferation and viability.

The inhibitor LY294002 inhibits the PI3K mediated activation of AKT. The effect of LY294002 on the inhibition of mES cell proliferation was assessed. The working concentration range of inhibitor was determined by titration in the nanomolar (Fig.5.1.1) and micromolar ranges (Fig.5.1.2). These findings demonstrate that LY294002 exerts a dose-dependent inhibition of mES cell proliferation. The concentration of 10μM inhibited mES cell proliferation by approximately 50%.

Figure 5.1.1

Dose-dependent effect of LY294002 on mES cell proliferation.

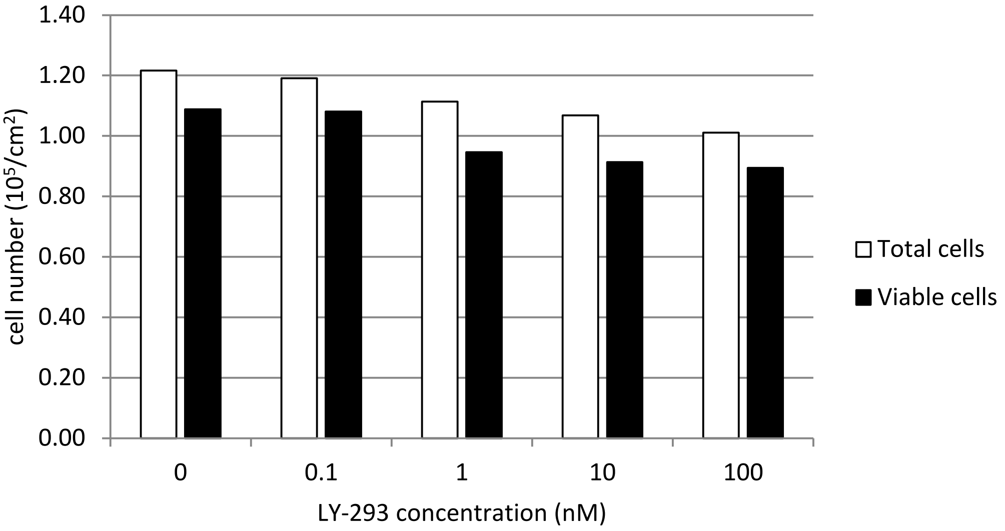

Fig.5.1.1

Dose-dependent effect of LY294002 on mES cell proliferation. Mouse ES cells were seeded into 6 well plates and cultured for 48h with complete growth medium containing 10^3 u/ml LIF and with a nanomolar concentration range of LY294002. At the designated time point, cells were harvested and counted by trypin blue exclusion assay using the Vi-Cell™ automated cell counter. Numbers of total cells and viable cells from a representative assay are presented.

Figure 5.1.2

Dose dependent effect of LY294002 on mES cell proliferation.

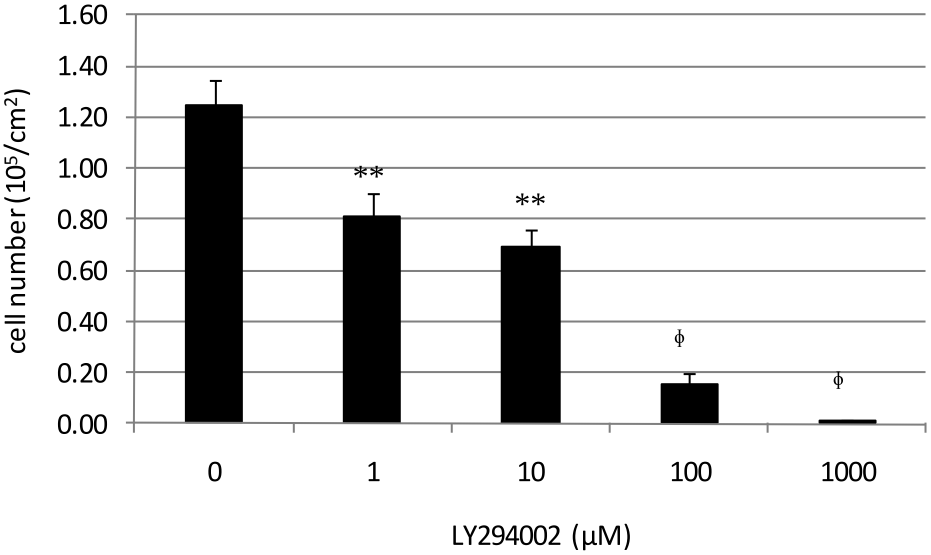

Fig.5.1.2

Dose-dependent effect of LY-290043 on mES cell proliferation. Mouse ES cells were seeded into 6 well plates and cultured for 48h with standard growth medium containing 10^3u/ml LIF and treated with a micromolar concentration range of LY294002 inhibitor. Control wells were treated with DMSO. At the designated time point, cells were harvested and counted by trypin blue exclusion assay using the Vi-Cell™ automated cell counter. Numbers of total cells from three independent culture assays are presented (n=3). Statistical analysis by parametric t-test revealed significant differences at an alpha level of $p<0.01$ (**) and $p<0.001$($^{\phi}$).

5.2 Combined inhibition of mTOR complex 1 and the PI3K pathway on mES cell viability.

This series of experiments were designed to assess the effect of combined inhibition of mTORC1 and PI3K activity on mES cell viability. Mouse E14 cells were seeded into 6-well plates and incubated for 48h in the presence of sub-optimal doses of rapamycin and LY294002 (10 nM rapamycin; 0.1µM LY294002) or combined treatment with both inhibitors at equivalent concentrations. Figure 5.2.1 shows the effect of single and combined inhibitor treatment on cell proliferation assessed by trypin-blue exclusion. Whereas treatment of mES cells with single inhibitors induced a marginal and non-significant inhibition of total cell numbers, the combined inhibitors produced a statistically significant reduction in cell numbers compared with the DMSO treated control and single inhibitors alone ($p<0.01$). This data demonstrates that the combined inhibition of mTORC1 and PI3K pathways synergistically inhibits mES cell proliferation. Treatment of mES cells with inhibitors alone or combined at low concentrations did not reduce mES cell viability (Figure 5.2.2).

Figure 5.2.1

Comparison between the effects of rapamycin, LY-294003 and combined inhibition on mES cell proliferation.

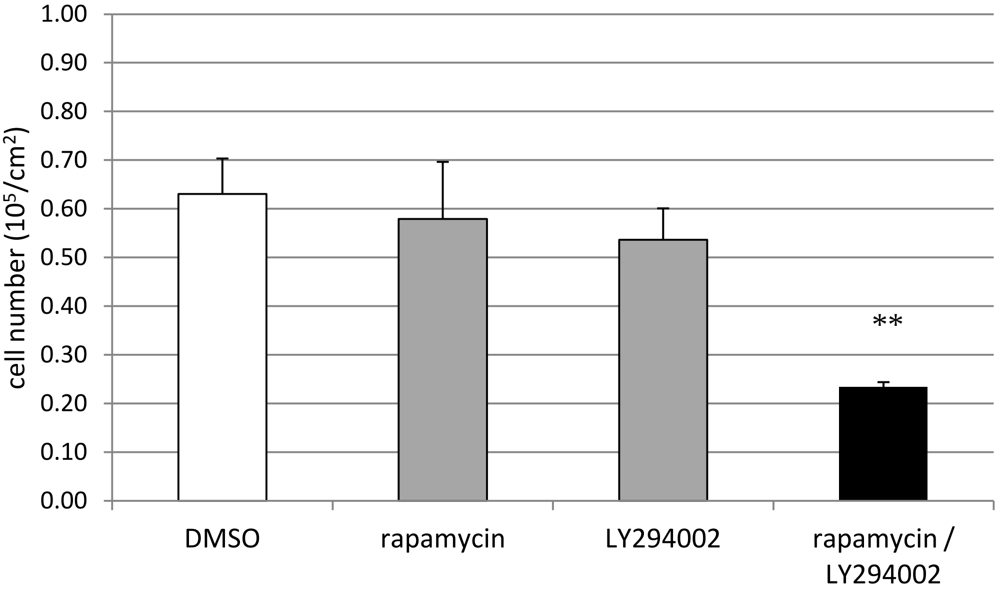

Fig. 5.2.1

Mouse embryonic stem cells were seeded into 6-well plates allowed to attach for 2h in complete growth medium containing LIF. Wells were then treated with sub-optimal doses of rapamycin (10 nM) and LY294002 (0.1μM) for the duration of the experiment. At the designated time-point cells were harvested and manually counted by trypin blue exclusion. Data presented from three independent experiments (n=3) and statistical significance was determined by one-tailed t-test (p<0.01 **).

Figure 5.2.2

Low dose rapamycin and LY294002 does not reduce mES cell viability.

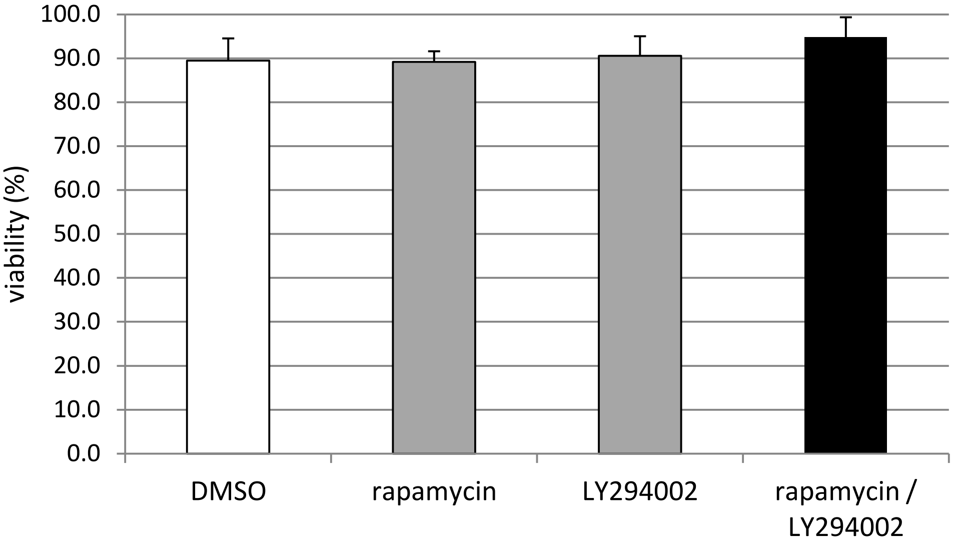

Fig. 5.2.2

Mouse embryonic stem cells were seeded into 6-well plates allowed to attach for 2h in complete growth medium containing LIF. Wells were then treated with sub-optimal doses of rapamycin (10 nM) and LY294002 (0.1µM) for the duration of the experiment. At the designated time-point cells were harvested and viability assessed by trypin blue exclusion. Data presented from three independent experiments (n=3).

5.3 The effect of the dual mTOR kinase inhibitor Ku-0063 on mES cell proliferation.

Rapamycin has great promise in cancer therapy as inhibitor of cellular proliferation. The efficacy of rapamycin treatments in vivo has not met the expectations of the in vitro studies. Consequently rapamycin analogues have been developed through drug screening programs in industry and academia. Recently, a number of dual TORC kinase inhibitors have been developed. One such inhibitor Ku-0063 has been shown to inhibit both TORC1 and TORC2 kinase activity without inhibiting 76 other kinases[134]. The effects of dual TORC kinase inhibitors have not been assessed on mouse embryonic stem cells.

The effect of this inhibitor on mES cell proliferation was assessed in Figure 5.3.1. Mouse ES cells were treated for 48h at the specified concentrations. The numbers of total cells were assessed by an automated trypin blue exclusion assay. The highest concentration used in this assay resulted in crystalisation of the inhibitor and ablation of cell proliferation was observed. Treatment of mES cells with Ku-0063 for 48h significantly inhibited proliferation at all concentrations tested with the concentration of 3μM producing a 50% inhibition of cell numbers.

.

Figure 5.3.1

Dose-dependent effect of Ku-0063 treatment on mES cell proliferation.

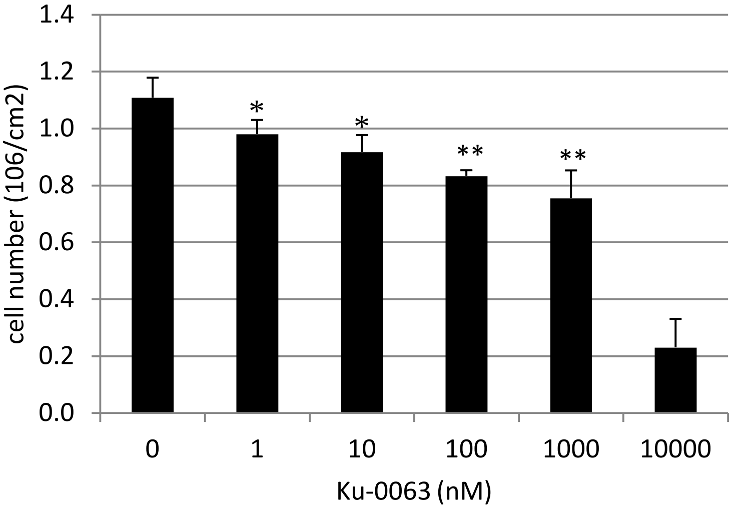

Fig 5.3.1

Dose-dependent effect of Ku-0063 inhibitor on mES cell proliferation. Mouse ES cells were cultured for 48h with complete growth medium supplemented with 103u/ml LIF and 10% FCS and treated with DMSO or a 5-fold titration of Ku-0063. At the assay end-point cells were harvested and counted by trypin blue exclusion with the Vi-Cell™ automated cell counter. Mean and standard deviation of triplicate culture assays (n=3). Statistical differences by parametric t-test (p<0.05*, p<0.01**). Dose of 1000nm resulted in crystallisation of inhibitor.

5.4 The effect of mTOR and PI3K inhibitors on mES cell viability.

To assess the effect of mTOR and PI3K inhibitors on mES cell viability, cultures were treated with inhibitors at a concentration that were shown to produce a 50% inhibition in cell proliferation after 48h. Mouse ES cells were cultured with complete growth medium containing serum supplemented with or devoid of LIF and treated with the inhibitors for 48h before harvesting for viability assessment. Treatment of mES cells with these inhibitors did not affect viability in LIF stimulated growth medium (Figure 5.4.1). Similar effects were observed when inhibitors were applied in growth medium devoid of LIF (Fig 5.4.2)

Figure 5.4.1

Inhibitors of the mTOR and PI3K pathways inhibit the proliferation but not viability of LIF stimulated mES cells.

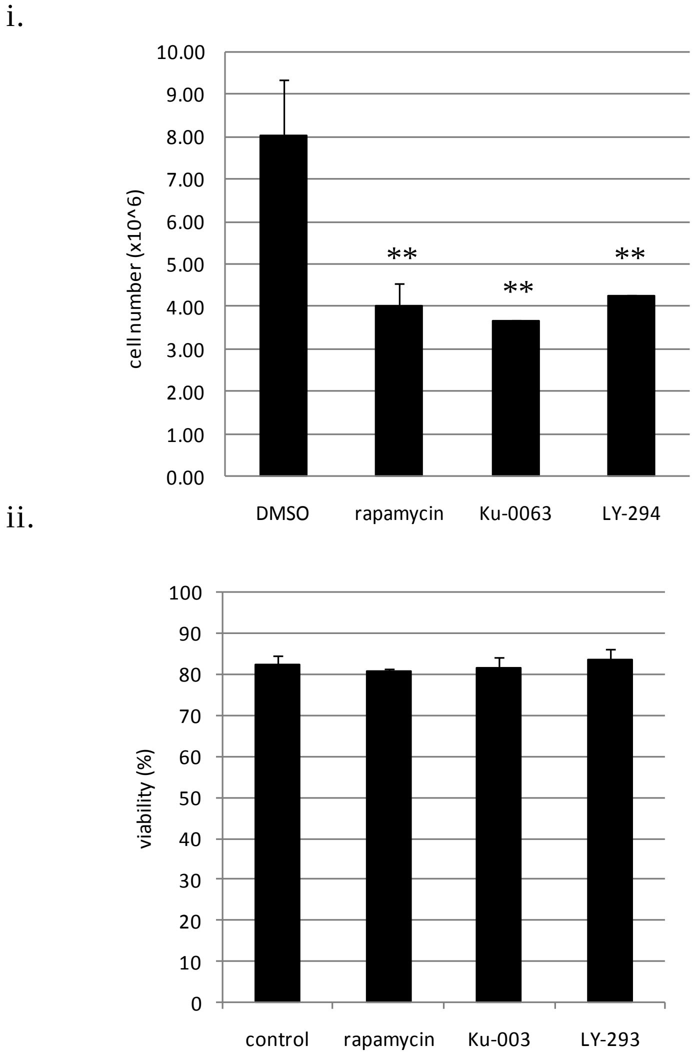

Fig. 5.4.1

Mouse E14 ES cells were cultured with complete growth medium supplemented with 10^3u/ml LIF and 10% serum and treated for 48h with DMSO (1µl), rapamycin (100nM), Ku-0063 (3µM) or LY-294 for 48h. Cells were harvested and analysed by trypin blue exclusion assay with the Vi-Cell™ automated cell counting system. Data presented as mean cell number (i) and viability (ii) from 3 parallel culture assays ($n=3^{tech}$) Statistical analysis was performed by parametric t-test adjusted for multiple comparisons p<0.016 (**).

Figure 5.4.2

Inhibitors of the mTOR and PI3K pathways inhibit the proliferation but not viability mES cells deprived of LIF.

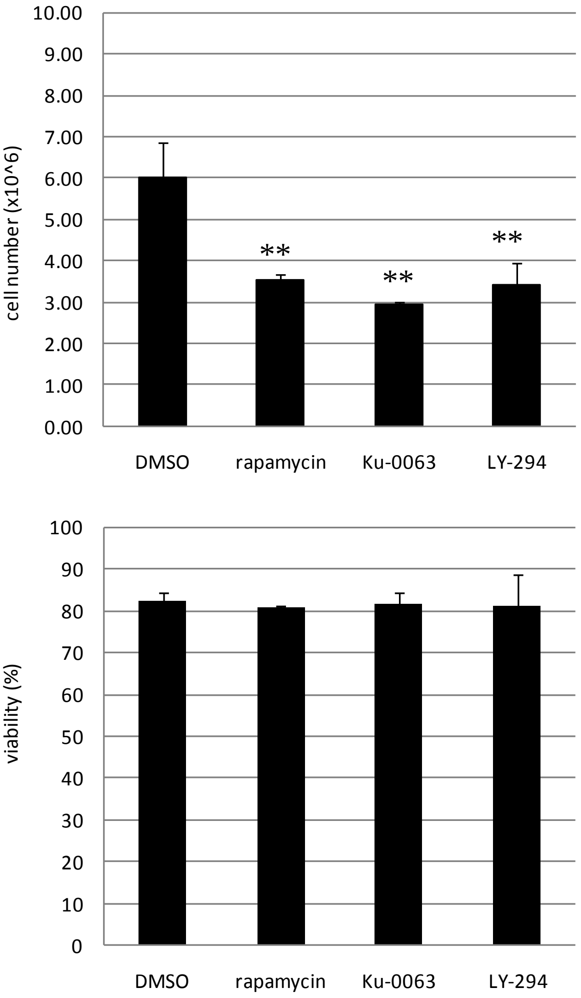

Fig. 5.4.2

Mouse E14 ES cells were cultured with complete growth medium supplemented with 10^3u/ml LIF and 10% serum and treated for 48h with DMSO (1µl), rapamycin (100nM), Ku-0063 (3µM) or LY-294002 for 48h. Cells were harvested and analysed by trypin blue exclusion assay with the Vi-Cell™ automated cell counting system. Data presented as mean cell number (i) and viability (ii) from 3 parallel culture assays ($n=3^{tech}$). Differences were deemed significant at the alpha level of $p<0.016$ (**) adjusted for multiple comparisons. No significant differences in cell viability were observed.

Figure 5.4.3

Inhibitors of the mTOR and PI3K pathways increase the numbers of detached mES cells when deprived of LIF.

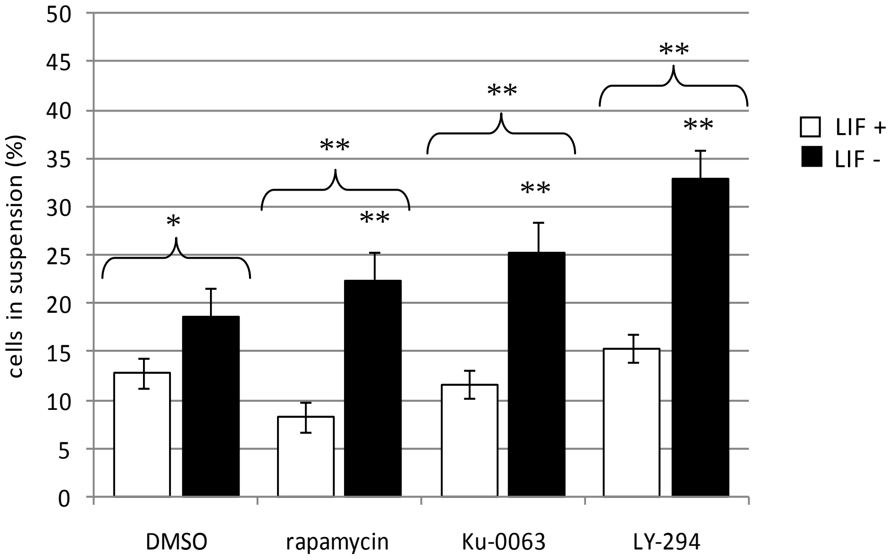

Fig. 5.4.3

Mouse E14 ES cells were cultured with complete growth medium supplemented with 10^3u/ml LIF and 10% serum and treated for 48h with DMSO (1µl), rapamycin (100nM), Ku-0063 (3µM) or LY-294 for 48h. Cells were harvested from spent medium and counted by automated trypin blue exclusion. The percentage of detached cell was calculated by dividing number of cells in suspension by the total number of adherent cells. Data presented as mean and standard error of three parallel cultures ($n=3^{tech}$). Statistical analysis was performed by parametric t-test adjusted for multiple comparisons $p<0.016$ (**). LIF deprivation increased cell detachment, an effect that was exacerbated by inhibitor treatment.

5.5 The effect of serum deprivation on mES colony formation.

This experiment was designed to assess the impact of mTOR inhibition on mES cell colony formation and integrity after 24h of serum deprivation. Cultures were imaged by phase contrast microscopy and assessed with the image analysis tool Method 2 (see Appendix 1). Representative examples of the phase-contrast and results images are shown (Figure 5.5.1).

Figure 5.5.2 shows that LIF supported colony expansion in serum deprived conditions as deprivation of LIF reduced the total cell area ($p<0.01$). Rapamycin inhibited colony expansion in serum deprived only in the presence of LIF. Viability was determined by dividing the non-viable cell area by the total area. It was observed that rapamycin but not Ku-0063 promoted viability during serum deprivation in the presence and absence of LIF ($p<0.01$)

Figure 5.5.1

Representative phase contrast and results images of mES cells following serum deprivation.

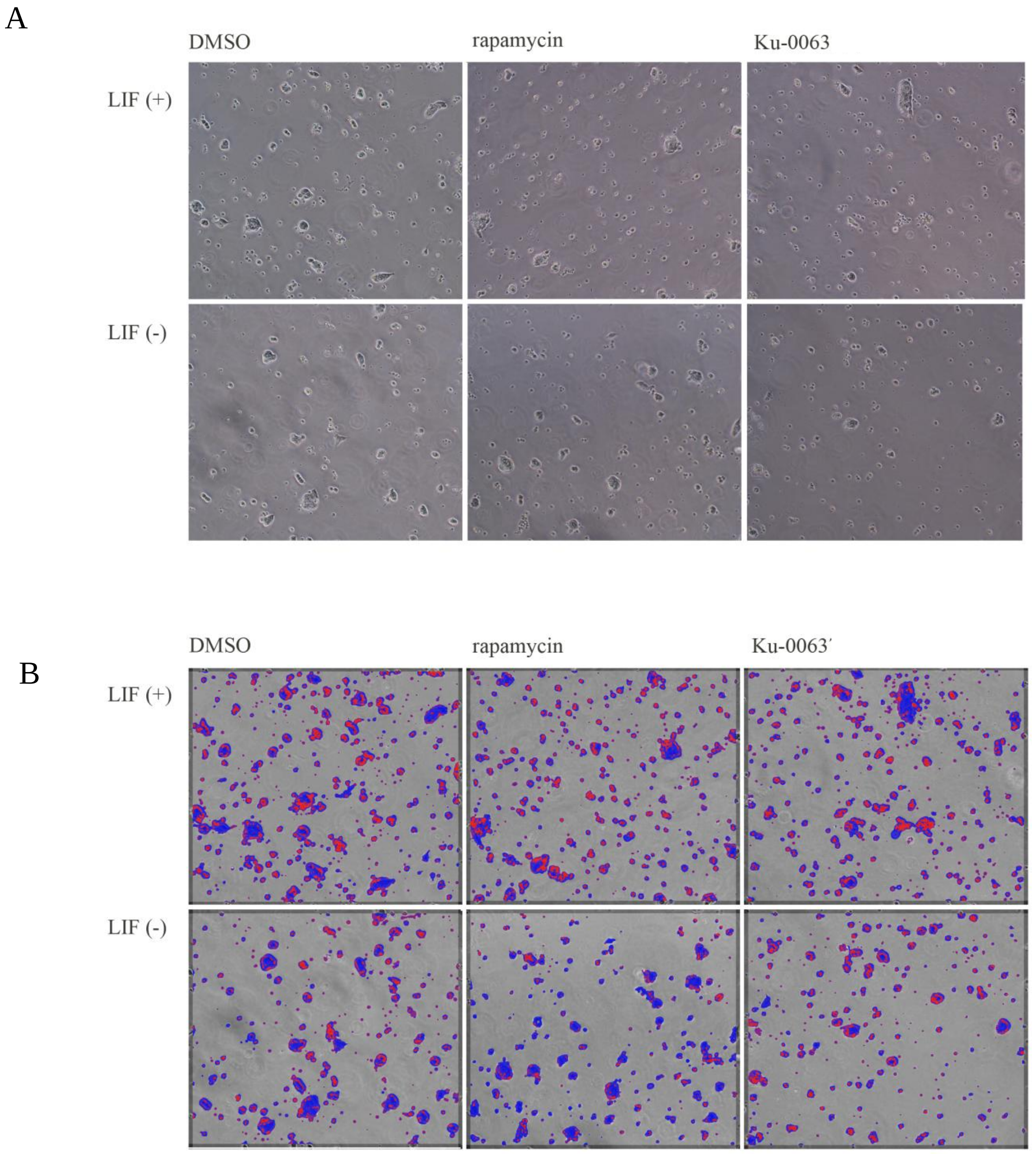
A
DMSO
rapamycin
Ku-0063
LIF (+)
LIF (-)
B
DMSO
rapamycin
Ku-0063
LIF (+)
LIF (-)

Fig.5.5.1

Mouse E14 Es cells were cultured in growth medium and starved of serum for 24h. Cells were either provided with 10^3u/ml LIF or deprived of LIF and treated with the mTOR kinase inhibitors rapamycin (100nM) or Ku-0063 (3µM) for 24h before analysis. Data is presented as phase contrast images (A) and results images generated by Method 2 image analysis tool.

Figure 5.5.2

Mouse ES cell colony expansion is impaired by LIF withdrawal during serum starvation.

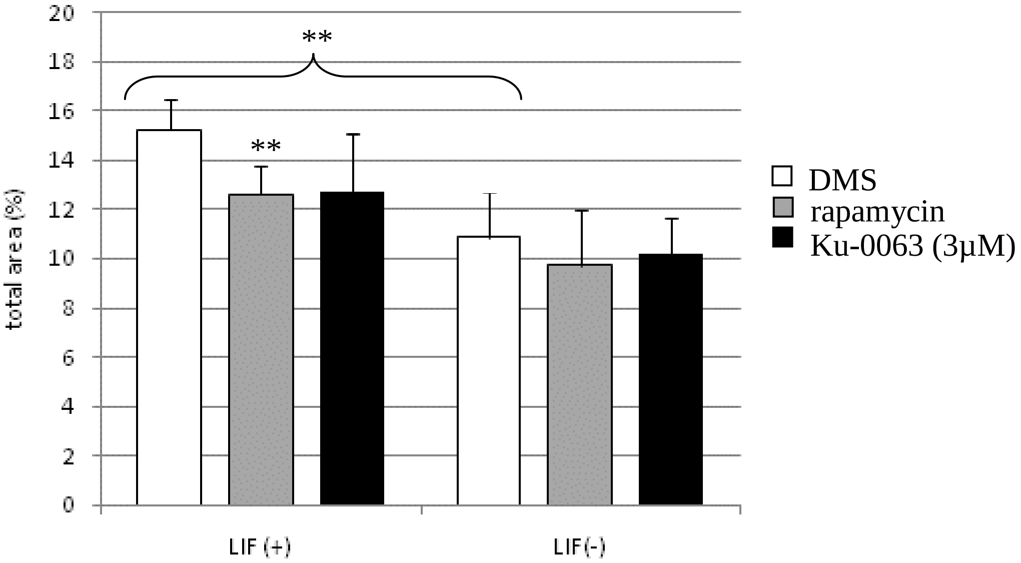

Fig.5.5.2

Data generated by Method 2 shows that LIF withdrawal impairs mES colony expansion during serum deprivation. Mouse ES cells were cultured for 24h without serum and LIF or supplemented with 10^3u/ml LIF. Total cell area was calculated from phase contrast micrographs. Data is expressed as the percentage of cell area relative to total measured area. Statistical differences were determined by parametric t-test adjusted for multiple comparisons ($p<0.01$).

Figure 5.5.3

Rapamycin treatment promotes mES viability independently of LIF during serum starvation.

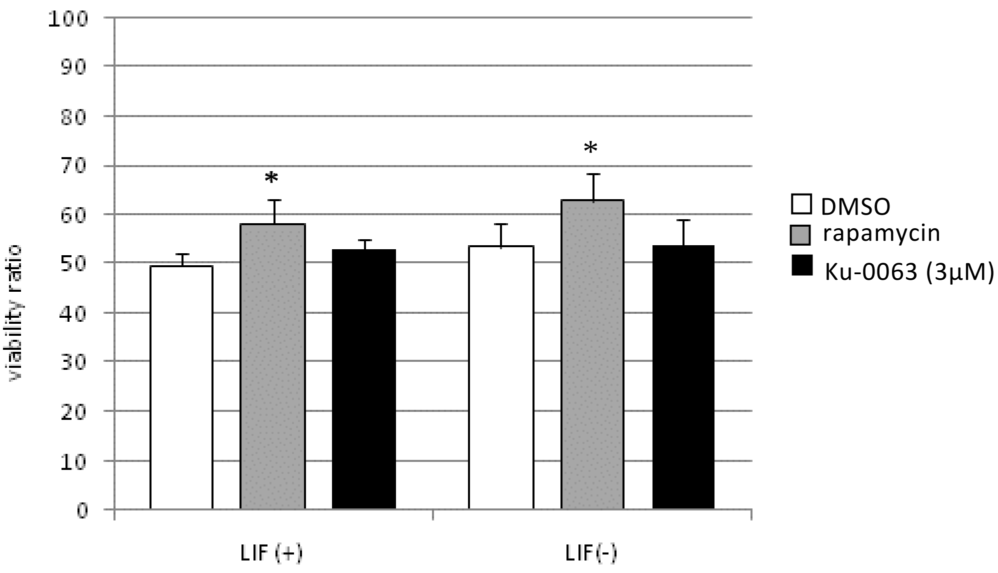

Fig.5.5.3

Data generated by Method 2 analysis shows that rapamycin treatment promotes viability independently of LIF during serum deprivation. Mouse ES cells were cultured for 24h without serum and LIF or supplemented with 10^3u/ml LIF. Cell area and phase (viable, non-viable cell area) was calculated from phase contrast micrographs. Data is expressed as the ratio of viable cell area relative to the total cell area. Statistical differences assessed by parametric t-test ($p<0.05$; *)

5.6 The effect of mTOR inhibition on mES colony expansion during differentiation.

Mouse ES cells were deprived of LIF for 96h to initiate differentiation. After 48h cells were detached and seeded into fresh flasks with growth medium containing or devoid of LIF. The mTOR inhibitors, rapamycin and Ku-0063 were applied for the final 48h of the assay. Total cell confluence and the percentage area containing compact and spread was assessed by the Method 2 image analysis technique. Figure 5.6.1 shows that both inhibitors reduced the total cell area in medium LIF-supplemented growth medium ($p<0.01$). Both inhibitors also reduced the area covered by compact cells but not spread cells ($P<0.01$). Similar findings were observed in LIF-deficient growth medium (Figure 5.6.2). Total confluence was decreased in each case and inhibitor treatment impaired the compact cell area but not the spread cell area (rapamycin $p<0.01$; Ku-0063 $p<0.05$); however, the effect of KU-0063 was not significant when the alpha level was reduced for multiple comparison errors to (α/number of tests). Representative images of the results returned from images of mES cells in LIF-deficient growth medium are shown in Figure 5.6.3.

Figure 5.6.1

Mammalian TOR complex inhibitors reduce the expansion of cells with compact but not spread morphology.

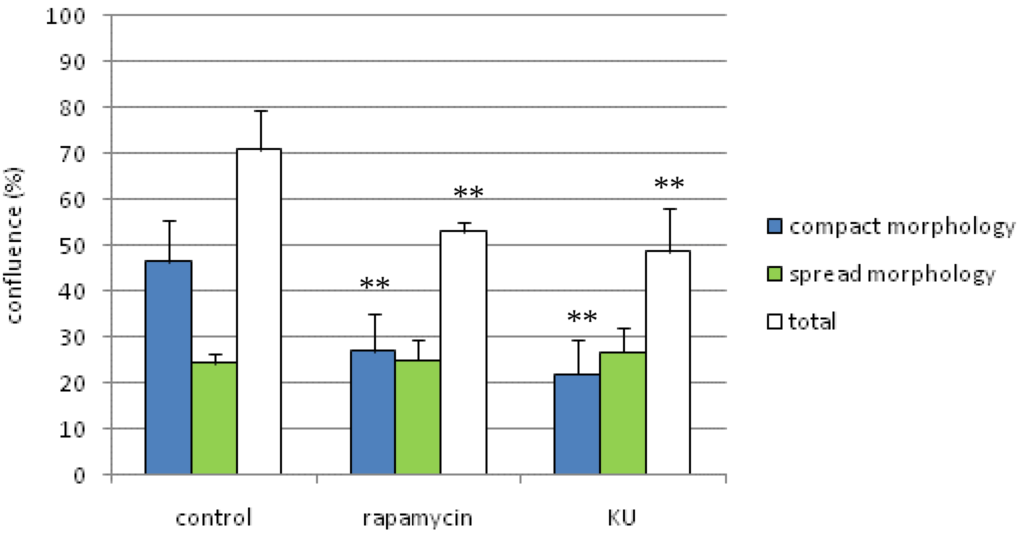

Fig.5.6.1

Mouse ES cells (E14) were seeded into parallel T25 flasks and cultured for 48h in complete growth medium devoid of LIF. After seeding, cultures were treated with 1ul DMSO (control), 100nM rapamycin or 3µM Ku-0063. Cells were then detached and seeded into 6-well plates at a density of 10^5cells/cm^2. Wells were treated with Inhibitors and growth medium containing 10^3u/ml LIF for a further 48h. After a total of 4 days in culture triplicate wells were imaged by phase contrast microscopy at 10x magnification (10x FOV)

Figure 5.6.2

Mammalian TOR complexes inhibitors reduce the expansion of cells with compact but not spread morphology during differentiation.

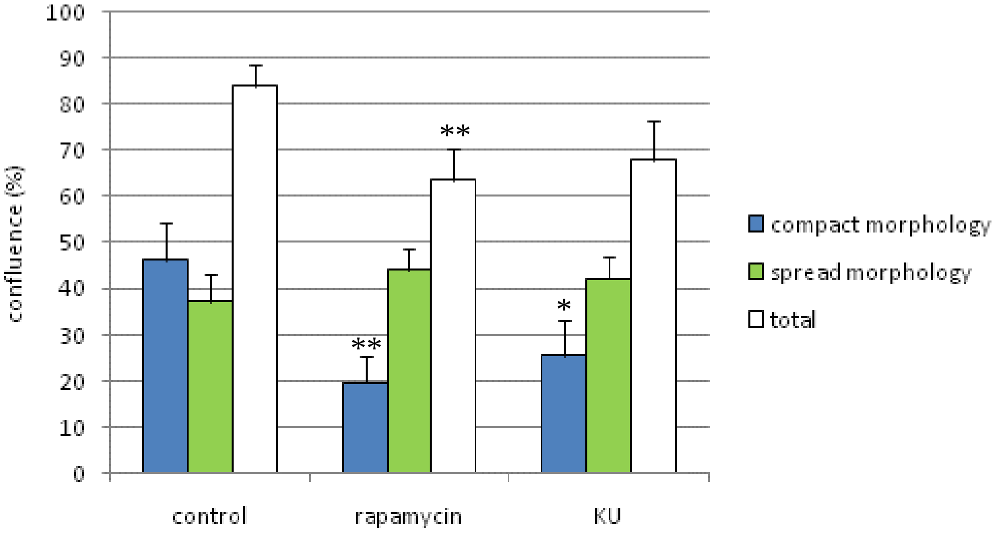

Fig.5.6.2

Mouse ES cells (E14) were seeded into parallel T25 flasks and cultured for 48h in complete growth medium devoid of LIF. After seeding, cultures were treated with 1ul DMSO (control), 100nM rapamycin or 3µM Ku-0063. Cells were then detached and seeded into 6-well plates at a density of 10^5cells/cm^2. Wells were treated with Inhibitors and growth medium containing 10^3u/ml LIF for a further 48h. After a total of 4 days in culture triplicate wells were imaged by phase contrast microscopy at 10x magnification (10x FOV)

Figure 5.6.3

Representative phase contrast and results images from Method 2 analysis of expansion of compact and spread cells during differentiation.

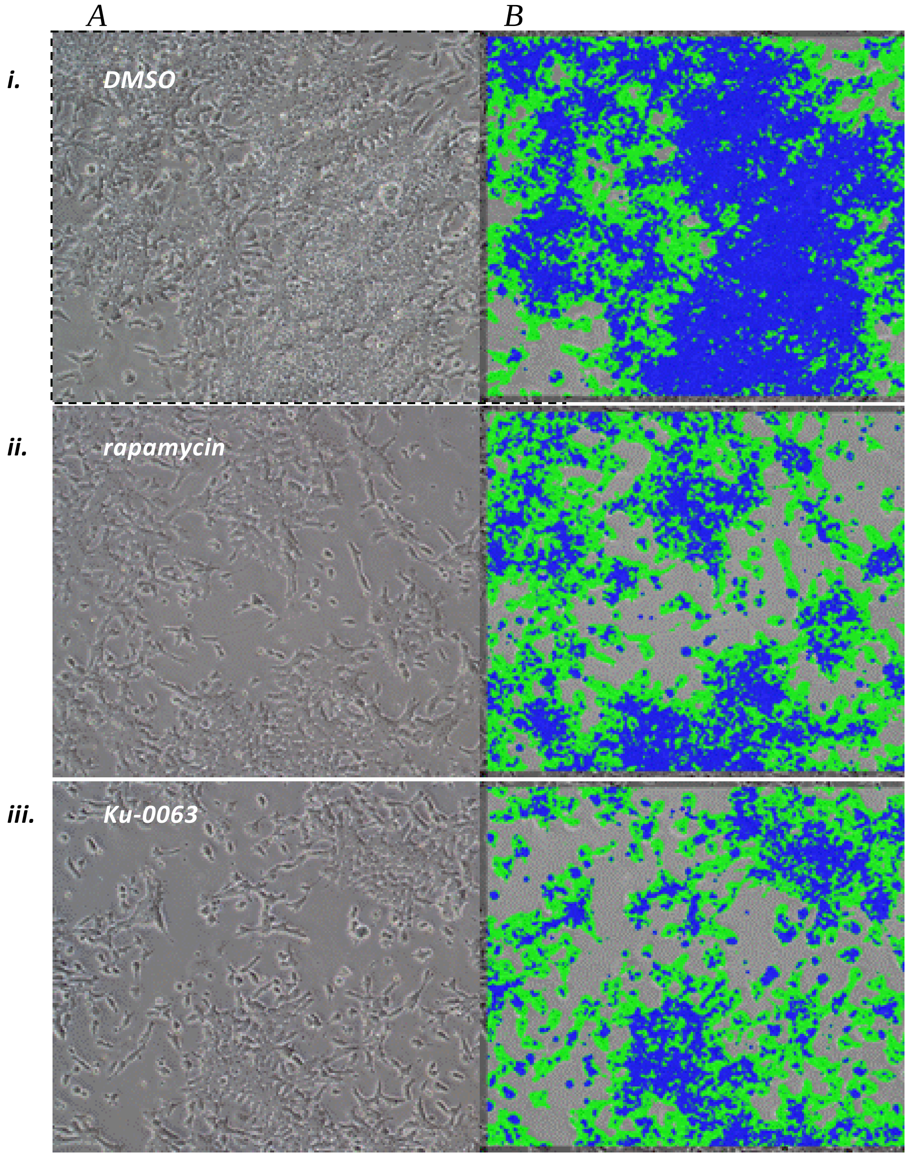

Fig. 5.6.3

Representative images of analysis of mES cell morphology after 4 days LIF deprivation. Phase contrast (A) and results images (B) by Method 2 analysis of compact cells (blue pixels) and spread cells (green pixels). Details of the validation of the MEthod 2 image analysis tool are documented in Appendix 1.

5.7 The effect of mTOR inhibition on mES cell apoptosis

Inhibition of mTOR complex signalling has been shown to reduce the proliferation of many cell types. It was demonstrated that mouse ES cell proliferation was impaired by treatment with mTOR inhibitors rapamycin and Ku-0063. In some cell types rapamycin treatment has been observed to promote cell death[135]. In this study, a series of experiments was designed to test the effect of mTOR inhibitors on mES cell viability and apoptosis under different growth conditions.

The assessment of apoptosis was undertaken using by flow cytometry using a commercially available apoptosis detection kit. Cells were harvested and processed for analysis within 1h. Apoptosis was determined by immunostaining for annexin IV and nuclear incorporation of the fluorescent dye 7-AAD using the Guava-Nexin™ kit. All analysis was performed with the Guava-EasyCyte™ flow cytometer. Details of the immunostaining protocol are found in Experimental Methods.

To assess the effect of mTOR inhibition on apoptosis levels, mouse E14-Tga2 cells were cultured in 6-well tissue culture dishes with complete growth medium supplemented with LIF (10^3 u/ml). After 45h, wells were washed to remove non-viable cells and then treated with 1µl DMSO, 100nM rapamycin or 3µM Ku-0063. After 3h treatment, cells were harvested for analysis.

The primary outcome measure for this assay was to determine whether rapamycin and Ku-0063 increased the levels of apoptosis in mES cells. Figure 5.7.1 shows that rapamycin did not have an effect on cell viability and did not modify the percentages of early and late apoptotic cells. However, treatment with Ku-0063 increased mES cell viability (DMSO = 79.2% +/- 1.4%; Ku-0063 = 84.5% +/- 0.9%; p = 0.01). This was complemented by a small reduction in the proportion of cells in late apoptosis (DMSO

= 13.5% +/- 1.0%; KU = 10.5% +/- 0.4%; p=0.01). Thus mTOR inhibitors do not appear to induce apoptosis in mES cells. Moreover, these findings suggest that Ku-0063 treatment may increase viability under normal growth conditions.

Leukaemia inhibitory factor (LIF) is known to activate cell survival pathways via activation of the PI3 kinase pathway and mitogenic pathways. Consequently the potential cytotoxic effects of the short-term application of mTOR inhibitors to mES cells may not seen when LIF is present. So to assess whether mTOR inhibition reduced the viability of E14 cells when LIF was absent the experiment was repeated without LIF supplementation.

Figure 5.7.2 shows the effect of 3h inhibitor treatment on mES viability and apoptosis in LIF deficient growth medium. Once again treatment with rapamycin did not reduce viability. Furthermore there was a small reduction in the percentage of cells entering apoptosis with Ku-0063 treatment (DMSO = 4.1 +/- 0.9%; KU = 1.6 +/- 0.2%; p<0.01). These findings confirm that short-term application of mTOR inhibitors does not induce impair viability, conversely dual inhibition of the two mTOR complexes appears to promote survival. The absence of LIF did not the affect the viability response of mES cells to the dual kinase inhibitor Ku-0063.

The effects of extended inhibition of the mTOR complex 1 with rapamycin and mTOR complexes 1 and 2 with Ku-0063on apoptosis was assessed in mES cells. Mouse E14 cultures were grown for 48h with complete growth medium without LIF or medium supplemented with 10^3u/ml LIF. Inhibitors were added after 24h, thereafter cells were incubated for a further 24h until the experiment was halted at 48h. Cultures were washed and adherent cells were collected for apoptosis assessment by flow cytometry.

Figure 5.7.1

Short term treatment of pluripotent mES cells with mTOR inhibitors does not induce apoptosis.

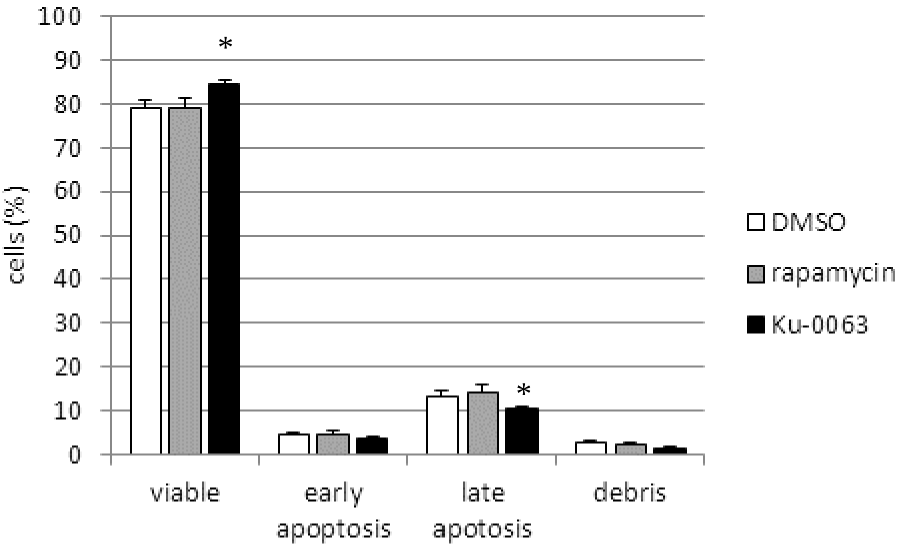

Fig.5.7.1

Short-term treatment with mTOR inhibitors does not increase mES cell apoptosis. Mouse E14 cells were treated for 3h with mTOR inhibitors rapamycin (100nM) or Ku-0063 (100nM) in the presence of LIF (103u/ml). The percentage of cells undergoing early and late apoptosis was assessed by flow cytometric assessment of 7-AAD incorporation and annexin V binding. Results presented from 3 experiments (n =3), statistical significance was determined by parametric t-test, single asterix denotes significance at alpha level of $p<0.05$ (*). Viability determined as the primary outcome measure in multiparameter apoptosis assays, other findings were designated as secondary outcome measures (Experimental methods 2.16).

Figure 5.7.2

Short-term mTOR inhibition (3h) does not induce apoptosis in mES cells in LIF deficient growth medium.

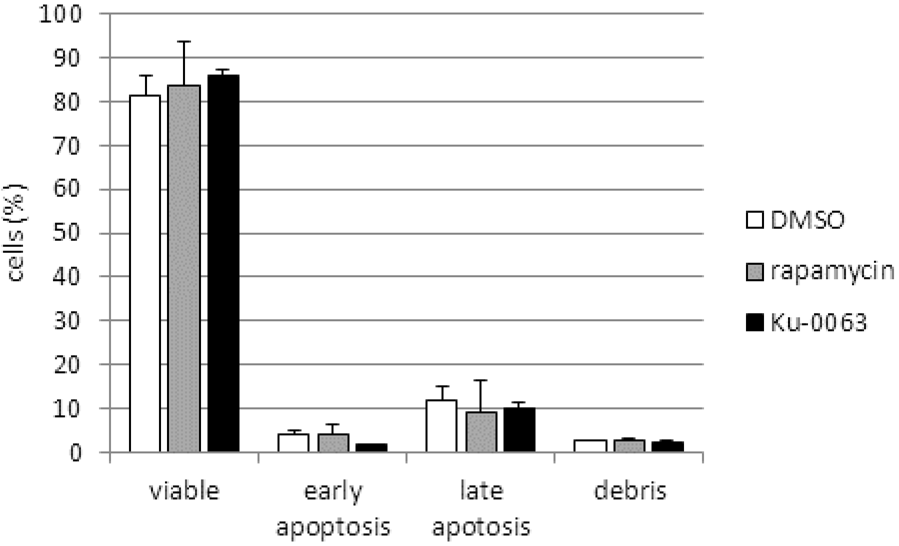

Fig.5.7.2

Short-term treatment of mES cells with mTOR inhibitors does not induce apoptosis. Treatment of E14 mES cells with 100nM rapamycin or Ku-0063 for 3h had no effect on viability. Ku-0063 reduced the percentage of cells entering apoptosis. Statistical analysis was performed with the two-tailed unpaired t-test and significance was determined at $\alpha = 0.01$ (*). Data is presented as mean plus standard deviation from 3 experiments (n=3).

Figure 5.7.3 shows the effect of 24h inhibition of mTOR on mES cell viability and apoptosis in LIF supplemented growth medium. Inhibition of the TORC1 kinase with rapamycin resulted in a significant increase in the proportion of viable cells relative to the DMSO treated control ($p<0.05$). Increased viability was associated with a decrease in the mean percentage of cells in early apoptosis. However, extended inhibition of TORC1 and TORC2 with Ku-0063 reduced viability ($p<0.05$) and increased levels of late apoptotic E14 cells after 24h.

Figure 5.7.4 shows the impact of 24h treatment with mTOR inhibitors on mES cell viability and apoptosis in LIF deficient growth medium. It was found that rapamycin treatment increased mES cell viability ($p<0.05$), and reduced the percentage of cells in early apoptosis.

The spent growth medium from the previous assay was collected and levels of apoptosis were assessed by flow cytometry. The primary outcome measure was defined as the effect of inhibitor treatment on the viability of detached cells in spent growth medium. A secondary outcome measure was defined as the impact of LIF on the mTOR mediated effect on inhibition on viability.

Figure 5.7.5 shows the effect of mTOR inhibition on the viability and apoptosis of detached mES cells in LIF-deficient growth medium. Rapamycin treatment increased the viability of detached cells (DMSO = 27.9% +/- 9.2%; rapamycin = 71.3% +/- 14.8%; $p=0.04$). Treatment with Ku-0063 also increased the mean percentage of viable cells (Ku-0063 = 60.1% +/- 3.8%; $p=0.04$) and decreased the percentage of late apoptotic cells.

Figure 5.7.3

Extended mTOR inhibition affects the viability and apoptosis of E14 mES cells cultured with LIF.

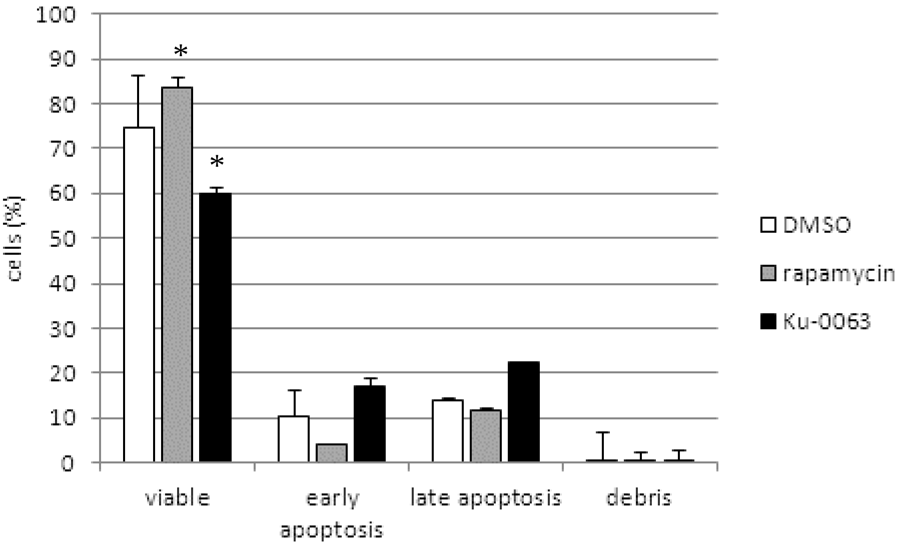

Fig.5.7.3

Treatment of mES cells with mTOR inhibitors for 24h under normal growth conditions. Rapamycin (100nM) and Ku-0063 (100nM) treatment generated significant alterations in the levels of viability and apoptosis of E14 cells. Data is presented as the mean and standard deviation of 3 parallel culture experiments ($n=3^{tech}$).Statistical significance was determined by two-tailed t-test at α <0.05 (*) and p<0.01 (**).

Figure 5.7.4

Extended mTOR inhibition affects the viability of E14 mES cells cultured in LIF deficient growth medium.

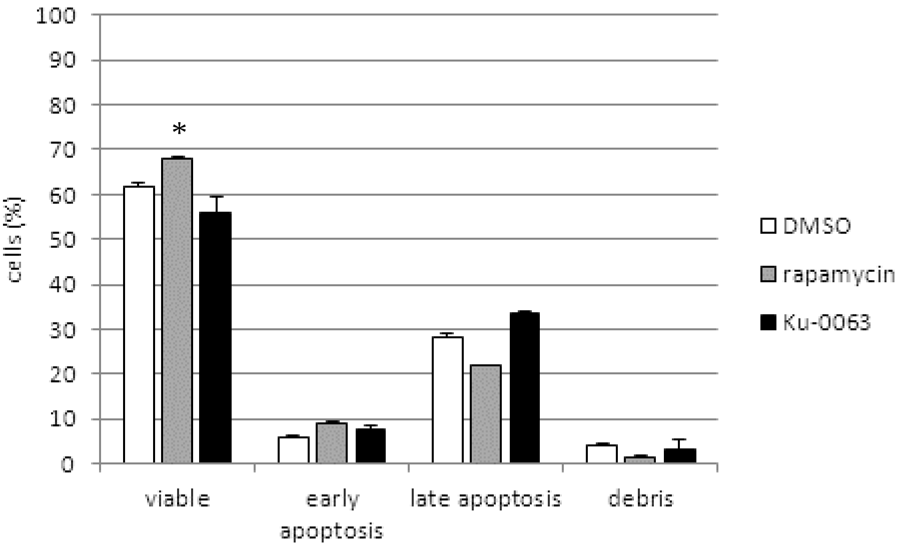

Fig.5.7.4

Treatment of mES cells with mTOR inhibitors for 24h under normal growth conditions. Rapamycin (100nM) and Ku-0063 (100nM) treatment generated significant alterations in the levels of viability and apoptosis of E14 cells. Data is presented as the mean and standard deviation of 3 parallel culture experiments ($n=3^{tech}$).Statistical significance was determined by two-tailed t-test at α <0.05 (*) and p<0.01 (**).

Figure 5.7.5

Inhibition of mTOR treatment increases the viability of detached cells in LIF-deficient growth medium.

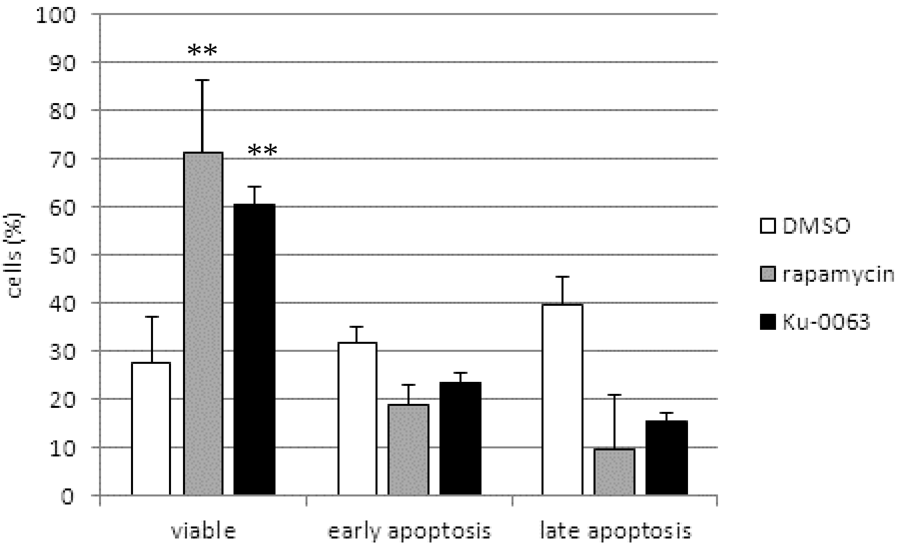

Fig.5.7.5

Treatment of mES cells with mTOR inhibitors for 24h under normal growth conditions. Rapamycin (100nM) and Ku-0063 (100nM) treatment generated significant alterations in the levels of viability and apoptosis of E14 cells. Data is presented as the mean and standard deviation of 3 parallel culture experiments (n=3^{tech}). Statistical significance was determined by two-tailed t-test at α <0.05 (*) and p<0.01 (**).

To assess the effect of mTOR inhibition on viability and apoptosis in differentiating mouse ES cells, cultures were deprived of LIF and expanded for 96h. Cells were pre-treated for the first 48h (D0-D2) with DMSO (control), 100nM rapamycin or Ku-0063 (5µM). Alternatively, cells were treated with mTOR inhibitors for 96h (D0-D4). After 48h, cultures were supplied with fresh growth medium and grown for a further 48hrs before harvesting for apoptosis analysis.

The effect of long-term mTOR inhibition on the viability of differentiating mES cells is shown in Figure 5.7.6. Rapamycin treatment reduced the percentage of viable cells, and increased the percentage of cells in early apoptosis; these findings were statistically significant by parametric t-test ($p<0.05$). Treatment of cultures with the dual TORC kinase inhibitor Ku-0063 resulted in a significant inhibition in cell viability and increased the percentage of cells in late apoptosis ($p<0.01$). These effects were not observed when cultures were pre-treated with inhibitors for the first 48h. Therefore, extended inhibition of TORC1 kinase activity impaired the viability of differentiating mES cells. Furthermore, dual inhibition of TORC1 and TORC2 exacerbates this effect and results in increased apoptosis.

Figure 5.7.6

Treatment but not pretreatment of differentiating mES cells with mTOR kinase inhibitors reduces cell viability.

i.

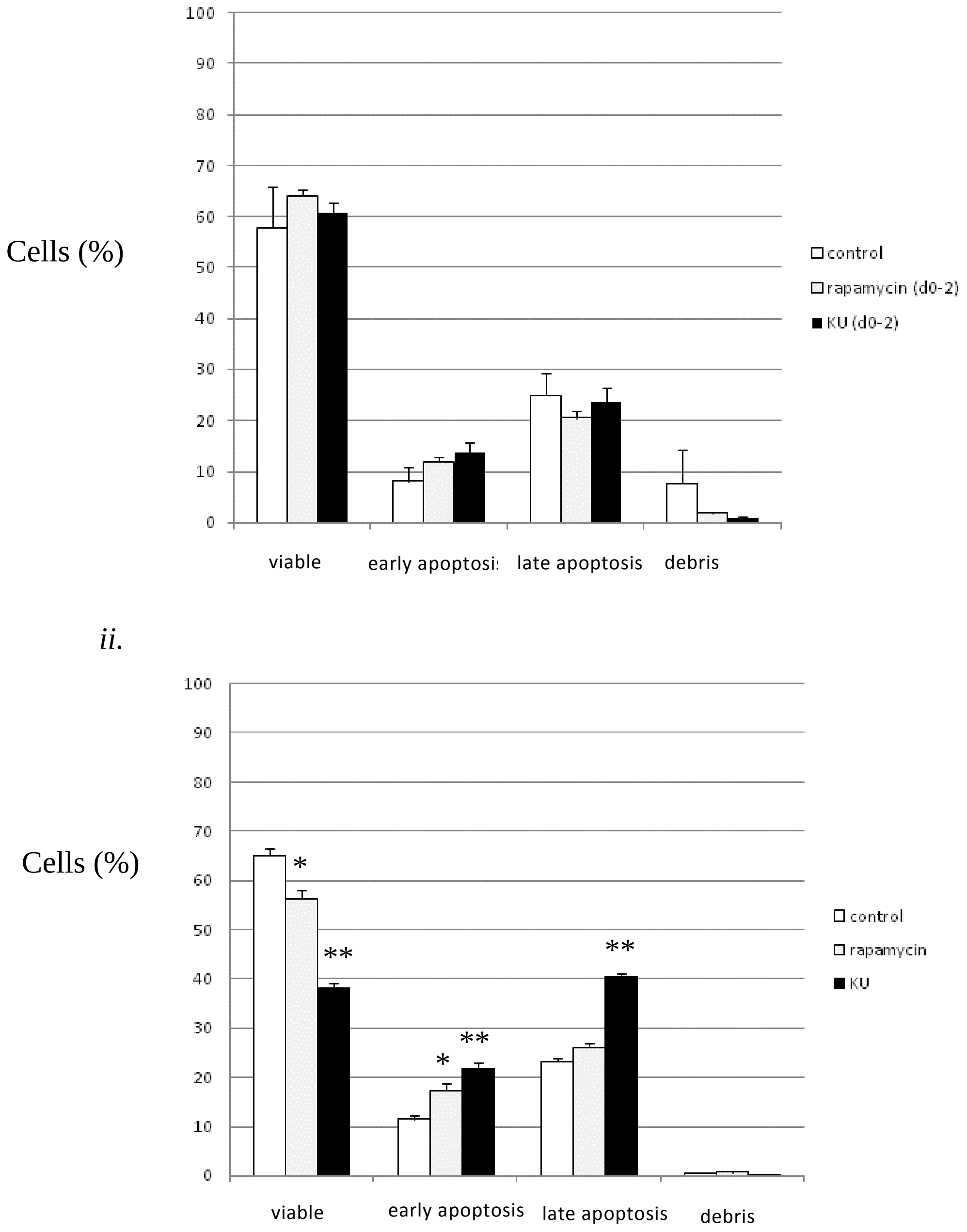

Figure legend

Fig, 5.7.6

Treatment of differentiating mES cells for 96h with mTOR inhibitors reduces viability and increases apoptosis. Mouse E14 cells were cultured for a total of 96h without LIF supplementation. Triplicate cultures (n=3) were pretreated for 48h or treated for 96h with the mTOR inhibitors rapamycin (100nM) or Ku-0063 (5µM). Assessment of apoptosis undertaken by flow cytometry after a total of 96h in culture; statistical differences determined by parametric t-test ($p<0.05$*; $p<0.01$**).

5.8 Summary of findings.

The aim of this study was to assess effects of mTOR inhibitors on the expansion of and viability of mES cells during normal culture and spontaneous differentiation.

Initially, the working concentration of the PI3K inhibitor LY294002 was established by a dose-response assay. Sub-optimal doses of rapamycin and LY294002 were applied to mES cells in culture. It was observed that single inhibitors alone did not reduce proliferation; however, combined treatment produced a synergistic inhibitory effect.

Mouse ES cells were then treated with a concentration of inhibitors that generated a 50% reduction in proliferation (I_c50). Rapamycin, Ku-0063 (dual TORC inhibitor) and LY294002 alone did not reduce viability either in the presence or absence of LIF. However, when LIF was absent, the percentage of detached cells in the spent medium increased. This effect was notable upon rapamycin treatment, greater with Ku-0063 treatment and was exacerbated with LY294002 treatment. These findings suggest that the activity of AKT may underlie the effects seen here as rapamycin, Ku-0063 and LY294002 are AKT inhibitors with increasing specificity.

Serum deprivation impaired mES colony formation, this effect was more apparent upon LIF deprivation. Rapamycin treatment inhibited colony formation in LIF-supplemented but not LIF-deprived conditions. Interestingly, rapamycin promoted viability in both treatment groups; this effect was not seen with Ku-0063 treatment. It can be deduced from this that TORC1 inhibition promotes the survival of serum-starved mES cells whereas additional TORC2 inhibition negates the survival advantage of TORC1 inhibition. As mTOR is known to regulate autophagy, this process may explain these observations as recycling intracellular proteins may provide a survival advantage in serum deprived conditions.

Mouse ES cells were induced to differentiate by withdrawal of LIF for 48h, after passaging and re-plating, cells were then provided with mTOR inhibitors and growth medium containing or devoid of LIF for a further 48h. The effects of LIF and mTOR inhibitors on cell expansion were then assessed. The objective was to induce cell spreading upon early differentiation and then test the impact of mTOR inhibitors on the expansion of morphologically distinct cells. The image analysis tool, Method 2 (see Appendix 1) was used to assess cell confluence and morphology. It was observed that both rapamycin and KU-0063 inhibited the expansion of compact but not spread cells in LIF-containing medium. In medium devoid of LIF similar effects were observed. This finding is key to the overarching hypothesis of this study, the implication of this data is that during early differentiation, inhibition of the mTOR pathway may selectively inhibit the expansion of pluripotent stem cells but not differentiated cells. Consequently it may be possible to achieve both a greater purity of differentiated cells and eliminate contaminating parent cells from mixed cell cultures. Interestingly these observed effects were independent of LIF stimulation and may therefore be applied to stem cells that are not dependent upon LIF to maintain pluripotency.

The effects of mTOR inhibitors on viability and apoptosis were also assessed. Short term treatment did not mediate a biological effect. However extended treatment with rapamycin increased viability whereas extended Ku-0063 treatment impaired viability, similar effects were observed in both medium containing and devoid of LIF. Inhibition of the mTOR pathway increased the percentage of cells in suspension when cultures were deprived of LIF, interestingly the viability of these detached cells was enhanced by rapamycin and Ku-0063. This supports the notion that inhibition of mTOR/PI3K signalling impairs cell attachment, an effect that is apparent when LIF stimulation of the PI3K pathway is removed and cells are allowed to differentiate. Putting these findings into the context of a bioprocess, it would be necessary to remove suspended cells by the addition of a washing step to ensure that viable pluripotent cells do not persist in the culture vessel.

Extending the differentiation period to 4 days, it was observed that mTOR inhibition impaired cell viability whereas pre-treatment with inhibitors had no effect on viability. Rapamycin treatment mediated a significant effect and Ku-0063 treatment exacerbated the effect on cell viability.

In conclusion, mTOR inhibition appears to promote the viability of pluripotent mES cells. When deprived of LIF, mES cells were prone to detach from the growth surface upon mTOR inhibition, as these detached cells were predominantly viable, apoptosis was not deemed to be responsible. This effect was enhanced by additional inhibition of TORC2 whereas LY294002 inhibition of the PI3K pathway further increased detachment. As differentiation proceeded during extended LIF deprivation, dual mTOR kinase inhibition but not TORC1 inhibition alone reduced viability. That these effects were observed when LIF was not present, it can be concluded that the activity and inhibition of AKT is likely to be a causal factor in this effect.

Finally, during differentiation, mTOR inhibition impaired the expansion of cells with compact but not spread morphology. The implication of this finding is that targeting the mTOR pathway during early differentiation may be an effective intervention to improve the purity of differentiated cells and reduce the prevalence of pluripotent cells in cultures. As the persistence of pluripotent cells in preparations for cellular therapies may have serious safety implications, this intervention may be useful in the context of industrial production of ES cell based therapies. That mTOR inhibition also increases cell detachment and promotes the viability of these detached cells, an additional washing step must be incorporated to remove pluripotent cells from the culture vessels.

In conclusion, mTOR inhibition during the early differentiation of embryonic stem cells may provide a bioprocessing advantage that both increases the purity of differentiated cells and removes potentially hazardous pluripotent cells from cultures. Further work will be necessary to find out if deprivation of branched-chain amino acids promotes similar effects to the inhibition of the mTOR pathway with small molecule inhibitors.

Chapter 6

Discussion

The primary objective of this study was to assess the principle that manipulation of the mTOR pathway during the expansion and differentiation of embryonic stem cells may provide a bioprocessing advantage that may be utilised at an industrial scale. The justification for this hypothesis stems from the fact that the mTOR pathway is central to the regulation of cell growth and proliferation, is highly conserved and is sensitive to the bioavailability of amino acids and glucose. Consequently the mTOR pathway may be modulated in a cost-effective manner by the provision and depletion of key nutrients. Pluripotent stem cells and somatic cells have different requirements regarding cell growth and proliferation, whereas embryonic stem cells proliferate rapidly and have little requirement for cell growth, differentiated somatic cells have a greater dependence upon cell growth and less requirement for proliferation. By targeting the mTOR pathway it may be possible to take advantage of these features for bioprocess improvements. However, the regulation of the mTOR pathway in ES cells is poorly understood. Consequently the experimental work presented in this study served to define the model system to be utlised, to characterise the mTOR pathway in the model system and finally to assess the effects of manipulating the mTOR pathway under different culture conditions. When this experimental data is taken together, conclusions are drawn to assess the validity of the central hypothesis. Furthermore, recommendations are made regarding the nature of intervention and caveats to mTOR modulation in the context of ES cell expansion and differentiation.

6.1 Preliminary observations.

Preliminary observations indicated that during the routine culture of mES cells, mTOR complex 1 activity was not maximal after 48h. It was observed that growth medium supplementation potentiated the phosphorylation of p70S6K th389. The relative level of phospho-S6K was assayed throughout the course of the passage cycle and twenty four hours after seeding, phosphorylation of S6K was at the highest observed level. Levels of S6K phosphorylation were then observed to decline after 48h. Interestingly, the pattern of S6K phosphorylation in mES cells over the 48h passage cycle was reflected in the growth rate curves presented in Appendix 1.2.2 and Appendix 1.4.2. This data demonstrates that after 30-35 hrs in culture the rate of colony expansion declines. Therefore there is an association between mTORC1 activity and colony expansion. This supports the notion that during the expansion of ES cells in vitro potentiating mTOR activation may provide a bioprocessing advantage. In this context, mTOR activity may be maintained by supplementing cultures with glucose and branched-chain amino acids. Whereas glucose will prevent mTOR deactivation via the AMPK-TSC complex in negative feedback loop, amino acids such as leucine act in a positive feedback system to promote mTOR activity. As both glucose and leucine are relatively cheap to produce compared with recombinant proteins it is therefore recommended that in the context of industrial production of ES cells, levels should be maintained to prevent mTOR pathway deactivation.

6.2 Subcellular localisation of mTOR phosphoproteins

In order to further characterise the activation of the mTOR pathway in mES cells under standard culture conditions, the cellular distribution of phospho-mTOR proteins were assessed by fluorescence microscopy. It has been documented that the cellular localisation of phospho-mTOR proteins is associated with the proliferative potential of cells. One such study documented a negative association between cytoplasmic localisation of mTOR and survival in gastric cancer patients[136]. In another study it was observed that both high levels of phospho-mTOR, and nuclear localisation were associated with tumour progression poor outcome in endometrial cancer[137]. Thus in the clinical context, mTOR activation and localisation is associated with neoplastic potential. It was not clear from these studies whether the differential activity and localisation of the two mTOR complexes related to the proliferation of cancerous cells or whether there was a relationship between discrete mTOR phosphorylation sites and proliferative potential.

In this study the total mTOR protein was stained and observed to reside in both nuclear and cytoplasmic compartments. However it was documented that the distribution of phospho-mTOR at serine residue 2448 was not uniform in mES cells. It was observed that phospho-ser2448 was marginally increased in cells undergoing mitosis. This finding is supported by reports documenting an increase in the phosphorylation of the mTOR ser2448 residue during the M-phase in ovarian granulosa cells[138,139]. Thus there may indeed be a relationship between phospho-specific mTOR localisation and proliferation.

The immunostaining pattern of phospho-mTOR serine-2481 exhibited marked nuclear localisation in mouse ES cell, and distinct phosphorylation patterns were observed in cells undergoing mitosis. The mitotic phosphorylation of mTOR at serine 2481 has been previously reported[140, 149]. In the first study by Vasquez-Martin et al in 2009, the intracellular localisation of phospho-mTOR ser2481 was documented in cancer cells. It was observed that some interphase cells exhibited punctate nuclear localisation and this was associated with proliferative capacity. As mitosis progressed through telophase, mTOR was localised at the midzone and midbody regions. Vasquez-Martin et al also reported that during late mitosis mTOR ser2481 formed a ring-like structure surrounded by microtubular bundles. They concluded that phospho-specific mTOR may be involved in the completion of mitosis, this hypothesis had not been previously considered.

A second study by the same group concurred with these findings, similar localisation patterns were observed in dividing cells in breast cancer tissue biopsies. It was also noted that phospho-mTOR ser2481 was an accurate marker of mitotic cells. However this technique appeared to identify mitotic cells from prophase until late anaphase. The localisation of mTOR phosphoprotein in dividing breast cancer cells revealed a close association with condensed chromatin in prophase, localisation with the mitotic spindle at anaphase and the midbody and intercellular bridge during telophase and cytokinesis. These published observations support the findings of this study where very similar if not identical expression patterns were documented.

It was observed in this investigation that there was an accumulation of phospho-mTOR ser2481 at the spindle pole in dividing mES cells. However, this association was not confirmed by co-staining for microtubular or centrosomal proteins. The pattern of phosphoprotein activation observed in prophase and prometaphase can also be seen with related phosphoproteins. In one such study by Vasquez-Martin, phospho-AMPK was shown to exhibit identical staining patterns to that seen here with mTOR ser2481[150]. Phospho-AMPK was colocalised with α-tubulin and significantly, centrosomal γ-tubulin. These localisation patterns were confirmed by co-staining for Aurora-A, a mitosis marker and a member of the chromosomal passenger complex[151]. Phosphoproteins within this complex have a role in the stabilisation of microtubules during spindle assembly, chromosome alignment and the completion of cytokinesis[152, 153].

Data presented in this study shows that mitotic phosphorylation of mTOR ser2481 was present in differentiated mES cells that exhibited a spread morphology. In these cells, phospho-mTOR ser2481 was distributed at the borders between adjacent cells. It was not clear if mTOR ser2481 was also localised at the cell membrane in ES cells with compact morphology. There is strong evidence to support the notion that mTOR activity occurs at lipid membranes[146]. It was reported that mTOR is membrane anchored, however active mTOR complexes are predominantly found at endomembranes. This is supported by the finding that the activity of Rheb, the upstream regulator of mTORC1 complex is localised at these endomembranes[147]. In yeast, it was reported that both TORC1 and TORC2 were associated with detergent resistant membrane fractions that were independent of lipid rafts. Proteins isolated from these preparations were associated with the plasma membrane, endocytic processes and the actin cytoskeleton.

Here, mouse ES cells exhibited uniform distribution of both total and phospho-th389 p70S6K. However, phsopho-th421 S6K was upregulated in a small percentage of cells. Upon examination of these images, it was apparent that the strong staining was restricted to cells in mitosis. This upregulation began at prophase and was maintained until late telophase. Cells undergoing cytokinesis did not exhibit high staining for this phosphoprotein.

Interestingly, similar findings were reported by Schmidt et al in 2007 [148]. Phospho-th421 S6K was visualised in cells from rat kidney sections. They observed an increase in phospho-th421 expression at early prophase that persisted throughout mitosis. In that investigation, localisation at specific intracellular organelles or structures was not observed. Findings presented here, showed high expression in mitotic mES cells, but not the distinct patterning seen with mTOR phosphoproteins.

Prior to this work, it was documented that phospho-ser421 was associated with mitosis in HeLa cells[149]. Phosphorylation of this S6K residue was correlated with the activity of the cell cycle regulatory protein cdc-2. Interestingly, p70S6K proteins that were phosphorylated at residues within the autoregualtory domain (eg: th421) were all elevated during mitosis. Interestingly, the converse was true for the th389 phosphorylation site. It was found that th389 phosphorylation was lost during mitosis. Furthermore, in cells arrested by nocodazole treatment, the kinase activity of S6K was absent. Thus, Shah et al demonstrated that the functional activity of S6K is lost during mitosis, an effect that is associated with increased phosphorylation of th421 and reduced phosphorylation of th389. They postulated that regulation of S6K activity differs in mitosis than in mitogen or nutrient stimulated cells.

In support of this hypothesis, Le et al demonstrated that paclitaxel treatment induced the upregulation of th421 phosphorylation and the concurrent inhibition of S6K activity[159]. Paclitaxel inhibits microtubule depolymerisation and arrests the cell cycle at G_2/M when tubulin polymerisation is necessary to form the mitotic spindle. It was observed that the paclitaxel mediated phosphorylation of th421 was impaired by an inhibition of the ACG kinase protein kinase-C (PKC) or the MAPK enzyme ERK. The mitotic phosphorylation of th421 may also be dependent upon other kinases that are active specifically during mitosis. Importantly, it was observed that paclitaxel treatment did not induce th389 phosphorylation and p70S6K activity was inhibited during mitosis.

The TORC2 kinase is known to directly phosphorylate AKT at serine residue 473 [77]. In mES cells, evidence shown here demonstrated that the intracellular localisation of AKT ser473 was restricted to mitosis. In these cells, AKT ser473 exhibited distinct patterning. Co-staining between α-tubulin and AKT ser473 was undertaken to determine if this patterning was associated with the microtubular network. This was found to be true and AKT expression mirrored the microtubular structure throughout the stages of mitosis. The percentage of AKT-positive and mitotic cells was concordant, this confirmed that the distinct AKT expression was a mitosis specific event.

Colocalisation between AKT ser473 staining and α-tubulin was confirmed by confocal microscopy. When tubulin polymerisation was disrupted with nocodazole, both the microtubular structure and AKT patterning were lost. This relationship was also observed in mouse embryonic fibroblasts, there was a significant correlation between α-tubulin and AKT ser473 in the x, y and z planes. Colocalisation was maintained after microtubules were disrupted with paclitaxel. Spindle formation was aberrant, however colocalisation was maintained. Thus, these findings showed that phospho-AKT ser473 is associated with polymerised microtubules.

To date, the mitotic association between AKT ser473 phosphorylation and spindle microtubules has not been shown. However, similar findings have been reported in mouse oocytes during meiosis. In these published studies, it was noted that AKT ser473 was localised with microtubules, and inhibition of PI3K activation impaired oocyte maturation. Meiosis involves asynchronous division resulting in the formation of a polar body after metaphase-1 (M1) and then spindle realignment. Following metaphase-2, emission of a second polar body completes meiosis. Inhibition of AKT phosphorylation with LY294002 impaired polar body formation at M1 and resulted in loss of the AKT ser473 distribution pattern[163].

Additionally, injection of an AKT ser473 binding antibody resulted in shortened, abnormal spindles. The actions of this AKT ser473 peptide in oocytes resulted in the failure of second polar body emission[164]. These findings were supported by a subsequent study undertaken by Kalous *et al* in 2006 who observed that AKT ser473 appeared localised ‘in the area of the condensed chromosomes’ and co-stained with pericentrin, a centrosomal protein[153]. These reports are the only published observations of phospho-AKT ser473 localisation with microtubules during cell division. Therefore, the data presented here represent the novel observation that AKT ser473 localised with spindle microtubules during mitosis in embryonic stem cells and embryonic fibroblasts.

Finally, it was observed that acute treatment of mES cells with mTOR inhibitors did not reduce the number of cells in mitosis. However, extended treatment with either rapamycin or the dual TORC inhibitor did inhibit mitotic cell numbers. This effect was enhanced with the dual kinase inhibitor. Consequently, these findings show that in response to TORC1 inhibition, cells continue to transit through mitosis, although in reduced numbers.

Dual inhibitors of the mTOR complexes also reduced the numbers of mitotic cells but did not arrest the cell cycle completely. Analysis of AKT ser473 staining in these cells was performed but not shown (Appendix 1), phospho-AKT persisted in mitotic cells under these conditions. It was documented that Ku-0063 treatment did not arrest mES cells at mitosis and at the high concentrations, proliferation was not abrogated. When cells were treated with 10μM Ku-0063, cell numbers were dramatically reduced and viability was very low. However, at this concentration of inhibitor, insoluble crystals formed in the aqueous culture medium. Consequently, whether AKT ser473 is essential for mitosis in mES cells could not be determined from these studies. Additional kinases have been reported to mediate AKT ser473 phosphorylation in other cells and may provide an alternative pathway to AKT phosphorylation during mitosis.

It has been reported that the serine-473 phosphorylation in the hydrophobic motif (HM) of AKT is a prerequisite for full activation. This mechanism has been postulated to involve a conformation change in the pleckstrin (PH) domain, facilitating membrane localisation. At the cell membrane, AKT is exposed to the Protein-Dependent Kinase-1 (PDK1) leading to phosphorylation at the threonine-308 residue[88].

In this study it was observed that the localisation of phospho-AKT ser473 in mitotic cells was also present in mouse embryonic fibroblasts. This suggests that mitotic association of AKT ser473 persists during embryonic development. It is curious that these observations have not been noted in cells other than oocytes, and here, embryonic stem cells and embryonic fibroblasts. It is possible that this AKT association is tissue specific or restricted during development. There are three AKT genes that transcribe similar molecules, AKT1, AKT2 and AKT3. Knockout studies have identified that these isoforms are tissue restricted during development. Expression of AKT1 and AKT2 is ubiquitous whereas AKT3 expression is restricted to neural, cardiac and renal tissues[154]. The AKT2 isoform confers glucose sensitivity and is abundant in adipose tissue[155] whereas AKT1 has been implicated in the growth of the organism. Knockout of all isoforms of AKT confers embryonic lethality and deletion of AKT1 and AKT2 results in lethality at the neonatal stage. However, these studies are complicated by functional redundancy between isoforms as just a single allele of one isoform can rescue observed defects[156]. Whether the mitotic AKT seen here can be attributed to a single isoform of AKT is not clear, however it has been suggested that AKT1 or AKT3 are likely candidates as AKT2 clearly mediates glucose and insulin sensitivity[153]. It has also been documented however, that AKT2 levels increase during mitosis and mediates cell cycle progression and importantly, tumorigenicity. It was concluded that AKT2 may promote aberrant cellular proliferation[157].

6.3 The viability of differentiating stem cells in response to mTOR inhibition.

The aim of this aspect of the study was to assess the effects of mTOR inhibitors on the expansion of and viability of mES cells during normal culture and spontaneous differentiation. Initially, the working concentrations of a PI3K inhibitor, and dual mTOR kinase inhibitor were established by a dose-response assay and the effect on mouse ES cell proliferation after 48h was determined. This data was the used to select concentrations that generated a 50% reduction in proliferation after 48h. Mouse ES cell cultures were then treated with rapamycin (TORC1 inhibitor), LY294002 (PI3K inhibitor) and KU-0063 (dual TORC1/TORC2 inhibitor). It was shown that in growth medium containing LIF, viability was unaffected after 48h. Similar findings were observed with LIF-deprived growth medium and it was concluded that mTOR and PI3K inhibition impaired proliferation but not viability.

It was observed that an increased percentage of detached cells were present in the spent culture medium without LIF and upon treatment with rapamycin, Ku-0063 and LY294002. This showed that cell attachment is negatively affected by inhibitors when LIF is not present. Rapamycin had less effect than both Ku-0063 and LY294002, with the greatest effect seen with the PI3K inhibitor. These findings suggest that AKT inhibition may underlie this effect. Rapamycin marginally reduces the T-loop phosphorylation (Fig.3.7), Ku-0063 inhibits the HM-motif phosphorylation (required for full activation) and has a weak effect on the T-loop phosphorylation[136]; and the LY294002 compound is a potent inhibitor of AKT activation. Interestingly these effects were only observed in the absence of LIF, a potent inducer of PI3K activation. Taken together these findings suggest that AKT activation may mediate this loss of attachment upon mTOR inhibition.

The role of PI3K activation upon cell adhesion molecule binding to extracellular matrix proteins is well documented. The adhesion of cell surface integrins to ECM proteins activates AKT in a PI3K-dependent manner[156], and focal adhesion kinase (FAK) molecules within focal adhesion complexes mediate survival and proliferation signals[157]. Focal adhesion complexes provide a direct link between cell surface molecules and the actin cytoskeleton and regulate processes such as migration and mitosis. The PI3K pathway also mediates the stabilisation of the microtubular cytoskeleton during migration, in one study it was found that stimulation of PI3K with platelet derived growth factor (PDGF) increased microtubule polymerisation, an effect that was prevented by PI3K inhibitors. Enforced expression of active AKT increased the amount of polymerised microtubules and a dominant negative form impaired microtubule stabilisation and cell migration in a wound healing assay[161]. Both AKT and TORC2 are recruited to the leading edge of migrating cells, whereas AKT is important for cell polarisation in response to chemoattractants[162], and TORC2 is known to regulate the actin cytoskeleton in budding yeast and somatic mammalian cells[73]. In yeast, rapamycin treatment inhibits microtubule assembly, elongation and stability[163].

Embryonic stem cells that exhibited a round, compact shape have been shown to be sensitive to mechanical forces. Application of the tip of an atomic force microscope to individual cells generated membrane protrusions called blebs. This effect was not observed in flat, spread cells that also had a complex, committed cytoskeleton[135]. It was concluded that as mouse ES cell begin to differentiate, the cytoskeleton develops and gives the cell rigidity. As ES cells spread, they gain complexity and structure at the interface between cytoskeleton and cell membrane. Thus, when ES cells commit to differentiation and develop a defined cytoskeleton, spatial and structural regulation of signalling pathways may be acquired. This supports the notion that in ES cells, differentiation and the acquisition of cytoskeletal rigidity may involve redistribution of signalling proteins to the cell membrane. Thus, in the spread cells observed in this study, the presence of mTOR serine2481 at the cell membrane may result in differential regulation of mTOR mediated processes. Consequently, the alterations in the survival and attachment response following mTOR inhibition may reflect this process.

6.4 Wider implications of mTOR signalling in mES cells.

Mammalian TOR is itself phosphorylated at a number of serine and threonine residues. In this study, the levels of phospho-specific mTOR proteins were assessed over the course of the passage cycle, however no changes were observed. To date it is known that mTOR is phosphorylated at serine residues 2448 and 2481 and threonine residue-2446. It has been shown that insulin promotes threonine-2446 and serine-2448 phosphorylation via AKT[163]. However, substitution of these domains with alanine does not impair the mTOR mediated phosphorylation of p70S6K. Deletion of the region containing amino acids 2430-2450 increases mTOR kinase activity suggesting that this region is important for the repression of mTOR activity. Indeed these amino acid residues lie within the NRD regulatory domain of mTOR and may therefore not potentiate kinase activity[59]. The AMP-kinase also phosphorylates threonine residue-2446 and inhibits mTORC1 kinase activity[164]. It has been demonstrated that p70S6K mediates the phosphorylation of the serine-2448 residue of mTOR as RNA interference inhibited serine-2448 phosphorylation. Furthermore, impairment of mTOR kinase activity by nutrient depletion reduced subsequent phosphorylation of ser2448 [165]. In a different study it was observed that both insulin and amino acid provision promoted this phosphorylation by independent mechanisms. Glucagon was also shown to increase ser2448 phosphorylation without activating AKT, leading to a reduction in mTOR kinase activity[166]. In summary, the serine-2448 phosphorylation appears to negatively regulate mTORC1 kinase activity and may operate as a self-regulating feedback mechanism to prevent excessive activation of mTOR.

The functional significance of the serine-2481 residue of mTOR is not clear. Recent studies have improved the understanding of the role this phosphorylation has on mTOR activity. It has been reported that the serine-2481 residue is an auto-phosphorylation site that is present in both TORC1 and TORC2 complexes. It has also been documented that rapamycin inhibits serine-2481 phosphorylation in mTOR1 complexes but not mTOR2 complexes[167]. It is now thought that the serine-2481 phosphorylation of mTOR is dependent upon the intact mTORC2 complex and is mTOR is rapamycin insensitive, whereas mTORC1 is found in association with phospho-serine-2448 [168]. In conclusion, mTOR serine 2481 is considered to be a marker of active TORC2 complexes whereas the 2448 phosphorylation is associated TORC1 but may represent a marker of inactivation. Drawing on these conclusions, it appears that the mitotic phosphorylation events observed in this study are TORC2 related events.

It has been well documented that the mTOR pathway interacts with other cell signalling pathways, including the mitogen activated protein kinase pathway (MAPK). In mouse ES cells LIF promotes MAPK pathway activation resulting in ERK1/2 phosphorylation[169] . The activation of ERK1/2 has a negative effect on pluripotency in mES cells[38] and promotes endoderm and mesoderm lineage specification [50]. This effect is negated by serum dependent signalling via ID proteins [40]. It is not currently known what impact rapamycin treatment has on ERK1/2 phosphorylation in mES cells under normal growth conditions and serum deprivation. Data presented here shows that in LIF-stimulated mES cells, rapamycin treatment results in the phosphorylation of ERK1 (p42) and ERK2 (p44). This effect is potentiated by serum deprivation. This is in concordance with the reported effect of serum on the inhibition of downstream ERK signalling in mES cells.

The mechanism of rapamycin mediated ERK phosphorylation cannot be inferred from data presented here. Published studies suggest that ERK interacts with mTOR pathway via multiple mechanisms. Inhibition of the upstream kinase of ERK, the mitogen-activated protein kinase kinase (MEK), also impairs PI3K activation and negatively regulates AKT phosphorylation in response to growth factor stimulation[170]. In embryonic stem cell-derived neural progenitor cells, insulin signaling promotes cell survival during hypoxia by activating the PI3K/AKT pathway. It was observed that this response was accompanied by an inhibition of ERK phosphorylation[171]. Activated ERK potentiates endoderm and mesoderm lineage commitment and inhibits neuroectoderm differentiation in the mouse. This suggests that there may be a dynamic equilibrium between the PI3K/AKT and the MAPK/ERK pathways that regulates cell survival and differentiation. However, as this study incorporated oxygen depletion, multiple factors may have influenced the cross-talk between the two pathways.

Other reported interactions between mTOR and ERK include the phosphorylation of raptor protein leading to TORC1 activation, and the phosphorylation of the S6-kinase-2 (S6K2) isoform by phospho-ERK [172,173]. Cross-talk between mTOR and ERK has also been implicated in self-renewal and tumorigenicity of glioblastoma stem-like cells[174].Of particular interest to this study is the documented role of ERK in the phosphorylation of p70S6K th421 [170].

It has been documented that ‘full’ activation of AKT is dependent upon phosphorylation at serine-473[176]. The search for a putative kinase (PDK2) identified a number of candidates including the mTOR complex 2 (TORC2)[77], integrin-linked kinase (ILK)[177] and DNA-protein kinase (DNA-PK)[178]. In this study the phosphorylation of AKT at serine-473 was found to be sensitive to rapamycin treatment. This is in accordance with published findings and supports the hypothesis that TORC2 mediates AKT serine-473 phosphorylation. Whereas the classical activation of AKT occurs at the plasma membrane, it is unclear in which cellular compartment the phosphorylation of serine-473 residue takes place. Upon activation AKT is known to exert its actions in the cytoplasm and nucleus where phosphorylation events induce the activation and repression of kinase substrates and gene transcription events[179,180].

Evidence for the membrane-activation of AKT ser473 suggests that this occurs at the in conjunction with the PDK1 phosphorylation of threonine-308 [154]. This is supported by investigations into novel PH-domain inhibitors which suppressed the Insulin-Like Growth Factor-1 (IGF-1) mediated phosphorylation of AKT at serine-473. However, levels of phospho-p70S6K also reduced, this implies that the PDK1-mediated regulation of mTORC1 activity may be involved. As PDK1 promotes TORC1 kinase activity indirectly through inhibiting the TSC complex; reducing AKT phosphorylation at the cell membrane may also relieve the inhibitory phosphorylation of TSC2. As the inhibition of TSC2 is necessary for mTOR complex-2 formation and kinase activity[87,181], the reduced serine-473 phosphorylation seen in response to the PH inhibitors may be due to TORC2 inhibition by the TSC complex. These studies do not provide convincing evidence that the phosphorylation of serine-473 AKT occurs at the cell membrane.

The activation of AKT is also regulated by additional phosphorylation events that are independent of nutrient and growth factor stimulation. It has been documented that TORC2 mediates the phosphorylation of a residue in the turn motif (TM) of AKT[146], and this phosphorylation, at threonine residue-450 stabilises native AKT protein from degradation. The TM phosphorylation was found to be dependent upon the functional TORC2 complex as this phosphorylation was lost in Sin1$^{-/-}$ cells. Enforced membrane localisation of AKT by myristolation (myr-AKT) induced constitutive phosphorylation of the threonie-308 residue by PDK1. The impaired TM phosphorylation observed in Sin$^{-/-}$ cells was not rescued by myristolated AKT. However, partial rescue of the HM (ser473) phosphorylation was observed[182]. This strongly suggests that the phosphorylation of AKT serine-473 can occur without active TORC2 and is a membrane localised event. It was hypothesised that the partial rescue was due to autophosphorylation, however, the evidence for this is not conclusive and additional membrane localised kinases may also been involved.

One such kinase is the integrin linked kinase (ILK), localised predominantly at the cell membrane, ILK transduces signals arising from integrin adhesion molecule binding, to stimulate cellular processes such as survival and proliferation[183]. The HM motif of AKT is a kinase substrate of ILK[177], and over-expression induces a dramatic upregulation in cellular proliferation, whereas inhibition impairs AKT ser473 phosphorylation and causes cell cycle arrest and apoptosis in PTEN-deficient PC-3 cells[184]. Interestingly, recent work has shown that ILK is also localised at centrosomes during mitosis, regulates the organisation of the mitotic spindle and colocalises with Aurora proteins[185]. This pattern of activity is similar to the observations documented here whereby TORC2 components localise at centrosomal areas and are upregulated during mitosis. Interestingly, the TORC2 associated protein rictor also interacts with ILK to mediate the phosphorylation of AKT ser473 and promotes the survival of cancer cells[186]. Both rictor and ILK were localised at the cell membrane and when mTOR protein was depleted, rictor, in cooperation with ILK mediated AKT ser473 phosphorylation and survival.

Recent findings show that the mTOR mediated phosphorylation of the TM residues of ACG kinases prevents protein degradation. The AGC kinase, AKT is known to drive cell survival and transit through the cell cycle. It has been show here, and by others that rapamycin treatment increases TORC2 activity resulting in the phosphorylation of AKT at the hydrophobic motif. This is understood to be mediated by feedback inhibition via IRS-1 and PI3K[176]. It was shown in this study that inhibition of TORC1 with rapamycin did not completely abrogate cell proliferation. Feedback between the two mTOR complexes may therefore provide a mechanism to enable cells to complete the current cell cycle upon the depletion of nutrient and growth factor stimulation. This theory is supported by the observation that in cancer cells with the PTEN deletion, proliferation continues independently of environmental cues. In MCF7 and PC3 tumour cells it was found that the mTOR complex-2 was essential for cell cycle progression and anchorage-independent growth[83]. This observation is interesting as the HM phosphorylation of AKT is also mediated by ILK. Thus, when signalling from adhesion complexes is ablated, TORC2 activation of AKT ser473 may drive proliferation. That the anchorage-independent proliferation of these cells is dependent upon TORC2 provides strong evidence for the dynamic balance between cell attachment signals via ILK, and nutrient mediated signalling via mTOR in mediating AKT ser473 phosphorylation and resulting in cell survival and proliferation.

6.5 Conclusion

The experimental data presented in chapter 3 defined the model pluripotent stem cells system utilised for further studies. The impact of mTOR activity on the proliferation of three cell systems was characterised. In mouse ES cells under standard growth conditions it was documented that mTOR activity modulates throughout the passage cycle and is sub-maximal after initial stimulation with growth medium. Supplementation of ES cells with factors that promote mTOR signalling is suggested in order to optimise cell proliferation rate during expansion of stem cells in a bioprocess.

Experimental data presented in Chapter 4 served to further characterise mTOR signalling in ES cells. Conclusions drawn from these findings are that mTOR phosphoproteins are spatially and temporally regulated in embryonic stem cells. Furthermore, phosphoproteins associated with the mTOR complex-2 were associated with cytoskeletal structures involved in cell division. As mouse ES cells differentiated they spread and lost their distinctive compact shape. These cells expressed a developed cytoskeleton and mTOR phosphoproteins appeared to localise to the plasma membrane. The implication of these findings is that the mTOR pathway may be differentially regulated in pluripotent stem cells and differentiated cells. Consequently, targeting the mTOR complexes independently may afford additional levels of control to manipulate cell proliferation and cell growth to achieve bioprocess improvements.

Observations documented in Chapter 5 build upon earlier findings by characterising the effect of mTOR pathway modulation on the expansion and viability of pluripotent and differentiated cells. Morphologically distinct ‘spread’ cells with a developed cytoskeleton were less susceptible than compact stem cells, to proliferation inhibition and apoptosis by mTOR inhibitors upon the withdrawal of growth factor signalling. Additionally it was observed that during differentiation mTOR inhibition resulted in increased cell detachment. These effects may be utilised to reduce the proportion of stem cells from mixed cell preparations during differentiation.

In summary, these findings suggest that the mTOR complex-2 may play an unrecognised role in proliferation via interaction with the cytoskeleton during mitosis. Furthermore, as stem cells differentiate, the regulation of mTOR signalling may be altered, affecting both proliferation and survival responses. This supports the notion that targeting the mTOR pathway may have differential effects in pluripotent and differentiated cells.

The data presented and discussed here offers a strategy to enhance the expansion of embryonic stem cells by stimulating the mTOR pathway. Furthermore inhibiting the mTOR pathway during early differentiation may improve the purity of differentiated cell populations by preferentially inhibiting pluripotent stem cell proliferation and attachment. The mTOR pathway is an ideal candidate for cost-effective bioprocess optimisation as it is both sensitive to the bioavailability of nutrients and a highly conserved global regulator of cellular growth and proliferation.

6.6 Future work

This investigation has highlighted key research questions that uncover novel biology regarding mTOR regulation in embryonic stem cells. An important aspect of future studies would be to assess the contribution of the respective AKT isoforms to the mitotic phosphorylation of AKT ser473. Targeted deletion or inactivation of the three AKT genes, both individually and in combination would enable isoform specific effects to be identified. This would determine whether the mitotic phosphorylation of AKT is essential for cell division in ES cells.

The second investigation would characterise the respective involvement of the integrin linked kinase (ILK) and TORC2 kinase in the phosphorylation of AKT during mitosis. The particular emphasis would be to assess whether ILK and TORC2 exhibit functional redundancy in mediating this phosphorylation event. Targeted deletion by RNA interference would enable this question to be answered.

Finally, the association of mTOR ser2481 with intracellular structures of the cytoskeleton and cell membrane would be probed in both compact stem cells and spread, differentiated cells. The relationship between membrane localisation and the acquired sensitivity to mTOR inhibitors would be addressed in the context of TORC2 and ILK knockdown.

This work would comprise of three projects that taken together would significantly advance the understanding of the relationship between mTOR and AKT activation in embryonic stem cells.

Modulation of the mTOR pathway as a route to generate bioprocess improvements for embryonic stem cell-based therapies would require additional investigation into the effect of nutrient supplementation and deprivation at the expansion and differentiation stages respectively. In support of this, the relationships between cell numbers, proliferation rate, cell morphology and nutrient levels should be addressed. The combination of a continuous perfusion system to enable dynamic control of nutrient levels coupled with a non-invasive image analysis system as documented in this study, this approach would deliver the cost-effective bioprocess advantages alluded to in this study.

Chapter 7

References

1. Martin, E. & Mathew, K. Establishment in culture of pluripotential cells from mouse embyros. *Nature* **292**, 154-156(1981).

2. Martin, G.R. Isolation of a Pluripotent Cell Line from Early Mouse Embryos Cultured in Medium Conditioned by Teratocarcinoma Stem Cells. *Proceedings of the National Academy of Sciences* **78**, 7634-7638(1981).

3. Yu, J. & Thomson, J.A. Pluripotent stem cell lines. *Genes & Development* **22**, 1987-1997(2008).

4. Smith, a G. Embryo-derived stem cells: of mice and men. *Annual review of cell and developmental biology* **17**, 435-62(2001).

5. Wobus, A.M. & Löser, P. Present state and future perspectives of using pluripotent stem cells in toxicology research. *Archives of toxicology* **85**, 79-117(2011).

6. Oh, S.K.W. & Choo, A.B. Human embryonic stem cells: Technological chalenges. *Clinical and Experimental Pharmacology and Physiology* **33**, 489-495(2006).

7. Blum, B. & Benvenisty, N. The tumorigenicity of diploid and aneuploid human pluripotent stem cells. *Cell cycle (Georgetown, Tex.)* **8**, 3822-30(2009).

8. Hentze, H., Graichen, R. & Colman, A. Cell therapy and the safety of embryonic stem cell-derived grafts. *Trends in biotechnology* **25**, 24-32(2007).

9. Kleinsmith, L.J. & Pierce, G.B. Multipotentiality of Single Embryonal Carcinoma Cells of Single Embryonal. *Cancer Research* **24**, 1544-1551(1964).

10. Finch, B. & Ephrussi, B. Retention of multiple developmental potentialities by cells of a mouse testicular carcinoma. *Proceedings of the National Academy of Sciences* **57**, 615-621(1967).

11. Evans, M.J. The isolation and properties of a clonal tissue culture strain of pluripotent mouse teratoma cells. *Journal of embryology and experimental morphology* **28**, 163-76(1972).

12. Rosenthal, M., Wishnow, R. & Sato, G. In vitro growth and differetiation of clonal populations of multipotential mouse clls derived from a transplantable testicular teratocarcinoma. *Journal of the national Cancer Institute.* **44**, 1001-14(1970).

13. Brinster, B. The effect of cells transfered into the mouse blastocyst on subsequent development. *Journal of Experimental Medicine* **140**, 1049-1056(1974).

14. Williams, R. et al. Myeloid leukaemia inhibitory factor maintains the developmental potential of embryonic stem cells. *Nature* **336**, 684-687(1988).

15. Smith, A. et al. Inhibition of pluiripotential embryonic stem cell differentiation by purified polypeptides. *Nature* **336**, 688-690(1988).

16. Moreau, J. et al. Leukaemia inhibitory factor is identicle to the myeloid growth fact human interleukin for DA cells. *Nature* **336**, 690-692(1988).

17. Bradley, A. et al. Formation of germ-line chimeras from embryo-derived teratocarcinoma cell lines. *Nature* **309**, (1984).

18. Thomson, J. a Embryonic Stem Cell Lines Derived from Human Blastocysts. *Science* **282**, 1145-1147(1998).

19. Kibbey, M.C. Maintenance of the EHS sarcoma and Matrigel preparation. *Journal of Tissue Culture Methods* **16**, 227-230(1994).

20. Xu, C. et al. Feeder-free growth of undifferentiated human embryonic stem cells. *Nature biotechnology* **19**, 971-4(2001).

21. Bazan, J.F. Structural design and molecular evolution of a cytokine receptor superfamily. *Proceedings of the National Academy of Sciences of the United States of America* **87**, 6934-8(1990).

22. Paonessa, G. et al. Two distinct and independent sites on IL-6 trigger gp 130 dimer formation and signalling. *The EMBO journal* **14**, 1942-51(1995).

23. Zhong, Z., Wen, Z. & Darnell, J. Stat3: a STAT family member activated by tyrosine phosphorylation in response to epidermal growth factor and interleukin-6. *Science* **264**, 95-98(1994).

24. Karin, M. & Hunter, T. Transcriptional control by protein phosphorylation: signal transmission from the cell surface to the nucleus. *Current biology* **5**, 747-57(1995).

25. Niwa, H. et al. Self-renewal of pluripotent embryonic stem cells is mediated via activation of STAT3. *Genes & development* **12**, 2048-60(1998).

26. Matsuda, T. et al. STAT3 activation is sufficient to maintain an undifferentiated state of mouse embryonic stem cells. *The EMBO journal* **18**, 4261-9(1999).

27. Cartwright, P. et al. LIF/STAT3 controls ES cell self-renewal and pluripotency by a Myc-dependent mechanism. *Development* **132**, 885-96(2005).

28. Burdon, T., Smith, A. & Savatier, P. Signalling, cell cycle and pluripotency in embryonic stem cells. *Trends in cell biology* **12**, 432-8(2002).

29. Sanghera, K.P. et al. The PI3K/Akt/mTOR pathway mediates retinal progenitor cell survival under hypoxic and superoxide stress. *Molecular and cellular neurosciences* **47**, 145-53(2011).

30. Liang, J. & Slingerland, J.M. Multiple Roles of the PI3K / PKB (Akt) Pathway in Cell Cycle Progression. *Cell Cycle* 339-345(2003).

31. Sasaki, A.T. & Firtel, R. a Regulation of chemotaxis by the orchestrated activation of Ras, PI3K, and TOR. *European journal of cell biology* **85**, 873-95(2006).

32. Cairns, P. et al. Frequent Inactivation of PTEN / MMAC1 in Primary Prostate Cancer Advances in Brief Frequent Inactivation of PTEN / MMAC1 in Primary Prostate Cancer. *Cancer* 4997-5000(1997).

33. Cheung, A.M. & Mak, T.W. PTEN in the haematopoietic system and its therapeutic indications. *Trends in molecular medicine* **12**, 503-5(2006).

34. Di Cristofano, a et al. Pten is essential for embryonic development and tumour suppression. *Nature genetics* **19**, 348-55(1998).

35. Meier, F. et al. The RAS/RAF/MEK/ERK and PI3K/AKT signaling pathways present molecular targets for the effective treatment of advanced melanoma. *Frontiers in Bioscience* **10**, 2986-3001(2005).

36. Watanabe, S. et al. Activation of Akt signaling is sufficient to maintain pluripotency in mouse and primate embryonic stem cells. *Oncogene* **25**, 2697-707(2006).

37. Takahashi, K., Murakami, M. & Yamanaka, S. Role of the phosphoinositide 3-kinase pathway in mouse embryonic stem (ES) cells. *Biochemical Society transactions* **33**, 1522-5(2005).

38. Kunath, T. et al. FGF stimulation of the Erk1/2 signalling cascade triggers transition of pluripotent embryonic stem cells from self-renewal to lineage commitment. *Development (Cambridge, England)* **134**, 2895-902(2007).

39. Hirano, T., Ishihara, K. & Hibi, M. Roles of STAT3 in mediating the cell growth, differentiation and survival signals relayed through the IL-6 family of cytokine receptors. *Oncogene* **19**, 2548-56(2000).

40. Ying, Q.L. et al. BMP induction of Id proteins suppresses differentiation and sustains embryonic stem cell self-renewal in collaboration with STAT3. *Cell* **115**, 281-92(2003).

41. Mitsui, K. et al. The homeoprotein Nanog is required for maintenance of pluripotency in mouse epiblast and ES cells. *Cell* **113**, 631-42(2003).

42. Nichols, J. et al. Formation of pluripotent stem cells in the mammalian embryo depends on the POU transcription factor Oct4. *Cell* **95**, 379-91(1998).

43. Scholer, H.R. et al. mouse embryogenesis : evidence for germline-specific expression of an Oct factor. *EMBO Journal* **8**, 2543-2550(1988).

44. Boyer, L.A. et al. Core transcriptional regulatory circuit in human embryonic stem cells. *Cell* **122**, 947-956(2010).

45. Chambers, I. Embryonic Stem Cells. *Cloning and Stem Cells* **6**, 386-391(2004).

46. Takahashi, K. & Yamanaka, S. Induction of pluripotent stem cells from mouse embryonic and adult fibroblast cultures by defined factors. *Cell* **126**, 663-76(2006).

47. Ivanova, N. et al. Dissecting self-renewal in stem cells with RNA interference. *Nature* **442**, 2006-2006(2006).

48. Masui, S. et al. Pluripotency governed by Sox2 via regulation of Oct3/4 expression in mouse embryonic stem cells. *Nature cell biology* **9**, 625-35(2007).

49. Ying, Q.-L. et al. The ground state of embryonic stem cell self-renewal. *Nature* **453**, 519-23(2008).

50. Nichols, J. et al. Suppression of Erk signalling promotes ground state pluripotency in the mouse embryo. *Development* **136**, 3215-22(2009).

51. Niwa, H. et al. A parallel circuit of LIF signalling pathways maintains pluripotency of mouse ES cells. *Nature* **460**, 118-22(2009).

52. Kudelski, A. & Sehgal, S.N. A new antifungal antibiotic taxonomy of the producing streptomycete and isolation of the active principle. *Journal of antibiotics* **28**, 721-726(1975).

53. Kunz, J. et al. Target of rapamycin in yeast, TOR2, is an essential phosphatidylinositol kinase homolog required for G1 progression. *Cell* **73**, 585-96(1993).

54. Helliwell, S.B. et al. TOR1 and TOR2 are structurally and functionally similar but not identical phosphatidylinositol kinase homologues in yeast. *Molecular biology of the cell* **5**, 105-18(1994).

55. Sabatini, D. et al. RAFT2: A mammalian protein that binds to FKBP12 in a rapamycin-dependent fashion and is homologous to yeast TORs. *Cell* **78**, 35-43(1994).

56. Brown, E. et al. A mammalian protein targeted by G1-arresting rapamycin-receptor complex. *Nautre* **389**, 756-758(1994).

57. Chiu, M.I., Katz, H. & Berlin, V. RAPT1, a mammalian homolog of yeast Tor, interacts with the FKBP12/rapamycin complex. *Proceedings of the National Academy of Sciences of the United States of America* **91**, 12574-8(1994).

58. Lynch, C.J. et al. Leucine is a direct-acting nutrient signal that regulates protein synthesis in adipose tissue. *American journal of physiology. Endocrinology and metabolism* **283**, E503-13(2002).

59. Hay, N. & Sonenberg, N. Upstream and downstream of mTOR. *Genes & development* **18**, 1926-45(2004).

60. Kim, D.-H. et al. mTOR interacts with raptor to form a nutrient-sensitive complex that signals to the cell growth machinery. *Cell* **110**, 163-75(2002).

61. Kim, D.-H. et al. GbetaL, a positive regulator of the rapamycin-sensitive pathway required for the nutrient-sensitive interaction between raptor and mTOR. *Molecular cell* **11**, 895-904(2003).

62. Vander Haar, E. et al. Insulin signalling to mTOR mediated by the Akt/PKB substrate PRAS40. *Nature cell biology* **9**, 316-23(2007).

63. Hara, K. et al. Raptor, a binding partner of target of rapamycin (TOR), mediates TOR action. *Cell* **110**, 177-89(2002).

64. Loewith, R. et al. Two TOR complexes, only one of which is rapamycin sensitive, have distinct roles in cell growth control. *Molecular cell* **10**, 457-68(2002).

65. Manteuffel, S.R. von et al. 4E-BP1 phosphorylation is mediated by the FRAP-p70s6k pathway and is independent of mitogen-activated protein kinase. *Proceedings of the National Academy of Sciences of the United States of America* **93**, 4076-80(1996).

66. Burnett, P.E. RAFT1 phosphorylation of the translational regulators p70 S6 kinase and 4E-BP1. *Proceedings of the National Academy of Sciences* **95**, 1432-1437(1998).

67. Hara, K. et al. Amino acid sufficiency and mTOR regulate p70 S6 kinase and eIF-4E BP1 through a common effector mechanism. *The Journal of biological chemistry* **273**, 14484-94(1998).

68. Fingar, D.C. et al. Mammalian cell size is controlled by mTOR and its downstream targets S6K1 and 4EBP1/eIF4E. *Genes & development* **16**, 1472-87(2002).

69. G, J., Pringle, J. & Hartwell, L. Coordination of growth with cell division in the yeast Saccharomyces cerevisae. *Experimental Cell Research* **105**, 98195-98195(2004).

70. Schmelzle, T. & Hall, M.N. TOR, a central controller of cell growth. *Cell* **103**, 253-62(2000).

71. Jacinto, E. et al. Mammalian TOR complex 2 controls the actin cytoskeleton and is rapamycin insensitive. *Nature cell biology* **6**, 1122-8(2004).

72. Sarbassov, D. et al. Rictor, a Novel Binding Partner of mTOR , Defines a Rapamycin-Insensitive and Raptor-Independent Pathway that Regulates the Cytoskeleton. *Current biology* **14**, 1296-1302(2004).

73. Yang, Q. et al. Identification of Sin1 as an essential TORC2 component required for complex formation and kinase activity. *Genes & Development* 2820-2832(2006).doi:10.1101/gad.1461206.insensitive

74. Pearce, L.R. et al. Identification of Protor as a novel Rictor-binding component of mTOR complex-2. *The Biochemical journal* **405**, 513-22(2007).

75. Woo, S.-Y. et al. PRR5, a novel component of mTOR complex 2, regulates platelet-derived growth factor receptor beta expression and signaling. *The Journal of biological chemistry* **282**, 25604-12(2007).

76. Guertin, D. a et al. Ablation in mice of the mTORC components raptor, rictor, or mLST8 reveals that mTORC2 is required for signaling to Akt-FOXO and PKCalpha, but not S6K1. *Developmental cell* **11**, 859-71(2006).

77. Sarbassov, D.D. et al. Phosphorylation and regulation of Akt/PKB by the rictor-mTOR complex. *Science (New York, N.Y.)* **307**, 1098-101(2005).

78. García-Martínez, J.M. & Alessi, D.R. mTOR complex 2 (mTORC2) controls hydrophobic motif phosphorylation and activation of serum- and glucocorticoid-induced protein kinase 1 (SGK1). *The Biochemical journal* **416**, 375-85(2008).

79. Facchinetti, V. et al. The mammalian target of rapamycin complex 2 controls folding and stability of Akt and protein kinase C. *The EMBO journal* **27**, 1932-43(2008).

80. Shor, B., Cavender, D. & Harris, C. A kinase-dead knock-in mutation in mTOR leads to early embryonic lethality and is dispensable for the immune system in heterozygous mice. *BMC immunology* **10**, 28(2009).

81. Guertin, D.A. et al. the mTOR complex 2 is required for the development of prostate cancer induced by Pten loss in mice. *Cancer* **15**, 148-159(2009).

82. Cybulski, N. & Hall, M.N. TOR complex 2: a signaling pathway of its own. *Trends in biochemical sciences* **34**, 620-7(2009).

83. Lee, C.-H. et al. Constitutive mTOR activation in TSC mutants sensitizes cells to energy starvation and genomic damage via p53. *The EMBO journal* **26**, 4812-23(2007).

84. Long, X. et al. Rheb binds and regulates the mTOR kinase. *Current biology : CB* **15**, 702-13(2005).

85. Burgstaller, S. et al. Tuberin, p27 and mTOR in different cells. *Amino acids* **36**, 297-302(2009).

86. Bai, X. & Jiang, Y. Key factors in mTOR regulation. *Cellular and molecular life sciences : CMLS* **67**, 239-53(2010).

87. Huang, J. et al. The TSC1-TSC2 complex is required for proper activation of mTOR complex 2. *Molecular and cellular biology* **28**, 4104-15(2008).

88. Bellacosa, a et al. Akt activation by growth factors is a multiple-step process: the role of the PH domain. *Oncogene* **17**, 313-25(1998).

89. McCampbell, A.S. et al. Loss of inhibitory insulin receptor substrate-1 phosphorylation is an early event in mammalian target of rapamycin-dependent endometrial hyperplasia and carcinoma. *Cancer prevention research (Philadelphia, Pa.)* **3**, 290-300(2010).

90. Fingar, D.C. & Blenis, J. Target of rapamycin (TOR): an integrator of nutrient and growth factor signals and coordinator of cell growth and cell cycle progression. *Oncogene* **23**, 3151-71(2004).

91. Beugnet, A. et al. Regulation of targets of mTOR (mammalian target of rapamycin) signalling by intracellular amino acid availability. *The Biochemical journal* **372**, 555-66(2003).

92. Liu, Z. et al. Unlike insulin, amino acids stimulate p70S6K but not GSK-3 or glycogen synthase in human skeletal muscle. *American journal of physiology. Endocrinology and metabolism* **286**, E523-8(2004).

93. Vary, T.C., Jefferson, L.S. & Kimball, S.R. Amino acid-induced stimulation of translation initiation in rat skeletal muscle. *The American journal of physiology* **277**, E1077-86(1999).

94. Du, M. et al. Leucine stimulates mammalian target of rapamycin signaling in C2C12 myoblasts in part through inhibition of adenosine monophosphate-activated protein kinase. *Journal of animal science* **85**, 919-27(2007).

95. Roos, S. et al. Mammalian target of rapamycin in the human placenta regulates leucine transport and is down-regulated in restricted fetal growth. *The Journal of physiology* **582**, 449-59(2007).

96. Yang, Z.-Z. et al. Protein kinase B alpha/Akt1 regulates placental development and fetal growth. *The Journal of biological chemistry* **278**, 32124-31(2003).

97. Van Winkle, L.J. et al. System B0,+ amino acid transport regulates the penetration stage of blastocyst implantation with possible long-term developmental consequences through adulthood. *Human reproduction update* **12**, 145-57(2006).

98. Martin, P.M. & Sutherland, A.E. Differentiation in the Mouse Blastocyst through an mTOR-Dependent Pathway. *Ambio* **193**, 182-193(2001).

99. Shaw, R.J. et al. The LKB1 tumor suppressor negatively regulates mTOR signaling. *Cancer cell* **6**, 91-9(2004).

100. Gwinn, D.M. et al. AMPK phosphorylation of raptor mediates metabolic checkpoint. *Molecular Cell* **30**, 214-226(2009).

101. Kim, Y.H., Heo, J.S. & Han, H.J. High glucose increase cell cycle regulatory proteins level of mouse embryonic stem cells via PI3-K/Akt and MAPKs signal pathways. *Journal of cellular physiology* **209**, 94-102(2006).

102. Kim, J. et al. AMPK and mTOR regulate autophagy through direct phosphorylation of Ulk1. *Nature cell biology* **13**, 132-41(2011).

103. Franke, T.F. et al. PI3K/Akt and apoptosis: size matters. *Oncogene* **22**, 8983-98(2003).

104. Tzivion, G. & Avruch, J. 14-3-3 Proteins: Active Cofactors in Cellular Regulation By Serine/Threonine Phosphorylation. *The Journal of biological chemistry* **277**, 3061-4(2002).

105. Harvey, D. & Sagar, L. No Title. *Future oncology* **3**, 2008-2008(2008).

106. Murakami, M. et al. mTOR Is Essential for Growth and Proliferation in Early Mouse Embryos and Embryonic Stem Cells. *Molecular and cellular biology* **24**, 6710-6718(2004).

107. Gangloff, Y.-G. et al. Disruption of the Mouse mTOR Gene Leads to Early Postimplantation Lethality and Prohibits Embryonic Stem Cell Development. *Molecular and cellular biology* **24**, 9508-9516(2004).

108. Naeslund, G. The effect of glucose-, arginine- and leucine-deprivation on mouse blastocyst outgrowth in vitro. *Upsala journal of medical sciences* **84**, 9-20(1979).

109. Martin, P.M., Sutherland, A.E. & Van Winkle, L.J. Amino acid transport regulates blastocyst implantation. *Biology of reproduction* **69**, 1101-8(2003).

110. Hentges, K.E. et al. FRAP/mTOR is required for proliferation and patterning during embryonic development in the mouse. *Proceedings of the National Academy of Sciences of the United States of America* **98**, 13796-801(2001).

111. Zhou, J. et al. mTOR supports long-term self-renewal and suppresses mesoderm and endoderm activities of human embryonic stem cells. *Proceedings of the National Academy of Sciences of the United States of America* **106**, 7840-5(2009).

112. Lianguzova, M.S. et al. Phosphoinositide 3-kinase inhibitor LY294002 but not serum withdrawal suppresses proliferation of murine embryonic stem cells. *Cell biology international* **31**, 330-7(2007).

113. Rossant, J. & Papaioannou, V.E. The relationship between embryonic, embryonal carcinoma and embryo-derived stem cells. *Cell differentiation* **15**, 155-61(1984).

114. Andrews, P.W. et al. Embryonic stem (ES) cells and embryonal carcinoma (EC) cells: opposite sides of the same coin. *Biochemical Society transactions* **33**, 1526-30(2005).

115. Sarbassov, D.D. et al. Prolonged rapamycin treatment inhibits mTORC2 assembly and Akt/PKB. *Molecular cell* **22**, 159-68(2006).

116. Huang, J. & Manning, B.D. A complex interplay between Akt, TSC2 and the two mTOR complexes. *Biochemical Society transactions* **37**, 217-22(2009).

117. Hernandez, D., Ruban, L. & Mason, C. Feeder-free culture of human embryonic stem cells for scalable expansion in a reproducible manner. *Stem cells and development* **20**, 1089-98(2011).

118. Richards, M. & Bongso, A. Propagation of human embryonic stem cells on human feeder cells. *Methods in molecular biology (Clifton, N.J.)* **331**, 23-41(2006).

119. Ding, L. et al. A genome-scale RNAi screen for Oct4 modulators defines a role of the Paf1 complex for embryonic stem cell identity. *Cell stem cell* **4**, 403-15(2009).

120. Davey, R.E. & Zandstra, P.W. Spatial organization of embryonic stem cell responsiveness to autocrine gp-130 ligands reveals an autoregulatory stem cell niche. *Stem Cells* **10**, (2006).

121. Thompson, S. et al. Cloned human teratoma cells differentiate into neuron-like cells and other cell types in retinoic acid. *Journal of cell science* **72**, 37-64(1984).

122. Viswanathan, S. et al. Supplementation-dependent differences in the rates of embryonic stem cell self-renewal, differentiation, and apoptosis. *Biotechnology and bioengineering* **84**, 505-17(2003).

123. Rosner, M. et al. Functional interaction of mammalian target of rapamycin complexes in regulating mammalian cell size and cell cycle. *Human molecular genetics* **18**, 3298-3310(2009).

124. Howe, C.C., Gmür, R. & Solter, D. Cytoplasmic and nuclear protein synthesis during in vitro differentiation of murine ICM and embryonal carcinoma cells. *Developmental biology* **74**, 351-63(1980).

125. Zhou, J. et al. mTOR supports long-term self-renewal and suppresses mesoderm and endoderm activities of human embryonic stem cells. *Proceedings of the National Academy of Sciences of the United States of America* **106**, 7840-5(2009).

126. Ferrari, S. et al. Activation of p70S6K is associated with phosphorylation of four clustered sites displaingdisplaying Ser/Thr-Pro motifs. *Proceedings of the National Academy of Sciences* **89**, 7282-7286(1992).

127. Wick, M.J. et al. Mechanism of phosphorylation of protein kinase B/Akt by a constitutively active 3-phosphoinositide-dependent protein kinase-1. *The Journal of biological chemistry* **275**, 40400-6(2000).

128. Zinchuk, V. & Grossenbacher-Zinchuk, O. Recent advances in quantitative colocalization analysis: focus on neuroscience. *Progress in histochemistry and cytochemistry* **44**, 125-72(2009).

129. Van Hooser, a et al. Histone H3 phosphorylation is required for the initiation, but not maintenance, of mammalian chromosome condensation. *Journal of cell science* **111 (Pt 2**, 3497-506(1998).

130. Bollen, M., Gerlich, D.W. & Lesage, B. Mitotic phosphatases: from entry guards to exit guides. *Trends in cell biology* **19**, 531-41(2009).

131. Mason, C. & Hoare, M. Regenerative medicine bioprocessing: building a conceptual framework based on early studies. *Tissue engineering* **13**, 301-11(2007).

132. Rosenblatt, J. Mitosis : Moesin and the Importance of Being Round. *Current Biology* **18**, 292-293

133. Veraitch, F. Precisely delivered nanomechanical forces induce blebbing in undifferentiated mouse embryonic stem cells. *Cell Health and Cytoskeleton* 23(2011).doi:10.2147/CHC.S13863

134. García-Martínez, J.M. et al. Ku-0063794 is a specific inhibitor of the mammalian target of rapamycin (mTOR). *The Biochemical journal* **421**, 29-42(2009).

135. Barilli, A. et al. In human endothelial cells rapamycin causes mTORC2 inhibition and impairs cell viability and function. *Cardiovascular research* **78**, 563-71(2008).

136. Murayama, T. et al. Relation between outcomes and localisation of p-mTOR expression in gastric cancer. *British journal of cancer* **100**, 782-8(2009).

137. Yoshida, Y. et al. Localisation of phosphorylated mTOR expression is critical to tumour progression and outcomes in patients with endometrial cancer. *European journal of cancer* **46**, 3445-52(2010).

138. Yaba, A. et al. A putative mitotic checkpoint dependent on mTOR function controls cell proliferation and survival in ovarian granulosa cells. *Reproductive sciences (Thousand Oaks, Calif.)* **15**, 128-38(2008).

139. Yu, J. et al. mTOR Controls Ovarian Follicle Growth by Regulating Granulosa Cell Proliferation. *PloS one* **6**, e21415(2011).

140. Vazquez-Martin, A. et al. The serine 2481-autophosphorylated form of mammalian Target Of Rapamycin (mTOR) is localized to midzone and midbody in dividing cancer cells. *Biochemical and biophysical research communications* **380**, 638-43(2009).

141. Lopez-bonet, E. et al. Serine 2481-autophosphorylation of mammalian target of rapamycin (mTOR) couples with chromosome condensation and segregation during mitosis : Confocal microscopy characterization and immunohistochemical validation of PP-mTOR Ser2481 as a novel high-cont. *International journal of oncology* **36**, 107-115(2010).

142. Vazquez-Martin, A., Oliveras-Ferraros, C. & Menendez, J. a The active form of the metabolic sensor: AMP-activated protein kinase (AMPK) directly binds the mitotic apparatus and travels from centrosomes to the spindle midzone during mitosis and cytokinesis. *Cell cycle (Georgetown, Tex.)* **8**, 2385-98(2009).

143. Yang, F. et al. Identification of a novel mitotic phosphorylation motif associated with protein localization to the mitotic apparatus. *Journal of cell science* **120**, 4060-70(2007).

144. Vader, G., Medema, R.H. & Lens, S.M. a The chromosomal passenger complex: guiding Aurora-B through mitosis. *The Journal of cell biology* **173**, 833-7(2006).

145. Sampath, S.C. et al. The chromosomal passenger complex is required for chromatin-induced microtubule stabilization and spindle assembly. *Cell* **118**, 187-202(2004).

146. Withers, D.J. et al. Expression, enzme activity, and subcellular localization of mammalian target of rapamycin in insulin-responsive cells. *Biochemical and Biophysical Research Communications* **241**, (1997).

147. Takahashi, K. et al. Differential membrane localization of ERas and Rheb, two Ras-related proteins involved in the phosphatidylinositol 3-kinase/mTOR pathway. *The Journal of biological chemistry* **280**, 32768-74(2005).

148. Schmidt, T. et al. Immunolocalization of phospho-S6 kinases: a new way to detect mitosis in tissue sections and in cell culture. *Histochemistry and cell biology* **127**, 123-9(2007).

149. Shah, O.J., Ghosh, S. & Hunter, T. Mitotic regulation of ribosomal S6 kinase 1 involves Ser/Thr, Pro phosphorylation of consensus and non-consensus sites by Cdc2. *The Journal of biological chemistry* **278**, 16433-42(2003).

150. Le, X.-F. et al. Paclitaxel induces inactivation of p70 S6 kinase and phosphorylation of Thr421 and Ser424 via multiple signaling pathways in mitosis. *Oncogene* **22**, 484-97(2003).

151. Hoshino, Y. & Sato, E. Protein kinase B (PKB / Akt) is required for the completion of meiosis in mouse oocytes. *Developmental biology* **314**, 215 - 223(2008).

152. Hoshino, Y. et al. Phosphatidylinositol 3-kinase and Akt participate in the FSH-induced meiotic maturation of mouse oocytes. *Molecular reproduction and development* **69**, 77-86(2004).

153. Kalous, J. et al. PKB/AKT is involved in resumption of meiosis in mouse oocytes. *Biology of the cell* **98**, 111-23(2006).

154. Moses, S.A. et al. In vitro and in vivo activity of novel small-molecule inhibitors targeting the pleckstrin homology domain of protein kinaseB/AKT. *Cancer* **69**, 5073-5081(2010).

155. Altomare, D. a et al. Akt2 mRNA is highly expressed in embryonic brown fat and the AKT2 kinase is activated by insulin. *Oncogene* **16**, 2407-11(1998).

156. Dummler, B. et al. Life with a single isoform of Akt: mice lacking Akt2 and Akt3 are viable but display impaired glucose homeostasis and growth deficiencies. *Molecular and cellular biology* **26**, 8042-51(2006).

157. Cheng, J.Q. et al. Transforming activity and mitosis-related expression of the AKT2 oncogene: evidence suggesting a link between cell cycle regulation and oncogenesis. *Oncogene* **14**, 2793-801(1997).

158. King, W.G. et al. Phosphatidylinositol 3-kinase is required for integrin-stimulated AKT and Raf-1/mitogen-activated protein kinase pathway activation. *Molecular and cellular biology* **17**, 4406-18(1997).

159. Reif, S. et al. The role of focal adhesion kinase-phosphatidylinositol 3-kinase-akt signaling in hepatic stellate cell proliferation and type I collagen expression. *The Journal of biological chemistry* **278**, 8083-90(2003).

160. Onishi, K. et al. The PI3K-Akt pathway promotes microtubule stabilization in migrating fibroblasts. *Genes to Cells* 535-546(2007).doi:10.1111/j.1365-2443.2007.01071.x

161. Lee, S. et al. Involvement of the Cytoskeleton in Controlling Leading-Edge Function during Chemotaxis. *Molecular Biology of the Cell* **21**, 1810 -1824(2010).

162. Choi, J.H. et al. TOR signaling regulates microtubule structure and function. *Current biology : CB* **10**, 861-4(2000).

163. Sekulić, a et al. A direct linkage between the phosphoinositide 3-kinase-AKT signaling pathway and the mammalian target of rapamycin in mitogen-stimulated and transformed cells. *Cancer research* **60**, 3504-13(2000).

164. Cheng, S.W.Y. et al. Thr2446 is a novel mammalian target of rapamycin (mTOR) phosphorylation site regulated by nutrient status. *The Journal of biological chemistry* **279**, 15719-22(2004).

165. Chiang, G.G. & Abraham, R.T. Phosphorylation of mammalian target of rapamycin (mTOR) at Ser-2448 is mediated by p70S6 kinase. *The Journal of biological chemistry* **280**, 25485-90(2005).

166. Mothe-Satney, I. et al. In rat hepatocytes glucagon increases mammalian target of rapamycin phosphorylation on serine 2448 but antagonizes the phosphorylation of its downstream targets induced by insulin and amino acids. *The Journal of biological chemistry* **279**, 42628-37(2004).

167. Soliman, G. a et al. mTOR Ser-2481 autophosphorylation monitors mTORC-specific catalytic activity and clarifies rapamycin mechanism of action. *The Journal of biological chemistry* **285**, 7866-79(2010).

168. Copp, J., Manning, G. & Hunter, T. TORC-specific phosphorlation of mTOR: phospho-Ser2481 is a marker for intact mTORC2. *Cancer* **69**, 1821-1827(2010).

169. Schuringa, J.J. et al. LIF-induced STAT3 signaling in murine versus human embryonal carcinoma (EC) cells. *Experimental cell research* **274**, 119-29(2002).

170. Hayashi, H. et al. Down-regulation of the PI3-kinase/Akt pathway by ERK MAP kinase in growth factor signaling. *Genes to cells : devoted to molecular & cellular mechanisms* **13**, 941-7(2008).

171. Zhao, Y. et al. Insulin rescues ES cell-derived neural progenitor cells from apoptosis by differential regulation of Akt and ERK pathways. *Neuroscience letters* **429**, 49-54(2007).

172. Carriere, a et al. ERK1/2 phosphorylate Raptor to promote Ras-dependent activation of mTOR complex 1 (mTORC1). *Journal of Biological Chemistry* **286**, 567-577(2010).

173. Wang, L., Gout, I. & Proud, C.G. Cross-talk between the ERK and p70 S6 kinase (S6K) signaling pathways. MEK-dependent activation of S6K2 in cardiomyocytes. *The Journal of biological chemistry* **276**, 32670-7(2001).

174. Sunayama, J. et al. Crosstalk between the PI3K/mTOR and MEK/ERK pathways involved in the maintenance of self-renewal and tumorigenicity of glioblastoma stem-like cells. *Stem cells* **28**, 1930-9(2010).

175. Iijima, Y. et al. c-Raf/MEK/ERK pathway controls protein kinase C-mediated p70S6K activation in adult cardiac muscle cells. *The Journal of biological chemistry* **277**, 23065-75(2002).

176. Hill, M.M. et al. Insulin-stimulated protein kinase B phosphorylation on Ser-473 is independent of its activity and occurs through a staurosporine-insensitive kinase. *The Journal of biological chemistry* **276**, 25643-6(2001).

177. Persad, S. et al. Regulation of Protein Kinase B / Akt-Serine 473 Phosphorylation by integrin linked kinase (ILK). *Biochemistry* **276**, 27462-27469(2001).

178. Feng, J. et al. Identification of a PKB/Akt hydrophobic motif Ser-473 kinase as DNA-dependent protein kinase. *The Journal of biological chemistry* **279**, 41189-96(2004).

179. Martelli, A.M. et al. Intranuclear 3’-phosphoinositide metabolism and Akt signaling: new mechanisms for tumorigenesis and protection against apoptosis? *Cellular signalling* **18**, 1101-7(2006).

180. Miyamoto, S., Rubio, M. & Sussman, M. a Nuclear and mitochondrial signalling Akts in cardiomyocytes. *Cardiovascular research* **82**, 272-85(2009).

181. Yang, Q. et al. TSC1/TSC2 and Rheb have different effects on TORC1 and TORC2 activity. *Proceedings of the National Academy of Sciences of the United States of America* **103**, 6811-6(2006).

182. Ikenoue, T. et al. Essential function of TORC2 in PKC and Akt turn motif phosphorylation, maturation and signalling. *The EMBO journal* **27**, 1919-31(2008).

183. Yoganathan, T.N. et al. Integrin-linked kinase (ILK): a “hot” therapeutic target. *Biochemical pharmacology* **60**, 1115-9(2000).

184. Yamabi, H. et al. Overexpression of integrin-linked kinase induces cardiac stem cell expansion. *The Journal of Thoracic and Cardiovascular Surgery* **132**, 1272-1279(2006).

185. Fielding, A.B. et al. Integrin-linked kinase localizes to the centrosome and regulates mitotic spindle organisation. *Cell* **180**, 681-689(2008).

186. Mcdonald, P.C. et al. Rictor and Integrin-Linked Kinase Interact and Regulate Akt Phosphorylation and Cancer Cell Survival. *Cancer research* **68**, 1618-1624(2008).

187. Tzatsos, A. & Kandror, K.V. Nutrients Suppress Phosphatidylinositol 3-Kinase / Akt Signaling via Raptor-Dependent mTOR-Mediated Insulin Receptor Substrate 1 Phosphorylation †. *Molecular and cellular biology* **26**, 63-76(2006).

Chapter 8

Appendix 1: Development and characterisation of image analysis methods for the assessment of stem cell expansion from phase contrast images.

In the laboratory setting, routine assessment of the quality of stem cell cultures is made by observations of cell morphology and confluence by light microscopy. Extensive cell differentiation or impaired proliferation can be quickly determined by this method. Empirical analysis of stem cell pluripotency is performed routinely by immunostaining for core pluripotency markers such as OCT4 and nanog or by PCR based assessment of gene expression. However, these analytical techniques are inapplicable for the routine monitoring of ES cell cultures in a large-scale process[133]. Therefore a microscopic method for the assessment of stem cell expansion will be explored in this study.

The principle objective was to accurately measure total cell area coverage and colony size distribution from phase-contrast micrographs of mES cultures. The validation of such a technique would have two roles. Firstly to enable the identification of changes in colony size and growth in response to treatment with mTOR inhibitors, and the secondly, to generate an analytical tool to provide rapid qualitative and quantitative data for the routine monitoring of stem cell cultures *in vitro*.

In order to investigate the effect of mTOR inhibition on mES cell colony expansion, image analysis tools were developed and optimised using the ImageJ analytical software platform.

A sequence of inbuilt ImageJ analytical modules were arranged into specific workflows and then packaged as macros enabling rapid analysis of individual images.

There is currently no true gold-standard technique for the measurement of stem cell colony area from phase-contrast images. The manual selection of confluent areas from digital images was considered a valid approach. However, analysis by this method was both inefficient and prone to subjective interpretation. Therefore, a number of computational methods were developed and test data were analysed and visually inspected. Finally, the techniques were compared to highlight the respective caveats and strengths of each method.

8.1 Intensity thresholding for determination of cell confluence from phase-contrast images (Method A).

Method A for the assessment of total mES cell area coverage was developed using mouse ES cells expressing green fluorescent protein (GFP) linked to the OCT4 promoter region (mES E14 OCT4/GFP). In these cells, GFP expression is related to the expression of OCT4 enabling the effective monitoring of pluripotent marker expression in live cells by fluorescence microscopy. Mouse E14 OCT4/GFP cells were cultured in complete growth medium for 48h. Plates were imaged by phase-contrast and fluorescence microscopy under defined illumination and exposure conditions. Captured images at 10x magnification were then used to develop the image analysis tool. I acknowledge the work of James Lawrence (Biochemical Engineering, UCL) for the initial development of the technique that preceded Method A.

The process described in Method A was based upon a simple thresholding approach with 8-bit greyscale images. The workflow involved three key steps. Firstly, the differences in greyscale intensity levels between background areas and cell areas were sampled and a threshold level determined. A binary image mask of selected area was then generated. Secondly, each contiguous area of cellular material was identified. Finally, the selected areas were measured and the total selected area was calculated relative to the total image area.

Intensity level thresholding was achieved by sampling the grey-level intensity of the background area by selecting numerous regions of interest (ROI). The mean intensity and standard deviation of the background region were then calculated. Regions of interest containing mES colonies were selected and the mean intensity and standard deviation calculated. Mouse ES OCT4/GFP cells grow *in vitro* as compact colonies that appear phase-bright relative to the background area. The threshold level was therefore set to a value greater than the mean plus two standard deviations of the background level (intensity>105) and a value lower than the mean minus two standard deviations of the cell area level (intensity<133). The image was then converted into a binary mask, theoretically enabling measurement of the total selected area. In practice, numerous modifications of the binary data were necessary to generate useful numerical data. Local intensity levels within the cell areas overlapped with the background levels, consequently these areas were incorrectly excluded from the threshold.

A series of functions were then utilised to generate contiguous areas around individual colonies. The selected areas were expanded with the ‘Dilate’ function. The non-selected areas within the colony were then ‘closed’ and gaps between selected areas were filled. Finally, the selected areas were ‘eroded’ back to a representation of the original mask area. To generate numerical data pertaining to the total cell area, number of colonies and mean colony size, the packaged ‘Analyze Particles’ function was utilised. In order to exclude cellular debris from the area calculation, a minimum size rule was included in the analysis protocol. Consequently, the binary mask area differs from the actual measured area.

Figure 8.1.1 represents images of OCT4/GFP mES cells at subsequent stages of the process. Before thresholding (A), after thresholding (B), the binary mask of threshold data after processing (C) and composite image of the final mask area (red pixels) overlayed onto the original image (greyscale) (D). Tabular data provides a summary of the mean intensity level and standard deviation of the background and confluent area determined to define the threshold value (E), and the numerical measurement of the total cell area (F).

Figure 8.1.2 is a visual representation of the relationship between the total calculated cell area from a test image and the expression of OCT4-GFP in these cells. Images A and B are the original phase-contrast image and the binary mask area described by Method A. To ensure that the analysis module correctly highlighted areas of mES colonies, OCT4/GFP expression was visualised by fluorescence microscopy (C). The intensity level of GFP was subjected to a threshold above the background level and a binary mask was generated (D). The relationship between the confluent colony area and OCT4/GFP positive area is represented in image 8.1.2. (F). In this image, the confluent colony area is represented by red pixels and the OCT4+ve area by green pixels (overlayed onto the original image). Yellow pixels indicate areas of overlap between the Method A binary mask area and the OCT4 binary mask area.

Image E represents the relationship between the threshold area defined by Method A (red pixels) and the actual cell area (greyscale).Visual inspection of test images revealed a close overlap between the measured colony area and actual cell area. There appeared to be good concordance between the measured colony area and OCT4/GFP-positive areas. However, analysis of test data by Method A resulted in some inaccuracy in cell area detection (white triangles; E, F). In some areas, cells were identified but did not exhibit high OCT4 expression (blue triangle). It was concluded that Method A generated a graphical and numerical description of the total area of mES cell coverage from phase-contrast micrographs. However, limitations of the method were apparent upon visual examination.

Figure 8.1.1

Method A analysis of confluence of OCT4/GFP mES colonies from phase-contrast micrographs

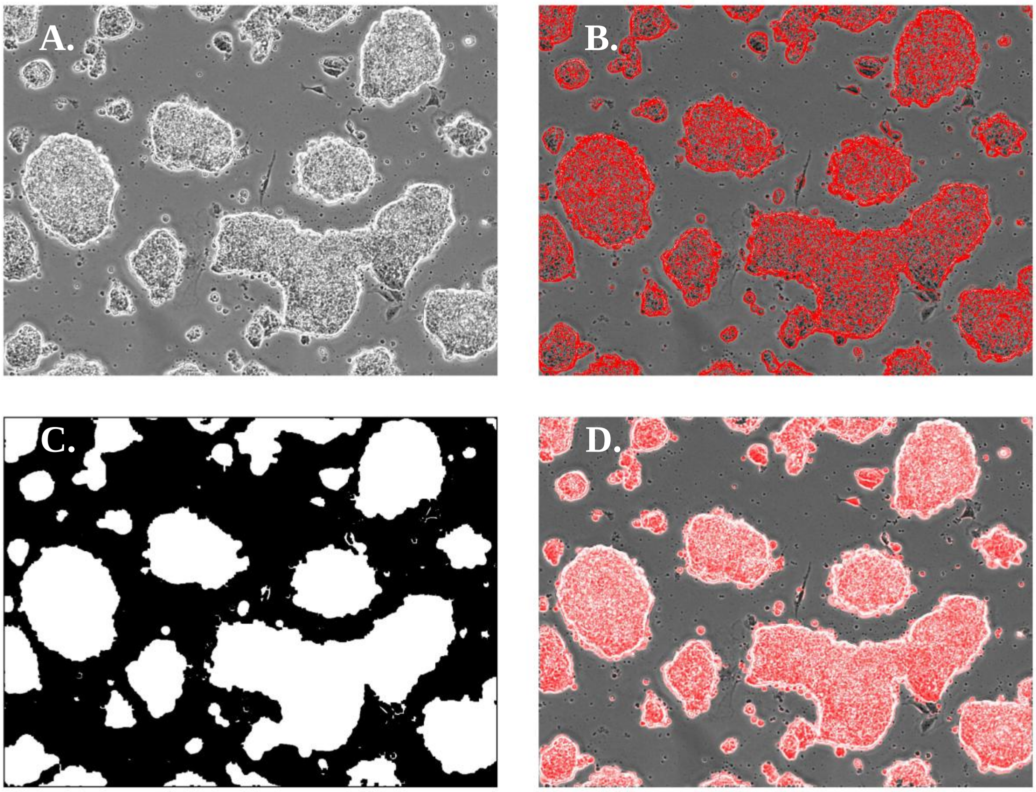

E.

threshold	mean intensity	standard deviation
background	98.2	3.3
colony	159.9	13.2

F.

size	pixels	μm^2
total area	526051	556.6
mean colony size	15030	94.1
number of colonies	35	

Figure 8.1.2

Relationship between the calculated cell area from Method A and OCT4+ve cell areas

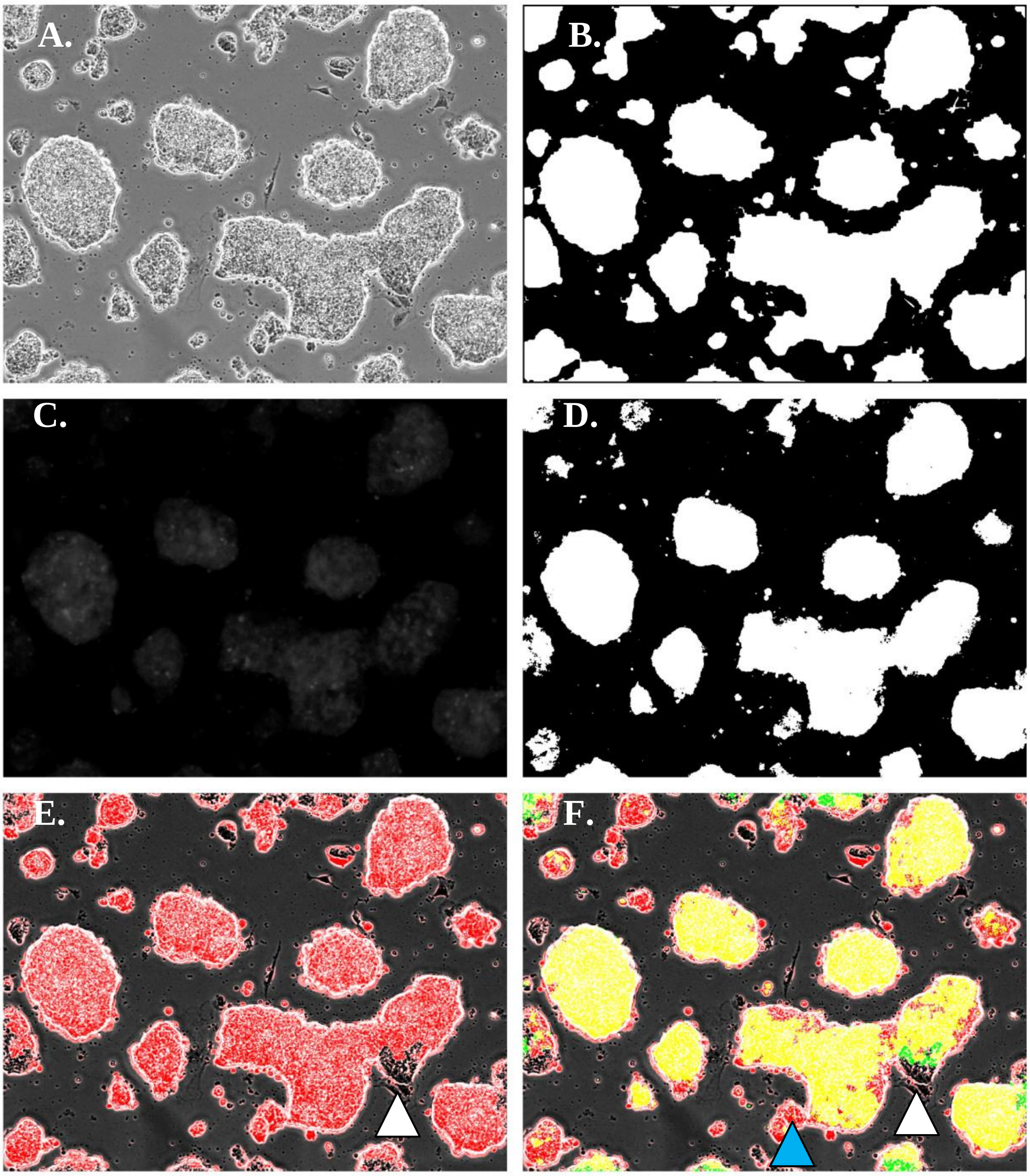

Figure Legends

Fig 8.1.1

Method A technique for the assessment of E14-OCT4/GFP cell coverage from phase-contrast micrographs. Original phase image (Image A) and threshold mask (Image B), final binary mask area (Image C) and the final mask area overlayed onto the original phase image (Image D). Tabular data (E) defines the threshold cutoff values and numerical results returned by the image analysis tool (F).

Fig.8.1.2

Visual representation of the relationship between Method A technique for identification of confluent cell areas and OCT4/GFP expression in E14-OCT4/GFP cells. Original phase image (A) and the final threshold mask area (B), OCT4/GFP expression (C) and the binary mask of OCT/GFP-positive areas (D). The original phase image (greyscale) is overlayed with the binary mask of the total cell area (red pixels) (E). A composite of the original phase image (greyscale), the mask area defined by Method A (red pixels) and the OCT4/GFP mask area (green pixels) (F). Yellow pixels define areas of overlap between calculated cell area and the OCT4/GFP binary mask. An area of cells that was incorrectly identified by Method A is indicated by a white triangle, and an area of OCT4/GFP-negative cell coverage identified by Method A indicated by a blue triangle.

Having established a basic tool to document the total area of mES cell coverage, the effect of rapamycin treatment was investigated. Mouse ES cells (E14 OCT4/GFP) were cultured with complete growth medium containing 10% FCS supplemented with 10^3u/ml LIF as previously. Cells were seeded into gelatin-coated Nunc™ brand tissue culture-treated T25 flasks and cultured in a humidified atmosphere with 5% $C0_2$. After an initial attachment period, cultures were treated with DMSO and 10nM or 100nM rapamycin for 48h. Triplicate wells were imaged at 10x magnification and a minimum of ten fields of view per well were captured for analysis. Data was generated with Method A is presented graphically (Figs.8.1.3-5). In these figures, Image A is the original phase micrograph, Image B the calculated binary mask area, Image C represents a line drawing of the actual measured area and Image D represents the mask area overlayed onto the original phase image.

It was previously established that rapamycin treatment inhibited mES cell proliferation in a dose-dependent manner (Figure 3.3.3). Therefore it was hypothesized that this inhibition in cell proliferation would manifest as a reduction in the total area of cell coverage (confluence). Analysis of imaging data by Method A revealed no significant difference in the total cell area coverage following treatment with 10nM rapamycin. At the higher concentration of rapamycin (100nM), there was a significant reduction in the total area of cell coverage compared with DMSO treated control cells ($p<0.01$).

Figure 8.1.3

Image analysis assessment of mES cell confluence following 48h treatment with DMSO (Method A).

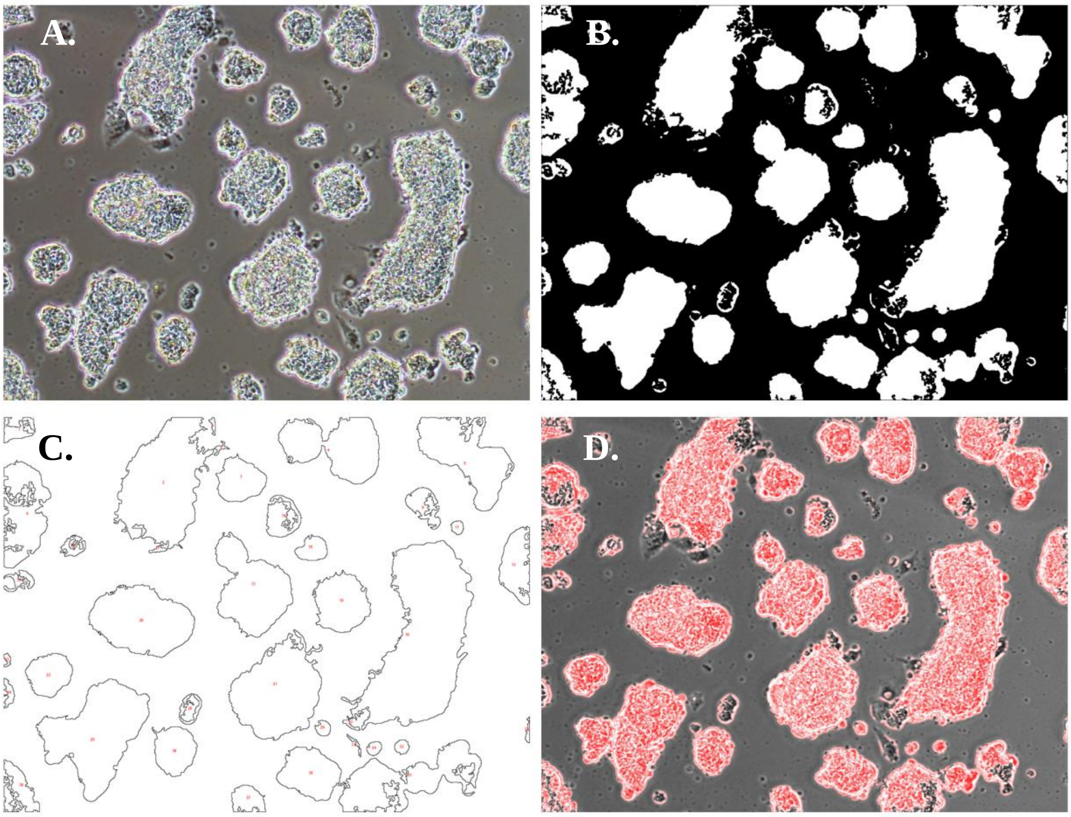

Fig.8.1.3

Method A analysis of E14-OCT4/GFP cells after 48h treatment with DMSO. Image A represents the original phase-contrast micrograph; the binary mask generated from Method A (Image B) and a line drawing of the actual measured area (Image C). Image D represents an overlay of the binary mask area (red pixels) and the original micrograph (greyscale).

Figure 8.1.4

Method A assessment of mES cell confluence following 48h treatment with 10nM rapamycin.

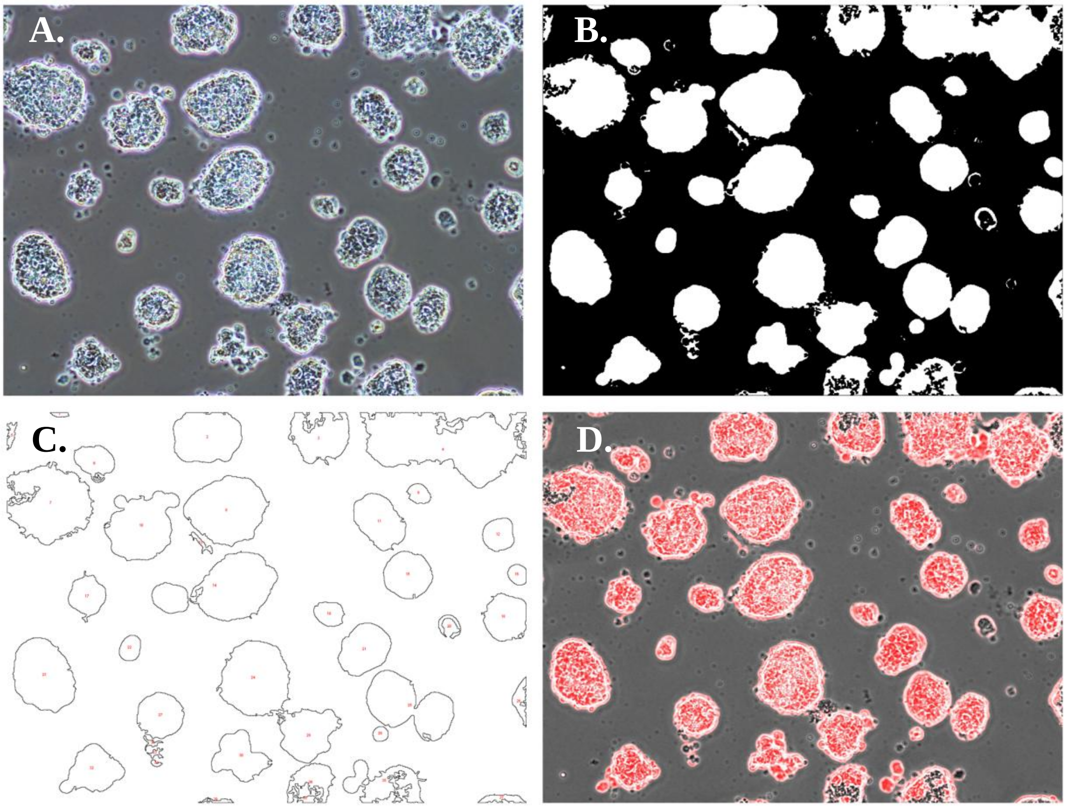

Fig.8.1.4

Method A analysis of E14-OCT4/GFP cells after 48h treatment with 10nM rapamycin. Image A represents the original phase-contrast micrograph; the binary mask generated from Method A (Image B) and a line drawing of the actual measured area (Image C). Image D represents an overlay of the binary mask area (red pixels) and the original micrograph (greyscale).

Figure 8.1.5

Method A assessment of mES cell confluence following 48h treatment with 100nM rapamycin.

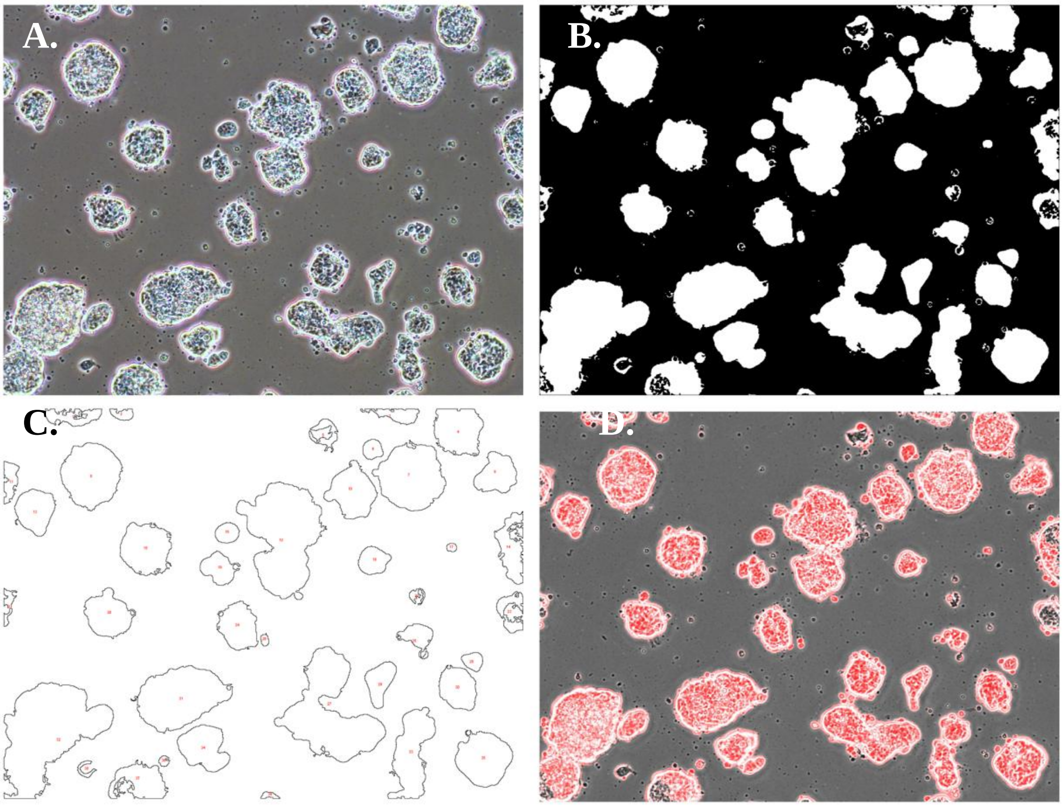

Fig 8.1.5

Panel of representative images of Method A analysis of E14-OCT4/GFP cells after 48h treatment with 100nM rapamycin. Image A represents the original phase-contrast micrograph; the binary mask generated from Method A (Image B) and a line drawing of the actual measured area (Image C). Image D represents an overlay of the binary mask area (red pixels) and the original micrograph (greyscale).

Figure 8.1.6

Assessment of the effect of rapamycin on cell area coverage by Method A analysis of phase-contrast images.

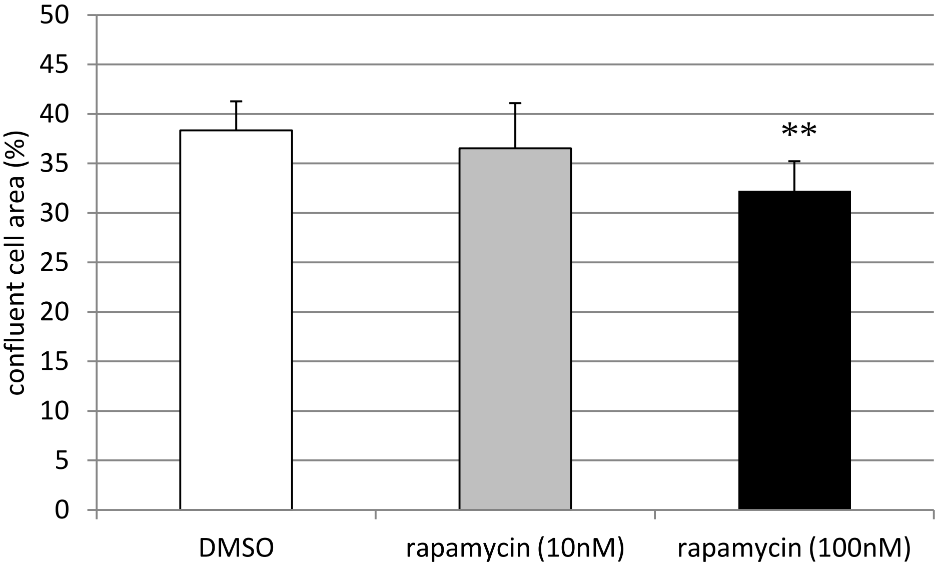

Fig.8.1.6

Method A analysis of total confluent cell area of DMSO and rapamycin treated E14 OCT/GFP mES cells. Ten unique fields of view per treatment group imaged at 10x magnification by phase-contrast microscopy. Results presented of data from three parallel cultures. Statistical analysis by unpaired t-test revealed a difference at the alpha level of p<0.01 (**).

8.2 Characterisation of Method A for determination of mES expansion from time-course images.

The aim of this experiment was to measure the expansion of the E14-Tga2 parent line over time by processing phase-contrast micrographs with the image analysis tool Method A.

Mouse ES cells exhibit variations in colony morphology depending on the cell line and culture conditions. It was noted that the E14-OCT4/GFP cells exhibited a clustered three dimensional morphology. In contrast, the E14 parent cell-line produced flat monolayer colonies (Figure 3.3.1). Therefore the E14 parent line was selected for mES colony area measurements. It was hypothesized that during the 48h passage the total area of cell coverage would increase, mean colony size would also increase but the total number of colonies would decrease. Therefore it was anticipated that analysis of mES cell expansion by Method A would generate data that was consistent with these traits.

Mouse ES cells (E14-Tga2) were seeded into 6-well plates and cultured within a proprietary live-cell imaging system (Cell-IQ™). Images were captured at 20x magnification over a 48h period. Control data was collected from 3 series of images. Micrographs from a biological assay were processed by Method A and the numerical data was plotted graphically, results images were then visually inspected to identify potential errors. Prior to analysis of the imaging data, modifications to Method A were applied to adjust for differences in the mean background intensity level of the imaging data. Additionally, the minimum size rule was modified to account for the increased magnification factor of the images.

Figure 8.2.1 represents graphical data of the total cell area coverage from triplicate fields of view imaged over 48h. Method A measured a time-dependent increase in the total confluent cell area. The rate of increase of the total cell area appeared to increase after 24h culture. An image series from a single field of view was then plotted and a 2nd order polynomial line was fitted (Figure 8.2.2). The coefficient of determination for the fitted line was 0.0997 indicating that the data closely matched a two order rate equation.

Data presented in Figure 8.2.3 indicated that after 48h the total number of colonies decreased, however, there was a large variation in the number of colonies at each time-point as indicated by large standard deviation values. The measurement of colony size over time demonstrated a steady increase in mean colony size (Figure 8.2.4). However, high standard deviation values precluded significance testing.

In summary, Method A generated data showing an increase in the total area of cell coverage over time. Measurements of colony size and colony number contradicted this trend. It was anticipated that the total area of cell coverage would relate to both colony size and colony number. Large standard deviations of the data points may have masked any trend. The results images from selected data points were then subjected to visual inspection to highlight the limitations of the analysis protocol.

Figure 8.2.1

Analysis of mES cell expansion from triplicate fields of view over 48h Method A.

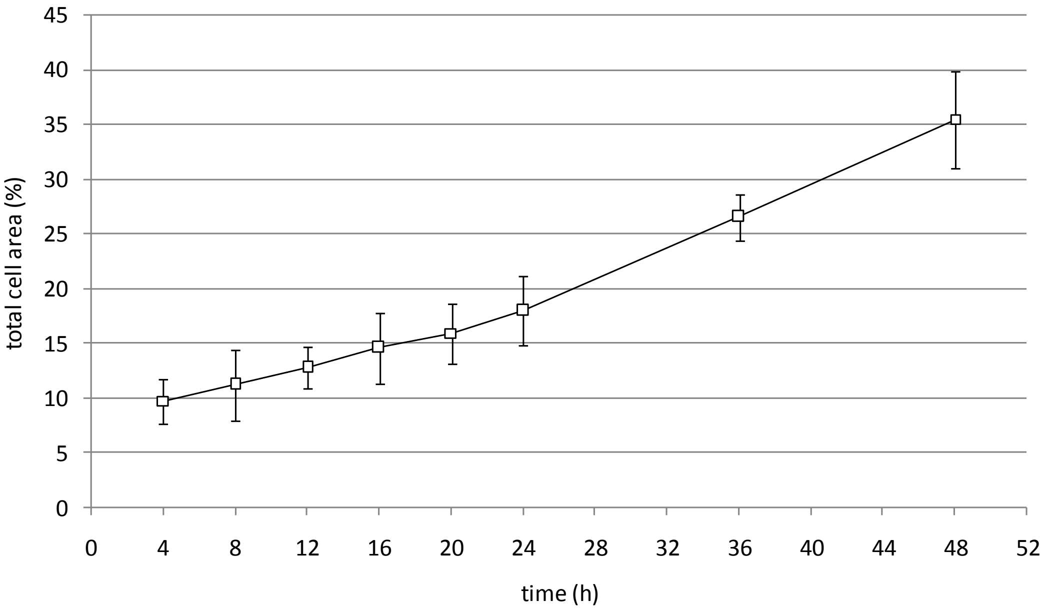

Fig 8.2.1

Analysis of mouse E14 cell expansion from triplicate fields of view by over 48h by Method A. Cells were seeded into 6 well plates cultured with complete growth medium containing 10% serum and 10^3u/m LIF. The Cell-IQ™ automated imaging platform for cell culture was used to capture phase-contrast images from fixed positions of the tissue culture plate over 48h. Images captured at 20x magnification.

Figure 8.2.2

Method A analysis of a single field of view describing mES colony expansion over 48h.

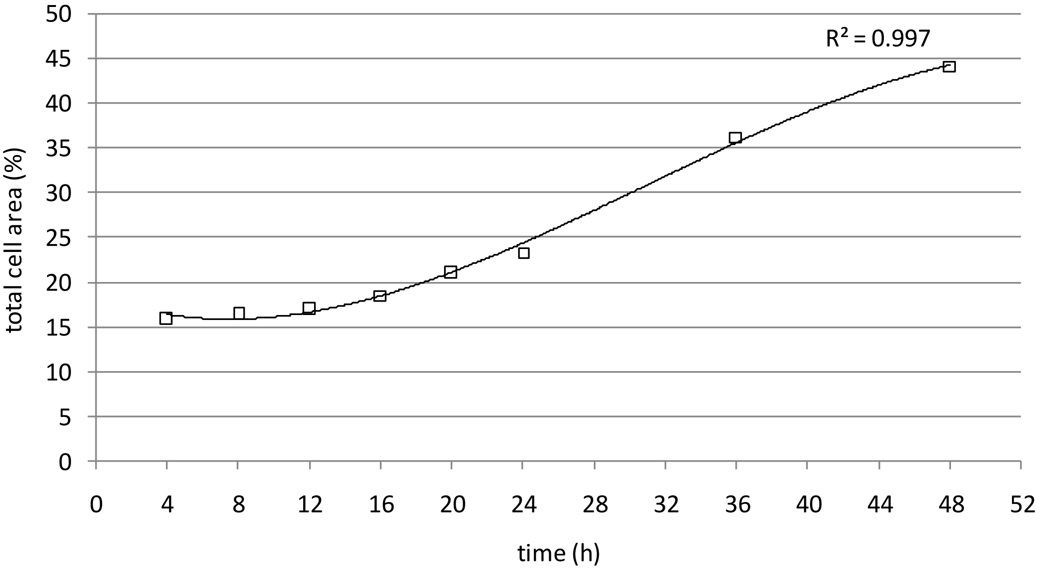

Fig.8.2.2

Analysis of mouse E14 cell expansion from a single view by over 48h by Method A. Cells were seeded into 6 well plates cultured with complete growth medium containing 10% serum and 10^3u/m LIF. The Cell-IQ™ automated imaging platform for cell culture was used to capture phase-contrast images from fixed positions of the tissue culture plate over 48h. Images captured at 20x magnification and subjected to analysis by Method A. The fitted line revealed a close concordance with a two order rate equation, assessed by the coefficient of determination statistic.

Figure 8.2.3

The mean number of mES cell colonies measured over 48h by Method A was highly variable.

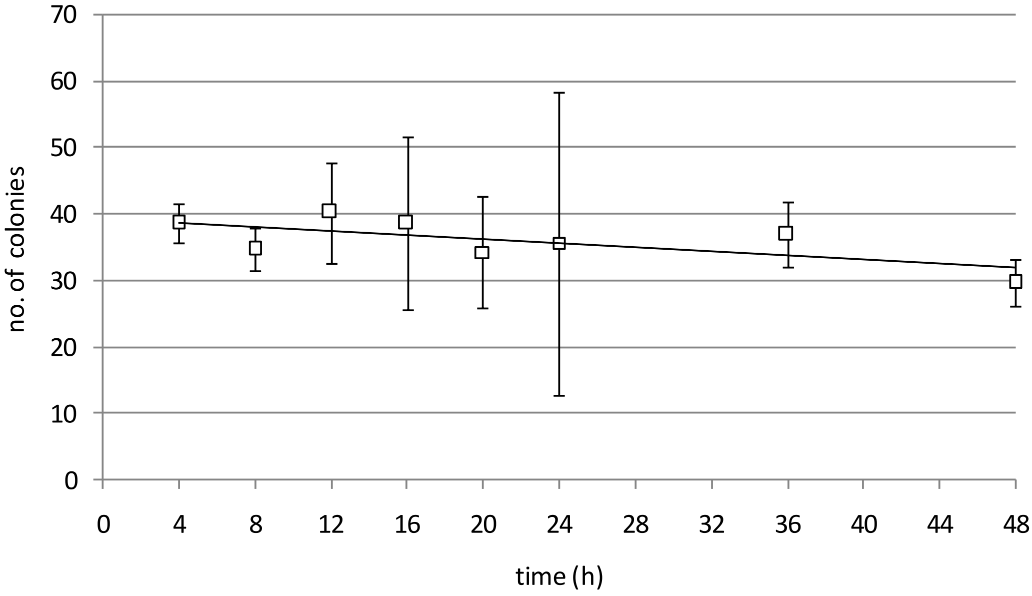

Fig.8.2.3

Analysis of mouse E14 cell expansion from triplicate fields of view over 48h by Method A. Cells were cultured and imaged as described in the previous figure. Data expressed as mean and standard deviation of the number of colonies at each time point.

Figure 8.2.4

High variance in the mean area of mES cell colonies over 48h calculated by Method A.

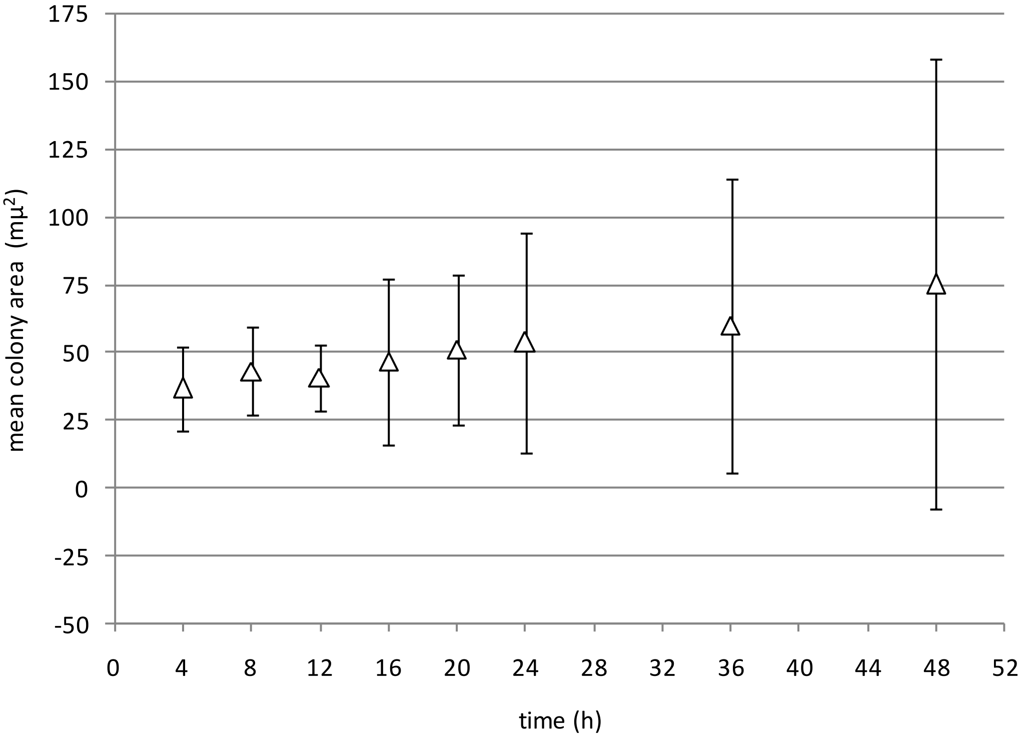

Fig.8.2.4

Analysis of mouse E14 cell expansion from triplicate fields of view over 48h by Method A. Cells were cultured and imaged as described in Figure 8.2.1 figure. Data expressed as mean and standard deviation of individual colony area measurements at each time point.

Examination of the results images generated by Method A revealed inaccuracies in cell area selection. Figures 8.2.5 and 8.2.6 represent a visual analysis of total cell area measurements at 4h and 12h respectively. Image panels consist of the original phase contrast image (A), a line drawing of the calculated area of cell coverage (B) and an overlay of the measured area (red pixels) and the phase-contrast image (C). Areas of false positive and false negative identification of mES cells are indicated by yellow triangles and white triangles respectively (Figure 8.2.6). Phase-bright areas of dead cells and cellular debris were inadvertently selected and counted as individual colonies by Method A, potentially skewing the distribution of colony size measurements (size distribution data not shown).

The principle factor for the determination of cell area by Method A was based upon identification of pixels with a grey level intensity greater than that of the background. Whereas the morphology of E14 OCT4/GFP mES cells *in vitro* was characterised by compact colonies that appeared phase-bright at 10x magnification. The E14-Tga2 parent cell line exhibited a less compact, monolayer morphology. Analysis of micrographs of E14 cells at 20x magnification by Method A revealed the limitations of this method. Areas of false negative identification were abundant after 12h culture (white triangles, Figure 8.2.6).

Figure 8.2.5

Images of mES cells in culture 4h after seeding analysed by Method A.

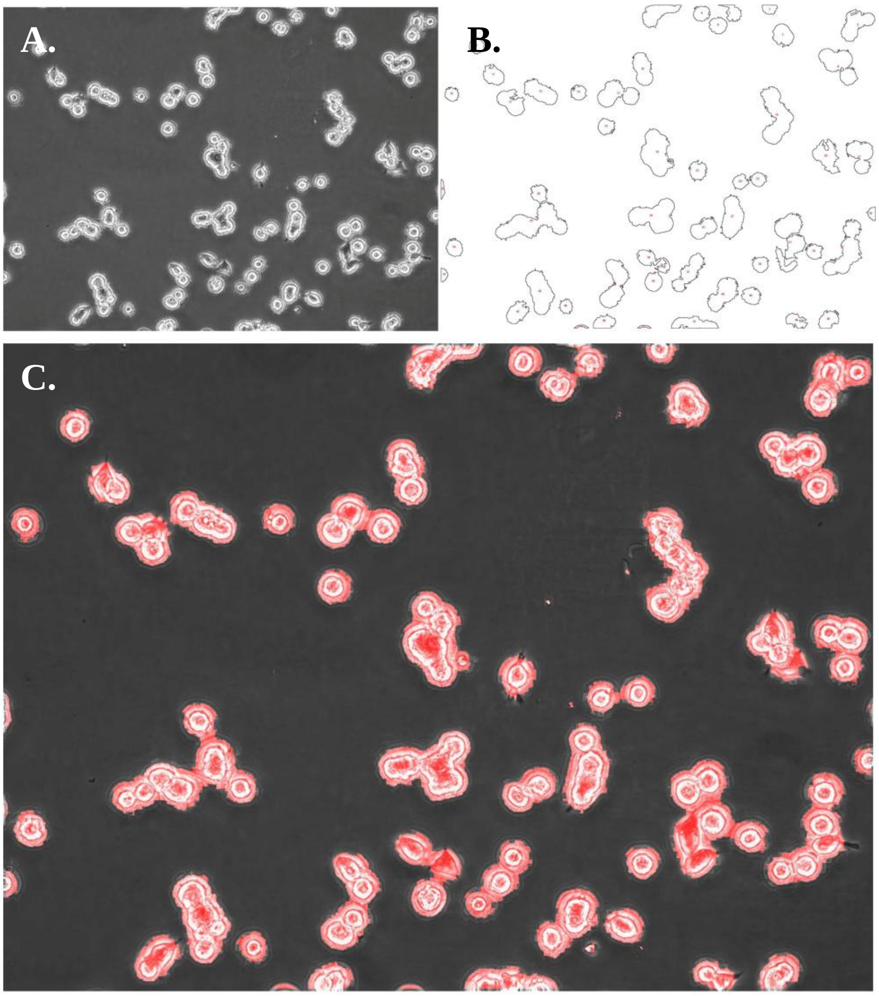

Fig.8.2.5

Visual representation of total cell area measurements at 4h and 12 respectively. Image panels consist of phase contrast image (A), a line drawing of the calculated area of cell coverage (B) and an overlay of the measured area (red pixels) and the phase-contrast image (C). Areas of false positive and false negative identification of mES cells are indicated by yellow triangles and white triangles respectively

Figure 8.2.6

Representative images of Method A analysis of mES cells in culture 12h after seeding.

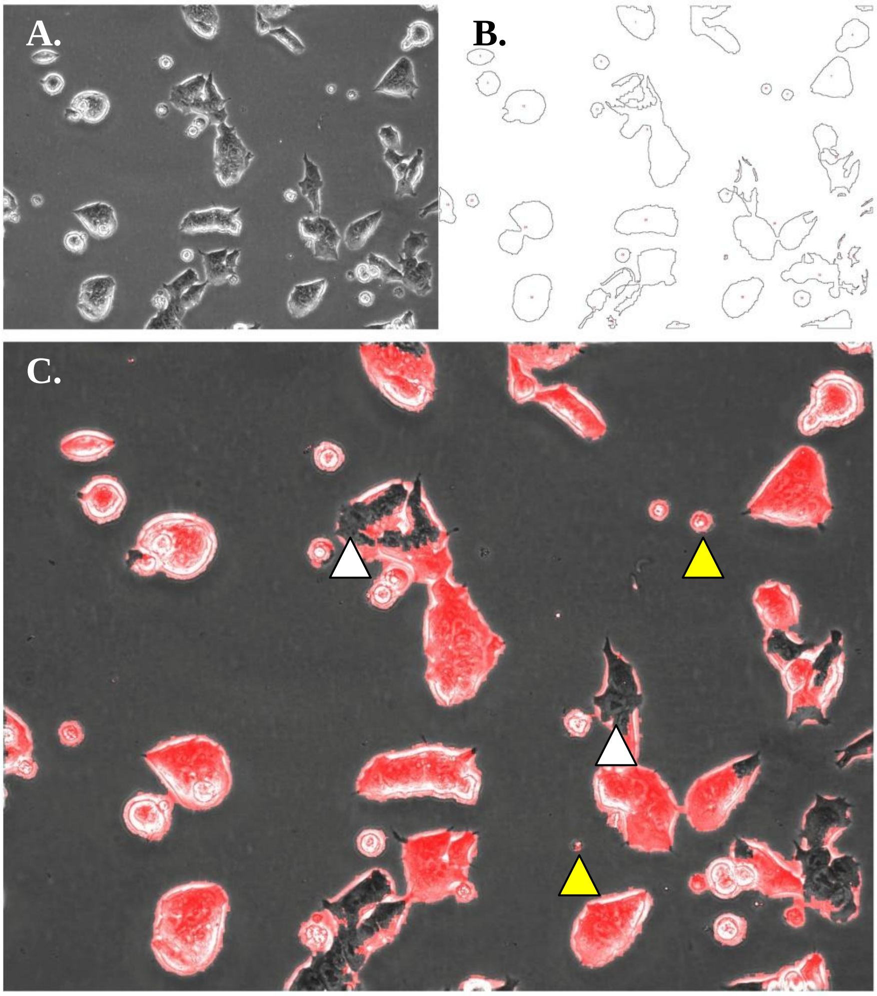

Fig.8.2.6

Visual representation of total cell area measurements at 4h and 12 respectively. Image panels consist of phase contrast image (A), a line drawing of the calculated area of cell coverage (B) and an overlay of the measured area (red pixels) and the phase-contrast image (C). Areas of false positive and false negative identification of mES cells are indicated by yellow triangles and white triangles respectively. Areas of the image incorrectly identified as background (white triangles) and non-viable areas and cellular debris identified by Method A Indicated (yellow triangles).

8.3 Development of a dual threshold technique - Method B

Method A was optimised for analysis of phase-contrast micrographs of E14 OCT4/GFP cells. However, application to the analysis of phase-contrast micrographs of the E14-Tga2 parent line at 20x magnification highlighted the limitations of the method. This discrepancy may have arisen from differences between colony morphology of the two cell lines, a feature exacerbated by increasing the magnification factor at image capture.

The principle concern with Method A was the false-negative identification of cell-areas. The grey-level intensity of these areas was measured, it was deduced that the intensity level of these regions was equal to or lower than the background level. Therefore, in order to develop a more accurate analytical tool, a dual threshold was applied to exclude pixels within the range of the background and include both high intensity and low intensity pixels. Additional concerns with Method A related to the high variability in the measurement of the total number of colonies and the large standard deviations resulting from the individual colony size measurements. It was observed that dead cells and cellular debris were included in the measurement. These individual elements were then measured from control images and a minimum size-rule was redefined. The impact of this modification will be discussed in section 8.5.

In order to assess whether Method B improved the measurement of cell area, mean colony size and the total number of colonies; time series data presented in the previous section (8.2) was reanalysed with Method B and compared with the results generated by Method A. Figure 8.3.1 shows a representative phase-contrast image after 12h culture (A), the overlay of the result from Method A (B), and the Method B result image (C). Visual inspection of these images revealed an improvement in the accuracy of Method B in the positive identification of cell areas.

Figure 8.3.2 shows the relationship between the area measurement calculation generated from the same data by the two methods. Data is presented as the measured area fraction over time. It is clear from this graph that Method B returned higher values than Method A at all time points. Plotting this data as a scatter graph revealed that there was a close correlation in the in the area calculation between the two methods (R^2=0.985). This analytical technique can highlight trends between two data sets independently of absolute values. However, as both data sets were based upon the same input data, a close correlation was to be expected. Consequently, this analysis does not effectively represent differences between the two methods. Therefore, the total cell area values were plotted against the difference between values generated by each method (Figure 8.3.3). Concordant data sets would align at the zero value at all data points. Examination of this chart revealed that when the area measurement was low, the difference between the methods was also low. As the measured cell area increased, the difference between the values generated by Method A and Method B also increased. In conclusion Method B provided a more accurate description of total cell area coverage than Method A.

Figure 8.3.1

Visual inspection of selected binary mask area from Method A and Method B for analysis of mES cell colony area in phase-contrast images 12h post-seeding

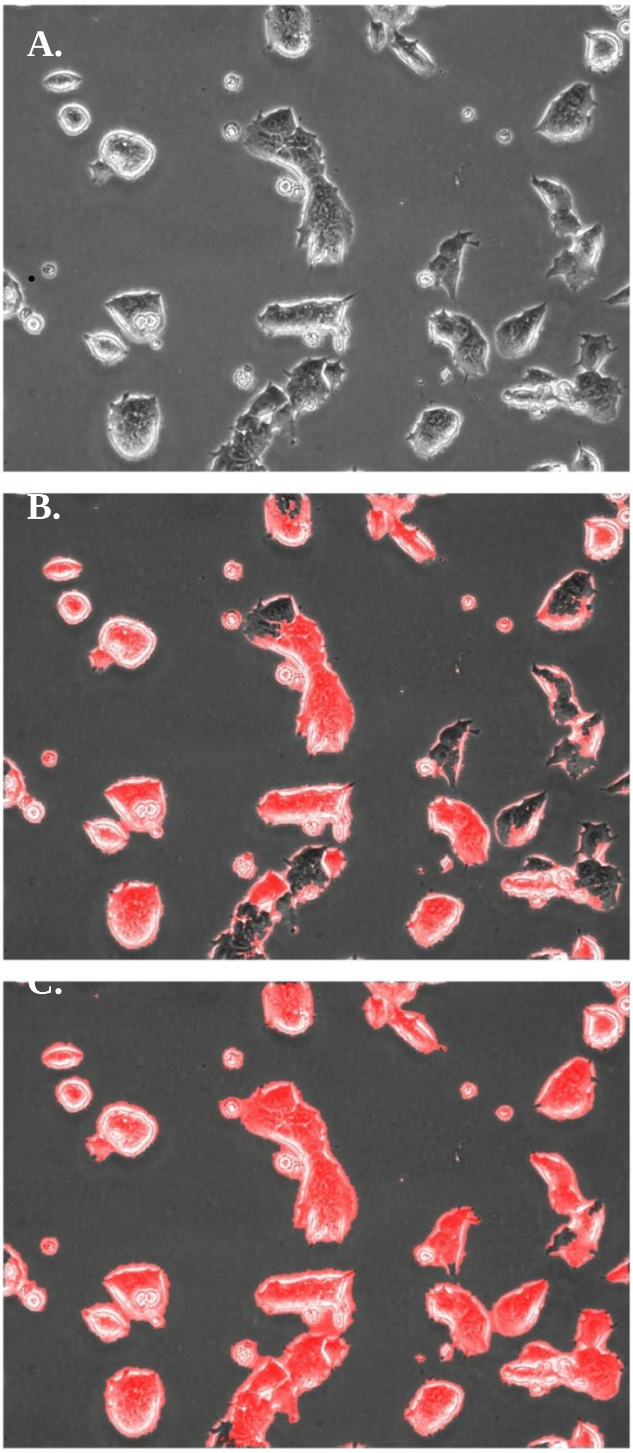

Fig.8.3.1

Panel of representative phase contrast images of mES cells after 12h in culture (image A) and results images from Method A (image B) and Method B (image C). Images reveal that Method B provides a more accurate description of total cell area.

Figure 8.3.2

Comparison between positive threshold analysis (Method A) and dual threshold analysis (Method B) for total cell area measurement from phase-contrast micrographs.

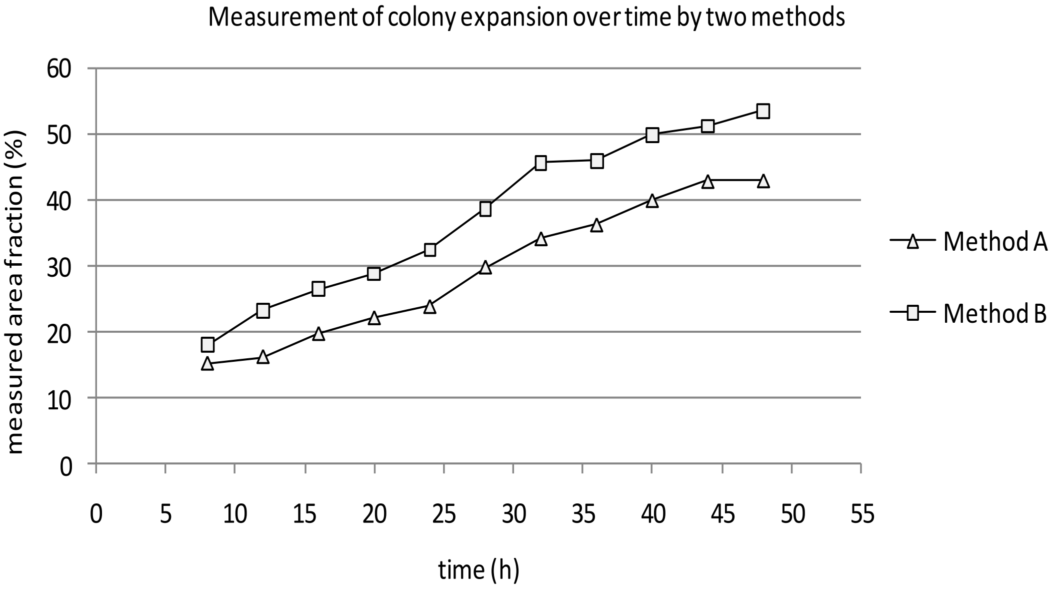

Fig.8.3.2

Total cell area measurement from phase contrast micrographs of mES cells in culture over 48h. A single field of view was analysed by Method A (open triangles) and Method B (open squares).

Figure 8.3.3

Correlation between the total cell area measurement calculated by two methods (A and B).

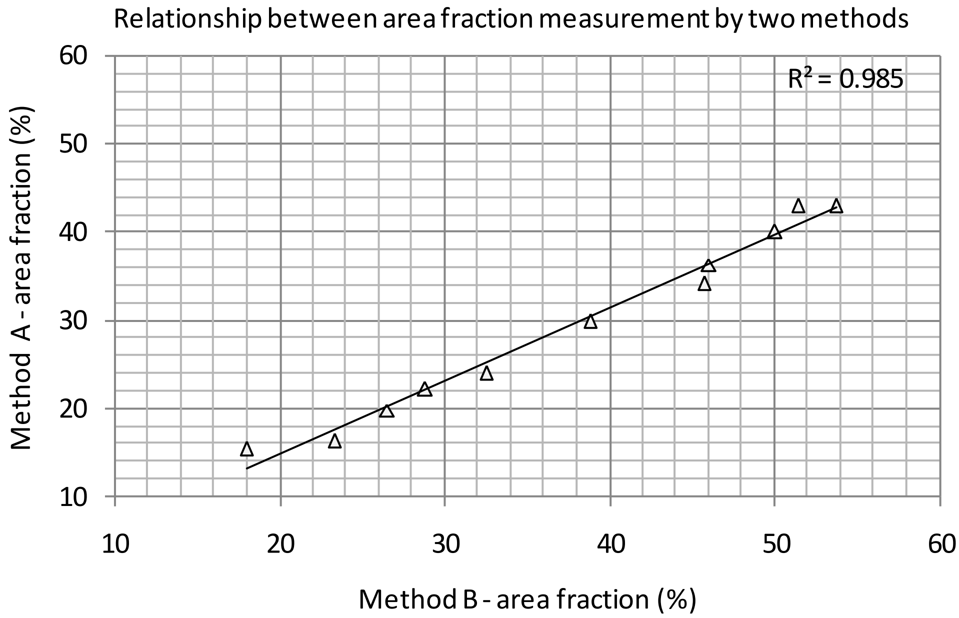

Fig. 8.3.3

Data from Fig.8.3.2 presented as a scatter plot to highlight the relationship between Method A and Method B calculation of total cell area (area fraction). Linear regression revealed a high correlation coefficient of distribution (R^2) between the two methods.

Figure 8.3.4

Relationship between total cell area measurements by two methods (A and B).

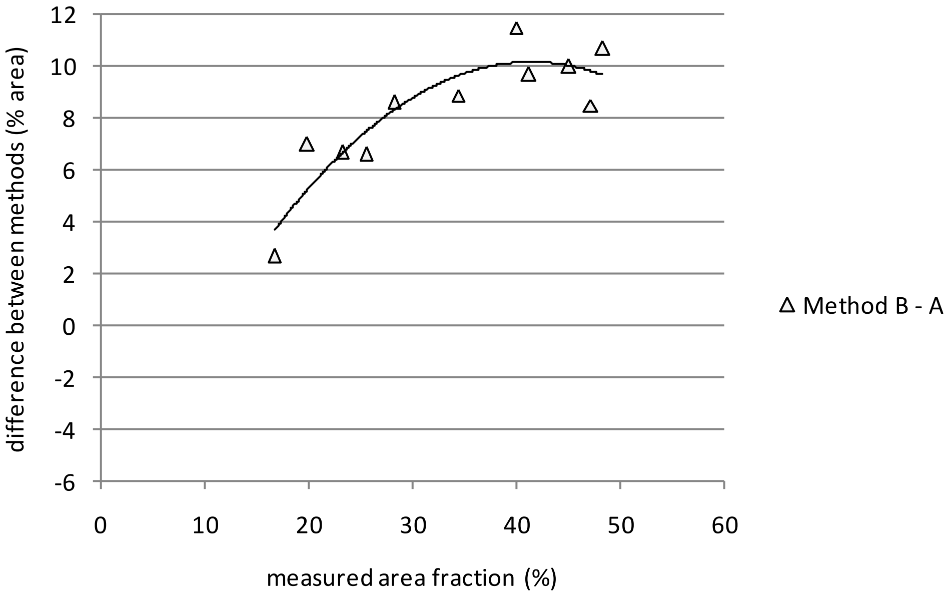

Fig. 8.3.4

The relationship between results generated from Method A and Method B from the same input data. Results are plotted as a scatter graph of total area measurement versus the difference between values at each data point. A polynomial regression line is included to highlight trends.

8.4 Characterisation of a robust, local contrast variation - Method C.

A prerequisite for the analysis of mES cell confluence from phase-contrast micrographs by Method A or B was a precisely defined background intensity level. However, analysis of images captured at different exposure settings may result in a reduction in the power of the technique to correctly identify areas of cell coverage. Analysis of images acquired over more than one imaging session therefore requires strictly controlled illumination and image capture settings. Alternatively, threshold calculations must be re-established from control images at each imaging session. Consequently, a more robust image analysis technique was developed. This alternative method functions on the basis of local variations in the contrast between adjacent pixels. This approach provided advantages over the threshold-based analysis as it was less susceptible to ‘between image’ variations in background intensity.

A principle feature of the background area (non-cell area) of a phase-contrast micrograph is the uniform distribution of pixel intensity levels (low local contrast). Conversely, areas of cell coverage exhibit high variability in pixel intensity. Therefore, the primary discriminator for selecting cell areas was based upon this local contrast variation. Areas of high local contrast variability were identified and a binary mask of the selected area was created as described for the previous methods. This process was termed Method C. Measurements of the total cell area, total number of colonies and mean colony size were compared with results generated by Methods A and B.

Figure 8.4.1 shows a panel of representative images of the results generated by Methods A, B and C. The same phase contrast image was analysed by each method and displayed as an overlay of the binary mask and original phase-contrast image (A) and a line drawing of the actual measured area (B). Inspection of these images revealed that Method C returned a similar result to Method B and accurately described total cell area. This was confirmed by the analysis of time-series data from a single field of view imaged over 48h (Figure 8.4.2). Mouse ES cells were cultured as previously described in the Cell-IQ™ imaging platform. Images of cells in culture were taken at 4h intervals and analysed using each method, data was presented as the total cell area over time.

The area fraction measurement at each time point was plotted against the difference between the results returned by each method. This data is presented in Figure 8.4.3. When Method C was compared with Method A, it was observed that the difference between values increased as cell area increased (i). This was not observed when Method C was compared with Method B (ii). Comparisons between these two methods revealed a linear relationship that remained close to the zero value (no difference between values). These findings, when taken together, show that Method C was equivalent to Method B and an improvement over Method A in the description of confluent cell area.

Figure 8.4.1

Visual representation of total cell area measurements of mES cells at 24h in culture by Methods A, B and C.

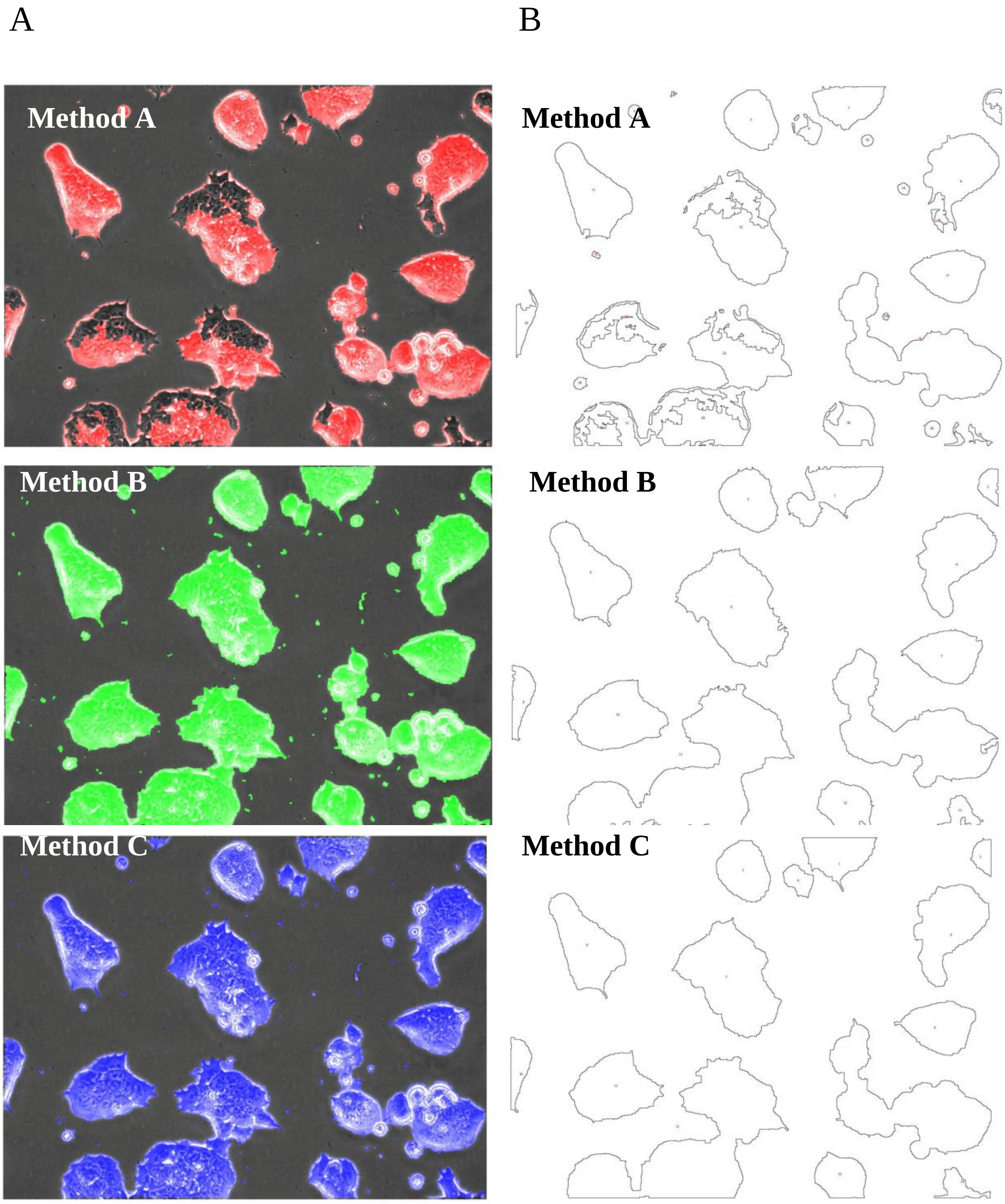
A
B
Method A
Method A
Method B
Method B
Method C
Method C

Fig.8.4.1

Binary mask result (A) generated from a representative phase contrast image analysed by Method A (red), Method B (green) and Method C (blue). Line drawings of actual measured area are also presented (B).

Figure 8.4.2

Total cell area measurement by Methods A, B and C

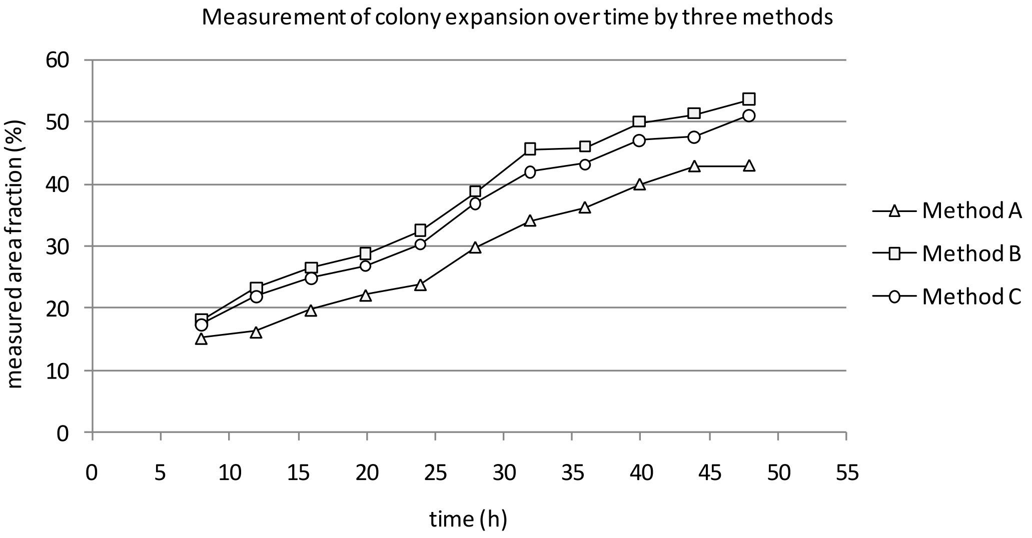

Fig.8.4.2

Total cell area measurement from phase contrast micrographs of mES cells in culture over 48h. A single field of view was analysed by Method A (open triangles), Method B (open squares) and Method C (open diamonds). Data shows that Method B generates similar results to Method B but not Method A.

Figure 8.4.3

Cell area measurements by Method C closely align with Method B but not Method A.

i.

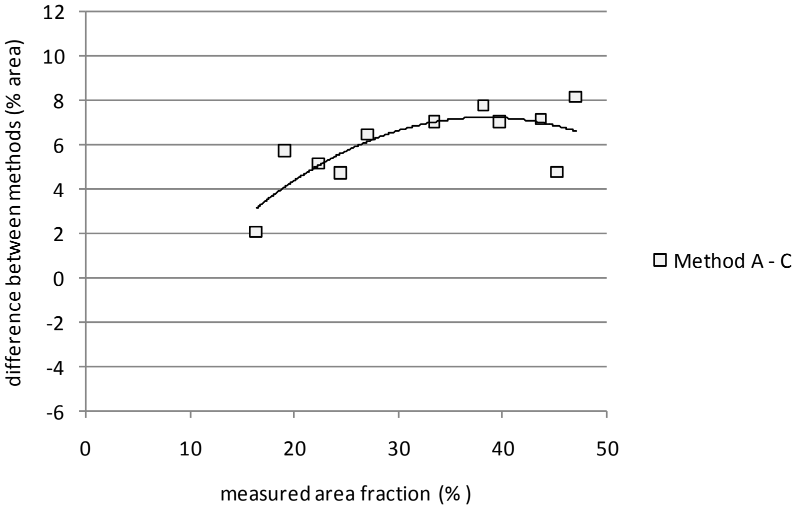

ii.

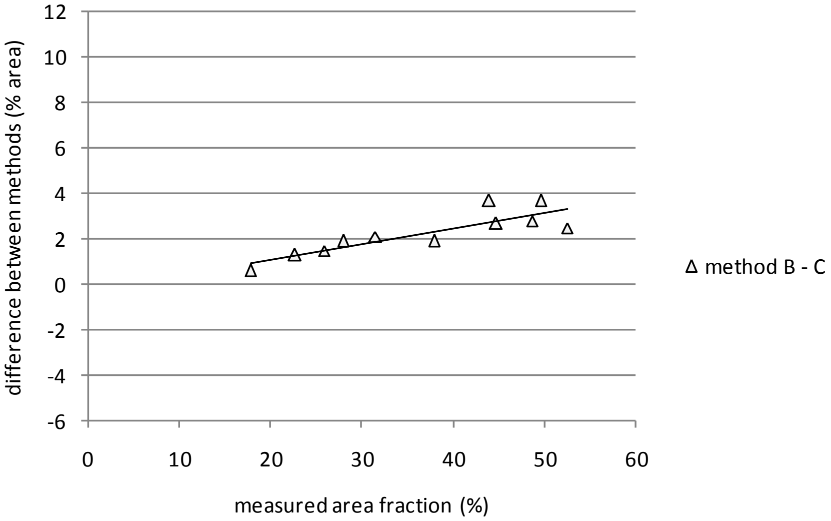

Fig. 8.3.4

The relationship between total area measurements generated by Method A and Method C(i), and Method B and Method C (ii). Results are plotted as a scatter graph of total area measurement versus the difference between values at each data point. Regression lines highlight the relationship between the methods. This data shows that Method C aligns closely with Method B but not Method A.

8.5 The relationship between mean colony area measurements and total number of colonies by the three methods.

During routine culture of E14 mES cells *in vitro,* it was observed that as cells reached confluence, individual colonies merged into large monolayers. Therefore, it was hypothesised that as the mean colony size increased, the total number of colonies would decrease. Moreover, a concordance between these parameters should be evident upon computational analysis.

To assess whether the image analysis methods described here, identified this concordance, the mean colony area measurements of mES cells in culture over 48h were plotted against the total number of colonies. This data is presented in Figures 8.5.1 (Method A), Figure 8.5.2 (Method B) and Figure 8.5.3 (Method C). Concordance was not found by Method A analysis. However, Method B and Method C exhibited a statistically significant concordance between the colony area and the number of colonies. The data from these two methods were described by a two-order polynomial equation with a coefficient of determination (R^2) of 0.994 and 0.963 for Method B and Method C respectively.

In summary, these findings demonstrate that Method B and Method C describe the *in vitro* expansion of mouse ES cell in accordance with the stated hypothesis. Method C operates independently of image capture settings and can therefore be applied post-hoc to imaging data. Consequently it was concluded that Method C provides a robust measurement of cell area, colony size and the total number of colonies and is therefore applicable for monitoring the expansion of embryonic stem cell cultures *in vitro* in the laboratory setting.

Fig 8.5.1

Relationship between mean colony size and the total number of colonies by Method A.

i.

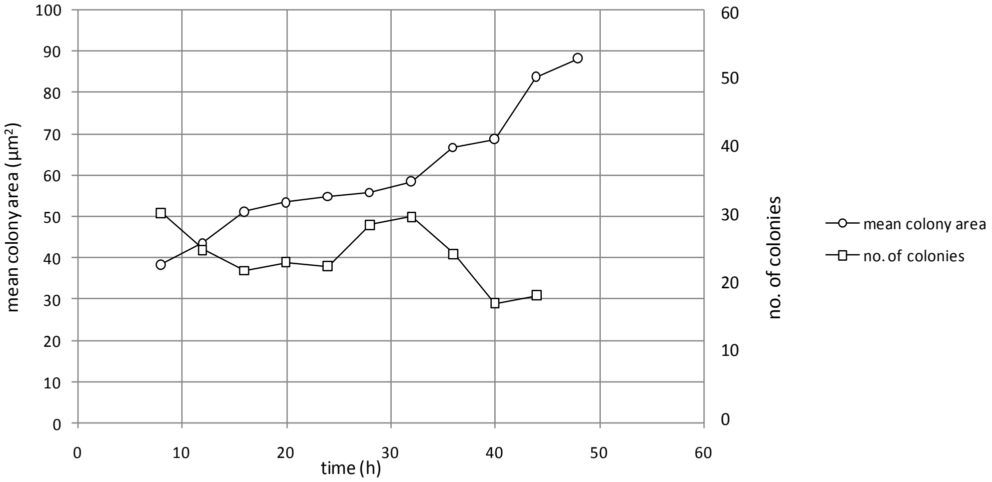

ii)

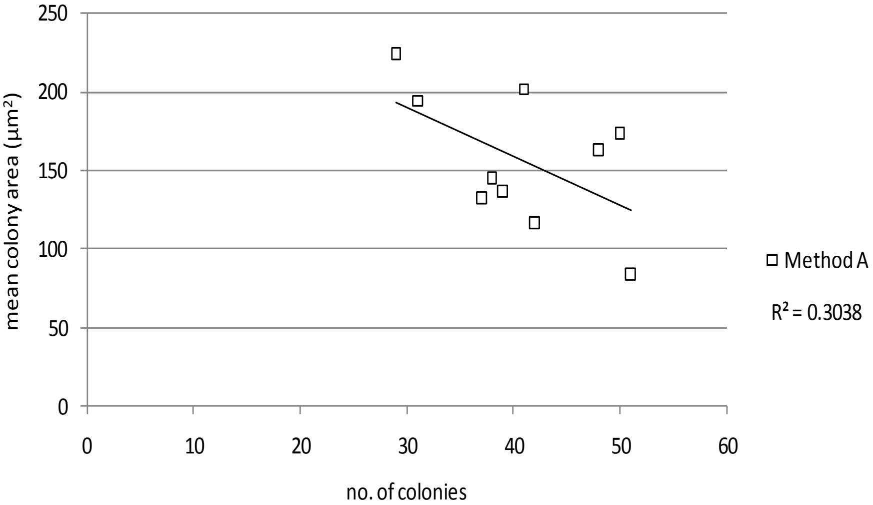

Fig. 8.5.1

Graphical representation of the number of colonies/field of view and mean colony size (μm^2) at each time-point over 48h (i) and the relationship between mean colony area and number of colonies (ii) from Method A. Linear regression analysis revealed no statistical concordance between the parameters,

Figure 8.5.2

Relationship between mean colony size and the total number of colonies by Method B.

i.

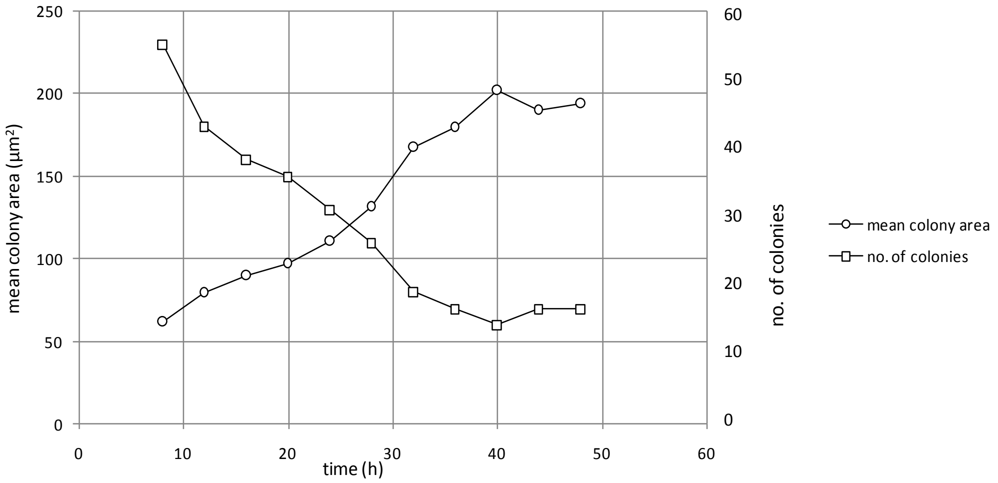

ii)

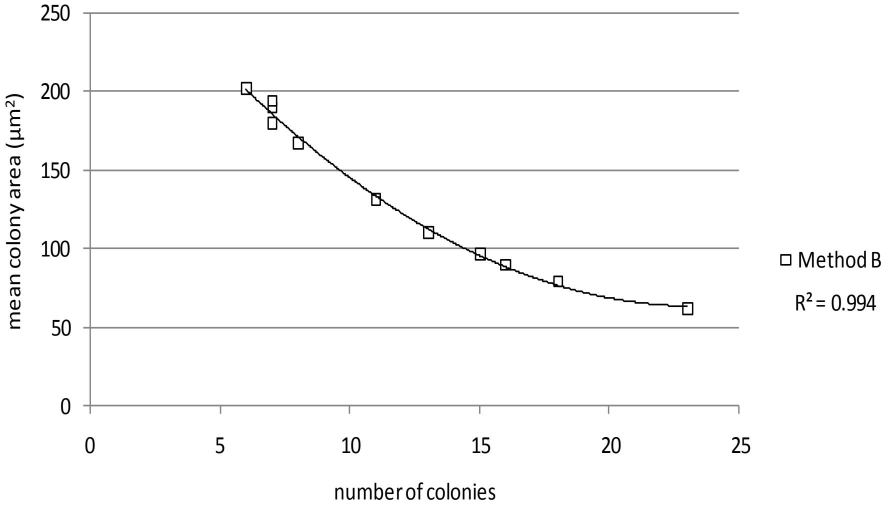

Fig. 8.5.2

Graphical representation of the mean colony area (µm^2) and number of colonies/field of view and at each time-point over 48h (i) and the relationship between mean colony area and number of colonies (ii) from Method B. A two-order polynomial equation described the relationship between values with a coefficient of distribution of 0.994 (R^2). Strong concordance between values was observed with Method B.

Figure 8.5.3

Concordance between the mean colony size and total number of mES cell colonies by Method C.

i.

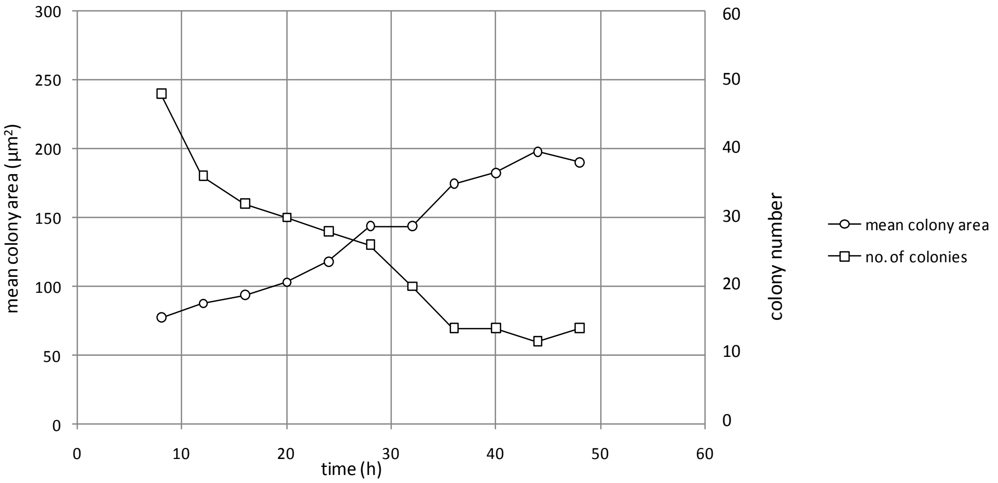

ii)

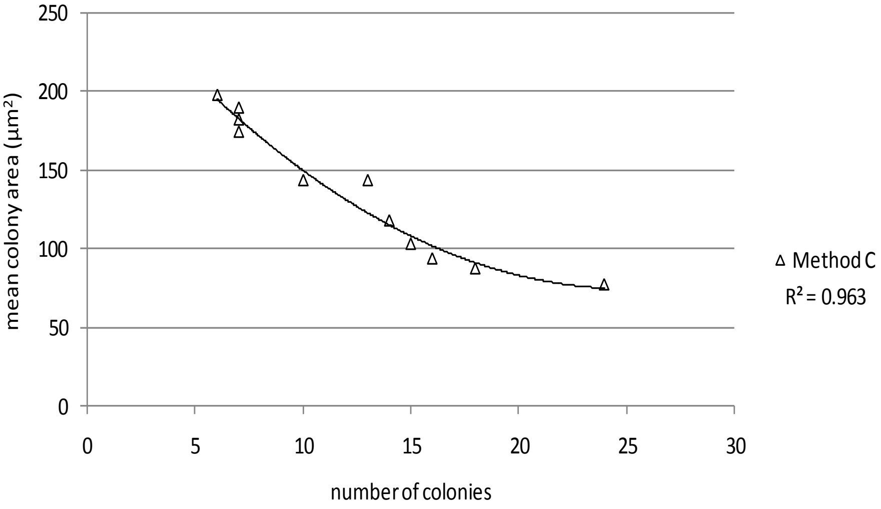

Fig. 8.5.3

Graphical representation of the mean colony area (µm^2) and number of colonies/field of view and at each time-point over 48h (i) and the relationship between mean colony area and number of colonies (ii) from Method C. A two-order polynomial equation described the relationship between values with a coefficient of distribution of 0.963 (R^2). Strong concordance between values was observed with Method C.

8.6 Characterisation of mES cell phase and morphology from phase-contrast micrographs by Method 2.

The methods presented in the previous sections describe the total cell area coverage, colony number and size distribution from phase contrast micrographs. The principle by which Method B operates is the identification of pixels with an intensity value that is either greater than or lower than the background level. The mode of action of Method C is by detecting local contrast variations differences in adjacent pixels. This enables areas of an image containing cells to be discriminated from the background. However, there are limitations in the scope of these methods as they are not sensitive to differences in cell morphology. Embryonic stem cells undergo morphological changes during differentiation, this can often be observed visually by light microscopy. The following section describes the development of an image analysis protocol that describes stem cell morphology utilising commercially available machine-vision software.

Pluripotent mouse ES cells also exist in numerous cell phases that exhibit discrete morphologies. Shortly after seeding into tissue-culture flasks, cells settle and begin to adhere to the substrate. At this stage cells appear compact with a phase-bright morphology observed by light microscopy. Twelve hours after seeding, small colonies exhibit a classical stem cell morphology containing cells with a large nuclear to cytoplasmic ratio. Proliferating stem cells undergo successive rounds of division, microscopically this can be observed as presents as circular phase-bright areas that form two-adjacent spheres which separate before returning into the colony. After 48h in culture numerous apoptotic and necrotic cells can be observed. Non-viable cells appear as small phase bright or phase-dark spheres. Thereafter, cellular debris forms which presents as small, phase-dark particles. Thus, pluripotent mouse

ES cells may be observed to exist with distinct morphological features that relate to the stage of their life-cycle.

The morphological identification of embryonic stem cells *in vitro* is complicated by their capacity to differentiate into lineage-specific progeny. Differentiated cells may present with an array of morphologies depending upon the lineage and stage of development. Morphological characterisation is therefore not an accurate predictor of cell phenotype. However, the initial stages of embryonic stem cell differentiation can be observed as an area of cell spreading, often proceeding from the edge of a colony of compact pluripotent cells[132,133].

In order to characterise changes in cell phase and morphology in response to inhibition of the mTOR pathway, proprietary software incorporating a machine-learning algorithm was utilised. The use of this software in biological systems has been well established but analysis of stem cell morphology has not been published in peer-reviewed publications.

A series of test images of mES cells in culture were captured and specific cell phase distinctions were identified visually. An analysis protocol was then generated by 'training' the software to recognise specific examples of distinct cell phases. Test data was then analysed and results visually inspected. Distinct cell morphologies were introduced into the protocol to provide a final iteration that included discrimination of cell phase (viable, non-viable, debris) and morphology (compact, spread, dividing). At least 100 samples for each group were visually identified and categorised according to cell phase and morphology. An analysis protocol was built based upon the sample library and this model (Method 2) was then tested with imaging data described in sections 8.4 and 8.5. Data generated from Method 2 was compared with the total colony area data generated by Method B and Method C.

Figure 8.6.1 shows the sample library for cell phase distinction generated from test images and Figure 8.6.2 shows the sample library for cell morphology distinction. Findings from Method B and Method C were then compared with Method 2. Figure 8.6.3 shows representative phase contrast and results images for cell phase and morphology calculations generated by Method 2. Coloured regions indicate cell phase and morphology. Viable (compact) area indicated by blue pixels, viable (spread) by green pixels, viable (dividing) by yellow pixels and non-viable (dead) cells indicated by red pixels. Cellular debris and background represented by grey pixels. Total viable cell area calculations (compact, spread and dividing) were then combined to give a total confluent area measurement to enable comparison with data generated from Methods B and C.

Figure 8.6.4 shows the total cell area calculations (confluence) from the three methods. This data reveals that the increase in cell confluence with time was accurately described by Method 2 as similar results were generated by each of the three methods. In order to assess the differences in the area calculations generated by these methods, the values returned by Method B and C were subtracted from values generated by Method 2. This data was plotted as a scatter graph of the total area value (confluence) versus the difference between the values at each data point (Figure 8.6.5). It is evident from this analysis that at low cell confluency, Method 2 returned a higher value than Methods B or C. As cell confluence increased beyond 40%, Method C returned a lower confluence estimate that Methods A and B. This occurred after 30-35 hours in culture.

Figure 8.6.5 shows that at this time point the total cell area measurement returned by Method 2 diverges from that of Methods B and C. When the relationship between measurements by Method 2 and Methods B and C were plotted, a two order polynomial rate equation was deemed appropriate to describe the concordance between the values (Figure 8.2.6). This was justified as Method 2 discriminated the viable cell area from the non-viable cell area the total cell area coverage measurements generated by Methods B and C may have included these non-viable cells.

The cell phase distinctions (viable, non-viable) for the area calculation generated by Method 2 were plotted individually in Figure 8.6.8. The total area of viable cells (compact, spread, dividing) and non-viable cells over 48h are shown in Figure 8.6.8.A. This chart indicated that the percentage coverage of non-viable cells increased with time. This was apparent after 30h in culture, from this time onwards there was also a decrease in the rate of colony expansion. Thus, the decline in the rate of mES cell expansion was associated with an increase in non-viable cells. Thus the differences between the area measurements described in Figure 8.6.5 and 8.6.6 can be explained by this increase in non-viable cell area.

Finally, the change in area coverage of compact cells and spread cells over 48h is plotted in Figure 8.6.8.B. Whereas the area covered by compact cells increased with time, the total area of spread cells remained constant. As mES cells will retain pluirpotency over extended passaging when supplemented with LIF and serum, an increase in the total area covered by spread cells in this assay was not expected.

In summary, Method 2 generated clear description of the total area of mES cell coverage from phase-contrast micrographs. Moreover, this method provided distinction between viable and non-viable cell phases and may further enable morphological changes that occur during early differentiation to be monitored in a non-invasive manner.

Figure 8.6.1

Representative sample library of mES cell phase distinction.

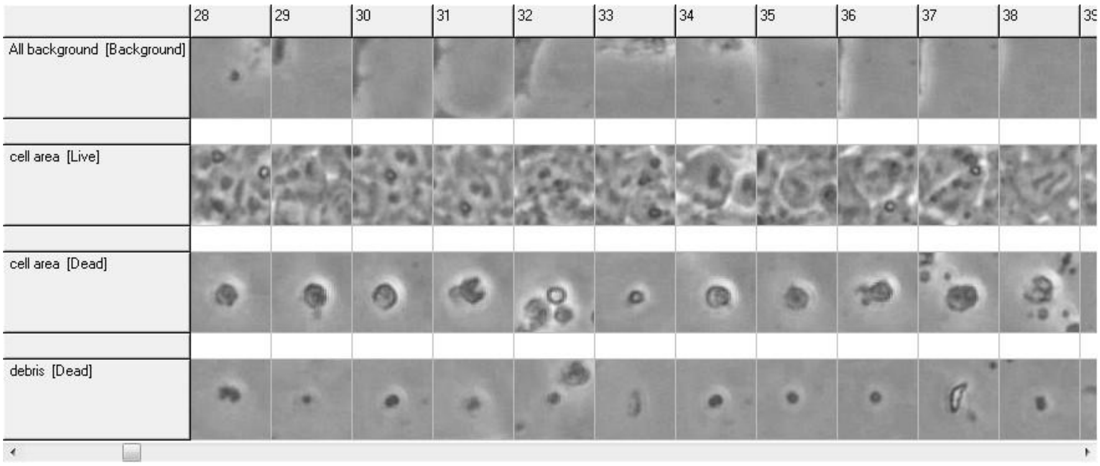
28
29
30
31
32
33
34
35
36
37
38
All background [Background]
cell area [Live]
cell area [Dead]
debris [Dead]

Fig.8.6.1

Generation of analysis protocol utilising the Cell-IQ Analyser Pro-Write™ v.2.0.1 software. Mouse ES cells were cultured within the Cell-IQ Analyser™ for 48h as previously described. Test images were visually inspected and cells exhibiting specific cell phase distinctions were identified and selected. At least 100 instances of each cell phase were included and a sample library was created. Cell phase distinctions include background recognition (358 samples); live cell phase (291 samples); non-viable cell phase (dead, 109 samples) and debris (227 samples). The analysis protocol was built with a recognition complexity factor of 1.4.

Figure 8.6.2

Representative sample library of mES cell morphology distinction.

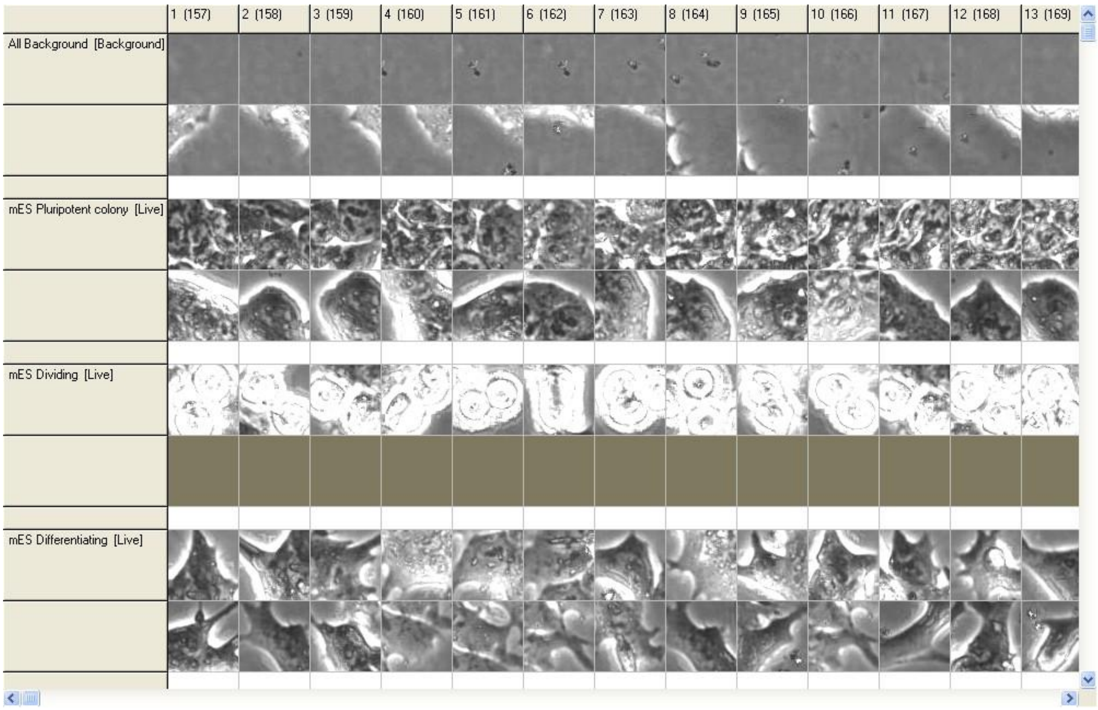
1 (157)
2 (158)
3 (159)
4 (160)
5 (161)
6 (162)
7 (163)
8 (164)
9 (165)
10 (166)
11 (167)
12 (168)
13 (169)
All Background [Background]
mES Pluripotent colony [Live]
mES Dividing [Live]
mES Differentiating [Live]

Fig.8.6.2

Generation of analysis protocol utilising the Cell-IQ Analyser Pro-Write™ v.2.0.1 software. Mouse ES cells were cultured within the Cell-IQ Analyser™ for 48h as previously described. Test images were visually inspected and cells exhibiting specific morphologies were identified and selected. At least 100 instances of each cell phase were included and a sample library was created. Cell phase distinctions include background recognition (358 samples); viable cell phase; compact mES cells (291 samples); dividing mES cells (124 samples) and differentiating cells (312 samples). The analysis protocol was built with a recognition complexity factor of 1.4.

Figure 8.6.3

Representative phase-contrast and results images of mES cells after 24h and 48h in culture by Method 2.

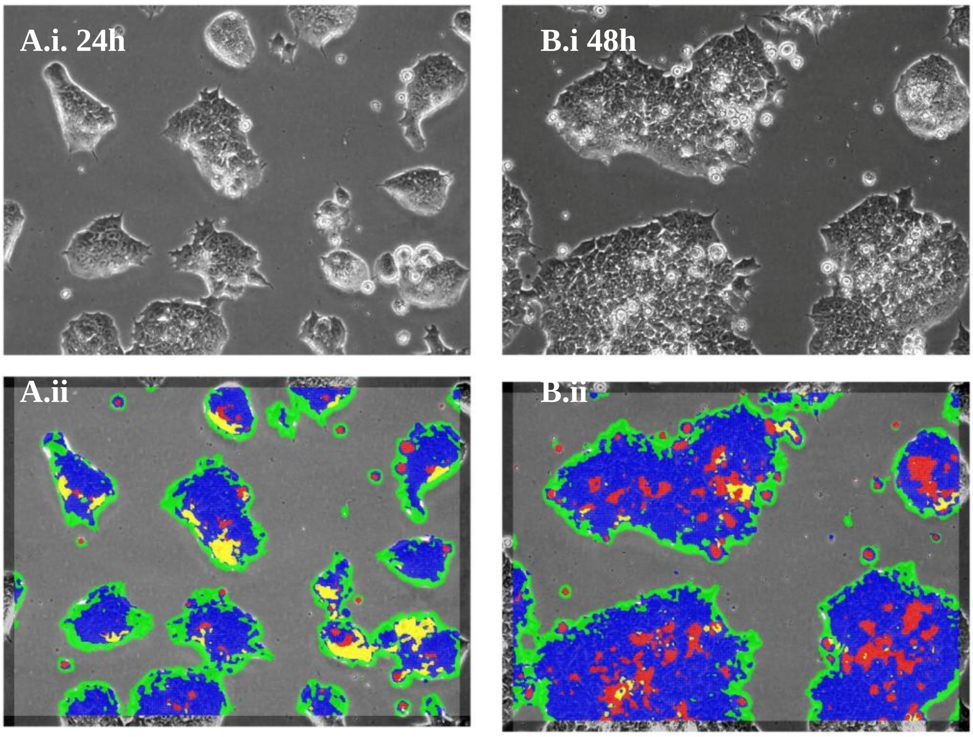

Fig. 8.6.3

Panel of representative images of mES cells in culture and results returned by the Cell-IQ analysis protocol (Method 2). Phase contrast images of mES cells after 24 (A.i) and 48h (B.ii) and corresponding results images at 24h (B.i) and 48h (B.ii). Automated image capture was undertaken at 20x magnification. Coloured regions indicate cell phase and morphology. Viable (compact) area indicated by blue pixels, viable (spread) by green pixels, viable (dividing) by yellow pixels and non-viable (dead) cells indicated by red pixels. Cellular debris and background represented by grey pixels.

Figure 8.6.4

Comparison of three computational methods to document mES cell confluence from phase-contrast images over 48h.

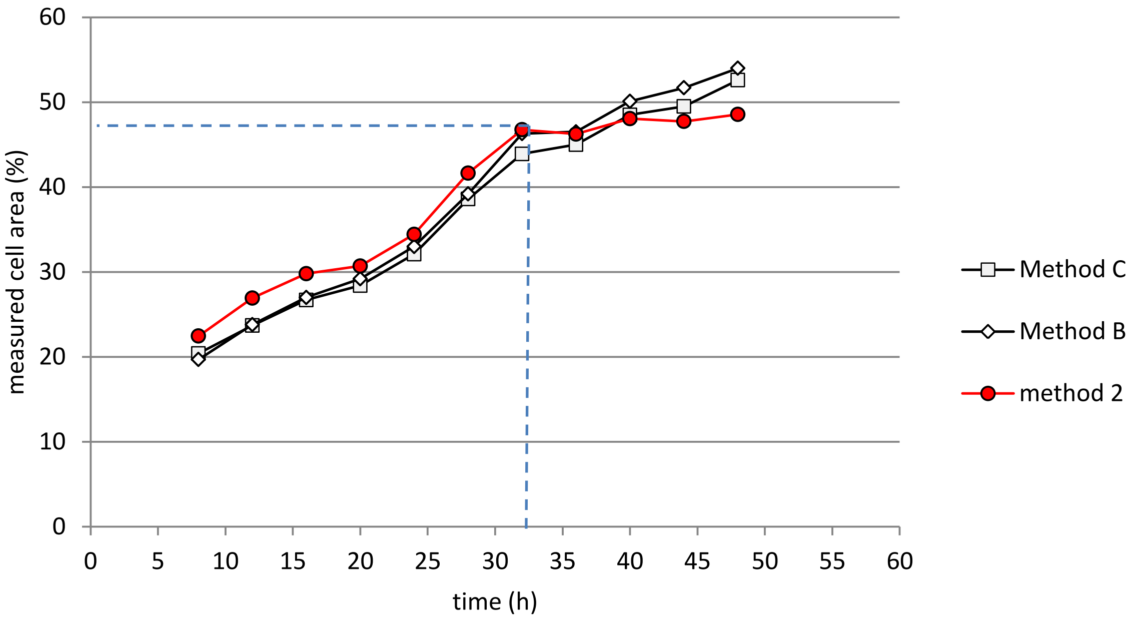

Fig.8.6.4

Total cell confluence was assessed by Method B (open diamonds), Method C (open squares) and Method 2 (red circles). A series of phase-contrast images of mES cells over 48h in culture were analysed by each method. The percentage cell area from each time-point was calculated and presented. Dashed line indicates the point at which rate of cell expansion measured by Method 2 declines.

Figure 8.6.5

The difference between cell area calculations by Method 2 and Methods B and C increases with cell confluence.

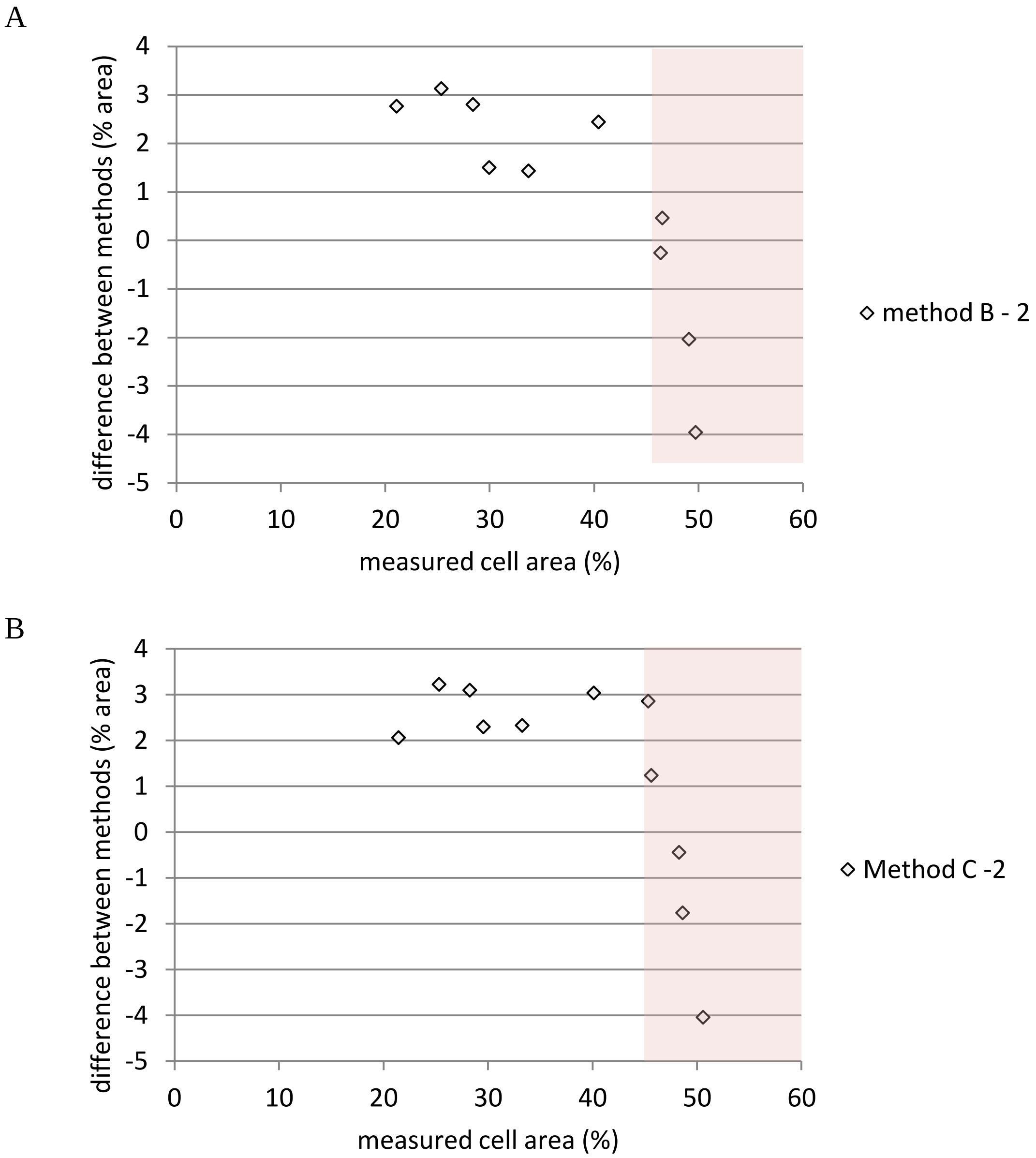

Fig. 8.6.5

The cell area measurements calculated by Method B and Method C were subtracted from the measurements calculated by Method 2 to highlight the difference between methods. This data was plotted as a scatter graph and shows that as the measured cell area increases beyond 45% the difference between the methods changes (pink shading).

Figure 8.6.6

The relationship between Method 2 and Methods B and C for the analysis of mES cell confluence from phase-contrast images.

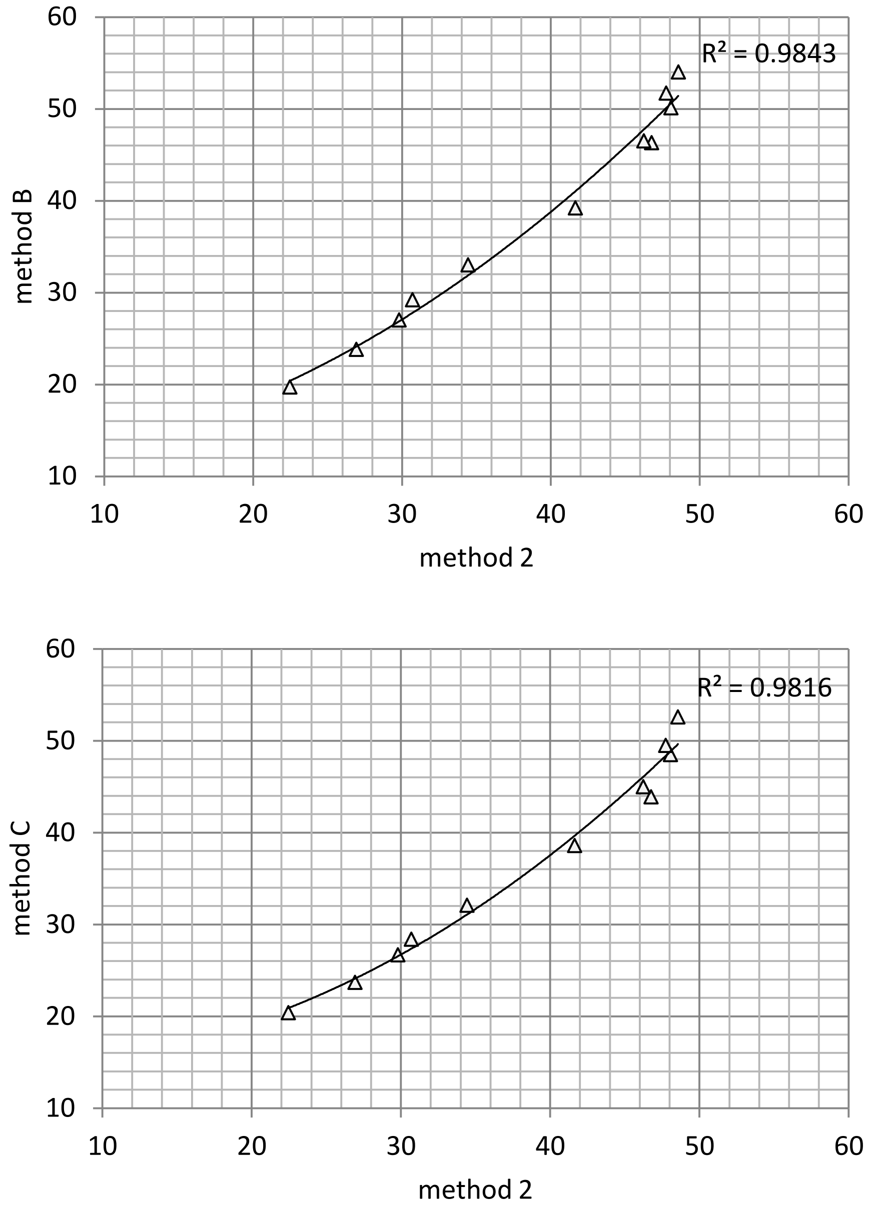

Fig.8.6.6

Total cell area calculations generated by Method 2 were compared with Methods B (chart A) and Method C (chart B). Data fitted a two order polynomial rate equation indicated by a fitted regression line and the coefficients of determination for the area calculation by Method 2 versus Method B (R^2=0.9843) and Method 2 versus Method C (R^2=0.9816).

Figure 8.6.7

Characterisation of mES cell morphology and phase by Method 2 image analysis technique.

A

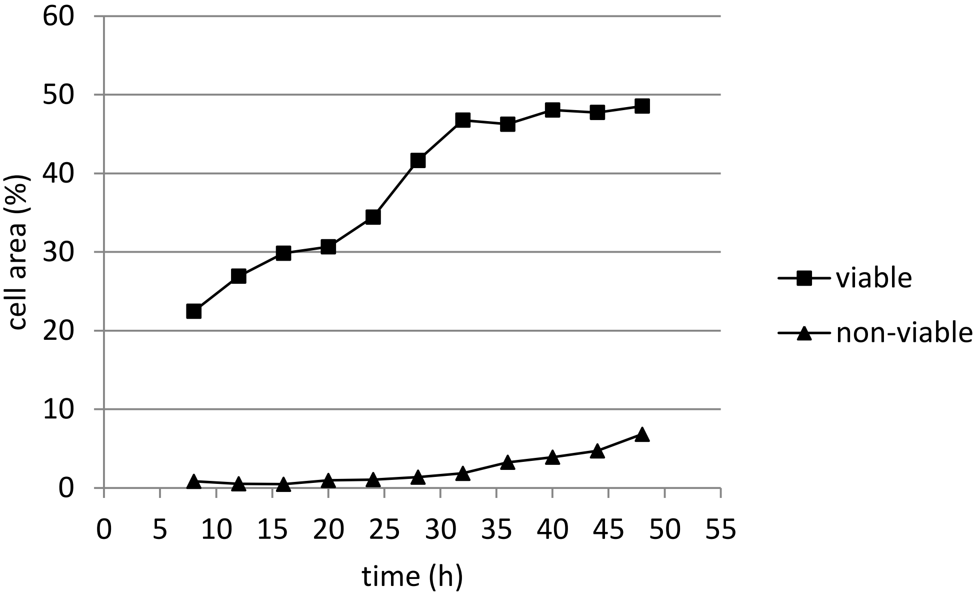

B

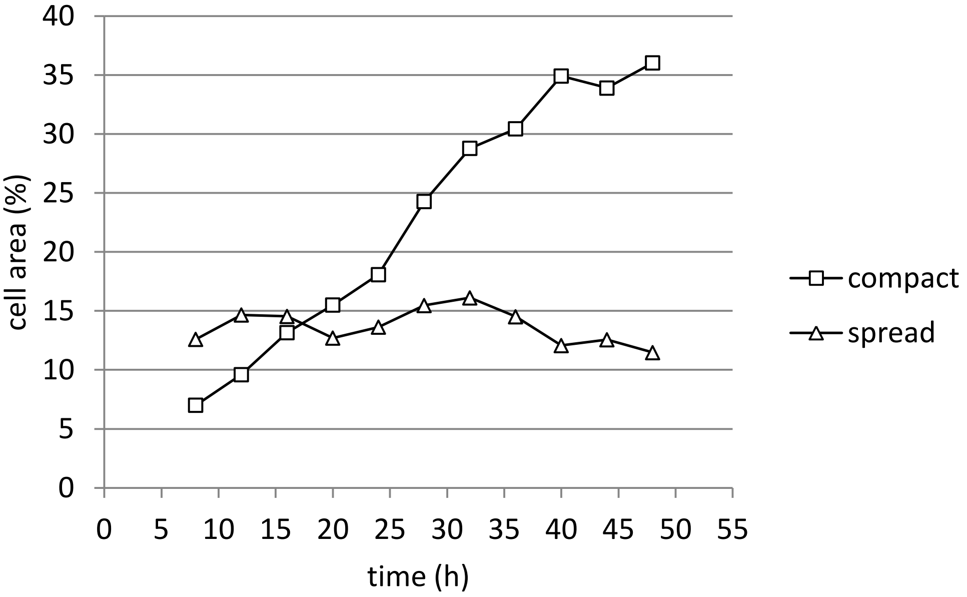

Fig.8.6.7

Method 2 analysis of mES cell expansion over 48h from phase contrast micrographs. Assessment of viable and non-viable cell area (i) and compact and spread cell morphology (ii).

8.7 Summary of findings.

The principle objective of this work was to generate an image analysis tool to analyse stem cell confluence from phase contrast micrographs. To achieve this, the ImageJ software platform was utilised. This program was developed and made available by the US National Institute of Health. The advantage of using ImageJ for this purpose was that it is an open source software with an extensive library of image analysis tools (macros). Thus, it is possible to develop new analytical routines that meet specific needs. The workflows developed here do not represent novel developments in the field of computational image analysis. Rather, they are arrangements of pre-existing macros that have been created by others and made freely available to the research community.

The approach presented in this chapter is a step-wise development of an analysis protocol for the assessment of mES cell confluence. The limitations of the protocol were assessed visually by comparing results images with the original phase contrast images. Modifications were then made to the protocols and images were reanalysed and inspected. Numerical data generated by the modified protocol was then plotted graphically against the original data to enable a statistical description of the iterative modifications. Successful enhancements were then incorporated into the next generation of the protocol.

Other parameters were also described by these image analysis methods. The total number of colonies was determined and the area of individual colonies was calculated. Consequently, the mean colony area measurement and corresponding standard deviations could be calculated for each image.

Method A was developed for the analysis of E14 OCT4/GFP cells, subsequently the effect of rapamycin of mES colony expansion was assessed. It was observed that rapamycin inhibited colony expansion after 48h. This was anticipated as rapamycin was also shown to inhibit mES cell numbers under these conditions. Therefore, Method A was determined to qualitatively document changes mES colony expansion.

This protocol was based upon a simple grey-level thresholding approach. When Method A was applied to images of the parent E14 cell line it was noted that some areas of cell coverage were not measured. Therefore, the protocol was modified to incorporate a dual threshold. This protocol, Method B was then compared with Method A by analysis time-course data from select fields of view over 48h. These results were inspected and limitations were identified. It was observed that Method B provided a better description of cell confluence than Method A as false-negative areas of cell identification were not apparent.

The limitations of the threshold-based approach arose from differences in the brightness and contrast of captured images during different imaging sessions. The images analysed in this aspect of the study were uniform in brightness and contrast as they were generated using an automated cell culture and image capture system. However, application of image analysis methods in the laboratory setting would necessitate a tool that was not sensitive to the image capture settings. To address the limitations of this method, a third iteration of the protocol was developed. This new technique, Method C was based upon local contrast variations that distinguished cellular material from the uniform background. This tool was then compared with previous iterations and was shown to be equivalent to Method B and an improvement to Method A in the assessment of cell confluence.

The final modification to the protocol defined a minimum size rule to exclude cellular debris. This modification was validated by testing a hypothesis that was determined from the observation of colony expansion over time. It is evident by observing cells in culture that as small colonies expand they join to form large colonies. Thus, an image analysis method should describe this as an inverse relationship between colony number and colony size. Method B and Method C both showed this correlation whereas Method A did not. Therefore, it was concluded that Method B and C effectively described individual colony area and the total number of colonies of mES cells from phase-contrast images.

Finally, these methods were compared with an alternative approach to image analysis. Commercially available machine learning software for cellular analysis enabled the discrimination of morphological parameters of cells in culture. This software was ‘trained’ with specific examples of cell morphology that included distinctions between viable and non-viable cells, and between compact cells and spread cells. This protocol, Method 2 effectively described cell confluence. Furthermore, it enabled distinction between areas of viable, non-viable, compact and spread cells. The major drawback of this technique related to the analysis time for each image. Whereas the ImageJ based methods generated numerical and graphical data from an image within 1 second, Method 2 processed each image within 4 minutes.

In conclusion, Methods B and C enabled the assessment of embryonic stem cell colony expansion. These techniques accurately described cell confluence, colony numbers and the individual and mean area of colonies. Method 2 described total cell area coverage and further, provided morphological distinction of mES cells.

Method A was developed for the analysis of E14 OCT4/GFP cells, subsequently the effect of rapamycin of mES colony expansion was assessed. It was observed that rapamycin inhibited colony expansion after 48h. This was anticipated as rapamycin was also shown to inhibit mES cell numbers under these conditions. Therefore, Method A was determined to qualitatively document changes mES colony expansion.

This protocol was based upon a simple grey-level thresholding approach. When Method A was applied to images of the parent E14 cell line it was noted that some areas of cell coverage were not measured. Therefore, the protocol was modified to incorporate a dual threshold. This protocol, Method B was then compared with Method A by analysis time-course data from select fields of view over 48h. These results were inspected and limitations were identified. It was observed that Method B provided a better description of cell confluence than Method A as false-negative areas of cell identification were not apparent.

The limitations of the threshold-based approach arose from differences in the brightness and contrast of captured images during different imaging sessions. The images analysed in this aspect of the study were uniform in brightness and contrast as they were generated using an automated cell culture and image capture system. However, application of image analysis methods in the laboratory setting would necessitate a tool that was not sensitive to the image capture settings. To address the limitations of this method, a third iteration of the protocol was developed. This new technique, Method C was based upon local contrast variations that distinguished cellular material from the uniform background. This tool was then compared with previous iterations and was shown to be equivalent to Method B and an improvement to Method A in the assessment of cell confluence.

The final modification to the protocol defined a minimum size rule to exclude cellular debris. This modification was validated by testing a hypothesis that was determined from the observation of colony expansion over time. It is evident by observing cells in culture that as small colonies expand they join to form large colonies. Thus, an image analysis method should describe this as an inverse relationship between colony number and colony size. Method B and Method C both showed this correlation whereas Method A did not. Therefore, it was concluded that Method B and C effectively described individual colony area and the total number of colonies of mES cells from phase-contrast images.

Finally, these methods were compared with an alternative approach to image analysis. Commercially available machine learning software for cellular analysis enabled the discrimination of morphological parameters of cells in culture. This software was ‘trained’ with specific examples of cell morphology that included distinctions between viable and non-viable cells, and between compact cells and spread cells. This protocol, Method 2 effectively described cell confluence. Furthermore, it enabled distinction between areas of viable, non-viable, compact and spread cells. The major drawback of this technique related to the analysis time for each image. Whereas the ImageJ based methods generated numerical and graphical data from an image within 1 second, Method 2 processed each image within 4 minutes.

In conclusion, Methods B and C enabled the assessment of embryonic stem cell colony expansion. These techniques accurately described cell confluence, colony numbers and the individual and mean area of colonies. Method 2 described total cell area coverage and further, provided morphological distinction of mES cells.

8.8 Appendix 2.

Cytoskeletal α-tubulin and nuclei in spread and compact cells from mES cultures.

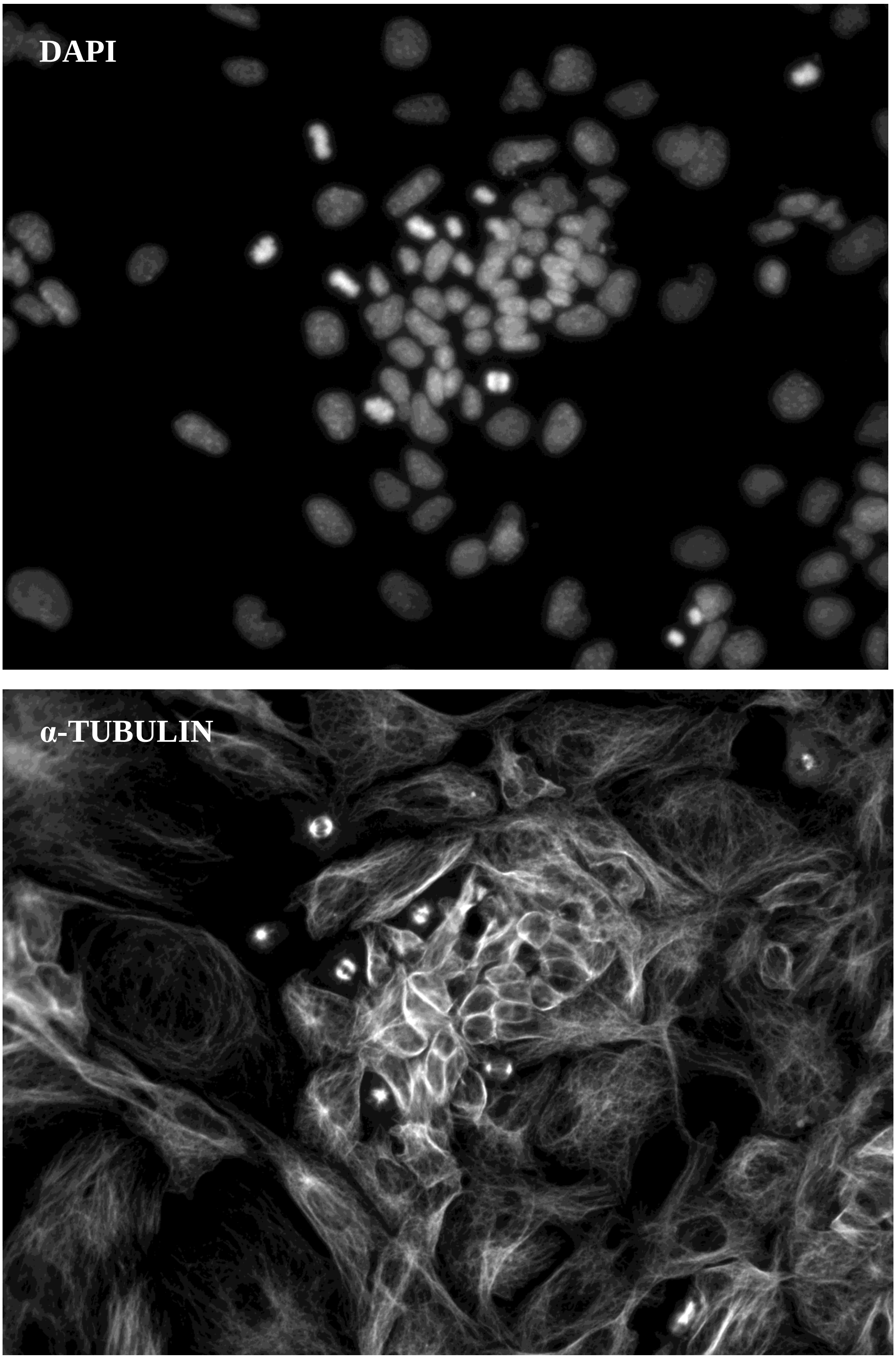
DAPI
α-TUBULIN

8.9 Appendix 3.

Total AKT protein staining in mES cells

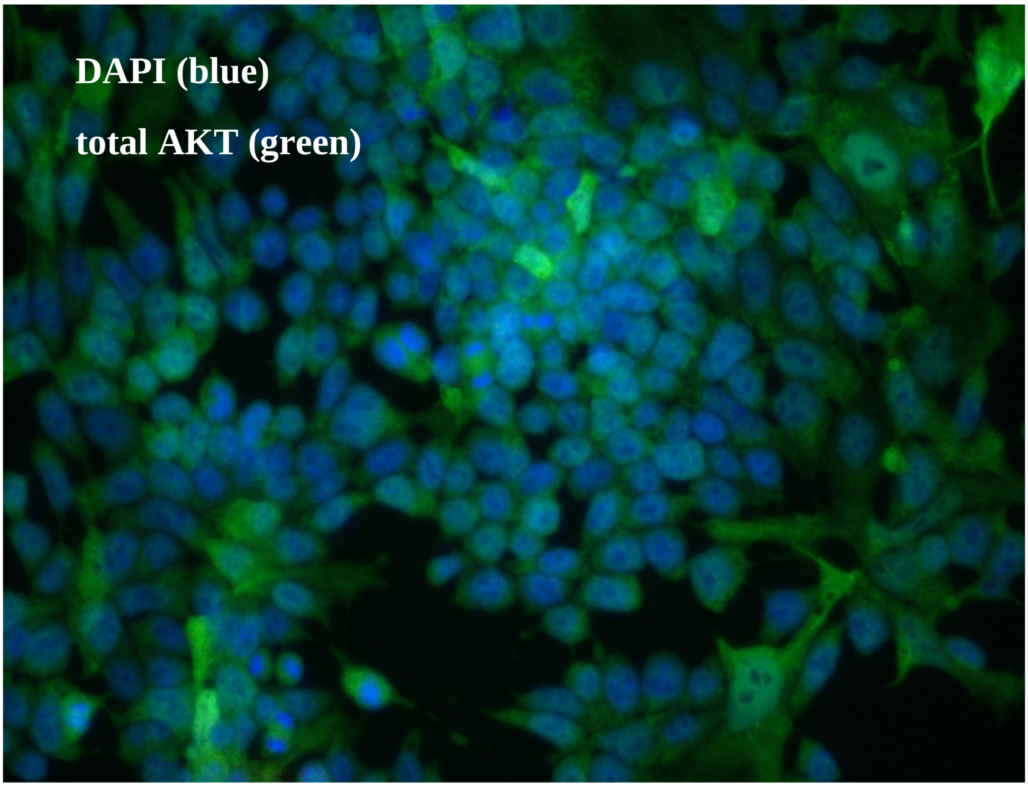
DAPI (blue)
total AKT (green)